AIX-MARSEILLE UNIVERSITE

FACULTE DE MÉDECINE DE MARSEILLE

ECOLE DOCTORALE DES SCIENCES DE LA VIE ET DE LA SANTÉ

T H È S E

Réalisée au

Centre de Résonance Magnétique Biologique et Médicale

Présentée et publiquement soutenue devant

LA FACULTÉ DE MÉDECINE DE MARSEILLE

Le 17 Avril 2014

Par Thomas TROALEN

IRM quantitative de la perfusion myocardique par marquage de spins artériels

Quantitative myocardial perfusion MRI using arterial spin labeling

Pour obtenir le grade de DOCTEUR d'AIX-MARSEILLE UNIVERSITÉ

SPÉCIALITÉ : PHYSIOPATHOLOGIE VASCULAIRE

<u>**Membres du Jury de la Thèse**</u> :

M. Emmanuel BARBIER Directeur de recherche	Université de Grenoble	Rapporteur
M. Gustav STRIJKERS Associate Professor	Technische Universiteit Eindhoven	Rapporteur
M. Benjamin ROBERT Ingénieur	Siemens France	Examinateur
M. Frank KOBER Chargé de recherche	Université de Marseille	Directeur
Mme. Monique BERNARD Directeur de recherche	Université de Marseille	Co-directeur

AIX-MARSEILLE UNIVERSITE

FACULTE DE MÉDECINE DE MARSEILLE

ECOLE DOCTORALE DES SCIENCES DE LA VIE ET DE LA SANTÉ

T H È S E

Réalisée au

Centre de Résonance Magnétique Biologique et Médicale

Présentée et publiquement soutenue devant

LA FACULTÉ DE MÉDECINE DE MARSEILLE

Le 17 Avril 2014

Par Thomas TROALEN

IRM quantitative de la perfusion myocardique par marquage de spins artériels

Quantitative myocardial perfusion MRI using arterial spin labeling

Pour obtenir le grade de DOCTEUR d'AIX-MARSEILLE UNIVERSITÉ

MENTION : PATHOLOGIE HUMAINE
SPECIALITE : PHYSIOPATHOLOGIE VASCULAIRE

Membres du Jury de la Thèse :

M. Emmanuel BARBIER Directeur de recherche	Université de Grenoble	Rapporteur
M. Gustav STRIJKERS Associate Professor	Technische Universiteit Eindhoven	Rapporteur
M. Benjamin ROBERT Ingénieur	Siemens France	Examinateur
M. Frank KOBER Chargé de recherche	Université de Marseille	Directeur
Mme. Monique BERNARD Directeur de recherche	Université de Marseille	Co-directeur

Remerciements

Abbreviation list

AHA   American Heart Association

AIF   Arterial Input Function

ASL   Arterial Spin Labeling

                              CASL   Continuous ASL

                              DASL   Dynamic ASL

                              PASL   Pulsed ASL

                              pCASL   Pseudo-Continuous ASL

                              spASL   Steady-Pulsed ASL

ATT   Arterial Transit Time

bpm   Beat Per Minute

bSSFP   Balanced Steady-State Free Precession

CI   Cardiac Index

CO   Cardiac Output

CT   Computed Tomography

DCE   Dynamic Contrast-Enhanced

ECG   Electrocardiogram

ED   End-Diastole

EDV   End-Diastolic Volume

EF   Ejection Fraction

EPISTAR   Echo-Planar Imaging and Signal Targeting Radiofrequency

ES   End-Systole

ESV   End-Systolic Volume

FAIR   Flow-sensitive Alternating Inversion Recovery

FLASH   Fast Low-Angle Shot

FM   Fluorescent Microsphere

GE   Gradient Echo

HFHSD   High-Fat High-Sucrose Diet

IR   Inversion Recovery

MBF   Myocardial Blood Flow

MBV   Myocardial Blood Volume

MCE   Myocardial Contrast Echocardiography

Moco   Motion Correction

MPI	Myocardial Perfusion Imaging
MPR	Myocardial Perfusion Reserve
MRI	Magnetic Resonance Imaging
MRS	Magnetic Resonance Spectroscopy
MT	Magnetization Transfer
MTT	Mean Transit Time
LA	Left Atrium
LAD	Left Descending Artery
LCx	Left Circumflex Artery
LGE	Late-Gadolinium Enhancement
LLFAIRGE	Look-Locker FAIR Gradient-Echo
LV	Left Ventricle
PE	Phase-Encoding
PET	Positron Emission Tomography
PRESS	Point-Resolved Spectroscopy
RA	Right Atrium
RCA	Right Coronary Artery
RD	Recovery Delay (or Regular Diet in Chapter 4)
RF	Radiofrequency
ROI	Region of Interest
RV	Right Ventricle
SD	Standard Deviation
SR	Saturation Recovery
SV	Stroke Volume
TE	Echo Time
TI	Inversion Time
TR	Repetition Time
SAR	Specific Absorption Rate
SNR	Signal-to-Noise Ratio
SPECT	Single Photon Emission Computed Tomography

Table of Contents

Introduction

The heart is a muscular organ that pumps blood throughout the blood vessels by repeated, rhythmic contractions. By providing this work, the heart muscle (the myocardium) depends itself on the constant supply of oxygenated blood and on the removal of metabolic waste products. These tasks are provided via tissue perfusion, i.e. blood flowing through the capillary system, which exchanges blood oxygen and nutriments with the tissue. The assessment of tissue perfusion therefore allows determining the regional and functional characteristics of the microvascular system of the examined organ. Perfusion MRI indeed gives access to regional blood flow in the capillary system as opposed to MR angiography, in which larger macroscopic vessels are directly visualized. The size of the capillary vessels is far below the spatial resolution of the imaging technique. Since the capillaries are the vessels that actually exchange oxygen and nutriments, only the amount of blood flow which is used by the tissue is measured.

In present clinical practice, perfusion MRI protocols are applied to patients with macrovascular lesions (coronary stenosis, myocardial infarction). Hypoperfused zones can be localized and evaluated in a direct comparison to healthy regions of the organ while providing important information on the extent of potentially jeopardized tissue. Capillary blood flow and volume can be assessed by MRI using two fundamentally different methods. The first, currently most widespread method, is first pass MRI. This technique is based on the injection of a contrast agent modifying the relaxation times dependent on its concentration in the vascular system and thereby producing concentration-dependent image contrast. An image series is acquired following a bolus injection to capture the time-course of the image contrast change. Similar to nuclear imaging techniques, the measurement occurs during the first pass of the contrast agent through the capillary system. In addition to the assessment of the amount of perfusion relative to surrounding regions, the latter technique can also be used to absolutely quantify regional capillary flow. Reliable quantitative perfusion MRI methods, however, are still in development process, and post-processing procedures remain too complex to be applied in clinical routine without the assistance of MR physicists. A reliable but simpler quantification of perfusion would allow the diagnosis and study of pathologies that are presently inaccessible by MRI.

The second method, which is the focus of this thesis, is arterial spin labeling (ASL) MRI. ASL makes use of magnetically labeled blood as an endogenous tracer. Image contrast differences are produced by inflowing blood whose magnetization is inverted prior to the measurement using radiofrequency pulses. The main advantage of ASL is that no injection is required to assess myocardial perfusion so that the measurement can be performed repeatedly. Another advantage of ASL as compared with first pass MRI techniques is that the quantification of perfusion with ASL is relatively easy and does not rely on bolus injection dynamics. Some of the major drawbacks include the inability to measure regional blood volume using the existing techniques as well as the relatively low sensitivity requiring longer acquisition time.

In the human heart, ASL was indeed reported to be limited in terms of acquisition efficiency and dominated by strong physiological noise, which impeded a reliable and robust perfusion quantification. However, for a number of reasons, a much more favorable situation for ASL perfusion measurements is found in the rodent heart, whose exploration is of interest in studies of

animal models of human pathology. Past approaches to measure perfusion with ASL in rodents were indeed more successful than in humans, although they were also characterized by long acquisition times and inherently low acquisition efficiency.

The aim of this thesis was therefore to develop new MRI sequences for a non-invasive quantification of myocardial perfusion using arterial spin labeling in both small-animal and human studies. For this purpose, a three-step translational approach has been carried out:

1. Implementation of a new sequence on a pre-clinical scanner.
2. Validation steps of the technique in healthy rodents.
3. Transition to human studies.

The context of this work will be introduced in the first chapter of this manuscript. The underlying anatomical and pathophysiological aspects will be initially broached to allow a better comprehension of the different mechanisms involved in myocardial perfusion. Secondly, a concise description of MRI techniques specific to cardiac imaging will be presented, insisting on the main differences between small-animal and human acquisitions. Thirdly, the different approaches concerning the assessment of myocardial perfusion will be reviewed. Finally, the main part of this chapter will focus on arterial spin labeling, from the origins of the technique to the various past applications of myocardial ASL, including a description of the different theoretical models developed for absolute perfusion quantification.

Chapter 2 presents the initial setup of an alternative ASL strategy developed within the scope of small-animal studies under the name cine-ASL. This technique uses a new so called steady-pulsed labeling (spASL) approach. The experimental setup will be illustrated, and a comparison with an existing technique setup earlier in the institution (LLFAIRGE) will be discussed in term of robustness to cardiac motion and sensitivity gain. Secondly, the dedicated theoretical model that allows absolute MBF quantification is presented.

Considering the gain in ASL sensitivity obtained using the new technique in small-animals, Chapter 3 focuses on the feasibility of the spASL approach when applied to the human heart. A recently developed free-breathing acquisition strategy combined with the spASL labeling scheme will be discussed in comparison to the FAIR labeling scheme. At the end of this chapter, specific work regarding the correction of respiratory motion under free breathing will be presented and discussed.

Chapter 4 deals with the development of cine-ASL versions that were specifically optimized for different application purposes. An accelerated cine-ASL sequence was developed to further reduce the acquisition time. This fast sequence has been used to investigate the dynamics of the hyperemic response to an infused vasodilator in rats and was also integrated in a multimodal MRI/MRS protocol to study cardiac alterations in type-II diabetes animal models. In a second cine-ASL version, the sequence was optimized with the goal of studying perfusion variations throughout the cardiac cycle. As an original feature, the cine-ASL sequence provides dynamic informations which can be used to correlate magnetization difference changes and perfusion variations across the cardiac cycle.

Chapter 5 summarizes the main findings of this thesis and discusses current limitations of our work. This chapter also presents potential future enhancements and possible future applications of the newly developed cardiac ASL techniques in both rodent and human hearts.

Chapter 1   -   State of the Art

Contents

1.1. The Heart

The physiology of the heart and the blood vessels are closely interrelated and represent the cardiovascular system. This section describes the following underlying aspects of cardiovascular physiology that are important for a comprehensive understanding of this thesis: the basic anatomy of the heart, myocardial architecture and vasculature, cardiac cycle and coronary physiology, myocardial perfusion and perfusion-related cardiac diseases.

1.1.a. Anatomy

The heart is a hollow, muscular organ that pumps blood throughout the blood vessels by repeated, rhythmic contractions. It is responsible for the systemic circulation which carries fresh oxygenated blood away from the heart to the body via the arterial pathway and returns deoxygenated blood back to the heart via the venous circulation. This physiologically based theory of circulation was first described in 1551 *[Lusitano 1551]*.

The heart is composed of four cavities: two right cavities, the right atrium (RA) and the right ventricle (RV) and two left cavities, the left atrium (LA) and the left ventricle (LV). Right and left cavities are completely separated by a bulkhead, the septum (Figure 1.1).
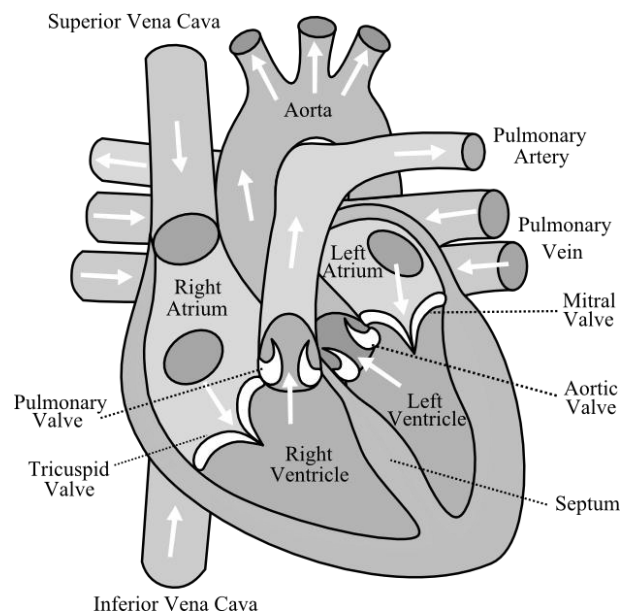
Figure 1.1 – Diagram of the heart. Adapted from [Wapcaplet 2006]

The right part of the heart is responsible for the blood supply to the pulmonary circulation. First, deoxygenated blood coming from the venous circulation is collected by the heart in the RA, from where it enters the RV during the relaxation period of the cardiac cycle, i.e. the diastole. During the contraction phase, i.e. the systole, deoxygenated blood is pumped to the lungs from where it exchanges carbon dioxide and oxygen before re-entering the heart within the LA via pulmonary veins.

The left part of the heart is responsible for the blood supply to the other organs of the body. In diastole, oxygenated blood is pushed from the LA to the LV and is then ejected from the heart through the aorta during the following systole. The aorta divides into smaller arteries, arterioles,

6

and finally capillaries. Waste and carbon dioxide diffuse out of the cell into the blood whereas oxygen in the blood diffuses into the cell. The blood transport continues via venous capillaries, venules and then the vena cava: the lower inferior vena cava and the upper superior vena cava, through which the blood re-enters the heart at the RA.

1.1.b. Myocardial architecture and vasculature

The four cavities are surrounded by the myocardium, a self-exciting muscle. In contrast to skeletal muscle, the latter has its own conduction system and does not require conscious or reflex nervous stimuli. The inner and outer layers of the myocardium correspond to endocardium and epicardium, respectively. The lowest superficial part and the highest part of the heart are named the apex and the base, respectively. The apex-base axis is called the long axis while the perpendicular plane is called the short axis. The LV wall can be divided into four myocardial segments, namely the anterior wall, the lateral wall, the posterior wall and the septum (Figure 1.2). As the blood pressure within the aorta is four times higher than within the pulmonary artery, LV myocardium is two to three times thicker than RV myocardium *[Fuster 2008]*. Consequently, cardiac function can be significantly reduced if the LV muscle is affected.
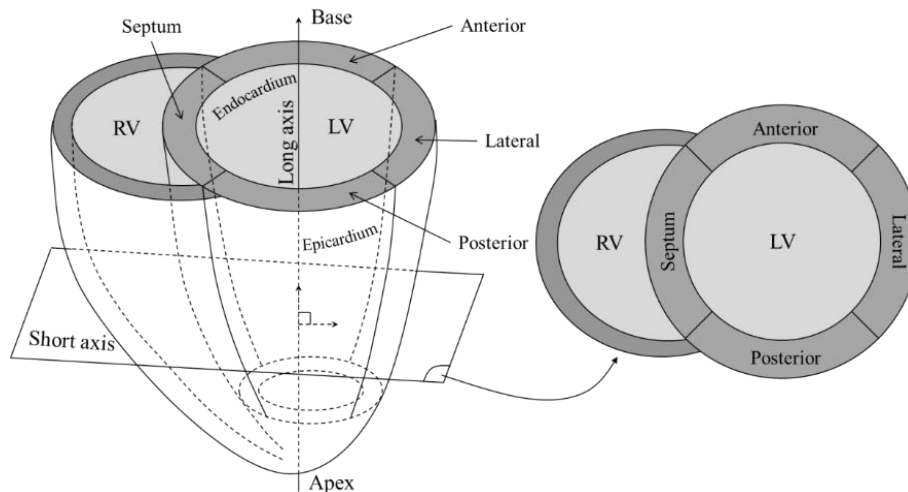
Figure 1.2 – Cardiac architecture and walls.

Arterial vascularization of the heart is provided by two main coronary arteries running along the surface of the heart. The larger left coronary artery divides into two branches, the left anterior descending artery (LAD) and the left circumflex artery (LCx). The right part of the heart is irrigated with fresh blood by the right coronary artery (RCA) going through the right atrioventricular canal (Figure 1.3A). The left and right coronary arteries and their branches lie on the surface of the heart, and therefore are referred to as the epicardial coronary vessels. These arteries give rise to a multitude of arterioles and capillaries that lie adjacent to cardiac myocytes (Figure 1.3B). A high capillary-to-cardiomyocyte ratio and short diffusion distances ensure both adequate oxygen delivery and removal of metabolic waste products. Once the blood has flowed through the myocardium, it is collected by cardiac veins returning to the right atrium, mostly through the coronary sinus located on the posterior side of the heart.
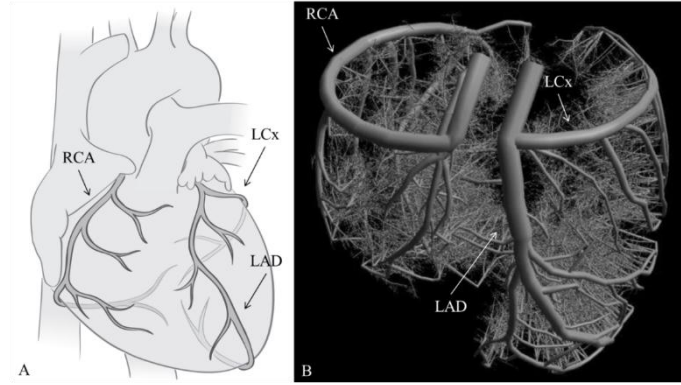
Figure 1.3 – (A) Schematic of the cardiac vascularization. (B) High-resolution ex-vivo angiography of the complex coronary network obtained with computed tomography and iodine-based contrast agent.

1.1.c.   Cardiac cycle and coronary physiology

The cardiac cycle is divided into two fundamental phases, the systole and the diastole (Figure 1.4). The systole corresponds to the ventricular contraction of the heart and occurs just after the QRS complex, or the 'R-wave', i.e. the electrical signal reaching the heart which triggers myocardial contraction. During that period, the blood is pushed out of the LV blood pool towards the body circulation. The second phase, the diastole, corresponds to ventricular relaxation and lasts longer that the systole. During that time, fresh oxygenated blood flows from LA into the LV through the mitral valve.

Between end-systole and early-diastole, the whole heart is relaxed and aortic blood pressure exceeds the blood pressure inside the LV blood pool. At that precise moment, the pressure gradient causes blood to move backward within the aorta, resulting in aortic valve closure and arterial coronary inflow (Figure 1.5).
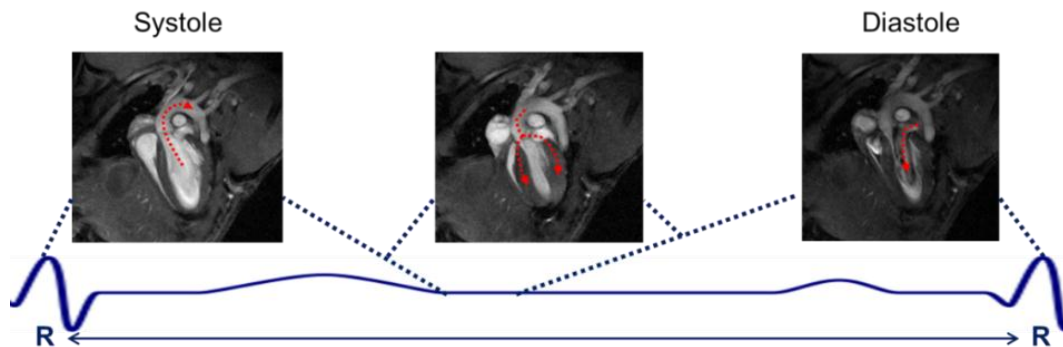
Figure 1.4 – The cardiac cycle. During systole (left), ventricular contraction causes blood to be pushed out of the LV towards the body circulation. During diastole (right), heart relaxation initiates ventricular filling with fresh oxygenated blood. The red arrows indicate macrovascular blood flow. Between systole and diastole (middle), high blood pressure within the aorta causes blood to move backward, resulting in aortic valve closure and arterial coronary inflow.
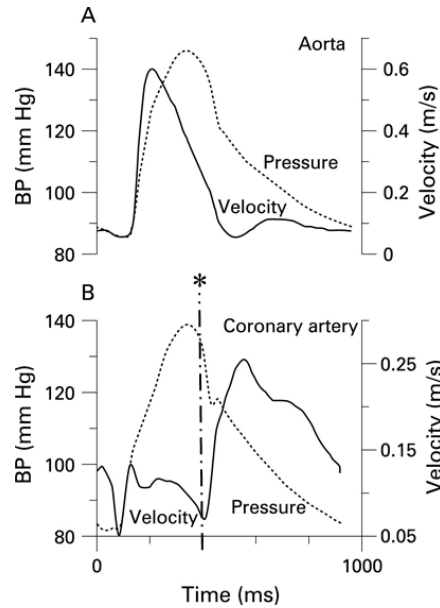
Figure 1.5 – Blood pressure and velocity in the aorta (A) and coronary artery (B). The asterisk and the dashed line correspond to the timing of aortic valve closure.

The phase opposition of blood velocity waveforms between coronary arteries (predominantly diastolic) and veins (systolic) is the most prominent characteristic of coronary hemodynamics. Scaramucci, also known as 'the father of coronary physiology', was the first to consider the effects of cardiac contraction on coronary flow, while hypothesizing that deeper coronary vessels are squeezed by the contraction of the surrounding muscle fibers and refilled from the aorta during diastole. The phasic nature of coronary flow (Figure 1.6) and its relation to the contractile cycle of the heart was originally described in 1957 *[Sabiston 1957]*.
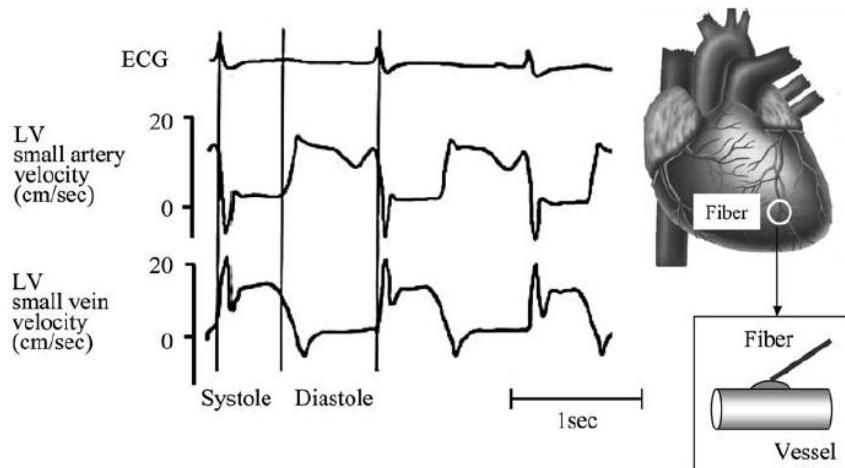
Figure 1.6 – Coronary arterial and venous blood velocity waveforms measured by Doppler velocimeter [Kajiya 2008]. A phase opposition between arterial inflow and venous outflow, i.e. diastolic versus systolic preponderance, can be seen. A reverse flow is frequently recognized in coronary artery in early-systole.

During contraction of the ventricular myocardium, the subendocardial coronary vessels are compressed due to high intraventricular pressures, whereas the epicardial coronary vessels remain

patent, thereby causing blood flow cessation in the subendocardium. As a result, higher myocardial perfusion occurs during heart relaxation in diastole when the subendocardial coronary vessels are patent and under low pressure.

1.1.d.   Myocardial perfusion

Perfusion refers to the delivery of oxygen and nutrients to tissues by means of blood flow and is one of the most fundamental physiological parameters. Perfusion disorders are among the most leading causes of medical disability and mortality.

Myocardial blood flow (MBF), at rest and during exercise, is controlled through an auto-regulation mechanism that is primarily mediated by the vascular resistance of pre-capillary arterioles (diameter less than 100 μm) and pre-arterioles (diameter from ~500 μm to ~100 μm). Coronary auto-regulation intrinsically maintains a constant blood flow despite changes in perfusion pressure under normal myocardial oxygen demand. However, several factors may increase myocardial oxygen demand and induce an increase in resting flow. Those factors include arterial hypertension, increased myocardial contractility, increased left-ventricular wall stress and tachycardia.

Increases in myocardial oxygen demand are additionally induced during physical exercise which increases cardiac workload secondary to heart rate, contractility and blood pressure elevation. In response to the exercise, the pre-capillary arteriolar resistance decreases which might lead to arteriolar vasodilation and increased MBF relative to the oxygen demand.

Myocardial perfusion reserve (MPR), also referred to as coronary flow reserve, signifies the ability of the myocardium to increase blood flow in response to stress. MPR is the ratio of MBF at peak stress, or maximal vasodilation, to the flow at rest. In healthy adults, as in rodents, flow reserve ratio is usually two or higher. Adenosine acts upon coronary arterioles and is one of the key mediators of metabolic blood flow regulation. It is formed in the myocytes by the degradation of adenosine nucleotides, i.e. adenosine triphosphate utilization, a process which is characterized by an increased energy demand. Adenosine stimulates the A2 adenosine receptors on arteriolar smooth muscle and exerts a powerful arteriolar dilator effect. As a result, increase in the interstitial adenosine concentration occurs in parallel to increase in coronary blood flow. Therefore, adenosine infusion can produce almost maximal vasodilation of the coronary microcirculation. This molecule is commonly used in clinical practice to induce myocardial hyperemia and to assess coronary flow reserve.

1.1.e.   Cardiac diseases and perfusion

While this section has no pretense at reviewing all cardiovascular diseases, it seems important to cite some pathologies responsible for perfusion regulation defects in the heart.

Since coronary arteries represent the only source of blood supply to the myocardium, they are classified as 'end circulation'. Failure of oxygen delivery caused by a decrease in blood flow in front of increased oxygen demand results in tissue ischemia, a condition of oxygen and substrate deficiency. Brief ischemia is associated with intense chest pain, known as angina. Severe ischemia can cause the heart muscle to die from hypoxia, such as during a myocardial infarction. Chronic moderate ischemia causes contraction of the heart to weaken, known as myocardial hibernation.

Impaired myocardial perfusion leads to a cascade of downstream effects depending upon its severity (Figure 1.7). With increasing impairment, metabolic abnormalities arise, such as change from glucose to fatty acid metabolism. Thereafter, this leads to abnormalities of first diastolic and then systolic LV function, and later to repolarization abnormalities that may be seen on the ECG accompanied by symptoms of chest pain. Cardiac functional imaging tests interrogate different parts of this cascade, but an assessment of initial perfusion abnormalities is likely to be the more sensitive and predictive marker to take decisions helping prevent this ischemic cascade.
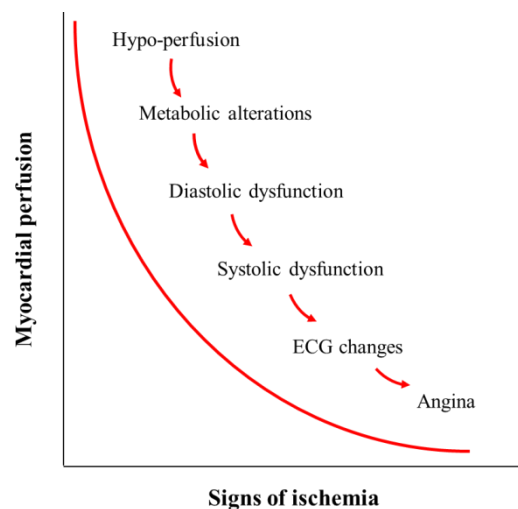
Figure 1.7 – The ischemic cascade.

The most common pathology is coronary artery disease (CAD) which occurs when fatty substances, cholesterol, cellular waste products, fibrin or calcium build up in the inner lining of an artery. Such condition, called atherosclerosis, causes the presence of stenosis, an abnormal narrowing of a blood vessel, which may be the cause of insufficient fresh blood supply to the heart muscle.

The resting tone of the coronary resistive vessels is intrinsically high. For stenosis up to 80-90 percent narrowing, resting MBF is fairly well maintained since baseline myocardial oxygen demand is not increased and the arteriolar auto-regulatory mechanism is able to compensate for the increased vascular resistance *[Gould 1974, 1990]*.

This might not be the case during peak exercise where MBF can increase three to four times to match the increase in myocardial metabolism and oxygen demand. The presence of a significant coronary stenosis reduces the ability of coronary circulation to increase MBF to match the increased workload. Thus, there is a progressive decrease in MPR with increasing stenosis levels. It is important to note that mild-to-moderate reduction in the blood flow with maximal vasodilation may be characterized as a flow deficit, but it may not be low enough to elicit ischemia. Peak flow and MPR reduction beyond a certain level, however, is associated with progressive ischemia with consequent metabolic changes in the cardiac myocytes. This makes flow quantification an important tool for characterization of at-risk patients.

Another important pathological category concerns patients with microvascular disease who usually demonstrate a diffuse reduction in myocardial perfusion and an impaired vasodilatory response. Thus, in the absence of coronary stenosis, a reduction in MPR reflects coronary

microcirculatory dysfunction, which is often associated with systemic diseases caused by endothelial dysfunction like diabetes, hyperlipidemia and hypertension. MBF and MPR estimation may identify early coronary artery disease, evaluate disease progression, and assess the effect of therapy and lifestyle modification.

Finally, MBF may also be altered in some cardiomyopathies that are classified as non-coronary heart disease. Non-ischemic pathologies, such as hypertrophic cardiomyopathy or dilated cardiomyopathy, are characterized by a generalized microvascular dysfunction which affects both resting MBF and MPR.

In conclusion, the heart is a complex system relying on mechanical, electrical, chemical and physiological mechanisms which are all cross-correlated. Cardiac defects can thus be of multiple orders among which myocardial blood flow represents one of the key parameters to characterize cardiac anomaly and to evaluate improvements following revascularization, as well as drug therapy response.

1.2. Cardiac MRI

Magnetic resonance imaging (MRI) is a multi-purpose imaging modality whose versatility is particularly apparent in a cardiovascular imaging context. It is frequently used to assess cardiac anatomy, ventricular function, myocardial mass, myocardial viability, macrovascular blood flow, perfusion, and even myocardial energetics. Simplistically, MRI is performed using a strong homogeneous magnetic field to align the nuclear magnetization of the hydrogen atoms or protons of water present in the body. Radiofrequency (RF) pulses are used to excite the magnetization which leads to signal generation. A group of orthogonal gradient coils is used to alter the magnetic field in a systematic way to achieve spatial encoding of the frequency of the detected signal, which can then be used for image generation. By modifying the timing and order of the sequence of activations of RF and gradient pulses, in combination with the natural abundance and relaxation properties (T_1 and T_2) of the nuclear spins of different tissue types, numerous types of MR images with different contrasts can be generated.

1.2.a. Generalities and specificities

Anatomical views

Tomographic imaging modalities, such as MRI or computed tomography (CT), traditionally orientate and display the body using planes that are parallel or perpendicular to the long-axis of the body. Every heart has, however, a unique orientation and anatomical configuration whereby cardiac planes generated by using the body's long-axis do not cleanly transect the ventricles, atria, or myocardial regions supplied by the major coronary arteries. Furthermore, slice selection, orientation and geometry may differ from one imaging modality to another, which may be confusing when comparing inter-modality exams. To circumvent this, the American Heart Association (AHA) has succeeded in standardizing all cardiac imaging modalities based on cardiac anatomy and clinical needs *[Cerqueira 2002]*. As part of these guidelines, theses authors have established a set of procedure to allow precise localization, orientation and display of the heart.

All cardiac imaging modalities should define, orient, and display the heart using the long-axis of the left-ventricle and selected planes oriented at 90° angles relative to the long-axis. As presented in Figure 1.8, the nomenclature of cardiac planes is thus standardized as short-axis (SA), vertical (or two-chamber) long-axis and horizontal (or four-chamber) long-axis.

Cardiac and respiratory motion

Compared with MRI of other organs, cardiac MRI is relatively complex mainly because of cardiac and respiratory motion. Since the timing of cardiac motion is comparable to the acquisition durations common in MR imaging, the acquisition has to be segmented and synchronized to the myocardial contraction.

Segmented acquisition means that at every heart beat a small set of k-space lines (a segment) is collected. The duration of such a segment is small compared with that of the cardiac cycle, and therefore motion during this short duration should remain small. Several such segmental acquisitions are then needed for complete coverage of k-space (Figure 1.9).
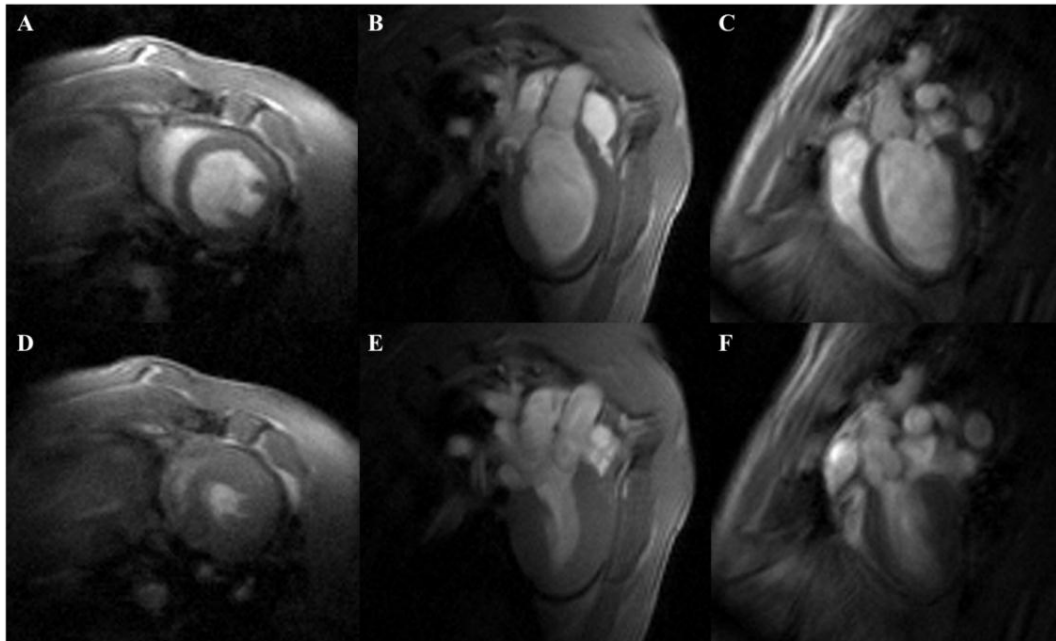
Figure 1.8 – MR images of a rat heart obtained at 4.7T in diastole (A-C) and in systole (D-F) representing the three main cardiac views (short-axis (A,D), two-chamber long-axis (B,E) and four-chamber long-axis (C,F)).

The small duration of each segment combined with cardiac synchronization thus enables the different phases of the cardiac cycle to be sampled. For cardiac MRI, as for other imaging modalities, an electrocardiogram (ECG) signal can either be used prospectively to gate or trigger the acquisition of the segments, or retrospectively at the time of image reconstruction. Prospective triggering is typically used for single-phase acquisitions (snapshot-MRI), usually chosen to coincide with diastases (when the heart is relatively still). Multi-phase acquisitions such as cine-MRI are used to acquire dynamic information. In this case, it is preferable to acquire the data continuously throughout the cardiac cycle, and to use the timing information from the ECG data at the time of image reconstruction for reordering of the segments (retrospective gating, Figure 1.9). The advantage of using a retrospective synchronization is the possibility of imaging the entire cardiac cycle, whereas in prospective gating, there is a lapse of time at the end of the diastole during which no data can be acquired. Due to this waiting time, the partially saturated magnetization has additional time to recover. In cine imaging with prospective gating, the first image therefore generally has a stronger signal (flash artifact). Partial saturation and the balancing of longitudinal magnetization only occur in the subsequent images. With retrospective gating, there is no interruption of the magnetization steady-state and no missing time window at the end of the cardiac cycle.

Moreover, as the heart is placed in the chest region, image acquisition can be disturbed by respiratory motion, which can cause image artifacts. In humans, most cardiac MRI images are obtained during breath-holds, typically of 10-20 seconds duration. In general, an end-inspiratory breath-hold is more comfortable for the patient and can be held longer; however, a breath-hold at the end of gentle expiration tends to be more consistent (minimizing slice misregistration) and is less likely to provoke cardiac ectopy. Another strategy to cope with respiratory motion is the use of a navigator-echo during free breathing acquisition. The subject is instructed to breathe regularly and consistently, and image information is only acquired when the diaphragm is in a pre-

determined position (e.g. end expiration). Navigator-gated acquisitions are, however, comparatively inefficient, since even in optimal situations, only about 30% of the available time is used for acquiring data.
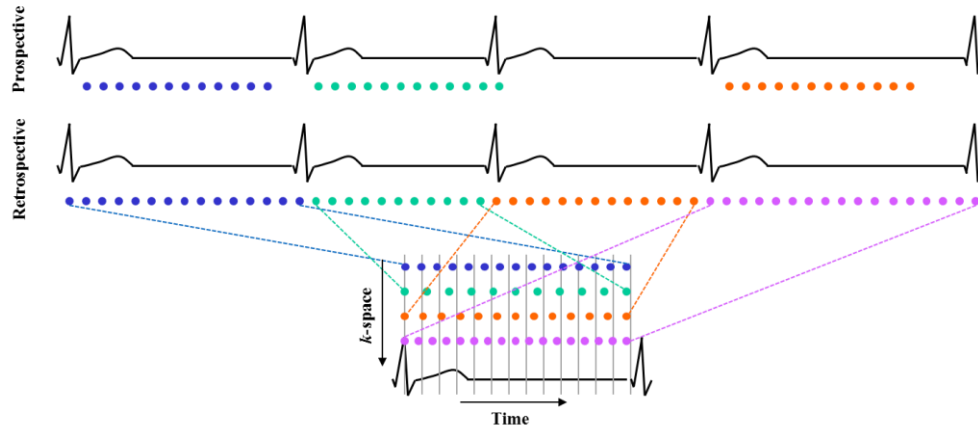
Figure 1.9 – Retrospective versus prospective synchronization. With retrospective gating, k-space segments are acquired continuously throughout the cardiac cycle and reordered as a function of their timing. For example, rapidly acquiring eight k-space lines per segment after each trigger until 128 lines of k-space are acquired in 16 triggers, thus makes image acquisition of multiple cardiac phases or anatomical slices possible in a single breath-hold.

1.2.b.   MRI pulse sequences

A pulse sequence is a carefully timed series of RF pulses and magnetic field gradients and provides the raw information by filling the *k*-space with spatially encoded information. The two broad families of pulse sequences are spin-echo and gradient-echo (GE). Classical spin-echo sequences give excellent quality images with T_1, T_2, or proton-density weighting, but they are characterized by a long time required to fill *k*-space. In the cardiac imaging context, one generally uses Turbo-Spin Echo (RARE) sequences, mainly for tissue characterization. In contrast, gradient-echo pulse sequences utilize a smaller initial RF pulse (between 10 and 90°) combined with magnetic field gradients to rephase magnetic moments to produce the signal. The main advantage of GE sequences is that GEs can be generated and repeated very quickly, so that scan times are reduced. The main disadvantage is an increased susceptibility to artefacts in the presence of inhomogeneity of the static magnetic field.

Imaging speed is a key concern in cardiac MRI, and parallel imaging is often used to reduce scan times or to improve temporal resolution. Such techniques rely upon multiple-element coils that permit undersampling of *k*-space. Missing lines are filled with data calculated using the available signal acquired in parallel from the elements along with the coil sensitivity profiles. These *k*-space undersampling techniques allow for 2-3-fold reduction scan times. The drawback of accelerated parallel imaging is a reduced signal-to-noise ratio (SNR).

Myocardial function

The workhorse of cardiac MRI is to acquire a dynamic dataset using cine-MRI (typically gradient echo) sequences. Usually, the cardiac cycle is divided into 20-30 phases, each of these phases being represented by a *k*-space segment of that duration (see section 1.2.a). Each phase is

represented by one image, and the resulting images are displayed as a cine loop. Cine-MRI is used primarily to evaluate cardiac anatomy and global function. The end-diastolic and end-systolic frames are selected, and then endocardial and epicardial contours are delineated. This allows calculation of global functional parameters, end-diastolic volume (EDV), end-systolic volume (ESV), stroke volume (SV), ejection fraction (EF), and myocardial mass. Cine-MRI is the reference standard for *in vivo* assessment of myocardial volume, global function, and mass *[Sakuma 1993]*.

Regional analysis of parameters, such as wall thickening or LV contractility, can be evaluated by employing approaches such as the AHA 17-segment model *[Cerqueira 2002]*. Many studies have used cine-MRI to evaluate changes in post-infarction myocardial function and remodeling following therapy. To tease out the more subtle regional changes in contractile function, including differentiating subendocardial from transmural changes, techniques such as myocardial tagging *[Zerhouni 1988, Axel 1989]*, displacement-encoding with stimulated echoes (DENSE) *[Aletras 1999, Gilson 2004]* and harmonic phase imaging *[Garot 2000]* have been applied to human and animal models of cardiovascular disease.

Myocardial viability

Late-gadolinium enhancement (LGE) is a particular contrast-enhanced MRI technique, which has rapidly become a key strength of cardiac MRI for *in vivo* assessment of myocardial infarction. LGE-MRI involves intravenous administration of a paramagnetic contrast agent (CA, e.g. Gd-DTPA or Gd-DOTA) which shortens the T_1 relaxation time leading to an increased intensity on T_1 weighted images. These agents are large molecules that rapidly diffuse from the intravascular space into the interstitium remaining in the extracellular space. The molecules are unable to enter cells, provided that tissue cell membranes are intact *[Saeed 1996]*. The technique is called 'late' or 'delayed' because images are typically obtained 10-20 minutes after injection, corresponding to the time needed for the contrast to 'wash-in' to the infarcted tissue and 'wash-out' of the normal myocardium. Imaging is then performed using sequences designed to null the signal in normal myocardium and enhance infarcted myocardium where the contrast agent temporarily collects. An example of LGE-MRI image is shown in Figure 1.10 demonstrating clear delineation of infarcted myocardium. In both animal and human studies, many research investigations on myocardial infarction have used LGE-MRI to compare infarct size between groups and over the time course of a study *[Kim 1999, Wagner 2003, Yang 2004]*.
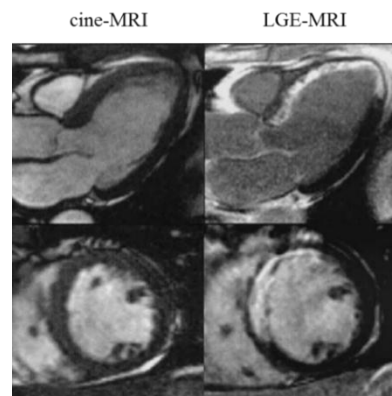

Figure 1.10 – Representative long-axis (top) and short-axis (bottom) T_1-weihted gradient-echo MRI (left) and LGE-MRI (right). Adapted from [Beek 2003].

Myocardial tissue structure - Parameter mapping

A significant number of developments regarding quantitative measurement and mapping of MR relaxation parameters dedicated to cardiac MRI were undertaken, covering mainly T_1, T_2, and T_2^* techniques.

The longitudinal relaxation time constant T_1 of the myocardium is altered in various disease states due to increased water content or other changes to the local molecular environment. Changes in both native T_1 and T_1 following administration of gadolinium are considered important biomarkers and multiple methods have been suggested for quantifying T_1 *in vivo [Moon 2013]*. More T_1 mapping techniques rely on Inversion-Recovery (IR) measurements. To achieve accurate T_1 estimates from a three-parameter curve-fitting procedure, data from at least 6 to 10 time points along the recovery curve should be available *[Zhang 1998]*. The multi-point approach, as first described by Look and Locker *[Look 1970]*, samples the relaxation curve multiple times after an initial preparation pulse. Although the Look Locker (LL) technique has been widely used for T_1 measurements of the brain, it is not suitable for pixel-by-pixel T_1 mapping in the heart because data acquisition is performed continuously throughout the cardiac cycle without regard for cardiac motion. To overcome the limitations of the conventional LL approach, Messroghli *et al.* proposed a modified LL inversion recovery scheme (MOLLI) *[Messroghli 2004]*. MOLLI allows acquiring data at a given time of the cardiac cycle over successive heart beats and merging image sets from multiple LL experiments with varying inversion times into one data set. MOLLI propelled the use of T_1-mapping in cardiovascular MRI and inspired many new methods. For instance, a shortened breath-hold adaptation with conventional curve fitting (ShMOLLI) was proposed as a means of mitigating heart rate dependence as well as shortening the breath-hold *[Piechnik 2010]*. Saturation recovery methods have been recently adapted for T_1-mapping using SSFP readout (SASHA) as a means of limiting the T_1 underestimation obtained with MOLLI *[Chow 2013]*. A review of all the developed methods for myocardial T_1-mapping has recently been published *[Kellman 2014]*.

Much attention has also been paid to the development of myocardial quantitative T_2 mapping techniques. T_2 is representative of tissue structure in general and of œdema, necrosis, fibrosis and collagen content in particular. Classical T_2 mapping techniques are based on Turbo-Spin Echo acquisitions with multiple echo times, but more recently T_2 preparation modules have been used and developed more and more frequently in both humans *[Knobelsdorff-Brenkenhoff 2013]* and small animals *[Beyers 2012, Coolen 2013]*.

Alternatively to T_2 assessment, T_2^* mapping can be used to obtain information on tissue structure and properties. For instance, T_2^* mapping has been used in humans to quantify myocardial iron deposition as a predictive variable for ventricular dysfunction treatment *[Anderson 2001]*. More recently, multi-gradient echo sequence and exponential fitting to produce T_2^* maps have been used in a coronary occlusion mouse model *[Aguor 2012]*. In this study, T_2^* mapping was found a useful addition to LGE-MRI for the follow-up of myocardial remodeling and the prediction of recovery from infarction.

Magnetic resonance spectroscopy

Though not generally considered as an imaging technique, another important MR technique is MR spectroscopy (MRS). Compared with MRI, MRS is the older MR technique, and it is

therefore available using the same imaging equipment. MRS offers the ability to quantify myocardial lipid accumulation or to investigate myocardial energetics.

Using proton MRS (^{1}H-MRS), it is indeed possible to quantify the triglyceride content in the heart. MRS uses the chemical shift of the resonance frequency of protons, which depends on their chemical environments. Hence, the resonances of protons contained in fat and water can be spectrally separated. For instance, spectral peaks corresponding to protons in lipid species (specifically the methyl CH_3 and methylene CH_2 groups) are distinct from those of water, thus permitting quantification by peak integration. As an example, ^{1}H-MRS in the human heart has recently been used by our group to assess the effects of bariatric surgery on cardiac ectopic fat deposition *[Gaborit 2012]*.

Phosphorus MRS (^{31}P-MRS) in general uses different localization techniques than ^{1}H-MRS but it also provides molecular information. In the past, this technique has been applied more widely in cardiac studies. ^{31}P-MRS is a powerful technique to assess bioenergetics and high-energy metabolism within the myocardium, allowing measurement of phosphocreatine and ATP concentrations *[Weiss 1990]*. Zeng *et al.* recently found that using ^{31}P-MRS one can detect improvement of bioenergetics in post-infarct swine following cell transplantation therapy, as measured by the subendocardial phosphocreatine/adenosine triphosphate ratio *[Zeng 2007]*. Moreover, they were able to demonstrate that these improvements were supported by improvements in regional and global contractility as measured by cine-MRI.

1.2.c.   Small-animal cardiac MRI

The interest in studying rodents using MRI is twofold, since rodents can be used not only to set up new imaging techniques, but also to study physiology and rodent models of human pathology using existing MRI techniques. The developments made during this thesis were carried out in a translational way, and a significant part of the work was therefore accomplished on rodent MRI techniques. The following section highlights the most relevant differences between humans and rodents to consider when developing techniques of rodent cardiovascular MRI.

As the most obvious feature, the size of the heart is proportional to the size of the body. The mouse heart is about 1 cm long while the rat heart is about 2 cm long and the human heart is about 10-15 cm long (Figure 1.11).

Despite this difference in size, the vascular physiology is quite similar between these species. While the major coronaries are also proportional to the size of the heart, the small arterioles and capillaries have the same size. Also, despite a significant difference in body weight, the velocity of the blood ejected through the aorta during systole is nearly the same, i.e. around 50 cm s^{-1}. Blood velocities in large vessels are therefore very high in rodents relative to their body size. Capillary tissue blood flow such as MBF is also much higher in rodents than in humans. In humans with normal coronary arteries, resting myocardial blood flow is in the range of $0.7 - 2.4$ mL g^{-1} min^{-1} *[Chareonthaitawee 2001]*, whereas in healthy rodents, resting MBF is in the range $3 - 7$ mL g^{-1} min^{-1}.
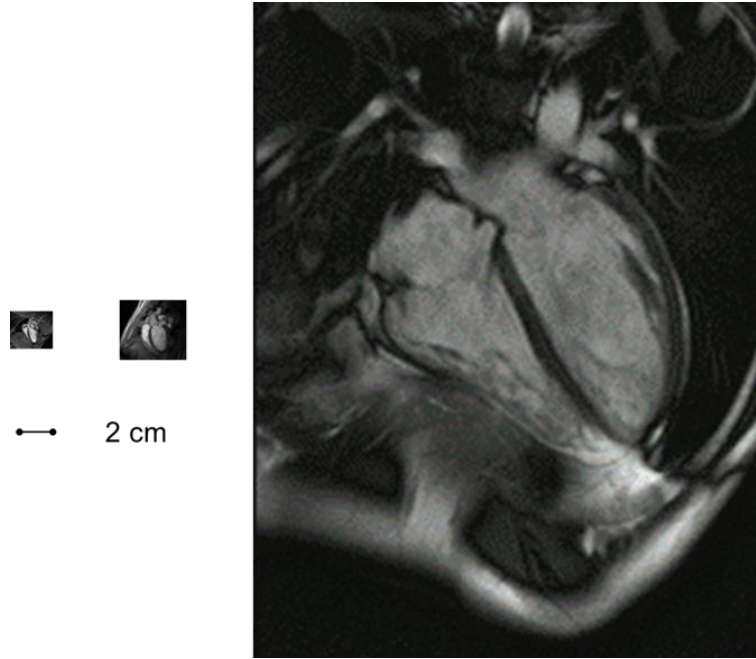
Figure 1.11 – Relative size of the heart between species. MRI 4-chamber long-axis views of a mouse (left), a rat (middle) and a human (right) heart obtained at 11.75T, 4.7T, and 3T, respectively.

Considering that typical spatial resolutions in MRI are of the order of 100 μm, whereas the mean capillary size ranges between 5 and 8 μm, it becomes clear that the measurement of tissue perfusion is not possible in a direct way. For this reason, only flow quantification in main arteries can be performed using a direct measurement (e.g. velocity-encoded MRI). Tissue perfusion needs to be addressed using indirect measurements and mathematical models allowing the calculation of mean blood flow within a voxel based on several assumptions such as the blood/tissue partition coefficient for water or the exchanges rates between vascular and extravascular space (Table 1.1).
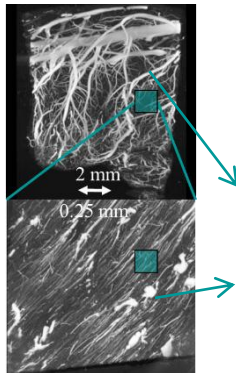
Table 1.1 – Blood vessels diameter and flow velocity.

Order of magnitude		
Typical MRI resolution	100 μm – 1 mm	
Main arteries diameter	> 100 μm	Direct measure
Flow velocity	~50 cm s^{-1}	
Capillaries diameter	5 – 8 μm	Indirect measure
Flow velocity	1 – 2 mm s^{-1}	

Heart- and breath-rates are fundamentally different between humans and rodents. Human heart-rate (50 - 100 beat per minute (bpm) at rest) is such that a complete image can generally be acquired within one cardiac cycle (a snapshot usually obtained in mid-diastole) without being affected by cardiac motion. Rodent heart rate is much higher (300 - 600 bpm), and a complete image acquisition of sufficient spatial resolution within one cardiac cycle is only possible using accelerated acquisition with parallel imaging. To cope with the timing constrains imposed by

these rapid cardiac contractions, the *k*-space is divided into segments that have to be acquired at different cardiac cycles. This *k*-space segmentation allows sufficient temporal and spatial resolutions when studying the rodent heart. The segmentation principle is similar to a segmented cine-MRI acquisition in humans, but in rodents *k*-space is generally fully segmented, acquiring one phase-encoding step per cardiac cycle in order to maximize temporal resolution.

The breath-rate is also higher in rodents (50-100 bpm) than in humans (15-20 bpm), and unless artificial respirators are used in intubated animals, there is no possibility for breath-hold acquisition. Keeping in mind that in rodents an image in the temporal domain is indeed integrated over several dozens of heart beats, respiratory motion is more likely to produce a smooth blur over the entire image than a specific motion artifact. Nonetheless, respiratory gating can be used in rodents to improve image quality.

A summary of the physiological values is reported in Table 1.2.

Another relevant difference between the cardiovascular systems of humans and rodents when it comes to MR sequence development is the time of blood recirculation in the body. This recirculation time is about one minute in humans (5L of blood volume with a cardiac output of about 5L/min), whereas it is only of the order of 10 seconds in rats (15 mL of blood volume with a cardiac output of about 90 mL/min). This implies for instance that contrast agents are transported very rapidly throughout the rodent body.

Table 1.2 – Order of magnitude of physiological parameters based on experimental observations.

	Heart rate (bpm)	Breath rate (bpm)	MBF (mL g^{-1} min^{-1}) [**]
Mouse [*]	400 - 600	80 - 120	4 - 7
Rat [*]	250 - 400	50 - 90	3 - 6
Human	50 - 100	15 - 20	0.7 - 2.4

[*] *Values obtained under the influence of isoflurane anesthesia.*
[**] *Order of magnitude based on experimental observations and literature. For references, see Chapter 2 (mouse), Chapter 3 (human), and Chapter 4 (rat).*

1.3. The Many Ways to Myocardial Perfusion Imaging

Nowadays, cardiovascular imaging techniques play a crucial role in clinical routine, especially in diagnostics, patient care and therapy follow-up. In present clinical practice, myocardial perfusion imaging (MPI) protocols are used in patients with macrovascular lesions such as coronary stenosis or myocardial infarction. By comparison with healthy regions of the organ, hypoperfused zones can be evaluated and localized giving important information on the extent of the jeopardized tissue. Nuclear cardiology, using either single photon emission computed tomography (SPECT) or positron emission tomography (PET), is the most widely used approach for assessing myocardial perfusion. Other imaging techniques, such as contrast echocardiography and MRI have been more recently proposed as alternative methods for the evaluation of myocardial perfusion.

Classically, tissue perfusion is quantified using a diffusible tracer that can exchange between the vascular compartment and tissue. This yields a perfusion measurement in units of milliliters of blood flowing through a gram of tissue per unit of time. However, since it is relatively easy to measure hemodynamic function from the passage of an intravascular tracer, the term 'perfusion imaging' has also been applied to measurements of perfusion-related parameters such as the mean transit time (MTT), the time for the blood to flow through the capillary system, and the myocardial blood volume (MBV) that can be related to perfusion through the Central Volume Principle:

$$MBV = MBF \times MTT \qquad [1.1]$$

Here, techniques that give access to myocardial perfusion will be reviewed while distinguishing between quantitative and qualitative techniques. 'Quantitative' refers to MBF quantification in absolute terms (i.e., in mL g^{-1} min^{-1}) and comprises invasive and non-invasive techniques, whereas relative or semi-quantitative MBF assessment will be considered as 'qualitative'.

1.3.a. Fluorescent microspheres

In small animals, the 'gold standard' to quantitatively assess MBF is the fluorescent microsphere (FM) technique. The FM experiment has been proposed as an alternative to the radioactive microspheres reference technique *[Rudolph 1967]*, which was still used until the late 90's *[Gervais 1999]*. Both techniques require sacrificing the animal and are based on the same principle: microspheres are trapped during their first pass in each organ of the body, and the flow of each organ is directly proportional to the number of spheres recovered within that organ after a fixed time of circulation. For cardiac experiments, microspheres are directly injected into the LV via the right carotid artery. For quantification, a reference blood sample needs to be withdrawn from the femoral artery after a fixed time of FM infusion. The animal is then killed, and the heart is removed, blotted, weighed and processed for fluorescent quantification using a spectrophotometer. Regional blood flow is quantified from microsphere data obtained from both the heart and the reference sample *[Gervais 1999]*. As a validation process, most of the techniques that are described hereafter have been compared to FM in small-animal studies.

1.3.b. Radionuclide MPI

Nuclear medicine uses radioactive isotopes to interrogate cellular and sub-cellular biological and metabolic processes. Generally, these radioactive isotopes or radionuclides are chemically bound

to complexes designed to specifically target certain physiologic processes. The capabilities of radionuclide MPI techniques to assess myocardial perfusion in the presence of coronary artery stenosis are related to the myocardial distribution of a perfusion tracer and corresponding regional blood flow.

SPECT perfusion imaging

SPECT operates by directly detecting gamma radiation from the tracer. During a SPECT scan, the gamma camera is rotated around the subject and projection images are acquired. Filtered back projection and iterative reconstruction are used to create a 3D volume out of the 2D projection data. The SPECT technique employs many of the back projection algorithms that have been applied to conventional radiographs for CT scanning.

Until the late 90's, myocardial scintigraphy was the most powerful technique available in clinic for the diagnostic of coronary artery disease *[Gibbons 2000]*. Although multiple view planar images were first employed, they have been largely replaced by SPECT, which is superior from the standpoint of localization, quantification and image quality. SPECT MPI requires radiopharmaceutical injection using either thallium-201 (^{201}TI) or technetium-99m (^{99m}Tc). Both are characterized by a rapid myocardial extraction and by a cardiac uptake proportional to blood flow. Thus, myocardial perfusion can be imaged and hypoperfusion can be detected as a relative uptake defect as compared with the normally perfused myocardium.

An important limitation of MPI with SPECT tracers is that absolute MBF cannot be measured. The standard qualitative approach remains a sensitive means for diagnosing the presence of obstructive CAD, but it often reveals only the coronary territory subtended by the vessel with the most severely flow-limiting stenosis, underestimating the true extent of the disease. Previous studies have suggested that it is possible to quantify myocardial perfusion reserve using dynamic planar scintigraphy and ^{99m}Tc tracers in humans or dynamic SPECT and ^{201}TI in animals *[Ben-Haim 2013]*. Although these studies provided initial proof of concept, they also highlighted the limitations of conventional SPECT systems for the dynamic collection of tomographic data necessary to quantify rapid changes in radiotracer concentration.

PET perfusion imaging

PET imaging operates on the following principle. The PET tracers emit positrons which annihilate with nearby electrons causing two gamma photons (511 KeV) to be emitted in opposite direction. The coincidence detection of these emissions by multiple detectors in the PET scanner allows direct localization of the annihilation events. Statistical analysis and tomographic reconstruction are then used to generate a 3D PET image.

PET perfusion tracers, such as ^{82}Rb, ^{13}N or ^{15}O, have short physical half-lives (~2 min for ^{15}O) and therefore often require that the cyclotron that produces them be on-site or nearby. These relatively short half-lives compared to SPECT tracers offers, however, the possibility of acquiring repeated MBF measurements in the same scanning session within a reasonable time (1 to 2 hours). Also a unique feature of PET is that MBF and MPR can be quantified in absolute terms using tracer kinetic modelling. ^{13}N-labelled ammonia and ^{15}O-labelled water have been well validated for this purpose in experimental studies using microspheres as well as in CAD patients *[Bergmann 1984, Sawada 1995, Kaufmann 1999]*.

Cardiac PET/CT combination has been proposed for MPI. Here, the PET scan is used for absolute MBF quantification with ^{15}O injection *[Harms 2013]* or ^{13}N injection *[Kim 2013]* while the CT scan is used for precise anatomical localization. This technique has recently been demonstrated to hold promising diagnostic value for the detection of CAD but methodological differences in post-processing and utilized analysis software can affect generated MBF values and potentially prohibits widespread applicability. An example for 3D myocardial perfusion assessment is presented in Figure 1.12.
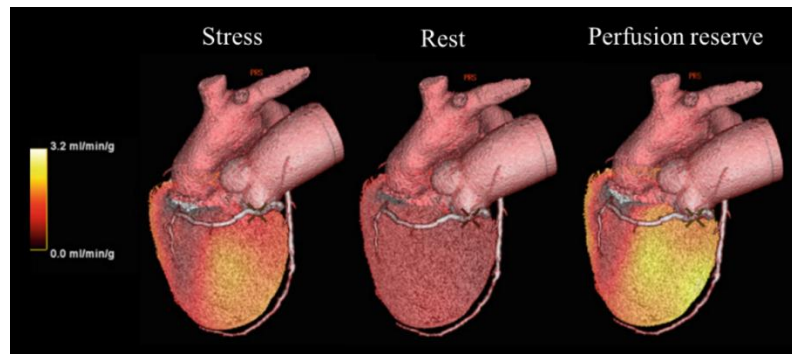
Figure 1.12 – Fused 3D views of quantitative $^{13}NH_3$ PET data (stress, rest, and perfusion reserve) and coronary artery anatomy obtained with CT. The stress-induced regional reduction in hyperemic flows is observable in the territory of right coronary artery while no significant MBF reduction is seen at rest. Adapted from [Marinelli 2013].

Limitations

It has been documented that radionuclide MPI is safe, particularly in comparison with invasive procedures. Over the past three decades, SPECT and PET have dominated MPI in clinical practice on the basis of an extensive amount of research. These techniques do, however, have several important limitations, which include the occurrence of attenuation artifacts and the inability to quantify MBF using SPECT. Both techniques have the intrinsic disadvantage of requiring the use of radioactive materials which prohibits close follow-up examinations. Furthermore, the low spatial resolution of nuclear techniques limits the accuracy of the diagnostic when a differentiation between subendocardial and subepicardial ischemia is needed, which is particularly limiting when focusing on small-animal studies.

1.3.c. Contrast echocardiography

Because of its low cost and its high availability, the most commonly used technique in the clinic is echocardiography which, for instance, allows evaluating the left ventricular systolic function or valvular diseases. Nevertheless, spatial resolution and variable patient's echogenicity, the ability of a tissue to reflect ultrasound, are restricting factors for this modality. Also, not all views of the heart are available due to the limiting incidence of the ultrasound beam. Echocardiography is characterized by a fast image acquisition so that ECG-gating with such technique is mostly unnecessary.

The evaluation and quantification of myocardial perfusion is an exciting application for myocardial contrast echocardiography (MCE). This technique is based on ultrasound-induced destruction of microbubbles. If microbubbles are administered as a continuous venous infusion, then their destruction within the myocardium and measurement of their myocardial reappearance

rate at steady-state provides a measure of mean myocardial microbubble velocity. Conversely, the measurement of their myocardial concentration at steady-state will provide an assessment of microvascular cross-sectional area. MBF can then be calculated from the product of the two quantities *[Wei 1998]*. A recent study proposed a direct comparison between MCE and the PET ^{15}O reference technique *[Dijkmans 2006]*. Although the authors found a significant correlation between both measurements, MBF quantification was more heterogeneous in the group of healthy subjects using MCE which might hamper the use of this technique in clinical routine. Although the general advantages of echocardiography include absence of radiation, wide availability and easy-performance, the major disadvantages of the technique are operator dependency, lack of reproducibility and technical difficulties to obtain good quality images in patients with high thoracic impedance.

1.3.d.   Gadolinium-based MRI

In the field of MRI, most people associate the concept of perfusion imaging with first-pass MRI, or dynamic contrast-enhanced MRI (DCE-MRI) as it is often called in the field of cardiovascular MRI. Such techniques rely on dynamic imaging of the first-pass signal changes in the myocardium after injection of a fast bolus of a CA causing alteration of regional tissue magnetic properties.

A complete description of these techniques goes far beyond the scope of this thesis. Although there is no standardized technical approach, most studies rely on saturation- or inversion-prepared T_1-weighted sequences to create images whose contrast enhances with the passage of gadolinium CA into the coronary bed, resulting in brightening of the myocardium compared with precontrast images. An advantage of 1st pass MRI techniques is the high amount of contrast change that is induced by the CA, making them relatively sensitive. The main issue in the design of MRI perfusion sequences is to find the best compromise between spatial and temporal resolution, acquisition time, and SNR. Several groups provided evidence that balanced steady-state-free-precession (bSSFP) sequences are superior to gradient echo techniques from the standpoint of image quality, spatial resolution, SNR and sensitivity to flow artifacts *[Schreiber 2002, Hunold 2004, Gebker 2005, Wang 2005]*. Consequently, bSSFP has become the standard MR perfusion sequence in most research and clinical trials focusing on human MBF.

An in-plane resolution of 2-3 mm allows separate visualization of the endo- and epicardial layers of the left ventricle. The consequences of an insufficient spatial resolution for the detection of small subendocardial infarcts are highlighted in Figure 1.13. Some studies showed that MRI perfusion imaging can identify regional reductions in MBF over a wider range than SPECT imaging *[Lee 2004, Schwitter 2008]*. Furthermore, direct comparison of 1st pass MRI versus SPECT for the detection of CAD demonstrated superiority of the MRI approach *[Ishida 2003, Schwitter 2012, 2013]*.

In addition to a visual inspection of the extent of the diseased tissue, various perfusion-related parameters for the distinction of ischemic and non-ischemic myocardial segments have been evaluated *[Gebker 2007]*. As an example, an index of the perfusion reserve can be calculated from the myocardial upslopes during stress and rest 1st pass MRI *[Al-Saadi 2003]*.
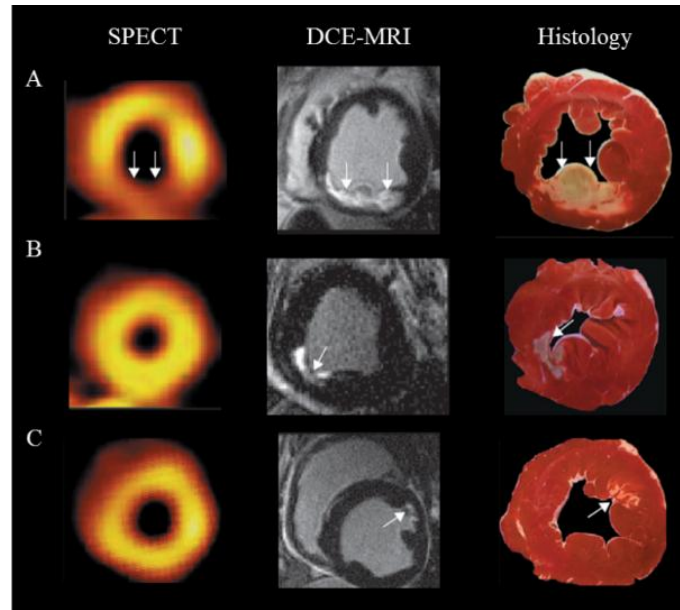
Figure 1.13 – Comparison of SPECT, DCE-MRI, and histology in three dogs. (A) When a transmural infarct is present, the spatial extent of the infarcted tissue is clearly delineated with both imaging techniques. (B and C) When a subendocardial infarct is present, the small subtle changes in myocardial perfusion is only visible using MRI due to the low spatial resolution of SPECT images. Adapted from [Wagner 2003].

Absolute MBF quantification

For absolute quantification with 1st pass MRI, additional requirements need to be met. It relies on measuring the rate at which the CA arrives in the myocardial tissue. As a first step, the CA concentration has to be obtained from the image contrast. By measuring T_1 in a homogeneous voxel, one can obtain an indirect measure of the contrast-concentration ratio. Quantitative analysis methods rely on time-intensity curves from the first pass of gadolinium through the tissue. It is measured from regions of interest (ROIs) in the myocardium, whereas the arterial input function (AIF) needed for quantification is obtained in the LV blood pool (Figure 1.14). While the use of higher doses of gadolinium is recommended for a visual assessment, lower doses are preferred to measure absolute changes in MBF *[Wilke 1995]*. Indeed, due to the non-linear relationship between contrast agent concentration and signal intensity especially at high contrast concentration, saturation of the signal occurs. If not accounted for this leads to an underestimation of the AIF peak and a resulting overestimation of MBF.

The group of Jerosch-Herold has contributed substantially to this field in the past, and already during the early studies, they have validated their approach in animal experiments by comparison with FMs *[Jerosch-Herold 2002]*. Absolute MBF (and therefore potential differences across myocardial regions and between patients) can be calculated using the mathematical process of Fermi model-constrained deconvolution *[Jerosch-Herold 1998]*.

The approaches which can be used for quantifying MBF from the observed contrast enhancement can be broadly divided in two categories, model-based and model-independent *[Jerosch-Herold 2010]*. For instance, the model-independent analysis of DCE-MRI data is based on the central volume principle, which relates the amount of tracer in a tissue region over time to the arterial input of tracer to the region.
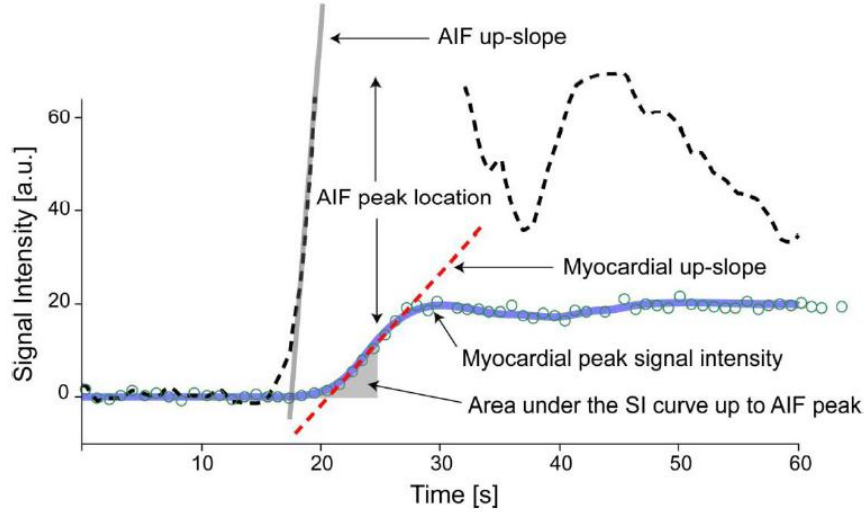
Figure 1.14 – The characteristics of myocardial contrast enhancement have been assessed in the literature using several parameters, as illustrated in this example, showing the initial intensity changes in the LV blood pool (arterial input function), and in an anterior segment of the myocardium (green circles). The blue line shows the fit to the measured data with a two-space distributed model. The dashed red line is commonly referred as the up-slope parameter, and gives the initial rate of contrast enhancement. It is often normalized by the up-slope of the AIF, as an empirical correction factor to account for hemodynamic changes between rest and stress experiments. Adapted from [Jerosch-Herold 2010].

For a single input system considered as linear and stationary, the tissue contrast agent concentration curve, $C(t)$, can be expressed as the convolution of the AIF and the tissue impulse response function, such that:

$$C(t) = MBF\left(AIF(t) \otimes R(t)\right), \qquad [1.2]$$

where $R(t)$ is the normalized impulse response function. MBF can therefore be determined by a direct deconvolution of the measured contrast agent concentration in the LV cavity, $AIF(t)$, from the measured myocardial tissue contrast agent concentration, $C(t)$.

Accurate cardiac 1st pass MR perfusion imaging, however, mandates profound knowledge of the MR acquisition details, the characteristics of paramagnetic CAs and the underlying pathophysiology of myocardial perfusion. Technical limitations of 1st pass perfusion MRI include the difficulty in the direct assessment of arterial input function (pre-bolus vs. double-contrast techniques) and the difficulty in modelling the myocardial kinetics of Gd-DTPA due to its rapid diffusion into the extracellular space. Also, the reproducibility of MBF quantification varies between intra-observer, inter-observer, and inter-study comparisons, mainly due to the use of a bolus injection and the relatively complex post-processing for absolute quantification *[Larghat 2013]*.

Some studies have directly correlated the MRI-derived flow with quantitative PET data from human subjects. One study compared ^{13}N PET and MRI, revealing a good correlation between the number of pathological segments per patient and high accuracy when implementing PET as reference *[Schwitter 2000]*. Miller *et al.* recently proposed to evaluate the effect of common methodological differences in cardiovascular MRI voxel-wise measurement of MBF using PET

as an external validation *[Miller 2014]*. An article reviews the currently available evidence on the use of both PET and CMR for MBF and MPR quantification, with a particular attention to the studies that directly compared these two diagnostic methods *[Bratis 2013]*.

Small-animal studies

Due to the high heart rate, 1st pass MRI has always been a challenge in small-animal studies. Quantification requires a good linearity between intensity and Gd concentration and a good sampling of the time-intensity curve, i.e. sufficient temporal and spatial resolution. Nonetheless, as in human studies, 1st pass bolus tracking techniques took advantage of new advances in MR technology. In the past years, two groups have independently reported successful myocardial 1st pass perfusion measurements in mice using *k-t*-acceleration or accelerated parallel detection *[Coolen 2010, Makowski 2010]*, thereby implicitly demonstrating the usefulness of *k*-space-accelerated acquisition for small-animal MRI. Particular efforts were made regarding absolute quantification of MBF. Makowski et al. introduced a *k-t*-SENSE technique for rodent MBF measurements on a clinical 3T scanner *[Makowski 2010]*. DCE-MRI was performed based on a saturation recovery spoiled gradient-echo method with 10-fold *k*-space and time domain undersampling. Fermi-function deconvolution of the image signal dynamics was then used to quantify regional MBF in healthy and infarcted myocardium. The same group later validated the technique in healthy mice by comparison with FMs at rest and during dipyridamole-induced vasodilator stress *[Jogiya 2013]*. There was good agreement between MRI and microsphere evaluation of the myocardial perfusion reserve with no significant difference between both techniques. This study demonstrated that 1st pass myocardial stress perfusion MRI is feasible in a mouse model with a 3T clinical system. In parallel, Coolen *et al.* proposed another approach to perform DCE-MRI in mice using a four-element detection coil and GRAPPA *k*-space acceleration allowing for semi-quantitative assessment of the myocardial perfusion status *[Coolen 2010]*. In order to perform absolute MBF quantification, the technique was enhanced using a dual-bolus approach and Fermi-constrained deconvolution of the myocardial tissue response *[van Nierop 2013]*. The low-dose prebolus was added to the original technique to keep the linearity of signal intensity in the left-ventricular lumen so as to reconstruct a non-saturated arterial input function necessary for absolute quantification. In a cohort of healthy mice, the authors assessed regional perfusion values in four segments and proved that the technique was repeatable within one week interval. Perfusion values were found to be comparable with previously reported studies. For both techniques presented here, however, only regional perfusion assessment was performed but no perfusion maps were presented, likely due to noise domination when performing pixel-wise analysis of first-pass perfusion data.

1.3.e.   Arterial spin labeling MRI

Arterial spin labeling (ASL) is an alternative perfusion MRI technique. Since it is the main subject of this thesis work, ASL will be introduced, reviewed and discussed in the next section.

1.3.f.   Summary

By using standard qualitative methods, evaluation of perfusion imaging assumes that the segment with the highest perfusion signal is normal, although that segment itself might be under-perfused in absolute terms. In multiple-vessels disease, for instance, the coronary flow reserve may be abnormal in all territories; thereby identifying segments with lesser degree of ischemia using

absolute flow quantification would help better define the true extent of ischemia and disease burden. Likewise, diagnosis and follow-up of non-ischemic pathologies with microvascular alterations, such as those associated with diabetes, would substantially benefit from a quantitative assessment. Fast and reproducible calculation of myocardial blood flow is thus of major importance in clinical practice.

The following table summarizes the advantages and drawbacks associated with these different imaging modalities for the assessment of myocardial perfusion.

Table 1.3 – Summary of existing techniques for myocardial perfusion imaging.

	Invasive	Spatial resolution	Temporal resolution	Absolute quantification	Reproducibility
FM	+ + +	+ + +	∅	+ + +	+ +
SPECT	+ +	-	- -	-	+
PET	+ +	-	+	+ +	+
MCE	+	+	+ +	+	- -
1st pass MRI	+	+ +	+	+	-

PET MPI seems the most appropriate technique to study myocardial perfusion, but the exposure of the subjects to a radioactive tracer and the low spatial resolution make this technique only suitable for diagnosis of more severe pathologies. MRI is superior to other imaging modalities in terms of spatial and temporal resolution, and the main advantages are good sensitivity and the ability to access blood volume and flow at the same time. Yet, one limitation is that the bolus injection makes it invasive, and the complexity and variety of modelling approaches hampers the production of commonly accepted normal values.

Another approach, which is the focus of our research, is ASL. This approach has emerged as a completely non-invasive method and consists in using magnetically labeled blood as an endogenous tracer. Quantification of perfusion using this method is comparatively simple because the arterial input function is well known and because no knowledge of a concentration-contrast relation is required. The main advantage of ASL is that no injection is required to assess myocardial perfusion so that the measurement can be performed repeatedly. Also, absolute quantification is relatively precise and simple as compared to 1st pass MRI. Some of the major drawbacks include the inability to measure regional blood volume while using the existing techniques, as well as the relatively low sensitivity requiring longer acquisition time, especially in the cardiac context.

1.4. Perfusion Assessment using Arterial Spin Labeling

The perfusion quantification techniques presented so far involve the use of exogenous CAs such as Gd-DTPA for 1st pass MRI. In a similar way, one can also use magnetically labeled endogenous blood water as a tracer for perfusion MRI. The principles behind ASL are quite similar to techniques utilizing exogenous tracers, except that ASL is completely non-invasive. Non-invasive is to be understood in the sense that no injection is needed, but also in the sense that MRI is a non-ionizing imaging technique, which can thus be repeated without limitations. These benefits make ASL very suitable for perfusion studies in healthy individuals, patients with renal insufficiency (who do not tolerate CA injection) and those who need repetitive follow-ups. Another advantage of ASL as compared with conventional bolus-tracking MRI techniques is that the quantification of perfusion with ASL is relatively easy and does not rely on bolus injection dynamics. Absolute perfusion quantification allows recognition of global and regional hypo- or hyper-perfusion states and also permits comparisons between multiple measurements in a longitudinal study.

In order to interpret ASL perfusion studies that have been developed during this thesis, basic knowledge about ASL techniques, pitfalls and limitations is important. This section first provides a historic review of ASL and physical principles underlying the technique, followed by a description of different labeling modules that have been developed in the past. The second part specifically addresses myocardial ASL in terms of organ specificity, validation of ASL techniques in the heart and recent developments in both clinical and pre-clinical studies.

1.4.a. Origins and principles

ASL perfusion MRI was conceived about 20 years ago with the first method for labeling arterial water spins *[Detre 1992, Williams 1992]*. In 1992 these authors published rat brain cerebral blood flow measurements using water as a freely diffusible tracer. Two years later, Detre *et al.* extended the application of ASL to human brain studies at 1.5T *[Detre 1994]*. Since then the technique has been mostly used in research, but recent refinements in sequence robustness, decreased acquisition time, increased image resolution and lesser artifacts have made ASL available for routine clinical practice, especially in brain disease studies.

The strategy of ASL perfusion MRI is to produce a flow-labeled image (also called 'tag' image) by modifying the magnetization of blood inflowing into the imaging slice, and to compare this image to one which upstream blood magnetization has not been modified. First, arterial blood water is magnetically labeled upstream the region of interest by applying a saturation or an inversion RF pulse (Figure 1.15). The result of this pulse is an alteration of the net magnetization of the blood water. The labeled water flows into the slice of interest and the labeled spins within the blood alter total tissue magnetization by a magnetization exchange between both compartments. The tag image is acquired after a certain amount of time known as the inversion time (TI). The experiment is then repeated without labeling the arterial blood to create a reference image, called the 'control' image. Finally, the control and tag images are subtracted to produce a perfusion-weighted image which reflects the amount of arterial blood delivered to each voxel of the slice during TI. Because the longitudinal relaxation is quite fast, only a small amount of labeled water accumulates in the tissue. The subtle magnetization difference between tag and

control images ΔM can be modeled to derive a calculated blood flow image showing absolute perfusion in mL g^{-1} min^{-1} at each voxel.
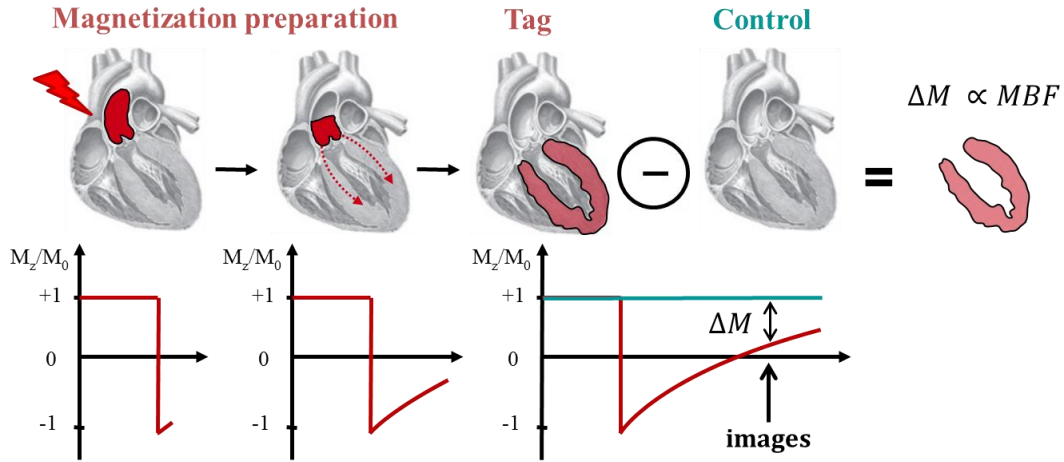
Figure 1.15 – Basic principle of arterial spin labeling. Arterial blood water is magnetically labeled using a radiofrequency pulse upstream the region of interest. The labeled blood flows into the tissue while T₁ relaxation occurs (red curve). Once the labeled blood has reached the microvascular compartment, the tag image is acquired. The same image is acquired without labeling the arterial blood (control image, blue curve). Finally, tag and control images are subtracted, yielding a difference signal ΔM that directly reflect quantitative local blood flow.

In the myocardium, as in the brain and other organs of the body, water is considered as freely diffusible, so that fast exchange between blood and tissue compartments can be assumed *[Detre 1992, Bauer 1996]*. When the exchange time constant is much smaller than T_1, the resulting fast exchange between blood and tissue compartments leads to rapidly homogenized magnetization. This assumption for the description of tissue magnetization is known as the single-compartment model. Diffusive water exchange is equilibrated, and the ratio of the magnetization in the two-compartments is given by the blood/tissue partition coefficient for water λ, defined as mL of water per gram of tissue / mL of water per mL of blood, such that:

$$\lambda = M_0{}^{tissue} / M_0{}^{blood} . \qquad [1.3]$$

If no labeling is applied on arterial spins, the arteries constantly feed the tissue with fresh unlabeled blood such that arterial magnetization M_a is constant and equal to $M_0{}^b$, the blood magnetization at equilibrium:

$$M_a(t) = M_0{}^b = M_0{}^{tissue} / \lambda . \qquad [1.4]$$

The fast exchange assumption implies that blood magnetization in the veins M_v is completely equilibrated with tissue magnetization M_z:

$$M_v(t) = M_z(t) / \lambda . \qquad [1.5]$$

In the imaging slice, the evolution of M_z freely relaxes towards equilibrium (M_0) in the presence of blood flow f. Tissue magnetization M_z is thus affected by incoming arterial flow ($+ f M_a$) and outgoing venous flow ($- f M_v$) and can be described by the following modified Bloch equation:

30

$$\frac{dM_z(t)}{dt} = \frac{M_0 - M_z(t)}{T_1} + fM_a(t) - fM_v(t),$$ [1.6]

where T_1 is the longitudinal relaxation time constant of free tissue protons *[Detre 1992]*. This master equation, first proposed by Detre *et al.*, constitutes the basis of all ASL techniques that have been developed during the past 20 years. The time constant governing tissue magnetization evolution is no longer only T_1 but an apparent relaxation time which depends also on blood flow:

$$T_1^{app} = \left(\frac{1}{T_1} + \frac{f}{\lambda} \right)^{-1}.$$ [1.7]

The general solution of equation [1.6] for tissue magnetization is described by a monoexponential expression:

$$M_z(t) = A e^{-t/T_1^{app}} + B,$$ [1.8]

where A is an integration constant that has to be determined depending on the initial conditions imposed by the labeling module and B is the asymptotic value of magnetization at infinite time.

Arterial blood labeling is usually performed using a saturation RF pulse or an inversion RF pulse. Assuming that the labeling is achieved with an inversion pulse, the initial arterial magnetization at $t = 0$ will be $M_a = - M_0^b$, while if a saturation pulse is applied, the initial arterial magnetization will be null. In both cases, arterial blood will then freely relax towards equilibrium magnetization of the blood $+ M_0^b = M_0/\lambda$.

The degree of labeling β describes the efficiency of the spin labeling and is defined as:

$$\beta = \frac{M_0^b - M_a}{2M_0^b}.$$ [1.9]

For a perfect saturation, M_a is forced to 0 leading to β=0.5 while for a perfect and complete inversion, $M_a = -M_0^b$ leading to β=1.

For example, if a saturation pulse is applied on tissue magnetization, equation [1.8] will become:

$$M_z(t) = M_0 \left(1 - e^{-t/T_1^{app}} \right),$$ [1.10]

while if an inversion pulse is applied, it will become:

$$M_z(t) = M_0 \left(1 - 2e^{-t/T_1^{app}} \right).$$ [1.11]

1.4.b.   Labeling modules

Currently there are three types of ASL techniques that differ mainly by their magnetic labeling process. Continuous ASL (CASL) was the very first implementation of ASL, while pulsed ASL (PASL) and pseudo-continuous ASL (pCASL) were developed to address limitations and

technical challenges encountered with CASL. A complete description of all these labeling modules can be found in a review on brain perfusion imaging *[Barbier 2001a]*.

Continuous ASL (CASL)

With CASL techniques, the blood magnetization is continuously labeled in a narrow plane of spins, usually just below the imaging plane. The continuous labeling allows forcing tissue magnetization to reach a steady-state while for the control condition the blood magnetization is at equilibrium. The comparison of the two experiments is directly proportional to blood flow.

In the first experimental ASL setup *[Detre 1992]*, arterial labeling was performed by continuously saturating the blood before it enters in the tissue. Tissue magnetization was thus altered by incoming labeled blood and reached a steady-state M_{Tag} after a certain amount of time. The authors showed that perfusion could be quantified by:

$$ f = \frac{\lambda}{T_1^{app}} \left(1 - \frac{M_{Tag}}{M_0} \right). \qquad [1.12] $$

Shortly after, Williams *et al.* proposed to use long and continuous RF pulses (2-4s) in combination with a slice-selective gradient aligned with the flow direction to induce flow-driven adiabatic inversion *[Williams 1992]*. The spins within a physiologic range of velocities traveling perpendicular to the tagging region can be inverted by carefully adjusting the amplitudes of the gradients and the RF pulse. A continuous inversion of arterial spins produces a tissue signal change two times larger than a continuous saturation, i.e. $\beta=1$ and $\beta=0.5$, respectively. The labeling efficiency β has been determined *in vivo* by imaging the large arteries downstream the labeling plane using a flow compensated imaging technique *[Zhang 1993]*.

The continuously inverted spins provide a theoretically higher SNR than that obtained with other ASL techniques such as PASL *[Wu 2007]*. But, due to the longitudinal relaxation that occurs during the transit time from the labeling plane to the perfusion site, the inversion state of the labeled spins in the imaging slice is no longer β but:

$$ \beta(t) = \beta_0 e^{-\tau/T_1^b}. \qquad [1.13] $$

Tagging efficiency of CASL may also be influenced by variation in flow velocities, which makes the averaged inversion efficiency of CASL (80-95%) lower than that of PASL (~95%) *[Pollock 2009]*.

In addition, CASL has several drawbacks. Even if low-power RF pulse are used, the long labeling pulses induce magnetization transfer (MT) effects *[Petersen 2006]* and cause large amount of RF energy deposition in the subject, resulting in a higher specific absorption rate (SAR) than other ASL approaches *[Detre 2009]*. MT effects can be compensated by applying a distal labeling during the control experiment. This induces identical saturation effects in both experiments that are canceled afterward by the subtraction. Nonetheless, such strategy is only valid for single slice acquisition, because the control RF pulse is applied symmetrically to the imaging slice causing MT effects to be slice-position dependent. Other strategies have been proposed to compensate for MT effects, like the double adiabatic inversion *[Alsop 1998]* or the simultaneously proximal and distal RF irradiation method *[Talagala 1998]*.

In 1994, Edelman *et al.* proposed the first pulsed ASL scheme as an alternative to the existing CASL techniques *[Edelman 1994]*. Instead of labeling blood as it flows through a plane, the first PASL techniques used short RF pulses (5 to 20 ms) to saturate or invert a thick slab (10-15 cm) of blood volume. Adiabatic pulses are generally used to obtain a homogeneous inversion across the slab, independent of magnetic field inhomogeneities. For PASL sequences, MT effects have to be considered as well, although these are much smaller compared with CASL. In the first PASL version with an 'echo-planar MR imaging and signal targeting radio frequency' (EPISTAR) sequence, inversion was performed distal to the imaging slice during the control experiment to induce identical MT effects in both cases. Shortly afterwards, an alternative to this symmetric method of labeling was proposed by Kwong *et al. [Kwong 1995]* and independently published by Kim, who named it 'flow-sensitive alternating inversion recovery' (FAIR) *[Kim 1995]*. In this approach, the label is applied using a non-selective inversion pulse, while the control employs a concomitant slice-selective gradient pulse. The symmetric nature of this sequence automatically compensates for MT effects, assuming the same RF power is used in both cases. Various kind of tagging methods have been developed that differ in the location of the labeling plane and the choice of magnetically labeled state of blood for control and labeled images. For most PASL techniques, the tagging efficiency is greater than 95% *[Wong 2005]*.

Pseudo-continuous ASL (pCASL)

Pseudo-continuous ASL (pCASL) has been introduced to match the inversion efficiency of CASL while having an intrinsically symmetric tag/control situation *[Wu 2007]*. First developed by Dai *et al.*, this technique employs a train of discrete RF pulses together with a gradient wave applied between two consecutive RF pulses to mimic CASL's flow-driven adiabatic inversion method *[Dai 2008]*. The pCASL labeling scheme provides less RF power deposition and MT effects compared to CASL without need of special hardware. pCASL has initially been developed for brain perfusion studies, as most of CASL and PASL strategies, but has also been recently applied to the mouse kidney *[Duhamel 2013]*, the human calf muscle *[Grözinger 2013]* and for human kidney and retina blood flow mapping experiments *[Park 2013]*.

In conclusion, the ease of implementation and reduced practical problems as compared with CASL have made PASL and pCASL popular choices for perfusion imaging studies in both clinical and pre-clinical practices. Potential problems with ASL methods are unwanted MT effects in the slice of interest due to the off-resonance inversion pulse, incomplete inversion of the arterial blood, relaxation during the transit from the inversion region to the slice, and signal contribution from large vessels *[Buxton 1998]*. When these effects are taken into account, ASL methods can provide a precise quantitative measurement of local perfusion in multiple organs.

1.4.c.   Myocardial ASL

Since the heart is an organ in perpetual motion, both blood labeling and image acquisition have to be synchronized to the ECG. Combined with respiratory motion, such constraints involve the use of fast imaging techniques, induce timing restrictions and increase the level of complexity for implementing an ASL technique in the heart.

One year after the first implementation in the brain, ASL has been employed to measure quantitatively perfusion in the isolated perfused rat heart *[Williams 1993]*. In this work, the authors also demonstrated the fact that T_1^{app} effectively depends on blood flow. Using CASL, the same limitations as those observed in the brain were found in the heart, i.e. a non-optimal labeling efficiency due to transit time and large MT effects. The flow-driven adiabatic inversion used in CASL and pCASL labels blood in a certain range of velocities. The high pulsatility of coronary flow irrigating the myocardium makes the use of such strategies virtually impossible in the heart. Hence, PASL using the FAIR labeling scheme has then been proposed as an alternative to study isolated rodent heart models *[Reeder 1996, Bauer 1997]*. Since the first *in vivo* experiment *[Belle 1998]*, the FAIR labeling scheme has dominated the development and usage of cardiac ASL.

As presented in the first section of this chapter, the heart has a complex geometry such that the tissue of interest, the myocardium, is surrounded by blood in both right and left ventricles as well as in the atria. ASL techniques rely on arterial blood labeling that has to exchange magnetization with the tissue of interest. The magnetization difference build-up between tag and control tissue magnetizations (ΔM) is low and far below the magnetization difference created in the blood itself. With FAIR tagging for instance, the difference signal in the LV blood pool is typically 30 to 40 times higher than the adjacent myocardium *[Epstein 2011]*. When the spatial resolution is insufficient, this large signal difference between LV blood and proximal tissue can significantly contaminate the ASL signal created in the myocardium.

ASL in the human myocardium, for instance, generates difference signals between tag and control images of only a few percent *[Zun 2009a]*. Acquiring reliable perfusion images in a short scan time is thus challenging, especially in the presence of cardiac and respiratory motion. In comparison to this, ASL in the rodent myocardium has relatively good sensitivity mainly because MBF and heart rates in rodents are roughly five times higher than in humans. Also, the magnetic fields used in rodent studies are generally strong leading to relatively long relaxation times, both directly influencing the perfusion signal $\Delta M/M$. These conditions and the fact that, for several reasons, bolus tracking is more difficult than in humans, have contributed to the success of the ASL technique when applied to the rodent heart.

The following sections present the model used for perfusion quantification and a chronological description of the major improvements published so far by differentiating small-animal from human studies.

Perfusion quantification using FAIR

In 1998, Belle and coworkers were the first to implement a FAIR ASL sequence to assess *in vivo* myocardial perfusion *[Belle 1998]*. The principle of this technique was based on the acquisition of two spatially resolved quantitative T_1 maps by means of an inversion recovery (IR) snapshot fast low-angle shot (FLASH) sequence *[Haase 1990]*. As shown in Figure 1.16, one T_1 map was obtained with a slice-selective inversion pulse (T_1^{sl}) and one with a global inversion pulse (T_1^{gl}). This work constitutes the foundation of all cardiac ASL studies that have been published subsequently. The major difficulty encountered is related to the very small difference between

T_1^{sl} and T_1^{gl} values, which imply the need for good SNR and strong accuracy in the determination of the T_1 maps are required, especially in the cardiac context.
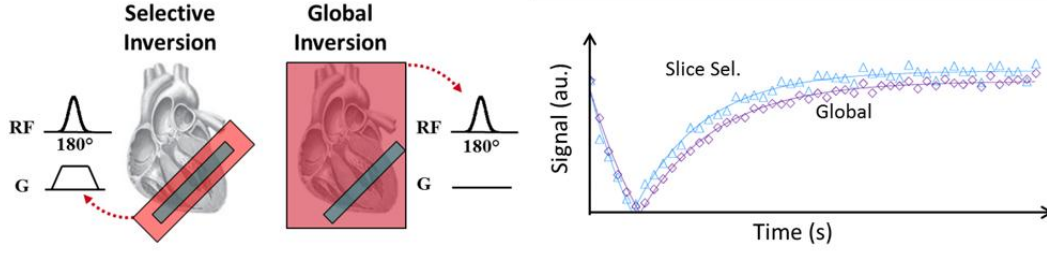

Figure 1.16 – Principle of the FAIR ASL sequence to assess myocardial perfusion. Two inversion recovery sequences are acquired following slice-selective and global inversions. The sampling of the T_1 recovery curves allows to quantify perfusion using equation [1.17].

Two years before, the same group proposed a model describing the effect of perfusion on longitudinal relaxation time in tissue *[Bauer 1996]*. This model was then adapted to the selective versus nonselective method, in which tissue is described as a two-compartment model, the intravascular capillary blood and the extravascular tissue. The model considers the effect of the superposition of two transport processes on relaxation enhancement: diffusion-exchange of nuclear spins between both compartments and perfusion that permanently transfers spins from the arterial system to the capillary space. Both compartments are characterized by their own longitudinal nuclear magnetization, governed by their intrinsic relaxation time and with exchange rates of water molecules from capillary space to extravascular tissue and reciprocally. From this complex two-compartment model, it can be shown that tissue magnetization $M_z(t)$ behaves like a biexponential function. Experimentally, the difference between a biexponential and a monoexponential relaxation behavior is in general not observable and $M_z(t)$ can therefore be approximated using equation [1.8], $M_z(t) = \mathrm{A}e^{-t/T_1^{app}} + B$.

The time course of the arterial magnetization $M_a(t)$ gives the arterial input function for tissue magnetization and depends on the T_1 experiment carried out, i.e. the spatial range of the inversion pulse. For the slice-selective inversion, only the spins within the slice of interest are inverted, and the magnetization of the inflowing arterial spins is therefore at equilibrium, $M_a(t) = M_0^b$. Thus, tissue magnetization freely relaxes towards equilibrium under the influence of perfusion of fresh unlabeled blood and solving equation [1.6] gives:

$$T_1^{sl} = T_1^{app} = \left(\frac{1}{T_1} + \frac{f}{\lambda} \right)^{-1}. \tag{1.14}$$

For the global inversion, the magnetization of the entire object is inverted, and the input function is:

$$M_a(t) = M_0^b \left(1 - 2e^{-t/T_1^b} \right). \tag{1.15}$$

Solving equation [1.6] and taking into account that approximation of the fast exchange between intracapillary and extravascular space may be assumed *[Bauer 1997]* leads to:

$$T_1^{gl} = \left(\frac{\dfrac{1}{T_1} + \dfrac{f}{\lambda}}{1 + \dfrac{fT_1^b}{\lambda}} \right)^{-1} , \qquad\qquad [1.16]$$

with T_1 the relaxation time of free tissue protons in the absence of perfusion. T_1 remains unknown since *in vivo*, static tissue spins do not exists without the influence of perfusion.

Combining equations [1.14] and [1.16] allows eliminating the unknown T_1 and yields the following master equation for absolute perfusion quantification:

$$\frac{f}{\lambda} = \frac{1}{T_1^b} \left(\frac{T_1^{gl}}{T_1^{sl}} - 1 \right) . \qquad\qquad [1.17]$$

As T_1^b can be easily measured from the T_1^{gl} map in the LV blood pool, the acquisition and reconstruction of slice-selective and global inversion T_1 maps provide the calculation of perfusion maps.

Rodent myocardial ASL

FAIR ASL in the rodent heart was first acquired using an ECG-gated snapshot-FLASH Look-Locker type readout sequence *[Belle 1998]*. In a cardiac context, snapshot means that an entire image is acquired per cardiac cycle and the temporal resolution is thus limited by the heart rate of the animal. To improve the temporal resolution and therefore the accuracy of T_1 measurements, two successive ECG-gated experiments were acquired with two different delays between the first ECG signal and the inversion pulse, allowing to double the number of points useful for the fit of the T_1 recovery curve (Figure 1.17). However, this also resulted in an inversion that did not occur during the same cardiac phase as the readout.
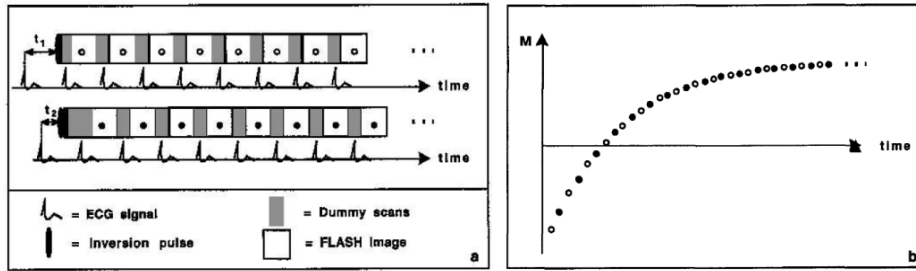
Figure 1.17 – Schematic diagram of T_1 determination with the ECG-gated IR snapshot FLASH sequence. (A) The sequence is performed two times with two different delays (t1 and t2). After the inversion pulse, a train of α RF pulses is applied. (B) Interleaving the images coming from both experiments leads to the determination of T_1 relaxation curve with a temporal resolution smaller than the heart rate. Adapted from [Belle 1998].

As presented in Figure 1.18, spatially resolved T_1 and MBF maps were calculated from images acquired in two IR snapshot-FLASH experiments with a total scan time of around 5 minutes. This calculation was based on a three-parameter least-square fit. The effects of saturation coming from the application of RF pulses trains to the spin system were corrected using the ratio of signal intensities of the first and the last image acquired in the Look-Locker train *[Deichmann 1992]*.
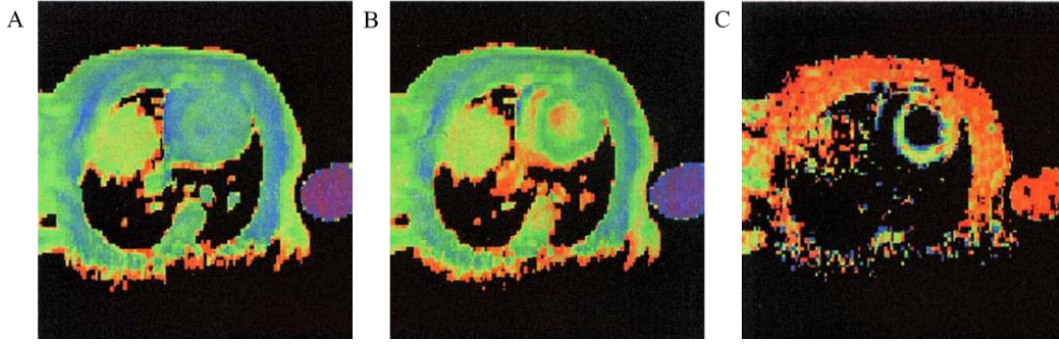
Figure 1.18 – T1 perfusion maps obtained with IR snapshot-FLASH from a rat at rest: (A) Global inversion T1 map, (B) slice-selective inversion T1 map, and (C) perfusion map. Adapted from [Belle 1998].

The IR snapshot-FLASH experiment was validated afterwards by the same group against the colored fluorescent microsphere technique in healthy rats, at rest and during adenosine-induced stress *[Waller 2000, 2001]*. The studies showed a good correlation between ASL and FM demonstrating that quantitative mapping of perfusion could be performed non-invasively by means of MRI in healthy animals.

An alternative to the FAIR snapshot-FLASH sequence has been proposed to counteract the spatial resolution limitation induced by the high heart rate of small animals *[Kober 2004]*. In this work, an ECG-gated IR gradient-echo technique with synchronization to the respiration of the animal was used to acquire T_1 maps, again using a Look-Locker type acquisition. ASL was still performed using the FAIR labeling scheme but in this approach, only one phase-encoding (PE) step per inversion pulse was acquired at each cardiac-cycle. The inversion pulse (global or slice-selective) and acquisition of one set of FLASH GEs was ECG-gated and triggered after a completed respiratory cycle (Figure 1.19). A series of 32 GEs was acquired after each inversion pulse followed by 3s of recovery delay to ensure full relaxation of the magnetization between two inversion pulses. The IR measurement was repeated for each PE step. Providing that the respiration is regular, only some images on the IR curve are submitted to respiratory movement artifacts. These images can then be easily excluded from the IR fitting algorithm. The in-plane spatial resolution achieved with this sequence was 234 x 468 μm² corresponding to 64 PE steps with 128 points per echo. At a mean heart rate of 350 bpm, this led to a total measurement time of about 25 min.

During IR measurements, the rapid repetition of small flip-angle excitation pulses causes the magnetization to be partially saturated. As a consequence, an apparent relaxation time T_1^* is observed, which is shorter than the actual T_1, and must be appropriately corrected. After the series of images were reconstructed, T_1^* maps were calculated by least-squares fitting the function $M\left(TI_n\right) = M_0^*(1 - 2e^{-TI_n/T_1^*})$ pixel-by-pixel. M_0^* is the magnetization under partial saturation and TI_n represents the TI of the nth image of the series. The TI_n values were obtained as an average of the measured TIs over all PE steps.
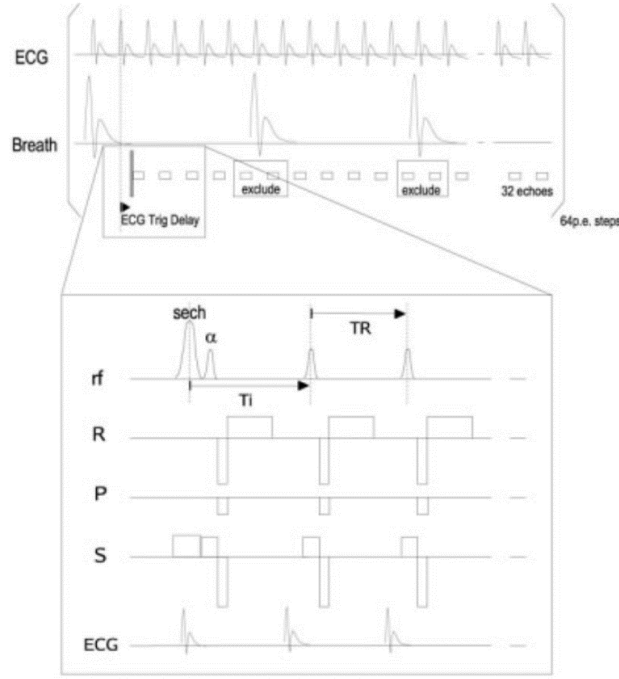
Figure 1.19 – IR gradient-echo pulse sequence used to acquire T_1 maps. The inversion pulse and the acquisition of one set of gradient-echoes are triggered after a completed respiration cycle. This series is repeated for each phase-encoding step. The experiment is performed with both slice-selective and global inversions. Images acquired during respiratory movements are excluded from least-squares fitting in postprocessing. Adapted from [Kober 2004].

For the saturation correction, the exact flip angle α was determined at each experiment by using a sample of a known T_1 value. For this purpose, the apparent T_1^* value in the reference vial was evaluated on the T_1^* map, and the flip angle was derived from the relation:

$$\frac{1}{T_1^*} = \frac{1}{T_1} - \frac{\ln(\cos\alpha)}{TR}, \qquad\qquad [1.18]$$

between true reference T_1 in a sample and T_1^* measured under partially saturated conditions *[Deichmann 1992]*. The corrected T_1 maps were obtained by applying the above saturation correction with the determined flip angle and repetition time TR to the T_1^* maps.

It was assumed that ventricular blood is nearly completely exchanged between two excitation pulses (i.e. two cardiac contractions), and that the saturation of LV blood magnetization could be neglected such that no saturation correction was necessary for the T_1^b determination in the LV cavity. Perfusion maps were finally computed using equation [1.17].

All small-animal myocardial ASL studies published so far made use of FAIR as labeling technique combined with a Look-Locker (LL) gradient echo readout *[Look 1970]*. To distinguish between the first proposed snapshot-FLASH experiments which also used a LL readout and the fully segmented FAIR technique suggested afterwards, the latter was given the acronym LLFAIRGE for 'Look-Locker FAIR gradient-echo' in subsequent studies.

Although this segmented single gradient echo readout scheme entails a relatively long experiment time of 25 minutes, the LLFAIRGE approach has major advantages over the first proposed IR snapshot-FLASH:

- On the scale of the RR-interval, the acquisition time per echo is small. This excludes the risk of errors due to through-plane movement of the myocardium.
- The spatially selective RF inversion labeling pulse and the image RF excitation pulse were both gated to the same phase of the cardiac cycle so as to ensure that both pulses excite the same volume of the heart.
- Small rodents have high heart rates, which allows for the short TR needed for a high density sample of the T_1 recovery curve and a precise T_1 measurement.
- At the expense of long measurement time, high spatial resolution can be achieved even at very high heart rates. It allowed an accurate separation of myocardium and ventricular blood and leads to reduction of partial volume effects at the borders of the myocardium (Figure 1.20).
- A longer excitation pulse than that used in IR snapshot-FLASH can be used, because the timing of the acquisition of one GE within one heart cycle is not critical.
- The animal can be left under spontaneous respiration conditions, while for all previous studies animals were ventilated throughout the imaging procedure. It is preferable to have freely breathing animals for both physiological and technical reasons.
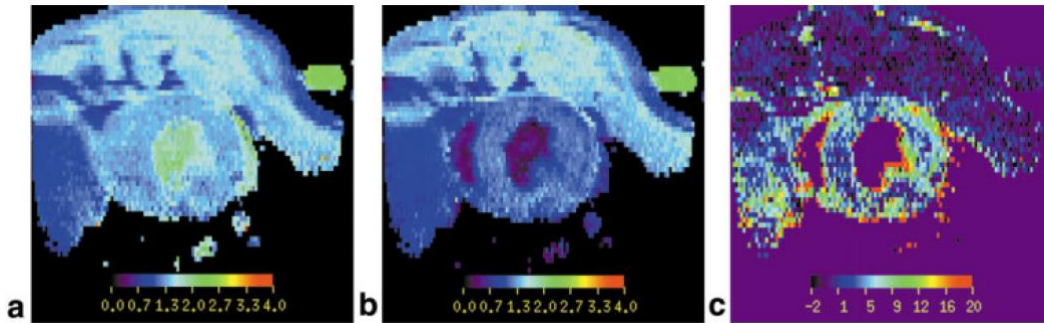
Figure 1.20 – T_1 perfusion maps obtained with LLFAIRGE from a rat at rest: (A) Global inversion T_1 map, (B) slice-selective inversion T_1 map, and (C) perfusion map. The color bar scale is given in seconds for the T_1 maps, and in mL g^{-1} min^{-1} for the perfusion map. Perfusion values above 20 mL g^{-1} min^{-1} and below -2 mL g^{-1} min^{-1} were masked in the perfusion map in order to suppress blood flow in large vessels and cavities. Adapted from [Kober 2004].

The LLFAIRGE technique has been used in a variety of protocols afterwards. For example it has been used to assess the influence of anesthetics commonly used in small-animal studies such as Ketamine/Xylazine, pentobarbital, or isoflurane *[Iltis 2005b, Kober 2005]*. It has been shown that, compared to other anesthetics, high-dose isoflurane anesthesia (~2%) induces vasodilation and increases MBF. This technique has also been used in two different diabetic rat models, showing that cardiac function and myocardial perfusion were affected by Type II diabetes *[Iltis 2005a, 2005c]*. Several other studies made use of the LLFAIRGE technique in cardiovascular disease models *[Vandsburger 2007, Merabet 2012, Zhang 2012, Caudron 2013]*.

The feasibility of adenosine-induced stress along with reasonable perfusion reserve values has been shown in rats under isoflurane anesthesia *[Jacquier 2011]*. In this work, results were also

confronted to microsphere MBF measurements validating the LLFAIRGE approach and stability against heart-rate variations during acquisition.

Recent improvements

More recently, the FAIR Look-Locker acquisition technique has been improved by Vandsburger *et al.* who have used fuzzy C-means clustering for a more accurate calculation of inversion times in a context of heart rate variations during acquisition *[Vandsburger 2010]*. The authors also used an interleaved spiral acquisition for readout, replacing the previously used Cartesian readout. Alike all radial approaches, this has the advantage that all signals contributing to the final image represent an equally weighted portion of *k*-space. The regional delineation of MBF maps obtained from mice with coronary occlusion was found more accurate when heart rate variations were taken into account. As a drawback, the acquisition time became again longer with this technique (50 minutes).

A modified version using segmented *k*-space acquisition has been implemented to acquire a single-slice MBF map with high spatial resolution (200 x 200 μm² in plane) with reduced acquisition time of 15 minutes *[Campbell-Washburn 2012]*. A data logger was also introduced to improve data quality by allowing automatic rejection of respiratory-corrupted images and by providing additional prospective gating to improve consistency of acquisition timing in case of missed ECG peaks. In addition, repeatability and reproducibility of myocardial perfusion measurements with ASL was tested. The 4-fold *k*-space segmentation has therefore accelerated the acquisition considerably, although loss of some image quality can be observed compared with previous studies.

The same authors also proposed the first attempt to perform multi-slice ASL in the mouse heart *[Campbell-Washburn 2013]*. Multi-slice acquisition combined with a pulsed ASL technique is not straightforward and has always been a challenge for the ASL community in terms of absolute MBF quantification. Partial saturation of imaging slices as well as the labeled blood input function have to be taken into consideration in the mathematical model based on the modified Bloch equations. *In vivo* experiments in mice were performed, and up to three slices could be obtained within 15 minutes when acquiring four *k*-space lines per heart-beat. Based on their simulations, the authors also showed that perfusion estimation using this method is robust against changes of the slice-selective inversion thickness, although MBF values obtained in mice seemed to overestimate perfusion compared to the reference single-slice technique.

Human myocardial ASL

As previously mentioned, myocardial ASL has been successful in small-animals where SNR is high mainly due to the relatively high blood flow and the strong magnetic fields. Rodent heart rates are high enabling apparent T_1 mapping to be performed accurately, i.e. the T_1 recovery curve can be sampled at many time points in a stable cardiac phase. In contrast, the development of human myocardial ASL is still at an early stage. Again, all previous studies used the FAIR labeling scheme and differ in the models used for quantification and the methods used for breathing control and image acquisition.

Poncelet *et al.* proposed to quantify myocardial perfusion based on a double-gated FAIR labeling and EPI readout sequence *[Poncelet 1999]*. In this study, the labeling inversion pulse and the image excitation pulse were both gated to the same phase of the cardiac cycle in consecutive heart

beats to maximize the signal difference ΔM and to ensure that both pulses excite the same volume. Images were acquired using a single TI corresponding to one heart beat that was repeated 46 times for each selective/non-selective pair. The quantification model was derived from the Bloch equation and requires a T_1 quantification to be fully quantitative. TIs of the 92 IR experiments were recorded for every acquired image and heart rate variations were used as an advantage to spread data along the T_1 recovery curve. In addition, 6 images at short TI (60 msec) and 6 images with no inversion were acquired to sample the beginning and the end of the recovery curve. This resulted in 108 image acquisitions for a total scan duration of 10-12 min. A data fitting procedure was then used to extrapolate the ASL signal from data acquired with different TIs.

Experiments were first performed on pigs and compared to the FM quantification at rest and during hyperemic stress. A good correlation was found between both techniques but a systematic underestimation of blood flow was obtained with ASL. The authors discussed that acquisitions were corrupted by noise coming mainly from respiration. The low SNR obtained with this technique has limited their ability to measure resting state fluctuation quantitatively in both pigs and humans. Here, the EPI readout was chosen because compared to FLASH the SNR is not limited by a low flip angle. However, EPI is known to produce susceptibility artifacts in the presence of field inhomogeneity. The authors acknowledged that other types of readout modules would have helped in reducing the noise level of their technique (>40% of the measured MBF in this study).

An *et al.* employed a similar quantification model using FAIR labeling and SSFP image acquisition *[An 2005]*. Experiments were for the first time performed at 3 Tesla which, in principle, gains from longer T_1 and increased SNR compared to 1.5T. The SSFP readout used here at 3T, however, caused additional problems such as banding artefacts induced by off-resonance. The authors concluded that these problems had to be eliminated before the SSFP ASL myocardial perfusion can be used at this field strength.

The FAIR gradient echo sequence was implemented on a 1.5T Siemens whole-body scanner for human studies *[Wacker 1999]*. The sequence was slightly modified for the determination of T_1 by using a saturation recovery (SR) TurboFLASH sequence with 9 progressing recovery delays ranging from 100 to 1400 ms. The saturation pulse used here avoids the need for full relaxation between measurements, leading to reduced scan time and improved performance in the presence of irregular heart rates. Experiments were conducted on 20 volunteers at rest and during dipyridamole-induced stress. MBF within the group was 8.5 mL g^{-1} min^{-1} at rest and 13.6 mL g^{-1} min^{-1} during stress, which is far above accepted standard values from the literature. The relative perfusion variation between rest and stress conditions was estimated from the slice-selective T_1^{sl} values using $\Delta P = \Delta\left(1/T_1^{sl}\right)\lambda.$ Data showed that changes in myocardial perfusion under stress were detectable using FAIR, but the mean MBF increase of 6.4 mL g^{-1} min^{-1} obtained from these measurements was unrealistic in the human heart. The authors acknowledged that these problems arose from inaccuracies of T_1 estimations, on which the entire perfusion quantification is based. Recovery delays were too small and acquiring another data set with long recovery times (~ 4 to 5 x T_1) would have helped stabilize the T_1 fit. Increasing the number of acquisitions for averaging would have also been a solution, but none of the two were obtainable within a single breath hold.

The FAIR SR TurboFLASH sequence was consecutively implemented on a 2T Bruker whole-body scanner. Experiments were first conducted on 12 healthy volunteers and 16 patients with suspected CAD *[Wacker 2003]* and then in a pilot study on 16 healthy volunteers *[Fidler 2004a]*. In both trials, experiments were performed under resting conditions and adenosine-induced vasodilation. By studying coronary flow reserve, a defect in perfusion was clearly detectable in 7 over 11 patients with suspected CAD who underwent pharmacological stress. These studies confirmed the feasibility of myocardial ASL techniques, but the measured perfusion values were still overestimated. The authors concluded that this was mainly due to the low spatial resolution causing a contamination of myocardial signal by LV blood.

In the approaches cited above, the ASL sensitivity was too low to give reliable MBF quantification, especially at rest. In the heart, cardiac motion requires the gating of tagging and imaging during a stable cardiac phase (mid-diastole or end-systole), and limits the tag delay to an integer number of R-R intervals. While this approach was particularly suited for the fast rodent heart-rate, it appears inadequate when applied to the human heart, because sampling of the recovery curve is not sufficient with TI increments of the order of a second. Also these studies have used common MRI readout techniques such as FLASH or EPI which are known not to be SNR optimal in the heart.

More recently, human cardiac ASL at 3 Tesla has been improved in term of SNR by using FAIR tagging combined with bSSFP readout *[Zun 2009a]*. Respiratory motion is a key concern in human myocardial ASL and requires the acquisition of tagged and control image pairs to be done during the same breath-hold. To improve sensitivity, a multiple-breath-hold approach has been carried out by acquiring 6 selective/non-selective pairs. Tag and control images were acquired at a single TI corresponding to one heart beat and the 6 tag/control pair signals were averaged for quantification.

Kim *et al.* proposed a quantification model for the FAIR labeling derived from Buxton's general kinematic model *[Kim 1995]*. The difference image intensity between selective and non-selective experiments, $\Delta M(t) = M_{sl}(t) - M_{gl}(t)$, is given by:

$$\Delta M(t) = -2M_0 e^{-t/T_1^b}\left(1 - e^{-tf/\lambda}\right). \qquad [1.19]$$

Since f/λ is small ($f \approx 1$ mL g^{-1} min^{-1}), the last term can be expanded, and the equation becomes:

$$\Delta M(t) = 2M_0 \frac{f}{\lambda} t e^{-t/T_1^b} \quad . \qquad [1.20]$$

For a single TI experiment, the perfusion rate f is thus given by:

$$f = \frac{\Delta M(TI)\lambda}{2TI M_0 e^{-TI/T_1^b}} . \qquad [1.21]$$

Based on this formula, Zun *et al.* proposed to acquire an additional baseline image with no preparation to obtain M_0 and to quantify MBF using:

42

$$MBF = \frac{C-T}{2B \cdot RR \cdot e^{-RR/T_1^b}} \ ,$$

[1.22]

where C, T and B refer to the mean signal in a ROI in control (slice-selective), tag (non-selective) and baseline images. Note that in this expression TI has been replaced by RR corresponding to one heart beat and that the blood/tissue partition coefficient λ has been neglected (≈ 0.92 in the human heart *[Bergmann 1984]*).

This study focused on the feasibility of robust MBF measurements at rest in healthy subjects. It also presented an analysis of thermal and physiological noise and their impact on MBF measurement error. Physiological noise was estimated to be 3.4 times higher than thermal noise at rest. The authors concluded that myocardial ASL in humans is critically limited by SNR and strong physiological noise, primarily due to respiratory motion.

The same sequence was evaluated in the setting of clinical stress testing to detect CAD *[Zun 2011]*. The major contribution of this study is the demonstration that ASL can detect reduced perfusion reserve in ischemic segments of patients with CAD proven by angiography. The average perfusion reserve in stenotic segments measured by ASL was 1.44, which was significantly lower than an average value of 3.18 in patients without CAD. Such results indicate that myocardial ASL is capable of detecting clinically relevant increases in MBF with vasodilation and that it has the potential to identify myocardial ischemia. Although the sensitivity was increased by acquiring six separated breath-holds prior to MBF quantification, the authors concluded that cardiac ASL in humans is still dominated by physiological noise. Because the difference signal resulting from the inflow of labeled blood is so small relative to the background image intensity, even small amounts of motion during a breath-hold can corrupt the difference image. Further respiratory artifact reductions are thus necessary for a robust quantification, especially at rest.

An alternative to breath-held acquisitions has been proposed by Wang *et al.* who recently published a free-breathing, navigator-gated myocardial ASL method with non-rigid motion correction (Moco) *[Wang 2010]*. By using a navigator-echo, a single-TI acquisition could be performed 32 times (16 pairs selective/nonselective) in 5 minutes. Experiments were repeated at multiple TIs ranging from 200 and 1700 ms so as to estimate the arterial transit time (ATT) based on a kinetic model *[Wang 2002]*. In their evaluation of this method in healthy volunteers, the authors observed a reduction of subtraction errors when using Moco. In a test-retest study, an increase in reliability has also been observed when using Moco. These encouraging results suggest that similar Moco algorithm could be applied to the multiple-breath-hold approach proposed by Zun *et al.* The measured dynamic curve of labeled blood signal showed an ATT of about 400 ms in the myocardium. To date, such estimation of ATT has not been reported in the literature. ATT is a critical parameter for accurate perfusion quantification using ASL because blood transit delay variations, which could occur in CAD for instance, could reduce the accuracy of perfusion quantification if not taken into account in the mathematical model.

Recent improvements

A short time ago, the multiple-breath-hold FAIR SSFP sequence was improved by using parallel imaging and accelerating the readout module using sensitivity encoding (SENSE) *[Do 2014]*. Experiments were performed on 7 healthy subjects at rest. While in the first study the authors

hypothesized that the major contribution to physiological noise was due to respiratory motion *[Zun 2009a]*, the same authors hypothesized here that cardiac motion during the long acquisition window was the major source of physiological noise in this experiment. Introducing the 2-fold SENSE acceleration within the readout scheme allowed them to reduce the duration of the acquisition window from 307 ms to 153 ms. This lead to a 60% decrease of the physiological noise compared to the previous readout scheme at the expense of an increased thermal noise.

1.4.d.   Summary and current limitations

ASL MRI appears to be an appropriate technique to non-invasively and reliably quantify tissue blood flow. Compared with brain studies, the application of ASL methods is less efficient in the heart leading to lower sensitivity and long acquisition time, which is mainly due to respiratory and cardiac motion. However, the major challenge associated with ASL is in overcoming its inherently low sensitivity to blood flow compared to 1st pass MRI.

Rodent myocardial ASL

Cardiac ASL has been developed and successfully used in small-animals providing high-resolution MBF maps *[Belle 1998, Waller 2001, Iltis 2005, Nahrendorf 2006, Vandsburger 2007, 2010, Jacquier 2011, Campbell-Washburn 2012]*. The most widely employed ASL technique in small animal hearts is based on a Look-Locker FAIR scheme with the analysis of apparent relaxation times measured after global and slice-selective inversions (T_1^{gl} and T_1^{sl}). Acquisition of a series of full FLASH images during each cardiac cycle has been proposed in the original work on rats by Belle and coworkers (FAIR-Snapshot FLASH). In mice, *k*-space segmentation proved to be necessary to shorten the acquisition window and to cope with the high heart rate *[Streif 2005]*. However, even with k-space segmentation, the acquisition windows within the cardiac cycle can remain relatively long, thus compromising the true spatial resolution which is of major importance when a clear distinction of myocardial tissue from LV blood is needed. With the Look-Locker FAIR gradient echo (LLFAIRGE) sequence, the reduction of the acquisition window to a single gradient echo along with additional respiratory gating had therefore been developed to yield spatial resolutions matching the nominal spatial resolution *[Kober 2004]*, and was successfully applied in the mouse *[Kober 2005]*. The Look-Locker sampling strategy was shown to increase acquisition efficiency compared with classical FAIR *[Günther 2001]*; but this accurate and motion-robust approach, however, led to longer acquisition times (~ 25 minutes). Consequently, the LLFAIRGE technique bears limitations regarding acquisition efficiency and therefore might allow for scan time reductions without loss in spatial resolution and accuracy in perfusion quantification. As in many time-resolved MR studies, a compromise has to be found between short acquisition time, spatial resolution and sufficiently high SNR.

With the aim of improving sensitivity without impacting the spatial and temporal resolution of the ASL acquisition, an alternative labeling approach named steady-pulsed ASL (spASL) was developed during this thesis. Steady-pulsed labeling in the aortic root was combined with continuous cine-MRI readout. The technique was setup in mice, and we have shown that it led to better acquisition efficiency compared, for instance, with the above cited LLFAIRGE technique. This new technique is presented in Chapter 2.

Following initial experiments and validation processes of the technique and the quantification model in mice, we have used this sequence in a variety of protocols. The different experiments subsequently performed are presented in Chapter 4.

In the original LLFAIRGE implementation *[Kober 2004]*, inversion times were obtained as an average over the measured TIs for all PE steps. A long scan time associated with variable heart rates can cause inconsistencies in the TIs used for the T_1 fitting process. Independently from the development of an alternative ASL scheme, a study was carried out during the period of this thesis to improve LLFAIRGE quantification. This work was done in partnership with Johannes Tran-Gia, a PhD student from the Institute of Radiology from the University of Würzburg and is presented annexed to this manuscript. An adjustment of the model-based acceleration of parameter mapping reconstruction *[Tran-Gia 2013a]* to a LLFAIRGE acquisition has been investigated. This work brings two major improvements: (i) the ability to take into account any variations of TIs in the reconstruction and (ii) the ability to apply *k*-space undersampling for eventually reducing the total acquisition time *[Tran-Gia 2013b]*.

Human myocardial ASL

In the past, progress has been made in the field of human cardiac ASL *[Poncelet 1999, Wacker 2003, Fidler 2004a]* at 1.5 and 2 Tesla scanners showing the feasibility of this technique on the human heart. The sensitivity, however, was still too low to give reliable quantification, mainly because the approaches cited above have used common MRI readout techniques such as snapshot-FLASH or EPI. More recently, human cardiac ASL at 3 Tesla has been improved using FAIR tagging combined with SSFP readout *[Zun 2009a, 2011]*. Respiratory and cardiac motions are a key concern in human myocardial ASL, which until now has required the acquisition of tagged and control image pairs to occur during the same breath-hold. Despite all these attempts, no robust ASL methods for the measurement of human MBF have been described.

A new approach to improving this situation using an alternative pulse sequence has been developed during this thesis. After initial experiments and development of quantification model validated in the rodent heart, the so called spASL scheme has been adapted for free-breathing human myocardial ASL acquisition. This technique is presented in Chapter 3. Again, a comparison with the existing multiple-breath-hold FAIR technique has been investigated in terms of robustness and repeatability of MBF quantification. Since the initial publications (congress presentations and article in revision), the technique has been refined regarding motion correction and spatial resolution using parallel imaging. These developments are also presented in Chapter 3.

Chapter 2 - Cine-ASL: Myocardial Perfusion Mapping in Rodents

Contents

2.1. Introduction – From PASL to spASL

The Look-Locker FAIR gradient echo (LLFAIRGE) scheme has become a well-established technique to quantify myocardial blood flow in the rodent heart. This technique is, however, relatively time-consuming since sufficient spatial and temporal resolutions are required to accurately separate the endocardial border from the LV blood, whose high ASL signal would contaminate the MBF signal measured in the myocardium. Acceleration of this technique is therefore desirable, but this acceleration should neither influence the temporal or spatial resolution significantly, nor the final signal-to-noise ratio obtained in the perfusion maps. The following chapter describes an approach that allows faster measurements through an increased acquisition efficiency, in which the only drawback is a reduced accuracy in absolute quantification.

As in other PASL techniques, a main drawback of the FAIR method is the relaxation of the labeled blood state along the experiment, which leads to a vanishing perfusion signal over time after each inversion (Figure 2.1). CASL and pCASL strategies maintain the labeled state over longer periods resulting in an increased sensitivity *[Wong 1998]*. Such flow-driven inversions have never been implemented and applied to the heart. Indeed, classical continuous tagging schemes would likely not be efficient because of the complex cardiac geometry and the strong flow pulsatility of aortic blood.
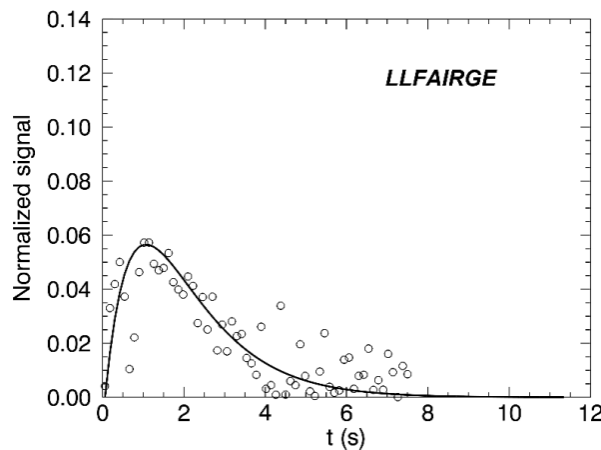
Figure 2.1 – Magnetization difference as a function of time between global and slice-selective inversion created with the LLFAIRGE sequence. Due to the pulsed ASL scheme, the perfusion signal relaxes with T_1 and vanishes over time after each inversion.

The main challenge of this project was thus to design a new ASL strategy that maintains the labeled blood state throughout the experiment while keeping compatibility with constraints imposed by cardiac motion and the highly pulsatile blood flow in the ascending aorta. This has been done by combining a steady-pulsed ASL (spASL) scheme with a steady-state acquisition in order to achieve quasi-continuous tagging of the blood. It allows driving tissue magnetization in a perfusion-dependent equilibrium state that is maintained as long as the sequence is running. The first part of this chapter focuses on the experimental feasibility of this new sequence in mice, and the second part describes the theoretical model developed for perfusion quantification.

2.2.   Experimental Study

This section is based on:

Cine-ASL: A Steady-Pulsed Arterial Spin Labeling Method for Myocardial Perfusion Mapping in Mice. Part I: Experimental Study. Magn. Reson. Med. 2013.

Troalen T, Capron T, Cozzone PJ, Bernard M, and Kober F.

In this work, we propose an original sequence under the name cine-ASL, based on a combination of a continuous cine-MRI gradient echo readout with a steady-pulsed arterial labeling approach. We focus on the experimental feasibility of the cine-ASL sequence in mice and discuss the quality of perfusion measurements and potential errors for this setting. In a direct experimental comparison with the LLFAIRGE method used in previous studies in mice *[Kober 2005]*, we show that this original scheme significantly improves acquisition efficiency over the previously established technique.

2.2.a.   Methods

Cine-ASL pulse sequence

A common ECG-gated cine-FLASH sequence was used as a basis for the new cine-ASL sequence (Figure 2.2). One cine block represents a series of gradient echoes (N_{echoes}) produced within one cardiac cycle. The steady-pulsed labeling is obtained by replacing one single gradient-echo acquisition by a spatially selective adiabatic hyperbolic secant inversion pulse in each cine bloc, which thus has ($N_{echoes} + 1$) repetitions. The labeling slice is positioned at the base of the heart and therefore inverts arterial blood in the aorta at end-systole, just before it enters the myocardial tissue via the coronaries. As a result, cine imaging across the cardiac cycle is achieved simultaneously with labeling of the arterial blood upstream of the myocardium. In order not to perturb the longitudinal steady-state in the imaging slice, the excitation pulse was also played out in the modified pattern. The repetition time TR between each echo was kept as short as possible to maximize temporal resolution.

The entire cine block is repeated N_{cine} times over several cardiac cycles in order to reach the steady-state of a FLASH experiment under the influence of perfusion. We will refer to this portion of the sequence as tag scan. Since the animal's high heart rate causes very rapid repetition of tagging pulses, magnetization transfer (MT) effects are likely to occur, and therefore a control slab was needed to ensure full compensation of these effects. The control scan needed to be positioned symmetrically to the labeling slab with respect to the short-axis imaging plane. Its position and orientation was therefore calculated automatically as a function of labeling slab and imaging slice. This symmetric labeling scheme is similar to the EPISTAR method *[Edelman 1994, Wong 1997]*.

Interleaved tag and control acquisitions were repeated for each phase encoding step (N_{PE}) to fill k-space. Consequently, a total of $2*N_{echoes}*N_{cine}*N_{PE}$ signals were acquired in a full data set. With this approach, continuous cine acquisition can be performed while maintaining quasi-continuous labeling of the blood feeding the coronaries.
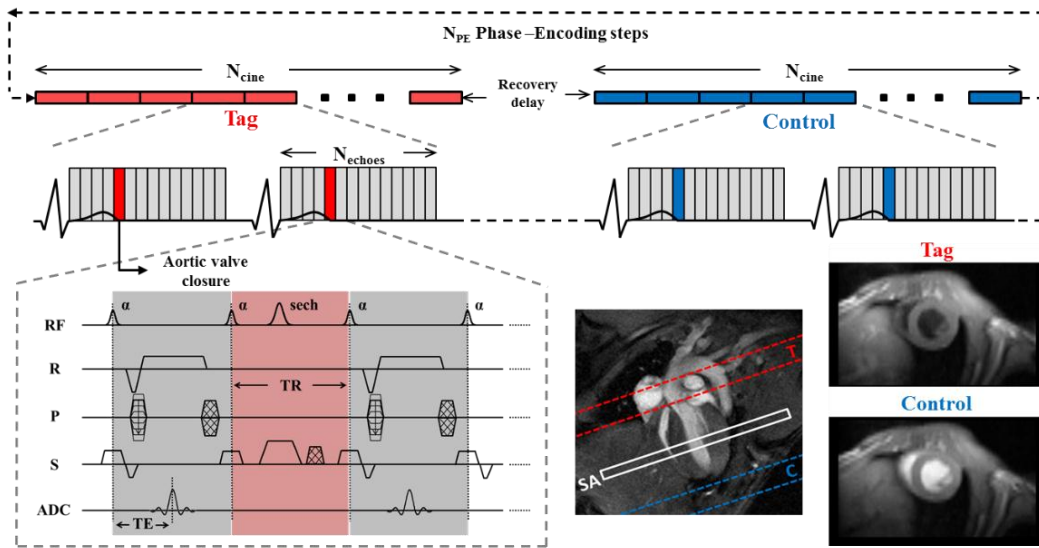
Figure 2.2 – Schematic description of the cine-ASL pulse sequence showing the customized triggered cine-FLASH acquisition combined with RF-pulse labeling applied in end-systole at each cardiac cycle (top). Sequence chronogram and position of the tag and control slabs in symmetry to the imaging slice, chosen on a four-chamber long-axis view (bottom left) and corresponding raw images (bottom right).

Experimental setup

The experiments were performed on a Bruker Biospec Avance 4.7T/30 imager with horizontal bore (Bruker, Ettlingen Germany) in fourteen healthy male C57Bl/6J mice (age 37 weeks, body weight 38-46 g) according to a protocol approved by the University's animal experimentation committee. Homogeneous RF excitation was achieved using a proton volume resonator (diameter 60 mm, homogeneous length 80 mm), and the animals were positioned prone on an actively decoupled surface receive coil (Rapid Biomedical, Wurzburg, Germany). A heating blanket with hot water circulation was placed on the back of the mouse to maintain body temperature throughout the experiment. Respiration was monitored using a pressure sensor connected to an air-filled balloon positioned under the abdomen of the mouse. The ECG signal was monitored by placing two subcutaneous electrodes into both forelegs of the animal. The electrodes were connected to an ECG trigger unit (Rapid Biomedical, Rimpar, Germany) to record the signal and to trigger the MRI sequence. During the MR protocol, mice were anesthetized with 1.5% of isoflurane added to 1L min^{-1} of pure O_2. Isoflurane concentration was regulated using a dedicated vaporizer (Ohmeda/General Electric, Milwaukee, WI, USA) so as to obtain regular breathing frequencies in the range of 100 breaths per minute. In order to stabilize physiological conditions prior to experimentation, mice were warmed for 10 minutes under an infrared lamp before isoflurane induction.

Protocol

Prior to the perfusion measurements, scout images were acquired to determine the short-axis plane used for the perfusion imaging sequences. A cine-FLASH sequence in four-chamber long-axis view was used to acquire dynamic images with a high temporal resolution of 5 milliseconds. This series was used to achieve precise spatial and temporal placement of the labeling pulse in end-systole, just before aortic valve closure.

Cine-ASL parameters were: flip angle $\alpha = 8°$, TE/TR = 1.64/8 ms, field of view = 25 x 25 mm², matrix size = 128 x 64, resolution = 195 x 391 µm², excitation pulse duration = 0.5 ms, inversion pulse duration = 6 ms, imaging slice thickness = 1.5 mm, labeling slice thickness = 2.5 mm, N_{echoes} = 10, N_{cine} = 30.

Using the same experimental setup as described earlier *[Kober 2005]*, a LLFAIRGE measurement was performed for comparison. A series of ECG-gated single phase-encoded gradient echoes was acquired following a global or slice-selective adiabatic inversion. The inversion pulses were ECG- and respiratory-gated to ensure that in the slice-selective case the inversion pulse was always applied at the same position. The number of gradient-echoes acquired for each inversion pulse was adjusted individually according to the heart rate to give measurements until 7 s after inversion (approximately 50). A repetition delay of 3.5 s was introduced after acquisition of a series of gradients echoes to allow for full relaxation between two inversion pulses. The LLFAIRGE acquisition was acquired with the same geometric parameters, pulse durations and echo time, the flip angle α was 12° and the TR was equal to the heart rate.

To evaluate the stability of the perfusion measurement throughout the protocol, a second cine-ASL acquisition was repeated with identical parameters. The acquisition time was 8 minutes for each cine-ASL sequence and 24 minutes for the LLFAIRGE sequence. Alos to investigate the response under vasodilation, both experiments cine-ASL and LLFAIRGE were repeated in one mouse for two different isoflurane concentrations (1.5% and 2%).

Perfusion quantification and image processing

As a result of the theory presented in the following section, the experimentally measured relevant quantity is the stationary signal difference between control and tag scans $\Delta M_\infty = M_\infty^c - M_\infty^t$. Once normalized to the control scan, one obtains the signal contrast $C_\infty = \Delta M / M_\infty^c$, which is related to myocardial blood flow MBF by the following equation:

$$MBF = \frac{\lambda M_{ss}}{T_1^* M_0} \frac{C_\infty}{2\beta - C_\infty} , \qquad [2.1]$$

where β is the average inversion efficiency ($\beta = 1$ for complete inversion and $\beta = 0.5$ for saturation), $\lambda = 0.95$ the blood-tissue partition coefficient for water *[Waller 2000]* and T_1^* the apparent relaxation time measured under the influence of rapid succession of small flip angle pulses *[Deichmann 1992]*. M_{SS} is the magnetization observed under FLASH partial saturation and can be directly calculated from M_0.

To obtain absolute MBF quantification, the only unknown parameter in equation [2.1] is the average inversion efficiency β. According to observations made in the LV chamber blood and taking into account the tagging mechanism analysis described in the discussion, the inversion efficiency can be supposed to be close to a saturation, and we have therefore set β to 0.5 for all post-processing steps.

To perform image analysis, an in-house developed program running in an IDL environment (ITT, Boulder, CO, USA) was used, and perfusion maps were generated by applying this model pixel-by-pixel. For the LLFAIRGE experiment, the method described earlier was used *[Kober 2004]*.

Two T_1^* maps (one global and one slice-selective) and a single MBF map, recorded 40 ms after the ECG trigger, were obtained from the LLFAIRGE approach. As the resolution was the same for both experiments, the global T_1^* map obtained with LLFAIRGE was corrected for partial saturation effect based on the formula proposed by Deichmann and Haase *[Deichmann 1992]*. The resulting T_1 map was thus corrected again to generate a T_1^* map with the cine-ASL parameters (flip angle and TR) and inserted into the cine-ASL perfusion quantification. To ensure good spatial and temporal concordance between both experiments, perfusion was quantified on maps with comparable time-frame within the cardiac cycle. Phases 4 to 6 of the N_{echoes} maps resulting from cine-ASL were averaged, and regional perfusion was assessed as an average of pixels for ROIs drawn on both perfusion maps. Global myocardium and three zones corresponding to septum, anterior and lateral area of the myocardium were evaluated.

All statistical processing was performed using Prism 5 software (Graph Pad, San Diego, CA, USA). To identify differences between myocardial regions, two-way analysis of variance (ANOVA) for repeated measures was performed on individual MBF values. The same statistical test was used to compare results between both cine-ASL scans and to compare the mean cine-ASL values obtained from both measures with the LLFAIRGE experiment.

Tagging mechanism and efficiency

In order to evaluate the labeling efficiency achieved with this method, an analysis of the signal dynamics inside the RV and LV blood pools was performed. In addition, a series of 9 cine-ASL sequences were acquired in one animal while successively shifting the labeling pulse frame to every possible position within the cardiac cycle (the temporal resolution of the labeling pulse timing is equal to TR, i.e. 8 ms in this experiment). On four mice, an additional cine-ASL scan was done with the labeling pulse occurring at the most unfavorable moment within the cardiac cycle, i.e. at the beginning of the cardiac cycle in early-systole.

2.2.b.   Results

Figure 2.3 shows perfusion maps obtained with both techniques from the same mouse using two different isoflurane concentrations. By inducing strong vasodilation with 2% of isoflurane instead of 1.5%, perfusion significantly increased by a factor of approximately 3 as consistently observed with both methods. Perfusion in the global myocardium increased from 5.6 up to 16.0 mL g^{-1} min^{-1} with cine-ASL and from 6.3 up to 18.7 mL g^{-1} min^{-1} with LLFAIRGE. This result demonstrates that cine-ASL has the potential to study and quantify changes in myocardial perfusion.

Perfusion signal dynamics

Figure 2.4 shows the time-dependent cine-ASL signal from a single isoflurane-anesthetized mouse. Data are shown from tissue ROIs in the myocardium and the chest muscle for both tag and control periods. For clarity, data were normalized to the first cine-block signal coming from the chest muscle. In the myocardium, the signal decreased during the ASL tag period (open circles), and then recovered during the control period (filled circles). This behavior is due to the presence or absence of labeled blood coming from the coronaries during each period, leading to a magnetization difference useful for perfusion quantification.
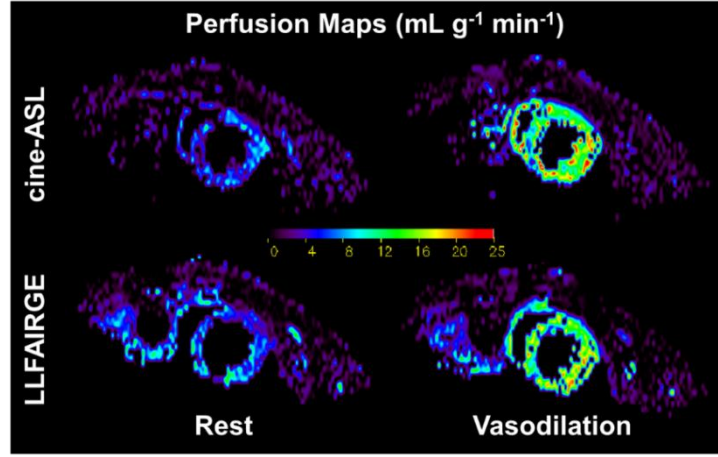
52

Figure 2.3 – Color-coded short-axis MBF maps resulting from a measurement series, in which isoflurane concentration was raised from 1.5% (left) to 2% (right). Perfusion increased from 5.6 to 16.0 mL g^{-1} min^{-1} with cine-ASL and from 6.3 to 18.7 mL g^{-1} min^{-1} with LLFAIRGE.

To roughly estimate the time for tissue magnetization to reach the steady-state in both control and tag periods, a three-parameter mono-exponential fit was used. In perfused regions, the signal decrease during the tag period was significantly faster compared to the signal recovery during the control period. It is also noteworthy that in weakly perfused regions like in the chest muscle, the signal remained in the steady-state throughout the experiment (open and filled triangles). The inserts in Figure 2.4 show the time evolution of the contrast C_∞ during the experiment, which remained approximately zero for the chest muscle (right) and reached a stationary level for myocardial tissue (left) after ten repeated cine blocks. Data in this stationary regime were then averaged to calculate a mean value for the perfusion-dependent contrast C_∞.

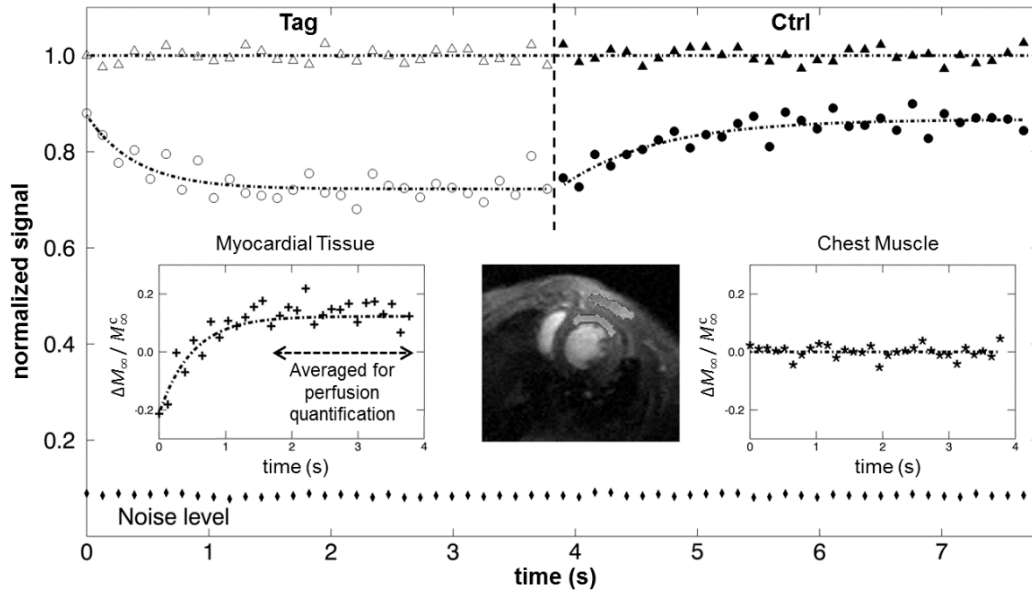*Figure 2.4 – Dynamic MR signal behavior during tag and control scan of a cine-ASL experiment acquired in a single animal. Myocardial tissue (open and filled circles), chest muscle tissue (open and filled triangles) and background noise (diamonds) are displayed. The inserts represent the time-evolution of the contrast parameter C_∞ in the myocardium (left) and the chest muscle (right). ROIs were drawn on a short-axis view.*

In Figure 2.5, dynamic signal plots from blood pool ROIs in the RV and in the LV are shown. It is clear that during the tag period (open symbols) the signal undergoes a magnetization preparation since it decreased already after the first cine block (one heartbeat), approaching the noise level in both RV and LV. A difference between RV and LV blood magnetization can, however, be seen during the control period (filled symbols). In the RV, the signal reached its maximum value after only one cine block whereas in the LV several cine blocks were needed for full recovery.
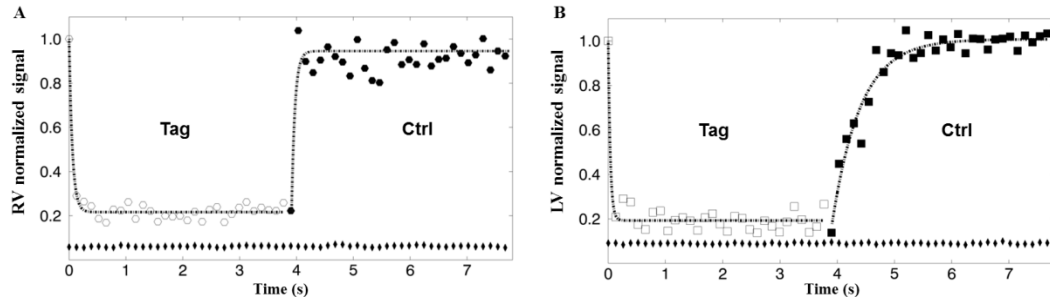
Figure 2.5 – Dynamic MR signal behavior during tag and control scan of cine-ASL data obtained from blood pool in the RV (A, open and filled hexagons) and the LV (B, open and filled squares).

Myocardial blood flow mapping

Averaging the contrast C_∞ over the second half of the scan time, i.e. cine blocks 15 through 30, along with equation [2.1] led to the MBF map series shown in Figure 2.6. In this example mean MBF across the cardiac cycle was 7.5 ± 2.0 mL g^{-1} min^{-1} for the myocardial tissue and 0.2 ± 0.3 mL g^{-1} min^{-1} for the chest muscle. One important feature of the cine-ASL approach is the capability of mapping MBF as a function of time within the cardiac cycle as shown in Figure 2.6A-J. Cine frames in which the cardiac contraction position was found similar could be summed-up (red and green squares) yielding averaged maps from early-systole (Figure 2.6K) and end-systole (Figure 2.6L).
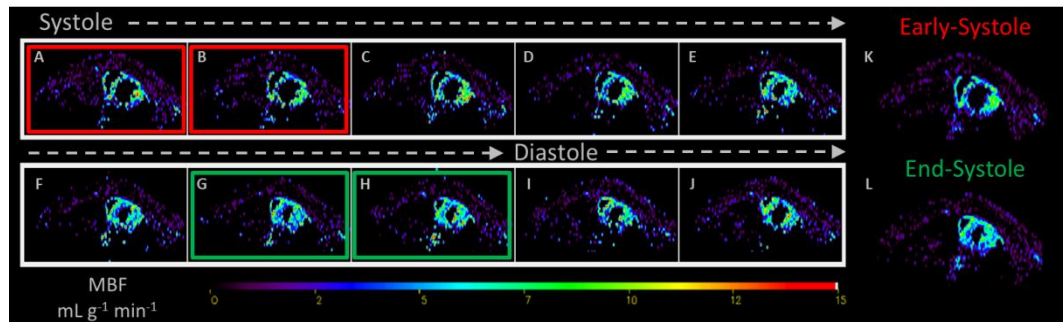
Figure 2.6 – (A-J) Perfusion map series as a function of the cardiac phase. Averaged map at early-systole (K=⟨A,B⟩) and early-diastole (L=⟨G,H⟩).

cine-ASL versus LLFAIRGE

Due to the use of a surface coil, we observed a lack of SNR in the most distant area from the coil, the posterior wall. For both methods, this area was excluded when performing a global analysis of MBF. Global MBF is expressed as group mean value (ROI standard deviation (SD))) ± group SD and was 5.0 (2.2) ± 0.8 mL g^{-1} min^{-1} for the first cine-ASL scan and 4.5 (2.1) ± 0.8 mL g$^-$

^{1} min^{-1} for the second scan. For the LLFAIRGE experiment, global MBF was 5.9 (3.5) ± 1.4 mL g^{-1} min^{-1}. In weakly perfused regions such as the chest muscle, the group mean value (ROI SD) ± group SD was 0.4 (0.8) ± 0.2 mL g^{-1} min^{-1} for the first cine-ASL scan, 0.3 (0.8) ± 0.2 mL g^{-1} min^{-1} for the second scan and 0.4 (1.1) ± 0.3 mL g^{-1} min^{-1} for the LLFAIRGE experiment.

Table 2.1 gives a summary of individual MBF values from the animal group obtained for the global myocardium. Minimum and maximum value, as well as the corresponding variation of the heart rate during the experiment is also reported for each subject. In this study the mean heart rate was 437 ± 45 (10%) bpm and the difference during the protocol did not exceed 15% in any individual subject.

Figure 2.7 is a Bland-Altman representation which gives a summary of all individual MBF values obtained from each subject for different myocardial regions (septum (triangles), lateral (squares) and anterior (diamonds)). In Figure 2.7A data are compared between LLFAIRGE and the first cine-ASL experiment, whereas in Figure 2.7B data are compared between both cine-ASL measurements. No significant regional differences were observed.

Table 2.1 – Individual Experimental Data Obtained From the Group of Fourteen Animals.

Mouse	Weight (g)	Heart rate (bpm)			Global MBF (mL g^{-1} min^{-1})		
		Min	Max	ΔHR (%)	cine-ASL 1	cine-ASL 2	LLFAIRGE
1	41.8	510	520	1.9	4.6 ± 2.4	5.0 ± 2.4	4.9 ± 3.9
2	44.2	380	430	11.6	4.2 ± 2.2	3.9 ± 2.4	4.8 ± 3.5
3	41.5	450	460	2.2	4.6 ± 2.0	3.9 ± 1.8	6.0 ± 2.9
4	46.5	375	415	9.6	4.3 ± 2.0	3.9 ± 1.9	6.4 ± 3.1
5	44.2	360	420	14.3	3.9 ± 2.5	3.3 ± 1.8	4.9 ± 3.2
6	44.6	430	500	14.0	5.5 ± 2.3	4.3 ± 2.5	5.5 ± 3.0
7	41.3	410	430	4.7	5.1 ± 2.0	5.2 ± 2.0	4.5 ± 3.3
8	40.8	410	450	8.9	6.4 ± 1.9	5.4 ± 1.5	7.2 ± 3.1
9	44.8	400	460	13.0	5.9 ± 2.0	5.7 ± 2.3	8.5 ± 3.2
10	44.8	430	500	14.0	5.6 ± 2.1	4.0 ± 1.8	8.1 ± 4.2
11	43.5	420	430	2.3	5.8 ± 2.1	5.4 ± 2.6	5.7 ± 4.4
12	46.6	360	400	10.0	3.7 ± 2.3	3.5 ± 2.4	3.5 ± 2.7
13	38.5	400	420	4.8	5.2 ± 2.2	5.1 ± 2.6	6.5 ± 4.6
14	42.3	510	550	7.3	5.5 ± 5.4	4.2 ± 2.0	5.6 ± 4.5
Mean ± SD	43.2 ± 2.3	437 ± 45		8.5 ± 4.6	5.0 ± 0.8	4.5 ± 0.8	5.9 ± 1.4

The average of the difference and the limits of agreement on both Bland-Altman plots were calculated for all data coming from the three regions. We observed a mean difference of -0.8 ± 1.3 mL g^{-1} min^{-1} between the first cine-ASL and LLFAIRGE and a mean difference of 0.6 ± 0.8 mL g^{-1} min^{-1} between the two cine-ASL experiments. However both differences remained within the corresponding limits of agreement.
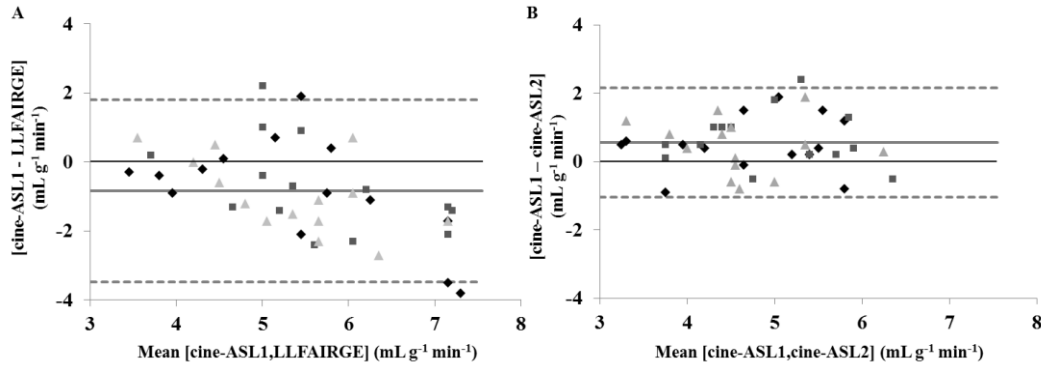
Figure 2.7 – Bland-Altman plots of all individual MBF values obtained in the n=14 mice for different myocardial regions: anterior wall (diamonds), lateral wall (squares) and septum (triangles). (A) Comparison between the first cine-ASL and the LLFAIRGE acquisition. Cine-ASL had a tendency to lower MBF values compared to those obtained with LLFAIRGE. (B) Comparison between the first and the second cine-ASL experiment. The scattered distribution above and below the equality line suggests that there is no consistent bias of one measurement versus the other.

Sensitivity considerations

A general definition of sensitivity in MRI is given by the image SNR that can be obtained in a given experiment time. Signal can be defined as the perfusion value in a specific region. However, in this study, perfusion maps were obtained using masks based on raw image signal intensity making a correct analysis of noise difficult, particularly for the LLFAIRGE technique, which uses pixel-by-pixel fitting to generate maps. We have therefore used the signal variation in the relatively homogeneous and weakly perfused chest muscle compartment as reference for our experimental sensitivity estimations, since these variations could be assumed to be dominated by noise.

The experimental sensitivity (ES) was defined as:

$$ES = \frac{\left\langle \mathrm{MBF}_{Myoc} \right\rangle / \sigma_{Muscle}}{\sqrt{T_{Acq}}} \, , \qquad [2.2]$$

where T_{Acq} is the total acquisition time of the method, $\langle$MBF$\rangle$ the mean perfusion found in the myocardium and σ_{Muscle} the standard deviation of signal in the chest muscle. ES was higher by a factor of 2.1 with cine-ASL compared to LLFAIRGE. We note, however, that ES only accounted for the ASL signal difference quantification and that an extra T_1 measurement might be required at least once per protocol for absolute perfusion quantification. LLFAIRGE has the advantage of providing T_1 inherently.

Labeling pulse timing

We define the optimal timing as the most favorable moment for the inversion pulse to occur within the cardiac cycle regarding the inversion efficiency, i.e. just before the aortic valve closure. To evaluate the impact of labeling pulse timing inside the cardiac cycle on the perfusion measurement, every possible position of the labeling pulse was tested on a single mouse. The results of this experiment are shown in Figure 2.8A where the measured MBF is plotted as a function of the labeling pulse time. One can easily see that one position emerges among others

56

with a maximum calculated perfusion of 9.3 mL g^{-1} min^{-1} obtained when the tag occurs between 56 and 62 ms after the R-wave. For the other positions, apparent perfusion was found lower with a minimum value of 4.9 mL g^{-1} min^{-1} when the tag occurred at the first position of the cardiac cycle, i.e. between 8 and 16 ms. Both extreme label timings were tested in four mice (Figure 2.8B) yielding averaged perfusion values of 3.9 ± 0.6 mL g^{-1} min^{-1} (labeling right after the R-wave) and 6.7 ± 0.7 mL g^{-1} min^{-1} (optimal timing).

2.2.c.   Discussion

In this study we report the absolute quantification of MBF by MRI with a new approach based on a cine-FLASH labeling and readout module. MBF maps were obtained with a high temporal resolution of 8 ms. The spatial resolution (195x391 μm²) and the sensitivity were sufficient to regionally measure perfusion and hemodynamic changes within the cardiac cycle in approximately 8 min.
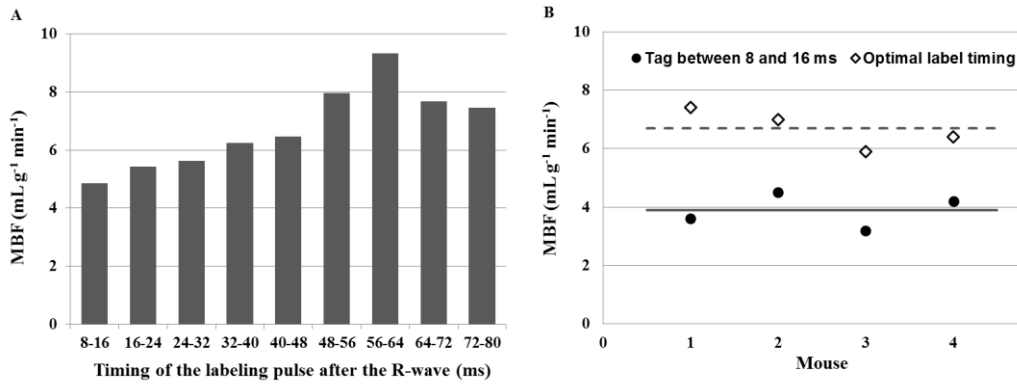
Figure 2.8 – (A) Measured perfusion as a function of the labeling pulse timing within the cardiac cycle. (B) Perfusion measured individually in a subgroup of four mice for two specific labeling times, 8 to 16 ms and the optimal label timing found by analysis of the Cine-FLASH 4 chamber view.

As a limitation common to many ASL techniques, cine-ASL also requires the acquisition of a T_1 map, which in this study was provided by the FAIR Look-Locker acquisition carried out for comparison. We note that it might be preferable to utilize faster alternative T_1-mapping techniques. In this context, the recently proposed driven-equilibrium (DESPOT1) T_1-mapping has advantages for 3D acquisition *[Coolen 2011]*.

Perfusion signal dynamics

The tagging scheme used in this approach consists in a rapidly repeated local inversion with precise timing within the cardiac cycle. For this purpose, the cardiac cycle was visualized on a 5 ms time resolution cine sequence in four-chamber view prior to the ASL sequences. By inspecting this four-chamber image series, the ASL label time point within the cardiac cycle was chosen just before aortic valve closure. In this setting, ideally, fully inverted blood from the aortic root flows into the coronary system at each cardiac cycle during the tag scan. Completely inverted magnetization would indeed be present at the entry of the coronaries if the blood entering the aorta were in a fully relaxed state. However, as shown in Figure 2.2, the tagging slab covers three blood-pool areas (both atria and aorta) such that blood entering the aorta has already been inverted several times with different inversion delays.

The dynamics of myocardial tissue magnetization (Figure 2.4) shows the build-up of the stationary regime for both scans tag and control. The myocardial magnetization difference is created by the difference in LV blood-pool magnetization whose time course for the two scans is shown in Figure 2.5B. The graph shows that the tagging steady-state is reached after only few cardiac cycles, but that the blood magnetization in that state is close to zero corresponding to a saturated rather than an inverted state. These experiments therefore show that the average tagging efficiency β is only about 0.5. Figure 2.5 also shows that the steady state is reached much earlier in the tag scan than in the control scan, in which tagged blood disappears only slowly from the imaged region. The time for tagged blood to leave the imaging slice is comparatively long and on the order of blood T_1, thus both relaxation and outflow play a role in the blood magnetization of the control scan. A likely reason for this difference in dynamics is the spatial extent of the labeling slab leading to a steady production of tagged blood in the entire thoracic region including atria and pulmonary vessels.

This assumption is supported by the blood magnetization behavior in the RV, which is shown in Figure 2.5A. While at the beginning of the tagging scan, RV blood magnetization closely follows LV blood magnetization, it is immediately replaced by fresh magnetization at the end of the tagging series. Thus, the slowly recovering blood magnetization in the LV at the end of tagging might be due to the fact that blood has undergone several inversions during its way through the pulmonary compartment. Complete recovery of LV blood magnetization can only be accomplished when fresh blood from the right atrium reaches the LV. In addition, blood entering the LV has undergone different transport stages across the cardiac chambers that all have incomplete ejection fractions. The graph in Figure 2.5A shows that already the RV contains a mix of tagged and fresh blood, since its magnetization in the tag scan is close to zero.

In summary, two factors impair the inversion's efficiency:

- The multiple exposure of blood spins to inversion pulses and the mixing with fresh blood leading to a reduced β.
- A significant amount of tagged blood perfuses the myocardium for as long as 10 heart beats after end of the tagging pulse series.

Inversion pulses with two-dimensional spatial selectivity could be one way of overcoming those limitations. However, since such pulses are characterized by longer duration, this approach might not be compatible with the elevated heart rate in mice.

We finally recall here that despite the loss in tagging efficiency described above, the new sequence showed significantly better acquisition efficiency than LLFAIRGE leading to comparable mapping quality within one third of the acquisition time. Experimentally, we found a roughly two-fold higher sensitivity with cine-ASL than with LLFAIRGE. The estimation of sensitivity obtained with both methods has two limitations. First, the resulting sensitivity is related to the absolute perfusion value found in the myocardium and second, the reference variation figure can contain other contributions than noise. From visual inspection, however, noise appeared to dominate variations in the chest muscle, and MBF was found stable across two successive measurements.

Motion robustness

In this approach, the compatibility with motion constraints in cardiac MRI in small rodents is maintained by a cine-FLASH readout that has a temporal resolution equaling the cine frame rate (here 8 ms). Even very high heart rates do therefore not affect the maximal spatial resolution. Across the cine blocks, frames with equal time within the cardiac cycle were summed up, and then a pairwise subtraction was done between tag and control scan. Also, each obtained perfusion map represents a single frame within the cardiac cycle. Optimized averaging over cardiac phases is therefore possible with this technique as opposed to segmented k-space acquisition, in which the time window has to be chosen before the acquisition. In this work, averaging within the cardiac cycle was done over frames across which motion was found minor by visual analysis as shown in Figure 2.6.

In this study, no efforts in experimental design were made toward respiratory motion robustness. One possible retrospective strategy for taking into account respiratory motion would be to record the timing of inspiration/expiration events along with the experiment to locate motion phases in time. k-Space lines acquired during the motion phases would then be set to zero before averaging. A prospective way (respiratory gating) would be to double-gate each k-space line acquisition, i.e. each cine pulse train, and to eliminate corrupted raw images by visual inspection. This has in the past been used for LLFAIRGE, but since the coherence of the respiratory patterns between k-space lines vanishes over time after the first respiration gate, it is less well suited for the present technique. Prospective respiration gating would also lead to regular interruptions of the pulsed steady-state and therefore to errors or loss of efficiency. More importantly and likely owing to the high number of averages and randomization over the several seconds long pulse train, no respiratory artifacts could be detected in the raw images so that respiratory gating is likely unnecessary.

Perfusion quantification

It should be noted that all MBF values reported in this study were obtained under the influence of isoflurane anesthesia and cannot be considered as physiological baseline values. For global myocardium, mean MBF values obtained from cine-ASL experiments were 5.0 ± 0.8 mL g^{-1} min^{-1} for the first scan and 4.5 ± 0.8 mL g^{-1} min^{-1} for the second scan. With LLFAIRGE, the mean perfusion value was 5.9 ± 1.4 mL g^{-1} min^{-1}. The mean group MBF values reported here are slightly lower than those obtained in previous studies reported in *[Kober 2005]* (6.9 ± 1.7 mL g^{-1} min^{-1}), *[Streif 2005]* (7.0 ± 0.5 mL g^{-1} min^{-1}) and *[Nahrendorf 2006]* (6.7 ± 0.3 mL g^{-1} min^{-1}). On the other side, Vandsburger *et al.* reported a mean group MBF value of 4.9 ± 0.5 mL g^{-1} min^{-1} and explained this difference with the literature by the sensitivity of methods to variability in heart rate and the effect of respiratory artifact which may increase the measured perfusion *[Vandsburger 2010]*. It may also be explained by differences in anesthesia concentration, as reported earlier *[Kober 2005]* and as demonstrated in Figure 2.3 of this work. Finally, warming-up the mice during 10 minutes prior to isoflurane induction may have been useful to counteract body heat decrease induced by anesthesia.

A LLFAIRGE MBF measurement was performed for comparison. This method has already been validated against fluorescent microspheres *[Jacquier 2011]*, which can be considered as the gold standard in absolute rodent myocardial perfusion quantification. MBF values in any region (septum, lateral and anterior wall, global myocardium and chest muscle) were not significantly

different between LLFAIRGE and cine-ASL measurements, although cine-ASL had a tendency to lower values as shown in the Bland-Altman plot in Figure 2.7A. We found an average difference between the two measurements of -0.8 ± 1.3 mL g^{-1} min^{-1}, i.e. about 14% lower MBF obtained with cine-ASL. However, the line of equality remained in the 95% confidence interval.

One likely reason for absolute MBF differences between the methods is that both use gradient-echo readouts, which are known to be more sensitive to bulk flow than spin-echo readouts because of the absence of efficient flow spoiling. Although the FLASH saturation in both techniques acts equally on both tag and control scans, it might lead to a net signal difference due to bulk blood flow in arterioles, because the initial blood magnetizations are not equal. This contributes to the perfusion signal and leads to an overestimation of perfusion. In this context, LLFAIRGE saturates static spins in the imaging slice with a higher flip angle and a much longer repetition time than cine-ASL and is therefore more sensitive to bulk flow than cine-ASL. Nevertheless, a drawback of the new cine-ASL method is that the inversion efficiency β is submitted to some uncertainty. Until now, the only way to estimate β is to assess the time-course of the magnetization within the RV and LV blood-pool as described above and shown in Figure 2.5. A complementary study correlating the inversion efficiency with the temporal position of the pulse and the heart rate could give additional information on β and might help improve its quantification in future experiments. One could further argue that the control slab might also label blood relevant to the perfusion signal measured in the myocardium, which would lead to underestimation of MBF. Arterial blood in large vessels is, however, first delivered to other organs and periphery, whereas venous blood such as that in the vena cava first goes through the lung before reaching locations relevant for myocardial perfusion. It is therefore justified to assume that the time for this blood to travel back to the coronaries is much longer than T_1, so that undesired control labeling is negligible.

The stability of perfusion quantification along the protocol was tested by repeating cine-ASL directly after the LLFAIRGE measurement. Very similar mean group values were obtained (5.0 (2.2) ± 0.8 mL g^{-1} min^{-1} and 4.5 (2.1) ± 0.8 mL g^{-1} min^{-1} for the first and second scans respectively) despite the 30 minutes delay between both scans. This comparison is detailed in the Bland-Altman plot shown in Figure 2.7b, which indicates no significant bias between both cine-ASL measurements.

Before perfusion quantification, cine-ASL frames were summed up in order to increase SNR. These maps were chosen at time-frames comparable with those obtained with LLFAIRGE (Figure 2.6D-F). On each individual map (Figure 2.6A-J) perfusion seems to be quite heterogeneous across the myocardium. Averaged maps, however, appear more homogeneous likely due to reduction of physiological noise.

Labeling pulse timing

The temporal position of the labeling pulse inside the cardiac cycle is a crucial parameter regarding the asymptotic regime reached by the magnetization during the tag part of the experiment and therefore the evaluation of the inversion efficiency β, as shown in Figure 2.8A. If, on the one hand, the labeling timing were chosen too short, the blood would be labeled too soon before closure of the aortic valve and would then be ejected toward the body circulation without feeding the coronaries and contributing to the ASL signal. On the other hand, if the labeling timing is chosen too long, the labeled blood stays inside the aorta until the next contraction of the LV and is then pushed into the body circulation instead of the coronaries. If

lost labeled blood were not accounted for in the inversion efficiency β, the result in both situations would be an underestimation of perfusion.

This shows the importance of two mechanisms contributing to the perfusion measurement in this approach. On the one hand, the labeling must take place at the right time within the cardiac cycle and at the right place. On the other hand, due to the geometric situation, the labeling slice also covers a portion of the atria. The tagged blood in these cavities also contributes to the perfusion measurement despite a longer pathway and partial relaxation during its transit delay. The second mechanism is undesired, since it leads to exposure of blood to multiple labeling pulses before entering the coronaries, but the label pulse timing is less critical in the second mechanism and leads to less error in case of imprecise timing situations. These observations are also supported by the result presented in Figure 2.8B where, even if the tag takes place at the most unfavorable moment, there is still a measurable perfusion signal.

As shown in Table 2.1, the heart rate variation in this group of healthy animals did not exceed 15%. Together with the analysis shown in Figure 2.8A, one can therefore expect limited impact of label pulse timing imperfections on MBF. Heart rate variations can, however, be larger in models of cardiac pathology and necessitate individual β determination.

2.3.   Theory and Sensitivity

This section is based on:

Cine-ASL: A Steady-Pulsed Arterial Spin Labeling Method for Myocardial Perfusion Mapping in Mice. Part II: Theoretical Model and Sensitivity Optimization. Magn. Reson. Med. 2013.

Capron T, **Troalen T**, Cozzone PJ, Bernard M, and Kober F.

Existing models for ASL describe free relaxation of the magnetization after a single pulsed inversion *[Detre 1992, Calamante 1996]* or during continuously labeled inflowing blood *[Buxton 1998]*. From a perfusion-weighting point of view, the spASL scheme is similar to the dynamic ASL (DASL) technique *[Barbier 1999, 2001b]*, which has been developed to simultaneously measure blood flow and kinetic parameters like transit time. This kind of periodic labeling method was shown to improve accuracy of blood flow quantification. DASL, however, remains a dynamic relaxation measurement and does not specifically address or overcome the low sensitivity weakness *[Meng 2012]*. Here, we present a theoretical model derived from the modified Bloch equations, specially developed to depict the magnetization behavior within the cine-ASL sequence. Tissue magnetization in this experiment was shown to evolve towards a perfusion-dependent stationary regime that can be used to quantify perfusion. We compare and discuss the predicted magnetization dynamics with the experimental observations made in the previous experimental study.

2.3.a.   Theory

Modified pulse sequence

A model was established for the sequence which combines steady-pulsed ASL and cine imaging. Continuous imaging is achieved by using a common ECG-gated cine-FLASH sequence, while the steady-pulsed labeling is obtained by replacing one single GE acquisition by a labeling pulse in each cine block. As a result, cine imaging across the cardiac cycle is achieved simultaneously with labeling of the arterial blood upstream of the myocardium. This scheme is repeated over N_{cine} heartbeats for each phase encoding step. For each PE step, both control and tag scans are acquired sequentially, separated by a recovery delay RD (Figure 2.2).

The magnetization is expected to reach a steady-state value that is characteristic for each tag and control scan. In the tag scan, this stationary value is affected by a continuous flow of labeled blood spins, whereas in the control scan, inflowing spins are in an equilibrium magnetization state. The signal difference between control and tag scans in the stationary regime should thus depend on MBF.

Theoretical model

In the myocardium, water is considered as freely diffusible, so that fast exchange between blood and tissue compartments can be assumed *[Bauer 1996]*. When the exchange time constant is much smaller than T_1, the resulting fast exchange between blood and tissue compartments leads to rapidly homogenized magnetization. Diffusive water exchange is equilibrated, and the ratio of the magnetizations in the two compartments is given by the blood-tissue partition coefficient for

water $\lambda = M_0^{tissue} / M_0^{blood}$. We thus use a single-compartment model for the description of tissue magnetization.

The magnetization time evolution can be decomposed in two phases. We call phase A the period during which the signal is acquired with the cine sequence and phase B the recovery period. During phase A, the cine-FLASH sequence leads to a well-known steady-state of the magnetization in the imaging slice. Note that in the experimental setup proposed previously, this steady-state is maintained all along the acquisition even when playing out the labeling pulse. The time evolution of the magnetization during the cine sequence is properly described by a mono-exponential expression *[Deichmann 1992]*, which can be written in the corresponding Bloch equation form:

$$\frac{dM_z}{dt} = \frac{M_{ss} - M_z}{T_1^*},$$
[2.3]

where

$$M_{ss} = M_0 \frac{1 - e^{-TR/T_1}}{1 - \cos(\alpha)e^{-TR/T_1}},$$
[2.4]

is the steady-state magnetization, and the decay time constant is given by

$$\frac{1}{T_1^*} = \frac{1}{T_1} - \frac{\ln(\cos\alpha)}{TR}.$$
[2.5]

In addition to the FLASH excitation, and assuming a constant blood flow f, tissue magnetization is affected by incoming arterial flow and outgoing venous flow, as described in the introduction. Magnetization brought to the tissue by arterial inflow is $f M_a$ and magnetization removed by venous outflow is $- f M_v$. Due to the fast exchange assumption, we consider that blood magnetization in the veins is completely equilibrated with tissue magnetization such that $M_v = M_z / \lambda$.

In the tag case, labeling is achieved with an inversion RF pulse, and the initial arterial magnetization can be set to $M_a (t = 0) = - M_0^b$, where M_0^b is the equilibrium magnetization of the blood. Blood flowing from the labeling slab into the imaging slice then relaxes towards equilibrium $+M_0^b$ with a time constant T_1^b, during one cardiac cycle. In small rodents, the interval between heart beats RR is about 130 ms and therefore short compared to T_1^b (RR << T_1^b). Arterial magnetization relaxation between two labeling pulses is therefore negligible. Moreover, we assume that the transit time of the blood from the left ventricle to the myocardium is short in comparison with T_1^b. In this model, we therefore consider that arterial magnetization remains constant during the whole tag scan. In order to take into account deviations from a true inversion of blood spins, we express the arterial magnetization during tag scan as $M_a^{tag} = -\varepsilon M_0^b$, where ε is a parameter that accounts for the inversion labeling efficiency, but also for other deviations that may arise from relaxation or transit time effects. ε can be expected to be close to 1, but strongly depends on the effective labeling efficiency build from the repeated tagging scheme.

In the control scan, we consider that the magnetization of blood feeding the coronary vessels is in equilibrium state, $M_a^{ctrl} = M_0^b$. The effective labeling efficiency of the experiment β is given by:

$$\beta = \frac{M_a^{ctrl} - M_a^{tag}}{2M_0^b} = \frac{1+\varepsilon}{2}.$$ [2.6]

Finally, the magnetization in phase A is described by the master equation:

$$\frac{dM_z}{dt} = \frac{M_{ss} - M_z}{T_1^*} + fM_a^{tag,ctrl} - f\frac{M_z}{\lambda}.$$ [2.7]

During phase B, the magnetization freely relaxes towards equilibrium in the presence of blood flow. Note that relaxation occurs in tissue but also in arterial blood. In a first approximation, we consider the wash-out of labeled blood by fresh blood to be fast on the scale of one heart cycle. Within this assumption, fresh blood immediately replaces the blood in the capillaries at each cardiac cycle. It can therefore be assumed that the arteries constantly feed the myocardium with fresh unlabeled blood such that $M_a = M_0^b$ remains constant during the recovery phase B (this also applies for the control scan).

The magnetization in phase B is then governed by the master equation:

$$\frac{dM_z}{dt} = \frac{M_0 - M_z}{T_1} + f\frac{M_0}{\lambda} - f\frac{M_z}{\lambda}$$ [2.8]

Solutions for the equations

The time constant governing the magnetization evolution in phase A is given by:

$$\frac{1}{T_1^{app*}} = \frac{1}{T_1} + \frac{f}{\lambda} - \frac{\ln(\cos\alpha)}{TR},$$ [2.9]

which is simply a combination of equations [1.7] and [2.5], taking into account partial saturation due to the cine-FLASH readout (T_1^*) and the influence of blood flow on the longitudinal relaxation time (T_1^{app}).

The general solution of equation [2.7] during phase A follows:

$$M_z^A(t) = Ae^{-t/T_1^{app*}} + M_\infty^{At,c},$$ [2.10]

where A is an integration constant to be determined with initial conditions. $M_\infty^{At,c}$ is the asymptotic value of the magnetization at infinite time, and depends on the arterial magnetization in tag or control cases:

$$M_\infty^{At,c} = \frac{M_{ss}T_1^{app*}}{T_1^*} + fM_a^{tag,ctrl}T_1^{app*}.$$ [2.11]

During the relaxation phase B, the decay time constant is T_1^{app} as described in the introduction such that:

$$\frac{1}{T_1^{app}} = \frac{1}{T_1} + \frac{f}{\lambda},$$ [2.12]

and the general solution is given by:

$$M_z^B(t) = Be^{-t/T_1^{app}} + M_0.$$ [2.13]

Accordingly, since $M_a = M_0 / \lambda$, the magnetization returns to equilibrium at long times: $M_z^B (t \rightarrow +\infty) = M_0$. The constant B will be determined with initial conditions.

As a result, detailed dynamics of the solutions $M_z^A(t)$ and $M_z^B(t)$ require initial conditions to be setup for each scan and each encoded line.

Tag and control scans are acquired in an interleaved fashion following the sequence:

Phase A, tag → Phase B, tag → Phase A, ctrl → Phase B, ctrl.

The initial conditions of a given phase thus depend on its preceding phase. We label each pair of phases (A+B) with an index n. We define t_p as the duration of the acquisition phase, that is, $t_p = N_{cine} (N_{echoes} + 1)$ TR. We define $M_{A,B,n}^{t,c}$ as the initial condition of the period (A,B),(tag,ctrl),n. Details of the initial condition calculations are given in the appendix (Supplementary Theory section). By solving the master equations, each initial condition is found to be expressed as a function of the previous one, with a recurrence relation of the form:

$$M_{A,B,n+1}^{t,c} = y_{A,B}^{t,c} + xM_{A,B,n}^{c,t},$$ [2.14]

where $y_{A,B}^{t,c}$ and x are constant factors depending on experimental parameters. Equation [2.14] can be expressed for an arbitrary n index, using a mathematical induction:

$$M_{A,B,n}^{t,c} = y_{A,B}^{t,c} \frac{1-x^n}{1-x} + x^n M_{A,B,0}^{t,c}.$$ [2.15]

The value of x thus governs the convergence of the signal with the line index n. This factor is given by:

$$x = e^{-RD/T_1^{app}} e^{-t_p/T_1^{app*}}.$$ [2.16]

The factor $y_{A,B}^{t,c}$ is detailed in the appendix of this chapter and depends on various experimental parameters M_0, β, T_1^{app}, $M_\infty^{At,c}$, t_p, T_1^{app*} and the recovery delay RD.

Magnetization dynamics during the scan

When we assume parameters $RD > T_1^{app}$ or $t_\mathrm{p} > T_1^{app*}$, the factor x becomes small ($x << 1$), and a unique signal behavior for all encoded lines is obtained with a common initial condition written as:

$$M_{A,B}^{t,c} = \lim_{n \to +\infty} M_{A,B,n}^{t,c} = \frac{y_{A,B}^{t,c}}{1-x}. \qquad [2.17]$$

Using this result, the magnetization time evolution in control and tag scans is analytically expressed with monoexponential expressions:

$$M_c(t) = M_\infty^{Ac} + \left(M_A^c - M_\infty^{Ac}\right)e^{-t/T_1^{app*}} \qquad [2.18]$$

and

$$M_t(t) = M_\infty^{At} + \left(M_A^t - M_\infty^{At}\right)e^{-t/T_1^{app*}}. \qquad [2.19]$$

However, as pointed out in the previous section, the control scan is affected by the previous tag scan, because the replacement of previously tagged blood with inflowing unlabeled blood takes several heart cycles. The "fast wash-out" assumption of our model therefore has to be refined.

Here, we assumed an arterial input function of the form $AIF(t) = 1 - e^{-t/T_{AIF}}$, which describes the delivery of the arterial magnetization to the tissue with a typical time constant T_AIF. The arterial magnetization M_a is thus recalculated in the four cases:

$M_a(t) = M_a^t\left(1 - e^{-t/T_{AIF}}\right)$: during phase A, tag, M_a evolves towards M_a^t.

$M_a(t) = M_a^c\left(1 - e^{-t/T_{AIF}}\right)$: during phase B, tag, M_a raises to M_a^c.

$M_a(t) = M_a^c\left(1 - e^{-(t+RD)/T_{AIF}}\right)$: during phase A, control, M_a continues to raise after RD.

$M_a(t) = M_a^c\left(1 - e^{-(t+RD+t_p)/T_{AIF}}\right)$: during phase B, control, M_a continues to raise after RD+t_p.

Asymptotic regime and quantification of perfusion

The resulting magnetization difference between control and tag scans is theoretically given by a mono-exponential expression as well:

$$\Delta M(t) = \Delta M_\infty + \left(\Delta M_0 - \Delta M_\infty\right)e^{-t/T_1^{app*}}, \qquad [2.20]$$

where

$$\Delta M_0 \approx \Delta M_\infty . e^{-RD/T_1^{app}}\left(e^{-t_p/T_1^{app*}} - 1\right) \qquad [2.21]$$

and

66

$$\Delta M_{\infty} = f \frac{2\beta M_0 T_1^{app^*}}{\lambda} .$$ [2.22]

Importantly, the magnetization difference in the stationary regime explicitly depends on the blood flow f. Another crucial quantity that should be evaluated is the signal contrast. Here we define this contrast C_{∞} as:

$$C_{\infty} = \frac{M_{\infty}^{Ac} - M_{\infty}^{At}}{M_{\infty}^{Ac}} = \frac{2\beta}{1 + \frac{\lambda M_{ss}}{fT_1^* M_0}} .$$ [2.23]

This formulation has the advantage to be independent of M_0, and the contrast only depends on the known parameters TR, α, T_1, λ, β, and the perfusion f. The capillary blood flow f can therefore be determined by a contrast measurement.

2.3.b.   Methods

Simulation of the signal evolution

The behavior of the signal coming from each phase-encoded line was investigated with exact simulations using equations [2.10] to [2.14] derived in the Theory section and calculating the initial conditions incrementally. Experimental parameters that do not significantly affect the acquisition behavior were fixed to realistic values: $T_1^{myo} = 1.4$ s, $\alpha = 8°$, MBF = 6 mL g^{-1} min^{-1}, $\lambda = 0.95$ mL g^{-1}, $\beta = 0.5$, $N_{echoes} = 12$. Other dynamic parameters were set with respect to physiological values to RR = 130 ms and TR = 10 ms. Two other parameters mainly govern the acquisition strategy: the recovery delay RD and the scan duration $t_p = N_{cine} (N_{echoes}+1)$ TR. Calculations of the magnetization were performed for the 6 first k-space lines, with interleaved control and tag scans, during imaging (phase A) and recovery (phase B) periods. From the set of simulation parameters, the time constants $T_1^{app} \approx 1.22$ s and $T_1^{app^*} \approx 0.56$ s were calculated. As the signal evolution between lines is governed by $x = e^{-RD/T_1^{app}} e^{-t_p/T_1^{app^*}}$, we chose in the simulation representative values for RD and t_p compared with T_1^{app} and $T_1^{app^*}$.

Theoretical versus experimental signal evolution

In addition to the data presented in the experimental study, further experimental data were acquired in the mouse heart in order to highlight some of the important features of the theoretical description. Parameters and materials were identical to those described previously. In this experiment, RR was 130 ms, and the number of frames N_{echoes} was set to 18 (TR = 6 ms). $N_{cine} = 30$ cine blocks were acquired, resulting in a scan time $t_p = 3.42$s.

A first acquisition was performed setting a long recovery delay RD = 6 s. Since RD >> T_1^{app}, full magnetization recovery between scans was ensured. A second experiment was performed on the same mouse, but setting RD = 0 s for comparison. In order to focus on signal dynamics, the experiment without recovery delay was performed again on another mouse (RR = 136 ms, $N_{echoes} = 10$, TR = 8 ms). Magnetization data was measured from a region of interest placed in the anterior septum and normalized by M_0 determined from the theoretical fit.

For sensitivity comparison with previously used methods, a LLFAIRGE was acquired with the same settings as previously described. A cine-ASL scan was acquired with $N_{cine} = 95$, yielding approximately the same total acquisition time as the LLFAIRGE scan (24 minutes). Field of view, resolution, slice thickness, bandwidth and TE were identical in both sequences. The sensitivity of each method was evaluated by integrating the signal over the scan time divided by noise level and the square root of the total acquisition time *[Pohmann 1997]*, both experimentally and theoretically. The noise level was obtained from the raw image noise in each experiment. In a ROI placed in the anterior septum, the experimental data points of all acquired echoes were summed, thus defining the total signal acquired as a function of the scan time.

2.3.c.   Results

Simulation of the signal Evolution

The initial behavior of the magnetization at onset of the sequence was simulated for long (3.5 s) and short (0.01 s) RDs and for two different scan lengths t_p (0.26 s and 3.12 s). Figure 2.9 shows the calculated longitudinal magnetization for the first six k-space lines acquired, in each of these situations. It can be seen that starting from the second phase-encoded line, the magnetization behaved similarly for all successive lines, provided RD $> T_1^{app}$ or $t_p > T_1^{app}$. Convergence of the magnetization behavior was therefore rapidly initiated.
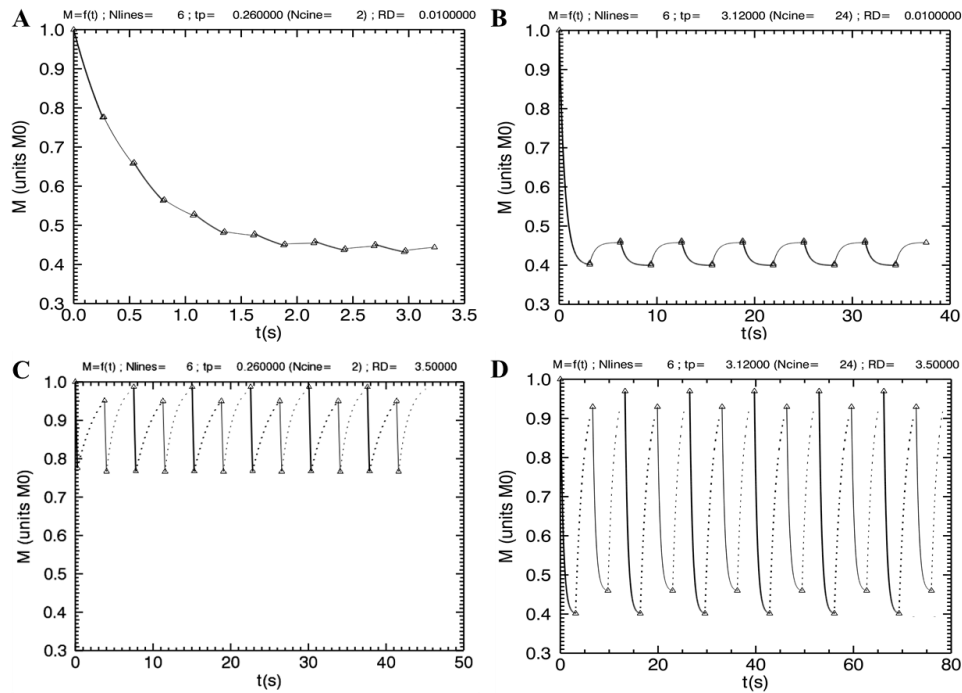
Figure 2.9 – Theoretical calculations for the normalized longitudinal magnetization time evolution during the proposed experiment. The course of the magnetization is shown with solid lines during imaging (phase A), and dotted lines during recovery (phase B). Tag scans are represented by thick lines, whereas thin lines describe control scans. The figure shows the behavior of the six first lines acquired, for representative values of the parameters RD and t_p. (A) short values RD=0.01 s, t_p=0.26 s. (B) short RD=0.01 s, long t_p=3.12 s. (C) short t_p=0.26 s, long RD=3.5 s. (D) long values RD=3.5 s, t_p=3.12 s.

Figure 2.10 shows the experimental magnetization time evolution obtained using a long recovery delay RD = 6 s (RD>>T_1^{app}). The data acquired in control and tag scans are well described by the theory, when setting the perfusion parameter f=MBF=12 mL g^{-1}min^{-1} and β=0.5. The data obtained with a short recovery delay RD≈0 s are shown in the same figure. Although the experimental points deviate from the theoretical prediction at short times after onset of the control scan, the measured signal is also well described by the theory using the same parameters as in the long recovery delay case.
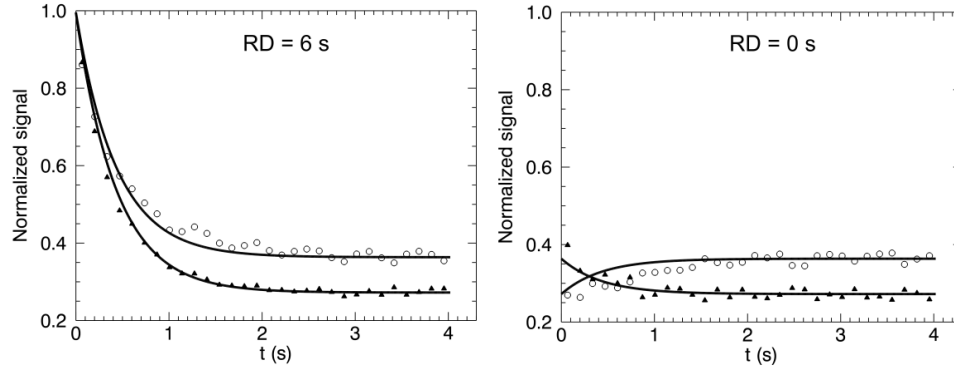

Figure 2.10 – Tissue magnetization time evolution experimentally obtained in control (open circles) and tag (filled triangles) scans, using a long recovery delay (left, RD = 6 s) and a short recovery delay (right, RD = 0 s). Solid lines show the theoretical prediction, adjusting β = 0.5 and MBF = 12 mL g^{-1} min^{-1} in both cases.

For illustration purposes, data obtained in the same experimental conditions are shown in Figure 2.11 and highlight the discrepancy between theory and the measured signal during the control scan. Using the exponential arterial input function correction proposed in the Theory section, with T_{AIF} = 0.35 s, the theoretical fit (dashed line in Figure 2.11) is significantly improved. The correction only applied to the control scan, since saturated blood was present at the input of the capillary compartment after only a few heartbeats during the tag scan, as observed in the experimental study.

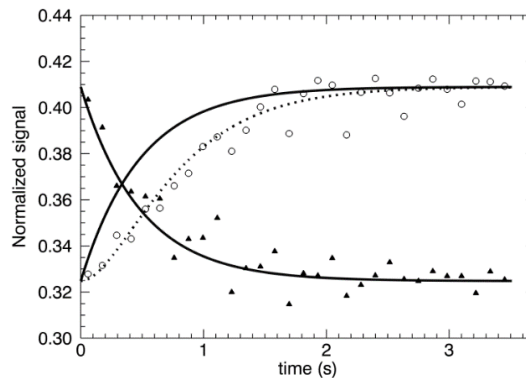*Figure 2.11 – Tissue magnetization time evolution experimentally obtained with a short recovery delay RD = 0 s. Signal during control (open circles) and tag (filled triangles) scans is shown, and solid lines represent the theoretical prediction, adjusting β = 0.5 and MBF = 10 mL g^{-1} min^{-1}. Dashed line shows the theoretical correction using an arterial input function with time constant T_{AIF} = 0.35 s.*

Figure 2.12 shows the magnetization contrast $C(t) = \Delta M(t) / M_c(t)$ obtained in the long (RD = 6 s) and short (RD = 0 s) recovery delay experiments carried out in the same mouse. Although the initial behavior is different, both signals converge to the same stationary value C_∞. The dashed line in Figure 2.12 shows C_∞ obtained with model parameters set to MBF = 12 mL g^{-1} min^{-1} and $\beta = 0.5$ This experiment shows that the asymptotic value of the magnetization contrast can be used to calculate perfusion as done in the experimental study.
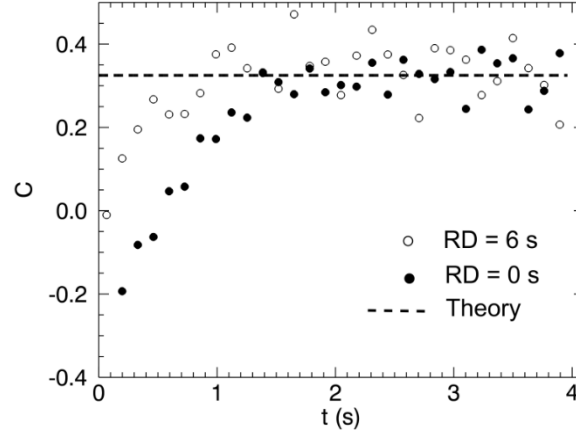

Figure 2.12 – Experimental contrast C (as defined in the text) as a function of time for short (open circles) and long (filled circles) recovery delays. The dashed line shows the asymptotic theoretical value C_∞ calculated with β=0.5 and MBF=12 mL g^{-1} min^{-1}.

Typical data obtained from the same subject with LLFAIRGE and cine-ASL are shown in Figure 2.13. The experimental absolute magnetization difference was normalized with respect to M_0. In the case of LLFAIRGE, the magnetization difference was found to be well described by a double-exponential law *[Kim 1995]*, using parameters $T_1^{gl} = 1.6$ s and MBF = 15.6 mL g^{-1} min^{-1}. In the cine-ASL experiment, a good agreement was found between theory and data using the same parameters as for LLFAIRGE, and setting $\beta = 0.5$ and MBF = 12.6 mL g^{-1} min^{-1}.
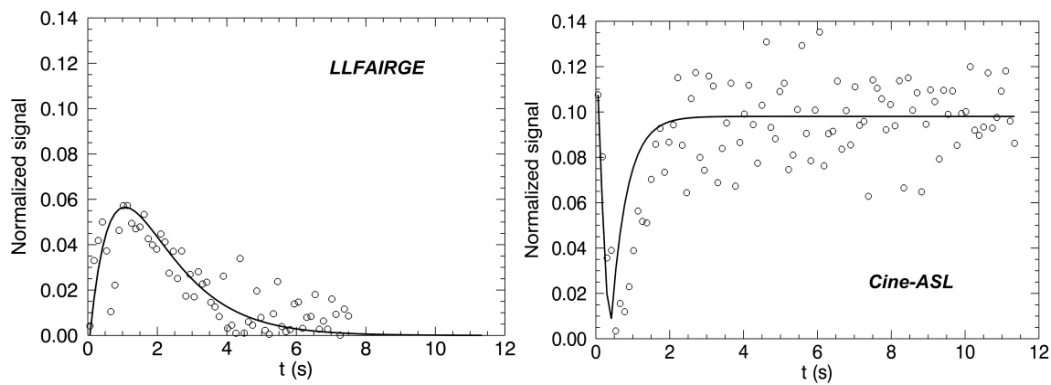
Figure 2.13 – Experimental signal difference obtained with LLFAIRGE (left) and cine-ASL (right). The corresponding theoretical curves are displayed as solid lines.

The corresponding sensitivities are shown in Figure 2.14. The experimental behaviors were well described by theory in both cases. The deviation of the cine-ASL data from the theoretical curve around $t \approx 0.5$ s is due to an increased uncertainty, since the signal $\Delta M(t)$ passed through zero

value at that time. Figure 2.14 shows that, for an equivalent acquisition time, cine-ASL provided more than three-fold higher sensitivity compared with LLFAIRGE.
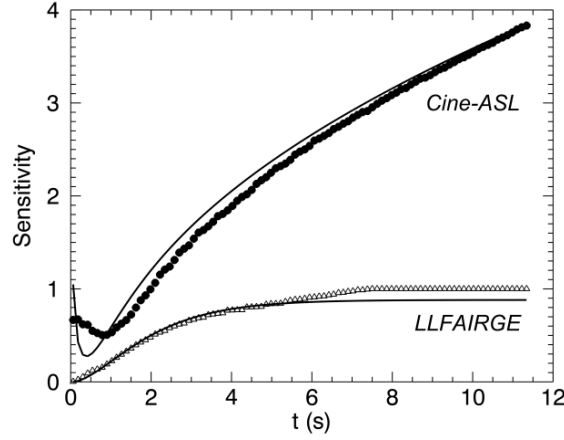
Figure 2.14 – Sensitivity of LLFAIRGE and cine-ASL as a function of the scan time, as defined in the text. Open triangles show the LLFAIRGE data, and black dots the cine-ASL data. Solid lines show the corresponding theory.

2.3.d.   Discussion

Myocardial ASL measurements have sensitivity limitations related to cardiac motion and acquisition strategy. The commonly used FAIR method is based on a measurement of magnetization difference that vanishes over time leading to losses in acquisition efficiency. To improve this situation, we propose a new experimental scheme in which the labeled state is maintained along a cine readout. We provide a theoretical model, which predicts that in such a situation tissue magnetization reaches a stationary perfusion-dependent regime that can be used for quantifying MBF. The proposed model was validated against experiments carried out in the mouse heart. The sensitivity of cine-ASL was calculated and shown to be more than three times larger than the previously used LLFAIRGE technique.

Considering a continuous labeling and readout, the model gives a compact and analytical expression for the magnetization time evolution, using few assumptions presented in the Theory section. The analytic magnetization description is justified, provided that the steady-state is preserved along the imaging process. The labeling state of the arterial magnetization can be taken as constant as long as blood circulation is fast, and labeling repetition time is short with respect to the blood relaxation time. Finally, it is also important that the blood-tissue magnetization exchange during the transit in capillaries is fast in comparison to the duration of a cardiac cycle. These assumptions have never been shown to fail in small rodent myocardium.

Simulation of the signal acquired for the six first lines (Figure 2.9) shows that all lines can be considered identical as soon as RD > T_1^{app} or t_p > T_1^{app}. This fast convergence is preserved even with short recovery delays RD, as long as t_p > T_1^{app}, which will be true in general experimental cases. Therefore, the signal of the resulting image after Fourier transform can be considered as governed by a unique set of initial conditions.

The long recovery delay used in the first experiment (RD $\gg$ T_1^{app}) ensured fully recovered magnetization between control and tag scans to exclude any inter-dependence between scans.

This experimental situation thus provides a reliable check of the theoretical model. The close agreement between theory and experiment validates our description of this type of experiment. The data of the experiment with short recovery delay RD shown in Figure 2.11 was also satisfactorily described by the theory. Tissue magnetization decreased in the tag case due to the flow of labeled spins whereas it increased in the control case, because myocardium is perfused with equilibrated spins. In this situation, the experimental data is sensitive to short time dynamics of inflowing magnetization, and the refined model incorporating a simple arterial input function was necessary to improve the fit. Fitting the experimental data with theoretical formula thus allows us to roughly estimate an arterial input function time constant, which dynamically describes the magnetization state of blood delivered to the tissue. One could raise the question of the time taken for the blood to fill the capillaries. This mean transit time would rely on the ratio of regional blood flow and regional blood volume. Blood volume was found earlier to be rather high in mice (12% according to a study by Streif *et al. [Streif 2005]*). Assuming MBF to be around 6 mL g^{-1} min^{-1} and a mean myocardial blood volume of about 0.12 mL g^{-1}, this would lead to a mean transit time of 1.2 s. As a result, the time constant for reaching the steady-state is not affected by mean transit time, as long as fast exchange (with respect to mean transit time) is assumed.

The theoretical model was found to well describe the experimental magnetization behavior, and the signal dynamics can indeed be used to quantify MBF. Such experimental determination, however, depends on the arterial input function as shown in Figure 2.11, and is subject to quantification errors that may arise from heart rate variability or other dynamical instabilities, as in common pulsed techniques. Further investigations may focus on the magnetization dynamical behavior and may bring new insights in those phenomena.

With cine-ASL, calculating MBF from experimental data can be accomplished in a more robust way by using the equilibrium regime. The tissue magnetization indeed reaches a stationary value, which is different for control and tag scans. A major result coming from theory and corroborated by the experimental observations shown in Figure 2.12 is that the asymptotic magnetization difference between control and tag scans does not depend on the recovery delay RD. Although the original signal difference depends on RD as described in the Theory section, and the time constant differs between short RD and long RD due to magnetization input dynamics, the data evolves towards a steady-state which is independent of RD. More generally, as the stationary value of the signal is cumulatively measured, dynamic variations are averaged out throughout the experiment. Therefore, the stationary magnetization difference ΔM_∞, or preferably the stationary contrast C_∞, yields a suitable measure for assessing perfusion, by means of equation [2.23].

The precision of the perfusion quantification using this method directly depends on the different experimental parameters. As outlined in the first part of this chapter, the tagging efficiency β is submitted to some uncertainty as a result of multiple tagging of blood in the different heart chambers, but we may consider as a good approximation that the resulting blood magnetization state is close to a saturation, that is $\beta \approx 0.5$. Among the key parameters that one might wish to optimize, the flip angle α has a minor influence on the perfusion assessment. The signal contrast C_∞ is almost independent of α in a wide range of low flip angles. Therefore, the determination of MBF is robust against errors in flip angle. However, as in all FLASH sequences, the signal-to-noise ratio has to be preserved by using α close to the Ernst angle (up to minor corrections due to flow effects). The contrast also depends on myocardial T_1, and for a precise perfusion mapping, it is therefore necessary to obtain a T_1 map of the same imaging slice, requiring a separate scan.

Note that T_1 might also be estimated directly from the same measurement by fitting the dynamic part of the signal, provided that T_{AIF} is known. Nevertheless, this measurement would depend on a number of experimental conditions and might therefore not be accurate enough.

As discussed before, RD can be chosen arbitrarily short without penalty on the assessment of the asymptotic magnetization difference. One can thus significantly reduce the total acquisition time by using RD = 0, as exploited in the experimental study. This possibility is not offered in FAIR Look-Locker, for which a relatively long recovery delay is required *[Kober 2004, 2008, Jacquier 2011]*, unless the short-TR approach is used *[Pell 1999]*.

A crucial point highlighted in Figure 2.13 is that in cine-ASL experiments the signal contributing to the perfusion measurement does not vanish with time, because the magnetization difference persists as long as the experiment is running. The number of cine blocks can be increased, and relevant data can therefore be accumulated, leading to an enhanced sensitivity of the perfusion assessment as shown in Figure 2.14. Indeed, the lowest detectable blood flow MBF_{min} with the cine-ASL method can be estimated from experimental uncertainty in Figure 2.13. The standard deviation of the cine-ASL data on the plateau yields $MBF_{min} \approx 2.4$ mL g^{-1} min^{-1}. By averaging N data values, the uncertainty diminishes with the square root of N, thereby lowering the detection minimum. As an example, averaging 30 cine blocks yields a detection minimum $MBF_{min} \approx 0.44$ mL g^{-1} min^{-1}, the detection threshold can thus be significantly improved.

The sequence proposed here maintains the labeled state by steadily repeating a pulsed inversion. Continuous and pseudo-continuous labeling schemes maintain the labeled state in an even more efficient way, but these methods are well adapted only when the labeling zone is well accessible (e.g. the carotid for brain studies). Indeed, these methods have proven superior sensitivity versus pulsed techniques *[Wong 1998]*, but the implementation of adiabatic flow-driven inversions is problematic in the heart for multiple reasons such as motion of the aorta, location, timing and pulsatile flow of the blood feeding the coronaries. The method proposed here provides a way of benefiting from the advantages of CASL or pCASL in the heart, although the labeling itself is pulsed.

Cine-ASL also has some of the known drawbacks of continuous labeling techniques. In the mouse heart, MT effects induced by the rapidly repeated inversion pulses can be considered as strong. Here, a PICORE-like scheme *[Wong 1997]*, placing a control labeling slab symmetrically to the imaging slice was used, although this approach cannot directly be used for multi-slice imaging, due to symmetry issues. We note, however, that the transfer insensitive labeling technique (TILT) labeling strategy *[Pruessmann 2000]* is intrinsically MT-compensated and would meet the requirements for a multi-slice acquisition. Compatibility of TILT in a context of tight timing and motion constraints would have to be proven first. Conceptually, specific absorption rate is not a limitation in this steady-pulsed scheme, which uses low flip angles for imaging and a typical duty cycle of 5% for the inversion performed once in a cardiac cycle.

2.4.   Conclusion

We present a new ASL tagging and readout scheme to quantify MBF in vivo in mice. The steady-state labeling approach combined with a cine-FLASH readout module were used to average the steady perfusion-dependent magnetization difference over several cardiac cycles to improve acquisition efficiency. The scheme is experimentally shown to be more sensitive than the previously employed LLFAIRGE method, although the latter has the advantage of providing T_1 maps inherently. According to our finding, MBF determined with cine-ASL technique in the fourteen isoflurane-anesthetized mice was 5.0 ± 0.8 mL g^{-1} min^{-1}. Results on MBF obtained with cine-ASL were not significantly different compared to LLFAIRGE measurements carried out within the same protocol. In addition to shorter acquisition time, this technique has the further advantage of being feasible with short transmit coils because it does not rely on global inversion of a large volume of blood.

We developed a model providing the ability to quantify MBF with the cine-ASL technique and giving insight into magnetization dynamics during the sequence. In agreement with experimental observations, the model showed that the cine-ASL technique yields significantly higher acquisition efficiency than previously used FAIR Look-Locker approaches. This sensitivity gain has been exploited to assess myocardial perfusion in humans as presented in the following chapter.

Some specific optimizations of the cine-ASL sequence have been done subsequently to this validation study and are presented in Chapter 4. Here, the repetition time of 8 ms was sufficient to obtain good temporal resolution within the cardiac cycle. Due to current hardware limitations on site, the inversion pulse duration was initially fixed to 6 ms, which was a limiting factor regarding repetition time and therefore cine frame rate. By using shorter inversion pulses and TR, higher temporal resolutions became feasible allowing to correlate magnetization difference changes and perfusion variations across time. High temporal resolution MBF maps were obtain in rats in order to study dynamic MBF changes over the entire cardiac cycle at rest and during adenosine-induced stress. Also note that in this work, k-space was fully segmented acquiring one line per tag/control series. Further investigations have been carried out to shorten the total acquisition time by optimized k-space segmentation. This fast and optimized version has first been validated and is now integrated in different protocols, including a multimodal MRI/MRS protocol to study cardiac function, perfusion and triglyceride content in two rodent models of type-2 diabetes.

Chapter 3 - The Steady-Pulsed Labeling Scheme: Transition to Humans

---

Contents

3.1. Introduction

ASL appears as a powerful, direct and non-invasive alternative to first pass MRI techniques for assessing myocardial blood flow in humans. Although ASL has become a routinely performed method in the rodent heart, its application to the human heart remains challenging. Low tissue blood flow compared with rodents, motion constraints and physiological noise are major difficulties in a reliable assessment of human myocardial perfusion by ASL. Despite these difficulties, several groups have successfully performed ASL in the human heart *[Wacker 2003, Northrup 2008, Zun 2009a]*. And shown its ability to assess myocardial perfusion reserve *[Zun 2011]*.

In these experiments, sensitivity and robustness of the perfusion assessment were limited by both a weak signal inherent to the ASL method (about 2%) and by low acquisition efficiency due to the alternation of pulse and relaxation periods in the acquisition scheme. As a result, these methods remain subject to strong physiological noise limiting the accuracy of myocardial blood flow (MBF) quantification *[Zun 2009a]*. Sensitivity improvement and the reduction of physiological noise are therefore still of major interest for assessing myocardial perfusion using ASL in the human heart.

As the new proposed steady-pulsed approach lowers the detection limit for the assessment of myocardial perfusion, there is great potential for a translation to the human heart provided that the experimental scheme can be made compatible with physiological constraints in human studies.

In this chapter, we propose to adjust the previously proposed steady-pulsed ASL (spASL) technique for improving sensitivity in human heart applications. The spASL approach was expected to be more efficient than PASL in a similar way as observed in the rodent heart. A similar technique was thus proposed to measure MBF in the human heart by keeping the spASL scheme but with a different readout strategy. This technique was implemented for a free-breathing acquisition along with a simple contour correlation-based image selection algorithm. The proposed spASL approach was compared in terms of signal and perfusion quantification with the earlier used multiple-breath-hold FAIR technique *[Zun 2009a]* in 13 healthy volunteers.

Subsequently to this initial feasibility study, optimizations have been made in the acquisition and in the post-processing algorithm. Regarding acquisition, these improvements include a higher spatial resolution and a shorter acquisition window within the cardiac cycle by use of accelerated parallel imaging. Post-processing was improved by developing a rigid motion correction (Moco) and a specific signal measurement algorithm. The Moco algorithm allows a larger portion of acquired data to be included in the perfusion quantification. Combined with the increased spatial resolution, these improvements represent another step toward the feasibility of MBF mapping in humans using ASL.

3.2. Myocardial Perfusion Assessment in Humans

This section is based on:

Myocardial Perfusion Assessment in Humans using Steady-Pulsed Arterial Spin Labeling. Submitted for publication in Magn. Reson. Med. (under revision).

Capron T, **Troalen T**, Robert B, Jacquier A, Bernard M, and Kober F.

Our first investigations made for the transition to human studies focused on a direct implementation of the cine-ASL sequence on our clinical scanner. The images obtained were strongly influenced by flow artifacts due to the FLASH readout. Thus, an adaptation of the cine-ASL scheme using bSSFP as readout module was attempted. Several groups have indeed shown that balanced steady-state-free-precession (bSSFP) sequences are superior to gradient echo techniques from the standpoint of image quality, spatial resolution, SNR and sensitivity to flow artifacts *[Schreiber 2002, Hunold 2004, Gebker 2005, Wang 2005]*. bSSFP images have greater contrast at the endocardial border (blood/tissue) with less blood flow dependence and also greater contrast at the epicardial border (fat/tissue). More importantly, they provide better signal-to-noise ratio compared with FLASH, although this advantage is more important at lower field strengths.

All fast gradient-echo sequences can be considered as a SSFP technique, even FLASH which could be seen as a spoiled-SSFP or as a spoiled-fast-gradient-echo. The major difference between FLASH and bSSFP comes from the gradient pattern between two excitation RF pulses (Figure 3.1). The bSSFP sequence is a particular SSFP with no spoiling gradients and in which all gradient waveforms are balanced, that is the gradient-induced dephasing within TR is exactly zero.
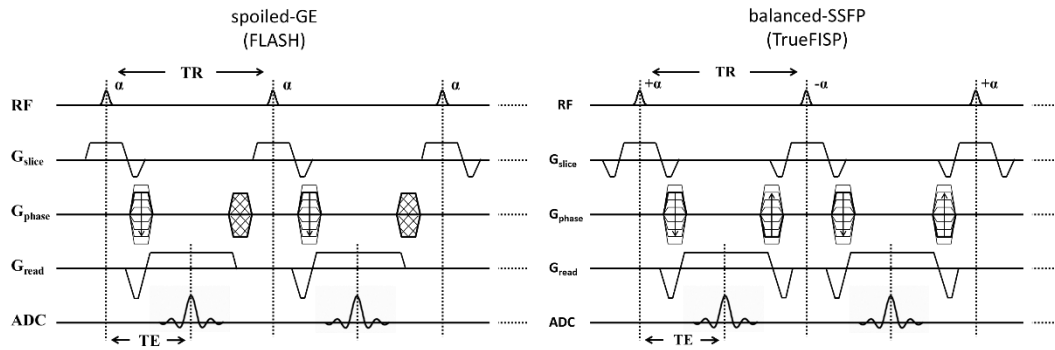
Figure 3.1 – Sequence chronograms: Spoiled gradient-echo or Fast Low-Angle Shot (left) and balanced Steady-State Free-Precession (right). For the FLASH sequence, a spoiler is applied after the echo such that the residual transverse magnetization is not refocused and can be neglected. For the bSSFP pulse sequence, all gradient waveforms are fully rewound, or balanced, over a repetition. The RF pulse sign usually alternates in bSSFP, so that a high signal is produced for on-resonant spins. Adapted from [Scheffler 2003].

The steady-state of bSSFP sequences is known to be less robust than in FLASH sequences *[Scheffler 2003]*, such that inserting an inversion pulse within the echo train as done in cine-ASL (cf. Chapter 2) is not straightforward. The technical constraints for such an implementation are that the duration of the inserted components (RF pulse and associated gradients) has to be shorter than the repetition time TR, which in SSFP must be equal to 2 TE, and that every inserted gradient shape must have a null moment within TR. However, adiabatic inversion pulses have

comparatively long durations. A scheme with a long TR and a magnetization preparation pulse inside a cine-bSSFP sequence (without steady-state interruption) was studied. The signal was subject to strong fluctuation due to transverse magnetization created by the labeling pulse itself causing a second and overlaying image signal, which indicated that the spoiling of the inversion pulse was insufficient.

An alternative way of magnetization-preparation during an bSSFP pulse train *[Scheffler 2003]* is to temporarily interrupt the transverse steady-state by storing the steady-state magnetization via $\alpha/2$ pulses before magnetization preparation, and to recall the steady-state after preparation (Figure 3.2). This type of interruption has not yet been implemented and will therefore be part of future work, which should enable the acquisition of a cine readout while preventing from the encountered signal disturbances.

Figure 3.2 – Principle of contrast modification during the steady-state of bSSFP. The steady-state magnetization is stored along the z-direction before magnetization preparation, and is recalled after preparation. Adapted from [Scheffler 2003].

In a simplified version, we thus decided to pursue a snapshot bSSFP strategy rather than using a cine readout. The spASL labeling was implemented as a classical magnetization preparation pulse occurring prior to snapshot bSSFP acquisition at each cardiac cycle. Considering that the pulsatility of coronary flow is similar between rodents and humans, the labeling still has to occur at end-systole while an entire image can be acquired later during a stable cardiac phase, i.e. mid- to end-diastole.

Compared to rodents, the efficiency of a spASL acquisition is further limited by the available duration of a breath-hold, which is of the order of 20 seconds. We recall here that the steady-state after start of a labeling block is only reached after 4-5 seconds. Therefore, 5 to 6 heart beats are necessary to build up the steady-state under the influence of labeled blood. Considering that the typical length of a breath hold in healthy subjects is around 20-25 seconds, only 12 tag/control pairs could be acquired within the available time. It would result in having about 6 pairs useful for perfusion quantification and we assumed that this was not sufficient for a reliable perfusion measurement in humans. We thus decided to develop a free-breathing acquisition allowing for longer data accumulation durations, though at the expense of a more complicated post-processing algorithm.

Using a bSSFP readout, one point of interest of this section therefore consists in the extension of the theoretical model that had been initially developed for FLASH type sequences *[Capron 2013]*. From a theoretical point of view, the steady-state establishment can be described by a mono-exponential formula as well *[Scheffler 2003]*, such that only the values for T_1^* and M_{ss} have to be updated.

78

3.2.a.   Methods

Sequence design

The steady-pulsed ASL technique was implemented in a standard bSSFP sequence using Siemens IDEA VB 17 software. An ECG-triggered bSSFP acquisition during diastole (T_{SSFP} = 334 ms / TR = 3.22 ms / TE = 1.61 ms, flip angle 50°, slice thickness 10mm) was combined with RF-pulse labeling applied in end-systole (Sech 15 ms) yielding one image at each cardiac cycle (Figure 3.3).
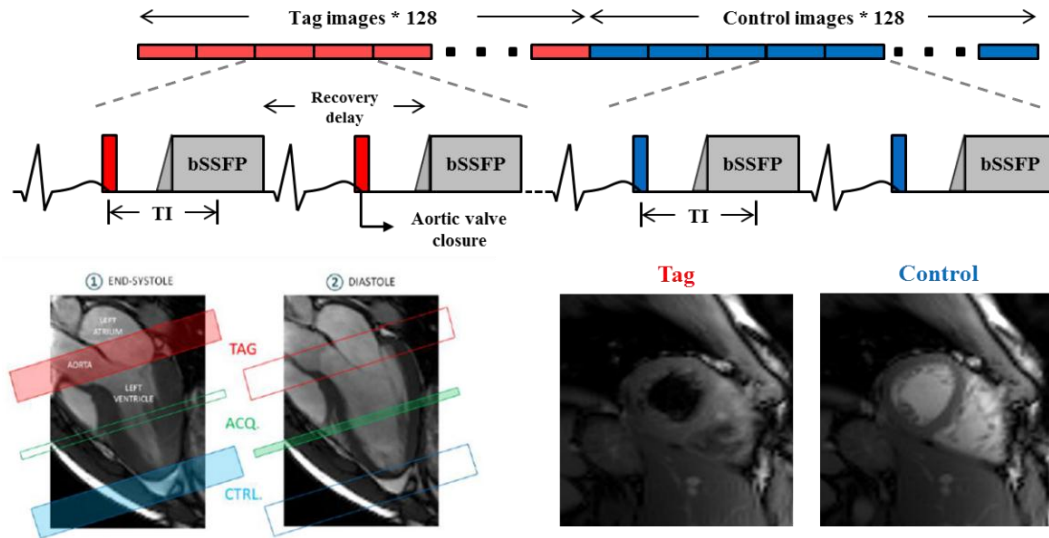

Figure 3.3 – Schematic description of the spASL sequence showing triggered bSSFP acquisition during diastole combined with RF-pulse labeling applied in end-systole at each cardiac cycle (top). 128 tag and control short-axis images are acquired sequentially under free breathing. Position of the tag and control slabs in symmetry to the imaging slice, chosen from a left ventricular outflow tract image of the heart (bottom left) and corresponding raw images (bottom right).

The block duration T_{SSFP} as defined here did not include the bSSFP state initialization pulses and dummy scans (10-tip linear ramp + 10 dummy scans). The labeling slab of 60 mm thickness was placed in the basal heart for the Tag scans so as to cover the aortic root. The gap between labeling slab and image slice was approximately 4 cm, but slightly dependent on the cardiac volume. Due to the high blood velocity in the main coronary arteries, the small distance variations should only weakly contribute to the arterial transit time ATT. As for the cine-ASL sequence, control scans were acquired with the inversion slab positioned in symmetry to the imaging slice so as to compensate for MT effects. A series of 128 tag images followed by a series of 128 control images (short axis view, FOV 244 x 300 mm², matrix size 104 x 128) were acquired in order to maintain the respective tag and control steady-states while the subject was freely breathing. Rectangular FOV was used to keep the acquisition block as short as possible. The total duration of the acquisition was about 4 minutes.

bSSFP acquisition modules were chosen for their robustness to flow artifacts and their higher SNR in the cardiovascular context. The image acquisition time T_{SSFP} = 334 ms was always much smaller than the respiratory period $T_{resp} \approx 3500$ ms. The position of the myocardium, however, was different in successive images due to the breathing motion. This sequence allowed for driving

the tissue magnetization into a perfusion dependent steady-state while maintaining compatibility with human heart constraints. In contrast to the cine-ASL sequence, however, the labeling pulse was played out prior to and not within each acquisition block in order to avoid signal disturbances and oscillations due to bSSFP steady-state interruptions.

Protocol

Thirteen healthy volunteers were included in the study, 8 men and 5 women (29.5 ± 6 years). All subjects gave written and informed consent to their participation in the study. The protocol was approved by the institutional ethics committee (CPP). Data were acquired on a Siemens Verio 3T clinical MRI scanner using a 32-channel phased array receiver coil. After standard adjustments and field map-based shimming, a cine-MRI scan was performed in left ventricular outflow tract orientation to visualize the aortic valve. This cine series was used to choose timing and location of the labeling pulse in the spASL sequence. The labeling slab was positioned in the aortic root, and the labeling pulse was played out at the instance of aortic valve closure measured for each subject.

A first set of data was obtained with the spASL sequence described above, setting the slab thickness to 60 mm. In order to prove that the signal indeed results from capillary blood flow and not from residual motion of any kind (respiratory, cardiac) during acquisition, a second spASL scan was performed with a slab thickness reduced to its minimum (3 mm), so that the resulting blood labeling was negligible. The slab thickness was minimized rather than the pulse removed, since this way all sequence properties inducing MT remained unchanged. Repeatability was investigated with a third scan, setting back the slab thickness to 60 mm. In order to evaluate the magnetization behavior at the onset of the sequence during the transient phase, all subjects were submitted to an additional spASL breath-hold acquisition allowing for a series of 8 tag/control pairs, and the group standard deviations during breath-hold were compared with the free breathing situation over a similar duration.

A comparison with a FAIR-SSFP method as published by Zun *et al.* was performed *[Zun 2009a]*. We implemented this sequence with FAIR labeling (selective/non-selective Sech pulses) in diastole and bSSFP acquisition in the following diastole such that the inversion time TI matched the duration of the cardiac cycle. The sequence parameters including FOV, slice thickness, matrix size, repetition time and flip angle were identical to those used with spASL. As proposed by Zun *et al.*, images were acquired during six breath-holds followed by an additional short breath-hold for baseline image acquisition.

Since both spASL and FAIR perfusion quantifications depend on T_1, a T_1-map was acquired for each subject using a sequence provided by the MRI manufacturer based on MOLLI *[Messroghli 2004]*. Heart rate and breath rate were continuously monitored during the experiment.

In order to assess the MBF response to modified physiologic conditions, two subjects were submitted to a cold pressor test (CPT) by immersing the volunteer's left hand into ice water during acquisition of an additional spASL scan (4 minutes). CPT has been shown to increase MBF in previous work using PET *[Schindler 2007]* or MR coronary sinus flow measurement *[Moro 2011]*. Blood pressure was measured by a cuff at calf level before and during acquisition. A summary of the CPT parameters is presented in Table 2.

With the theoretical description of the cine-ASL sequence, the signal behavior has been described for a similar steady-pulsed experimental scheme. The model was based on the fast exchange assumption in the mouse heart, which can be considered valid for human myocardium as well. The main difference arises from the fact that in this work, bSSFP readouts were used instead of FLASH.

With bSSFP sequences, the signal evolution can be described using:

$$M_{ss} = \frac{M_0\left(1 - e^{-2TE/T_1}\right)}{1 - \left(e^{-2TE/T_1} - e^{-2TE/T_2}\right)\cos\alpha - e^{-2TE/T_1}e^{-2TE/T_2}} \cdot \frac{\sin\alpha}{\tan(\alpha/2)} \qquad [3.1]$$

and

$$T_1^* = \left(\frac{1}{T_1}\cos^2(\alpha/2) + \frac{1}{T_2}\sin^2(\alpha/2)\right)^{-1}, \qquad [3.2]$$

where M_{ss} is the steady-state longitudinal magnetization, M_0 the equilibrium magnetization, α the flip-angle, T_1 the longitudinal relaxation time, T_2 the transverse relaxation time and T_1^* the apparent longitudinal relaxation time *[Scheffler 2003, Schmitt 2004]*. Note that the right hand side of the equation for M_{ss} had to be multiplied by the projection term $\sin(\alpha)/\tan(\alpha/2)$, since no flip-back pulses were used at the end of the bSSFP pulse train, leading to only partially exploited magnetization in bSSFP. In order to restitute the longitudinal magnetization at the end of each acquisition train, the flip-back pulse has been integrated in the latest version of the spASL sequence and is expected to increase the ASL signal.

With cine-ASL, the following relation between perfusion and magnetization difference was obtained for a FLASH perfusion-dependent steady state:

$$C_\infty = \frac{2\beta}{1 + \dfrac{\lambda M_{ss}}{f T_1^* M_0}} . \qquad [3.3]$$

This formula has the advantage to be independent of M_0, and the contrast only depends on known parameters TR, α, T_1, λ, β. The capillary blood flow f can therefore be determined by a contrast measurement in a similar way as with cine-ASL.

Using SSFP acquisition, an important simplification occurs, since $2TE \ll T_{1,2}$:

$$\frac{M_{ss}}{T_1^*} = \frac{M_0}{2T_1}\frac{\sin\alpha}{\tan(\alpha/2)}, \qquad [3.4]$$

and therewith

$$C_\infty = \cfrac{2\beta}{1 + \cfrac{1}{2}\cfrac{\lambda}{fT_1}\cfrac{\sin\alpha}{\tan(\alpha/2)}} \;,$$ [3.5]

which was used for quantification in this work. The contrast C_∞ was experimentally obtained from the measurement of the control $\left(M_\infty^c\right)$ and the tag $\left(M_\infty^t\right)$ steady-state values:

$$C_\infty = \frac{M_\infty^c - M_\infty^t}{M_\infty^c} \;.$$ [3.6]

Within the proposed experimental scheme, image acquisition occurs during the time $T_{SSFP} = 334$ ms, and a recovery delay RD is set between each acquisition block. As a result of ECG-triggering, RD = (RR - T_{SSFP}) for each cardiac cycle as presented in Figure 3.3. The equations do not depend on RR as long as the RR variations remain small compared with T_1. Therefore heart rate variations had a small impact on signal stability.

For estimating β, we took blood signal in the LV as a starting point and the following considerations. Ventricular blood is ejected in systole and flows through the coronaries to the capillary bed in the following diastolic phase. The initial state of blood magnetization before entering the coronaries can therefore be measured in the LV blood region on the ASL raw images. In our series, the relative amount of remaining blood magnetization in the LV was $M_{tag}^b/M_{ctrl}^b =$ 15.5%, and we therefore assumed saturated LV blood for the tag image series. On its way from the LV to the capillary bed, LV blood first undergoes a period of relaxation with T_1^b. The duration of this period is taken as the delay between the image k-space center and the following inversion pulse in the next cardiac cycle (duration RR – TI). Blood is then inverted again by the inversion slab in the aortic root and again relaxes during an arterial transit time ATT before reaching the capillary bed. Using a single-exponential Bloch-model to describe relaxation during each of these two consecutive periods of durations (RR-TI) and ATT, the magnetization at the entry of the capillary system can therefore be estimated by two Bloch relaxation terms separated by an inversion leading to:

$$\beta = \left(1 - 1/2 e^{-(RR-TI)/T_1^b}\right)e^{-ATT/T_1^b} \;.$$ [3.7]

Using FAIR ASL in the human heart with different inversion times, ATT was estimated by Wang *et al.* to be around 400 ms *[Wang 2010]*. We assumed that similar ATT values can be considered in the spASL experiment as well, since the distance traveled from the aortic root to the imaging slice is only slightly longer than that in FAIR, and the velocity in the coronary vessels is high. T_1^b was set to 1.69 s as measured in the MOLLI T_1 experiment. Using Equation [3.7] with these values, we obtained β values of around 0.5.

The magnitude image series obtained with the spASL sequence was first filtered by global intensity, such as to exclude images acquired during the transient regime after start of the series or after switch from control to tag scan. This filter also excluded images acquired after occasionally missing ECG trigger pulses that led to loss of steady-state and signal increase. This resulted in keeping about 80% of the acquired data. Since the acquisition was done during free

breathing, the myocardium underwent position changes throughout the series (Figure 3.4). All control/tag difference images were then averaged and the resulting signal was evaluated in the myocardium and the chest muscle.

To assess regional perfusion only when the myocardium was at equal positions, the following contour-based selection algorithm was applied. A Canny-Deriche edge-enhancement filter (upper threshold 0.8, lower threshold 0.4, and sigma 0.6) was applied to each image. A region covering the analyzed myocardial segment was manually drawn, and within this region, the cross-correlation coefficient (CC) of contour image pairs was calculated for every possible control and tag combination. The contour-based selection and signal evaluation were done in each ROI separately. A CC acceptance level was set such that the 30% best-correlated pairs of the scans were retained. However, the measured signal showed only slight changes when the acceptance level was varied between 10 and 50%. In order to remove potential bias related to the very high bulk-flow blood signal in the LV cavity, the signal difference maps were masked with an intensity threshold. The threshold was symmetric to zero and set manually and individually until the endocardial rim introduced by limited spatial resolution and partial volume disappeared (Figure 3.5). Perfusion was assessed from the signal averaged from all unmasked remaining pixels in the ROI. After removal of the endocardial rim, about 35 to 50 pixels were retained for each region, and there were three transmural pixel ranges available for quantification. The group average myocardial T_1 measured with the MOLLI sequence was used for all calculations.

For the FAIR-SSFP sequence, signal was quantified as described in the introduction *[Zun 2009a]*. In order to allow for comparison with the steady-pulsed method, the relative FAIR-SSFP signal was defined as $S_{FAIR} = (C - T)/B$ where C, T and B refer to the mean signal from a ROI in control (slice-selective), tag (non-selective) and baseline images. C, T and B were obtained as average in regions that were manually segmented in the same four locations assessed with spASL for each breath-hold, averaged over multiple breath-holds. MBF was then obtained using:

$$MBF = \frac{S_{FAIR}}{2RR\,e^{-RR/T_1^b}}\,.$$

[3.8]

3.2.b.   Results

Selection procedure

A series of images approximately covering a complete respiratory cycle, with tag (top) and control (bottom) labeling, is shown in Figure 3.4. The image selection process is also illustrated on the right side. The contour cross-correlation is calculated for each pair in a manually defined ROI shown in the last images. Among all control/tag pairs, the top right image of Figure 3.4 shows the best cross-correlation, whereas the bottom right shows the worst case for illustration. Grey pixels indicate discordance between control and tag contours, whereas white and black pixels show well overlaying contours.
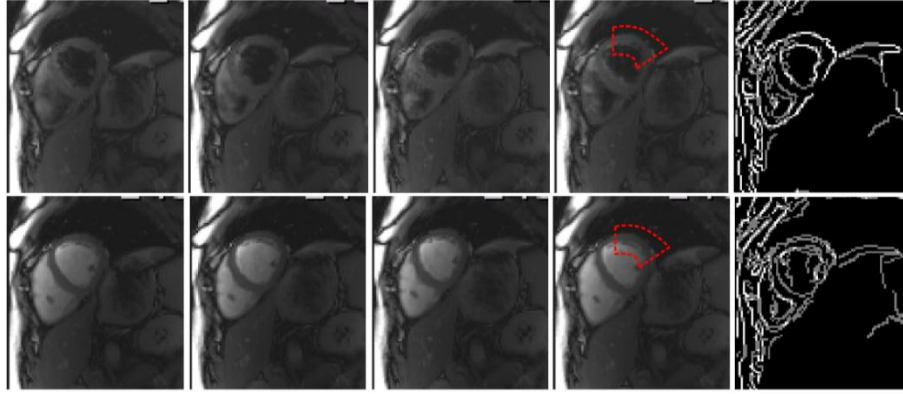
Figure 3.4 – Series of four tag (top) and control (bottom) images showing respiratory motion and motion handling. A lateral myocardial region was defined (dashed lines in the fourth column), and control/tag pairs were chosen based on their contour cross-correlation coefficient within the chosen region. For illustration, the top right image shows the best correlated pair and the bottom right image the worst correlated case. Grey pixels represent discordance between contours, whereas black and white pixels are displayed when control and tag contours are superimposed.

Signal measurement

The signal difference map calculated from selected images of a freely breathing subject is shown in Figure 3.5A. For this map, the selection was based on contour correlation within a region covering the entire heart. To show the initialization of the steady state under free breathing compared with breath-hold, the average myocardial signal difference measured for 8 successive tag and control scans in all subjects is shown in Figure 3.5B under breath-hold and free-breathing. The stationary magnetization difference, which is related to perfusion by equation [3.5], was reached after about 5 to 6 heartbeats, and the signal stability was found to be comparable between breath-hold and free breathing acquisitions (dispersion 8%).

The group average of signal difference values are shown in Figure 3.6 for the tag experiment (labeling slab 60mm) along with the 'no tag' experiment (labeling slab 3mm). The chest muscle can be assumed to be perfused with unlabeled blood, since the time for blood to travel from the heart to the chest muscle is long compared with T_1. In two subjects, insufficient stability of the signal over time was found in the 'no tag' scan and were excluded from the analysis. For comparison, Figure 3.6 also shows the FAIR signal difference measured in the group.

MBF calculated from the spASL signal using equation [3.5] as well as that obtained with FAIR is shown in Figure 3.7 for four segments of myocardium. Global MBF was obtained by averaging the values from the four segments. For comparison, perfusion procedure was also applied to the signal obtained in the chest muscle with FAIR and spASL techniques. From the MOLLI sequence at 3T, the group mean ± SD T_1 values in myocardium, chest muscle and blood were found as T_1^{myo} = 1.16 ± 0.03 s, T_1^{muscle} = 1.06 ± 0.05 s and T_1^b = 1.69 ± 0.04 s respectively. MBF averaged over all myocardial regions was MBF$_{spASL}$ = 1.28 ± 0.36 mL g^{-1} min^{-1}. Using the FAIR technique, MBF was calculated using equation [3.8], with T_1^b = 1.69 s and RR measured for each subject. The FAIR data yielded a group average MBF$_{FAIR}$ = 1.32 ± 0.47 mL g^{-1} min^{-1}. Individual results are summarized in *Table 3.1*.

84

A

Signal Map $\Delta M_\infty = \frac{M_\infty^C - M_\infty^T}{M_\infty^C}$ (%)
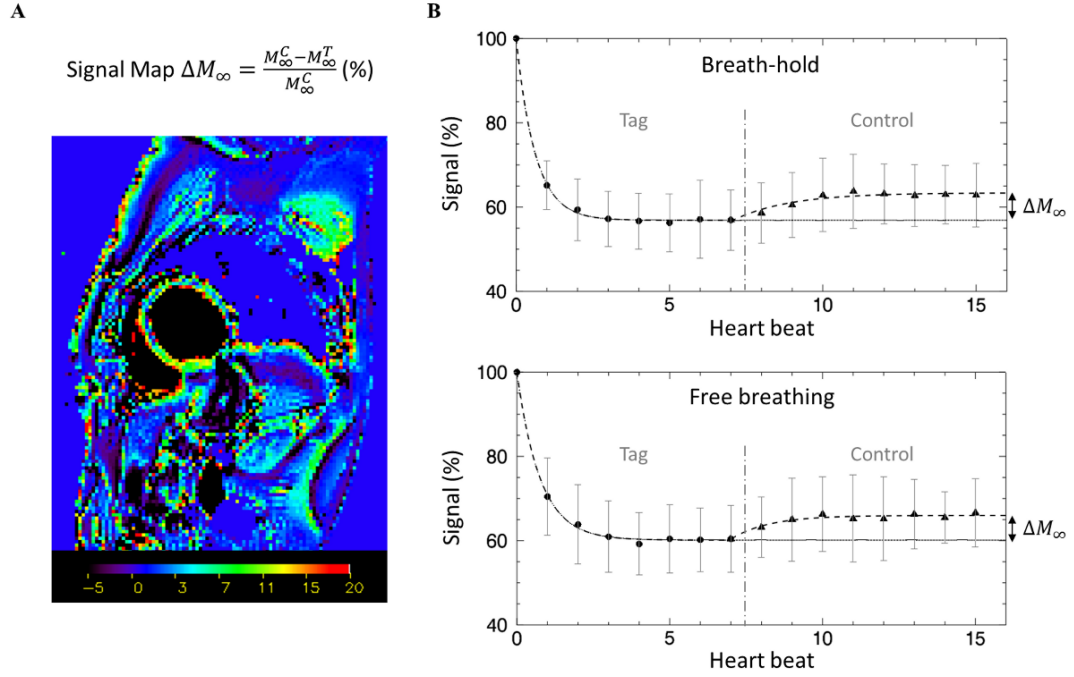

B

Figure 3.5 – (A) Typical signal map obtained in a representative subject. (B) Myocardial signal evolution during steady-state initialization. The data were experimentally obtained for the first 8 successive tag and control scans during the breath-hold experiment (top) and during free breathing (bottom). In the stationary regime, the magnetization difference ΔM∞ depends on perfusion. During the steady state, the standard deviations of signal over time were comparable between breath-hold and free breathing acquisitions (~ 8%).
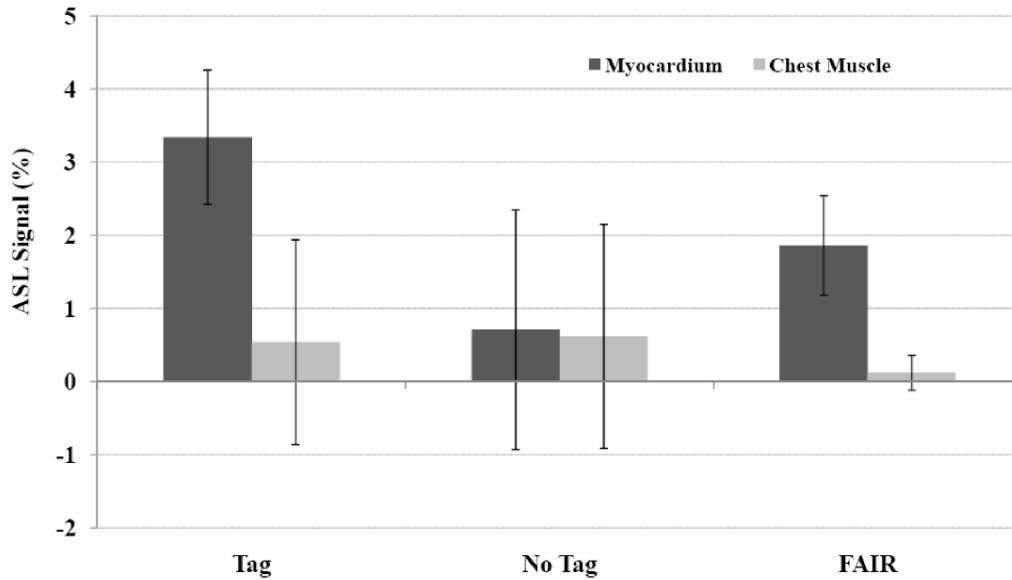

Figure 3.6 – Mean contrast signal in % obtained in the myocardium (dark grey) and the chest muscle (grey). Signal was measured with the "Tag", "No Tag" and "FAIR" procedures as described in the text. Error bars show group standard deviation (N=11).
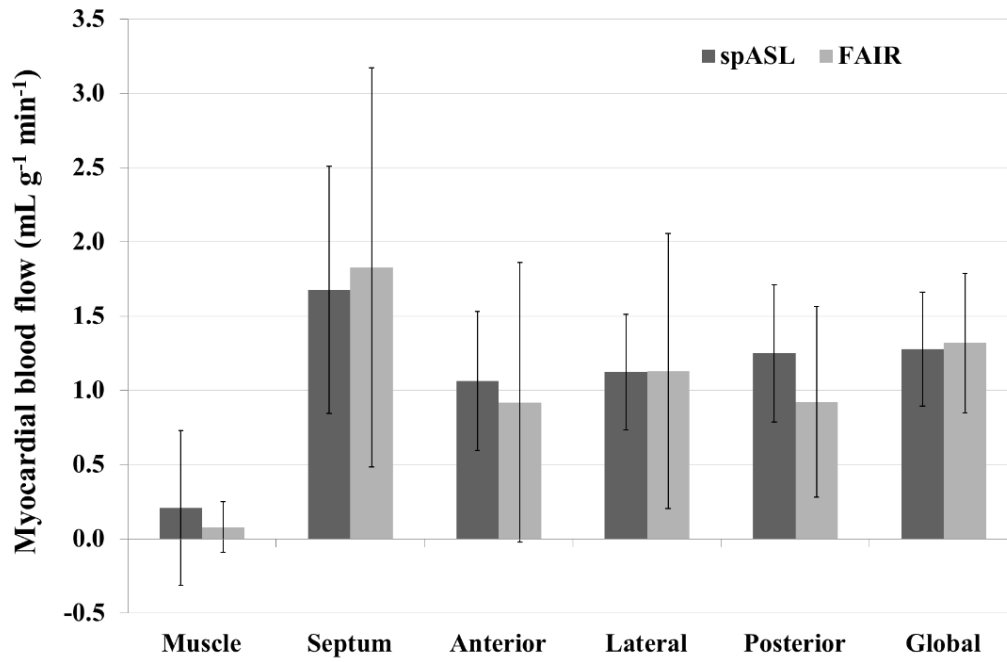
Figure 3.7 – Mean MBF in mL g^{-1} min^{-1} obtained in four regions of the myocardium, chest muscle, as well as global MBF, comparing spASL (dark grey) and FAIR (light grey). Error bars show group standard deviation (N=13).

Table 3.1 – Individual characteristics and results of MBF measurements using FAIR and spASL in the group of healthy volunteers as well as repeatability across consecutive measurements. SD_{Rep}^{FAIR} for FAIR represents the standard deviation across six repetitions, whereas Δ_{Rep}^{spASL} is the variation between the two spASL measurements. N_{Avg} corresponds to the number of tag/control pairs averaged for MBF quantification with spASL. The two subjects undergoing CPT are marked with an asterisk.

Age Gender	HR (bpm)	BR (bpm)	MBF$_{spASL}$ (mL g^{-1} min^{-1})	MBF$_{FAIR}$ (mL g^{-1} min^{-1})	$\Delta_{Re\,p}^{spASL}$	$SD_{Re\,p}^{FAIR}$	N_{Avg}
28M	64	17	1.46	2.33	0.12	1.23	23
26F	56	13	1.41	1.06	0.03	0.74	23
25M	65	16	1.36	1.47	0.41	0.40	29
44M	67	14	1.02	1.45	0.13	0.59	26
29F	69	18	1.79	1.11	0.02	0.91	22
29F	76	18	1.22	1.94	0.04	2.83	30
24F	70	17	1.65	1.44	0.10	0.68	27
26M	54	16	0.43	0.73	0.19	0.65	14
20M	89	17	1.60	1.57	0.44	0.62	27
30F	81	16	1.00	0.71	0.08	5.43	24
28M	80	14	1.47	0.85	0.21	0.9	23
*32M	65	18	0.94	0.98	0.01	0.67	34
*33M	66	19	1.29	1.50	0.12	1.08	30
Average	69	16	1.28	1.32	0.15	1.75	26
± SD	± 10	± 2	± 0.36	± 0.47	± 0.14	± 1.41	± 5

Intra-subject repeatability was evaluated from the two measurements performed at about 4 minutes interval during the protocol. Results are depicted as a Bland-Altman plot in Figure 3.8A (grey). Since the placement of the different regions of interest and image thresholding might vary from one observer to another, inter-observer variability was evaluated by comparing MBF values obtained from two different readers following the procedure described in the Methods section. Results are shown in the Bland-Altman plot in Figure 3.8A (dark grey).

Results of the stress test carried out in two subjects are shown in Figure 3.8B. Hemodynamic response to CPT was characterized by a significant blood pressure increase and stable heart rate. MBF was found larger for both subjects, although one subject only showed a minor increase (8 % and 56 %, respectively). Parameters of this experiment are summarized in

Table 3.2. Heart rate varied by less than 5% in a single subject along the 4 minutes acquisition, at both rest and moderate-stress states. The standard deviation of RR interval variability was estimated at 28 ms in the group at rest. During stress test, blood pressure was measured three times yielding systolic and diastolic pressure variabilities of 7 mmHg and 4 mmHg, respectively.
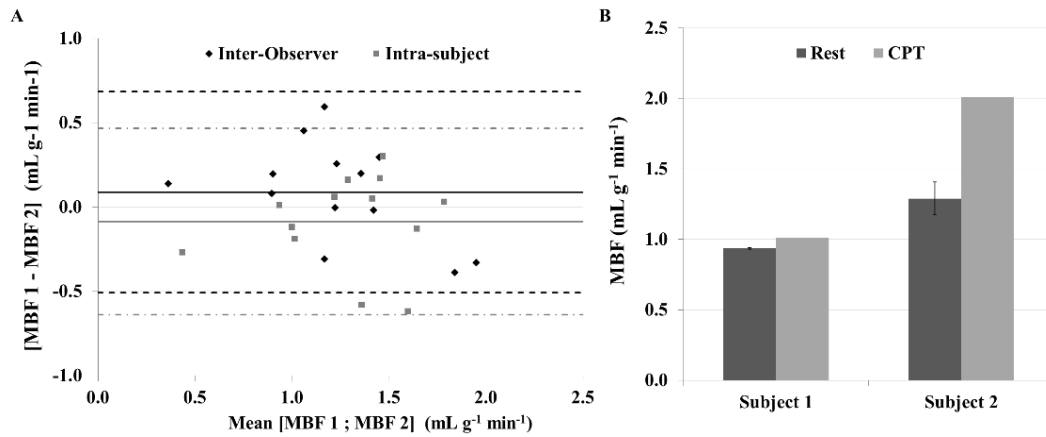
Figure 3.8 – (A) Bland-Altman plot of individual MBF measurements illustrating inter-observer (black diamonds, N=13) and intra-subject (grey squares, N=13) repeatability. (B) MBF increase in response to CPT for two subjects. Error bars show standard deviation of repeated measurements at rest.

Table 3.2 – Cold pressor test parameters in two subjects. Blood pressure (BP) was measured at calf level during acquisitions. MBF was assessed with the spASL technique.

		HR (bpm)	BP Sys/Dia (mmHg)	MBF (mL g^{-1} min^{-1})	ΔMBF (%)	ΔMBF/ SD_{Rep}
T12	Rest	65	117/57	0.94	8	13.0
	CPT	64	154/81	1.01		
T13	Rest	66	105/56	1.29	56	4.7
	CPT	69	139/68	2.01		

3.2.c. Discussion

In order to improve the sensitivity of myocardial ASL in humans, we have implemented an alternative steady-pulsed labeling method for acquiring a series of perfusion-weighted cardiac images under free breathing. The results obtained in 13 healthy volunteers showed that the technique yielded a higher intrinsic signal than the FAIR method. Although the post-processing procedure can still be improved, the method offers efficient averaging capability and good reproducibility. Signal increase during CPT could also be shown.

Free-breathing acquisition is an important advantage as compared to breath-hold techniques when targeting pathological populations. Concerning the selection of free-breathing images, we note that from a perfusion-weighting point of view, all steady-state image pairs contain the same information. Any pair can therefore be formed within the series. Out of the 128*128 possible combinations, only 30% were typically accepted by the algorithm. As presented in the following section, the post-processing can be improved regarding respiratory motion handling.

The signal difference within image pairs was related to perfusion by an equation derived from the previously reported theoretical model used for cine-ASL acquisition in rodents. Using bSSFP sequences with short TE, the quantification simplifies to equation [3.5]. As a result, a single T_1 map was sufficient for quantification. The transient signal behavior reported in Figure 3.5 arises from the successive alternation of labeling-acquisition and relaxation periods. Such a steady-pulsed scheme was modeled in previous theoretical work, and showed that the transient regime is mainly characterized by TR and RD. In our setting, we used $T_{SSFP} = 334$ ms and RD ≈ 470 ms in group average, and observed signal convergence to the steady-state after about 5 to 6 heart beats, in accordance with theoretical predictions. Nevertheless, the contrast itself is independent of RD, so that arrangement of the steady-pulsed scheme only affects the signal convergence, as illustrated in this case.

As presented in Figure 3.6, spASL consistently provided signal in the myocardium, whereas insensitive regions like chest muscle showed no measurable signal although a tendency to a positive offset existed. Also, when neutralizing the labeling, good signal nulling was obtained. In comparison with the earlier employed FAIR-SSFP technique, a larger signal was found with the spASL method. Due to the perfusion-dependent steady-state feature, spASL gives intrinsically larger signal than the single-TI FAIR method. When comparing the results between FAIR and spASL, one has to keep in mind that the sensitivity advantage of spASL is also owing to the large number of acquired signals, since it was applied in a free-breathing implementation, whereas the labeling efficiency including arterial transit times should be significantly better with FAIR. Since relatively long relaxation periods are required for FAIR-SSFP, it does not acquire a sufficient number of images per time for allowing retrospective image exclusion.

Global MBF obtained with both methods was in good agreement. A paired Student's t-test carried out on global MBF yielded $P = 0.77$, although the regional values had a rather large distribution particularly for FAIR. Also, both methods showed higher values in the septum. Since the septum is bordered on both sides by chamber blood the higher blood flow values are likely due to residual influence of LV and RV chamber blood signal that was not completely masked. As this variation was small, however, it shows that masking was relatively efficient in our experiment.

88

Table 3.1 shows also some particularly strong-differing values between FAIR and spASL. This might be caused by breathing motion that influences the data differently for spASL and FAIR. In some cases, breathing patterns on the one hand and stability of the cardiac position under breath-hold on the other hand might have caused a particular difference in response. Note, however, that the FAIR reproducibility SD cannot directly be compared to the spASL variation, since the number of measurements was six for FAIR and only two for spASL.

As a limitation, there is a remaining uncertainty in quantification, and a potential loss of sensitivity related to the labeling efficiency. The labeling slab was chosen rather large to ensure compatibility with a free-breathing acquisition. This led to multiple labeling of blood before entering the LV and labeling in the left atrium in particular. As previously discussed for cine-ASL experiments in the mouse heart, multiple fast labeling likely leads to a saturation, that is $\beta = 0.5$. In humans, however, the delay between two labeling events is larger, and labeling efficiency should be reconsidered. Based on our observations of blood signal in the LV blood chamber throughout the tag series, the assumption of nulled blood magnetization described in the method section was fulfilled for all subjects studied. When using equation [3.7] for estimation, the error in β even with heart rate or ATT variations of 20% should thus remain within 10%. This introduces errors and a potential bias in perfusion quantification, which varies linearly with β, i.e. of the order of 10%. The use of a 2D spatially selective labeling pulse as proposed by Botnar *et al.* in a different context is likely to improve the labeling efficiency and to remove uncertainties regarding β *[Botnar 2001]*. Myocardial ASL using pulsed 2D tagging of the proximal aorta has been proposed in the past but investigations remained at an early stage *[Zun 2009b]*. On the other hand, the relatively large slab thickness ensured good robustness to breathing motion. As a future improvement, real-time slice-tracking might be employed for improving the robustness of the steady-state regime against respiratory motion. Indeed, through-plane motion during respiration leads to loss of the steady state and associated signal transients that might affect quantification, and these were not taken into account in the current version of the sequence. Figure 3.5 shows, however, good stability of the myocardial signal under free breathing during the steady state initialization. Also, signal transients due to respiratory motion should affect tag and control scans in a similar way so that the influence on perfusion quantification remains limited. A second step of improvement should be the use of flip-back pulses at the end of each bSSFP readout, which will remove the major part of flip-angle dependency from the perfusion quantification. Note, however, that flip-angle variations of 10% lead to an error of 2.5% in MBF, so that the sequence still remains relatively robust to potential B_1^+ inhomogeneities.

For improving robustness against long-term motion and heart rate variations, one might also consider to acquire several tag and control blocks in an interleaved fashion as it was done with cine-ASL. We note, however, that this would introduce a higher number of discarded scans, since the transitory regime between tag and control blocks cannot be taken into account for signal measurement.

With the spASL technique, perfusion values were found with a good intra-subject and inter-observer repeatability. The upper masks were indeed necessary to delimit ROIs in a way that ensures that all pixels lie entirely within the myocardium and to exclude pixels from the myocardial border. Despite the mask, MBF values in the septum were higher for both techniques indicating non-negligible partial volume effects. To ensure minimal operator bias, a more uniform and robust post-processing procedure has been developed and is presented afterwards.

The sequence was also able to report perfusion changes induced by the CPT carried out in two subjects, although one only showed a small increase. A large inter-individual variation in response to CPT was also observed in other studies *[Schindler 2007, Moro 2011]*, and a larger number of subjects will ultimately be required for a proper comparison.

3.3.   Towards MBF Mapping

In this section, several approaches to improve the method described above are presented.

1- Improvement of the spatial resolution by accelerated parallel imaging.
2- Implementation of a simple rigid motion correction.
3- Improvement of the regional signal evaluation by using smaller regions of interest.

3.3.a.   Spatial resolution improvement

The spatial resolution used in the previous study was higher than that used by Zun *et al.*, yet, further resolution improvements are desirable to increase the number of pixels available for processing on the relatively thin myocardium. However, no lengthening of the acquisition window within the cardiac cycle should occur to avoid blurring by contractile motion. On the other hand, segmented acquisition across several cardiac cycles cannot be done under free breathing without advanced reconstruction. We thus implemented *k*-space acceleration using parallel imaging allowing for higher spatial resolution.

For bSSFP acquisition of the heart, high spatial resolution images are essential to clearly delineate the endocardial border from the LV blood pool to limit partial volume effects. Resolution is usually increased by increasing the number of phase encoding steps, which leads to longer acquisition periods. However, spASL uses snapshot acquisitions during each heart beat limiting the available time and therewith the maximum achievable resolution. Hence, snapshot acquisitions were accelerated with a 32-channel phased array receiver coil using integrated parallel imaging techniques (iPAT) together with the generalized auto-calibrating partially parallel acquisitions method (GRAPPA) *[Griswold 2002]*. GRAPPA acceleration allows skipping *k*-space lines in each acquisition, which are later on replaced by spatial information coming from each phased array elements. Using GRAPPA, additional *k*-space reference lines are required for the reconstruction algorithm. These lines can be acquired separately before the readout module series or integrated within each readout module. Due to the free-breathing acquisition in which signal can differ from one scan to another, we chose to keep the reference lines inside each bSSFP readout at the expense of small loss in acceleration possibilities. The factor of acceleration depends on the number of *k*-space lines skipped during acquisition, from 1 (no lines skipped) to 4 (only every fourth line is acquired).

In addition to breathing motion, some of the physiological noise could be due to cardiac motion, if the acquisition window is too long. In order to keep a good SNR while reducing the scan time, the chosen acceleration factor was 3 with 16 references lines, allowing for an increased matrix size from 104 x 128 to 156 x 192 while decreasing the acquisition duration from 334 ms (TE/TR = 1.61/3.22 ms) to 241 ms (TE/TR = 2.01/4.02 ms).

3.3.b.   Dedicated motion correction and signal evaluation

> This section constitutes the work of Julien Pugnaire, a Master student under my co-supervision.

The simple selection algorithm initially used (Figure 3.4) has several limitations. As described in the previous section, only a small portion of the data acquired under free breathing was used

(around 30%). In a further step, the associated post-processing has been improved by an additional retrospective motion correction of the heart in the image series such that a greater percentage of the acquired data can be used for averaging.

The spASL signal maps are obtained by the pairwise subtraction of each tag and control image. Even a small misplacement between those two images leads to pixels whose signal contains a false value, due to the subtraction of muscle with blood, fat or air instead of myocardium only (Figure 3.9). In addition, due to free-breathing acquisition, the heart is subjected not only to rigid displacement within the field of view, but also to distortions induced by breathing motion.
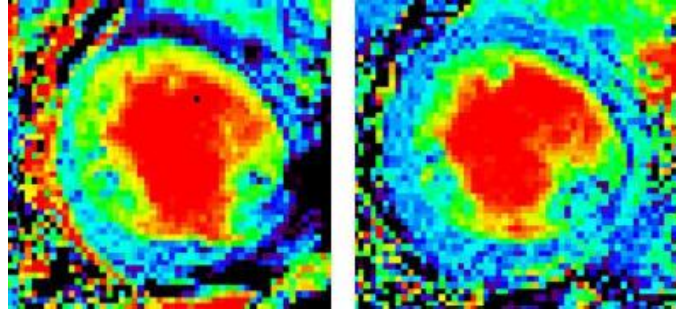

Figure 3.9 – Images resulting from the subtraction of one pair of tag/control images without (left) and with (left) correct positioning.

A major difficulty with applying Moco to the spASL dataset is that in the case of tagged blood, the signal in the LV chamber can be close to the myocardial signal, which makes the limit between these two compartments hardly detectable. Many Moco algorithms are based on easily (automatically) detectable image landmarks to calculate displacements. For the spASL approach, this landmark detection represents a particular challenge, since the Moco has to be applicable to both image sets (tag and control) although they strongly differ by their blood/tissue contrast. In order to overcome this problem, a homemade three-step motion correction and signal quantification algorithm has been developed.

In this work only rigid motion correction was used in order to guarantee conservation of the signal. Thus, the developed algorithm can only roughly correct for global motion, and a more precise procedure has to be elaborated to correctly assess myocardial perfusion in a specific segment. Both of these aspects have therefore been developed more thoroughly in this part of the project.

Originally developed processing algorithm

The following summarizes the different steps initially proposed to select images for myocardial perfusion assessment.

Step #1: Data exclusion.

The first step was to detect images acquired during the transient regime after start of each tag/control series and after occasionally missed ECG (Figure 3.10). These images have to be excluded since they are not in the steady-state regime. As initially proposed, images were excluded using a simple mean intensity selection on the whole left ventricle. This selection procedure lead to keep 80 ± 5 % of the acquired data.
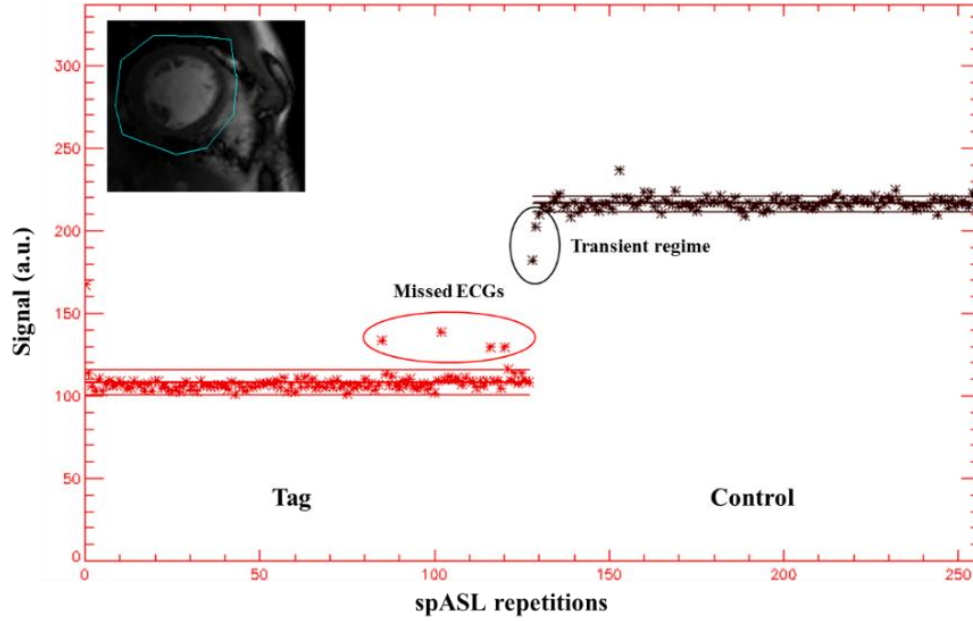
Figure 3.10 – Mean intensity selection algorithm to exclude images that are not in the stationary regime.

Step #2: Contour-based selection.

A Canny-Deriche edge-enhancement filter was applied to all images, and a specific segment was selected with a manually defined ROI (Figure 3.11). The contour cross-correlation (CC) was then calculated for each tag/control pair out of the N_{data} = 128*128*80% possible combinations.

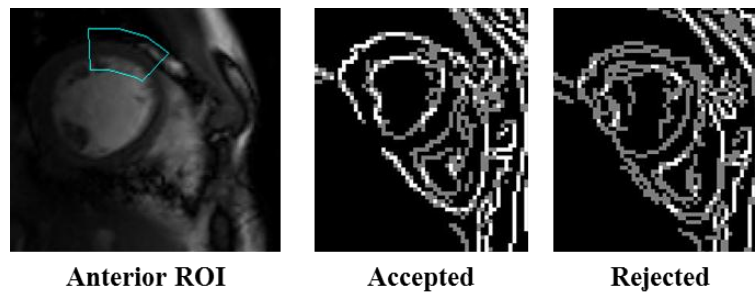**Anterior ROI**   **Accepted**   **Rejected**

Figure 3.11 – Selection procedure based on contour superposition, see Figure 3.4 for more details.

Step #3: Cross-correlation acceptance level.

A CC acceptance window was then defined by the user to choose the percentage of best correlated combinations that have to be kept (Figure 3.11). It was found that without motion correction of any kind, the signal measured in a particular region of the myocardium was independent of the number of included tag/control combinations within a certain range of acceptance levels (approximately when keeping between 10% and 40% of the pairs).
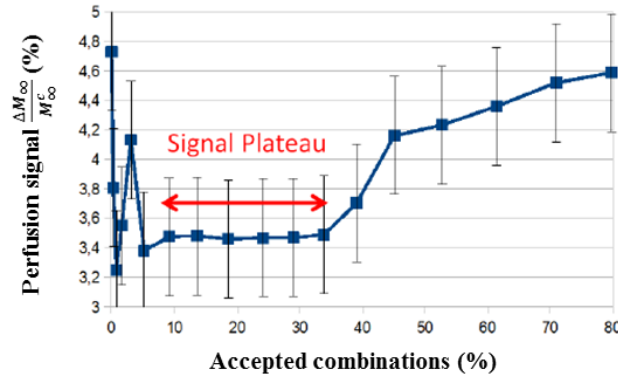
Figure 3.12 – Signal measured in the anterior myocardium of a single subject as a function of the percentage of accepted tag/control combinations. Numerous data have to be rejected in order to obtain signal stability.

In the following, N_{data} will be used when referring to the number of all possible tag and control combinations and the term 'signal plateau' will be used to specify the range in which the perfusion signal $\dfrac{\Delta M_\infty}{M_\infty^c}$ does not vary significantly when changing the acceptance level.

Step #4: Perfusion quantification.

In the original post-processing procedure, the perfusion signal was averaged over the accepted combinations in the same region of interest as that used for the contour-based selection procedure. Perfusion was finally quantified using equation [3.5].

The proposed ameliorations based on motion correction and a more precise quantification procedure will now be presented. This procedure adds three independent steps to the originally proposed post-processing.
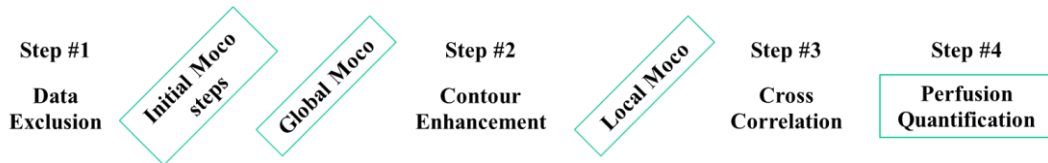

Figure 3.13 – Initial and new post-processing chain. Moco and signal quantifications improvements are highlighted by a green square.

Initial Moco steps

Reference images.
Since tag and control images are strongly different in their blood tissue contrast, both sets of images have to be post-processed separately. Reference images are automatically selected by the software for both image series (Figure 3.14). This procedure is based on the minimization of the subtraction over the N_{data} pairs available. Tag images will then be corrected according to the tag reference and the same will apply to control images. If a shift remains between the two tag and control references (in the case of false references chosen by the software), the user can manually define the reference based on visual inspection.
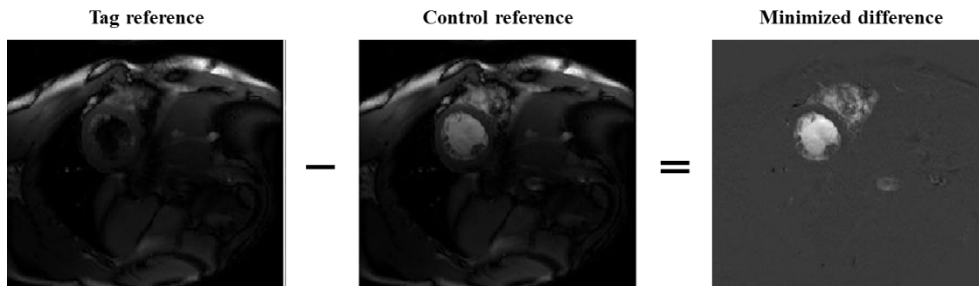
Figure 3.14 – Automatic tag and control references selection. The algorithm calculates the difference of all possible tag/control combinations and chooses the minimum to define references. If tag and control images are not well overlaid, the user can manually designate references images.

Regions of interest.

As shown in Figure 3.15, a ROI is drawn on the whole LV and will be used for the following global Moco. Keeping in mind that the heart is moving in the field of view, this ROI is drawn to roughly cover the LV and its surroundings. Also, it is important to cover a part of the lung since it is the only region of the image in which the signal is constant over the entire tag and control series. In order to minimize blood signal impact on the Moco procedure, additional ROIs are drawn in blood chambers to suppress this signal.
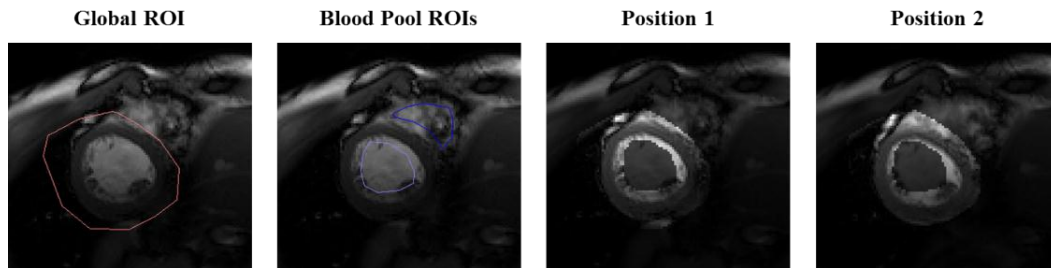

Figure 3.15 – ROI selection procedure. A global ROI is drawn around the LV (red). Additional ROIs are drawn in the blood chambers (blue) to designate regions to be excluded from analysis. All ROIs have to fit their compartment for the entire series during which the heart undergoes displacement. They are therefore chosen slightly larger or smaller than their compartment on a specific image. The global Moco will work with the remaining signal as highlighted on the right side for two different positions.

Global Moco using signal differences

The algorithm consists in correcting for motion using global signal differences of two images, one being the reference (tag or control) and one being the image to correct for motion (Figure 3.16). The algorithm is applied on all images independently for both tag and control sets. The corrected image is sequentially shifted in both horizontal and vertical directions to best overlap the whole LV, i.e. when the integral of the difference image between both is minimal.

Local Moco using contour correlation

This algorithm so far performs a gross motion correction. Due to non-rigid deformations of the heart, a second step was implemented acting with references to a specific region. This step uses local contour correlation between the image pairs within a specific segment of the myocardium. For simplicity, we will use the term 'local Moco' for this step, although the global image is shifted.
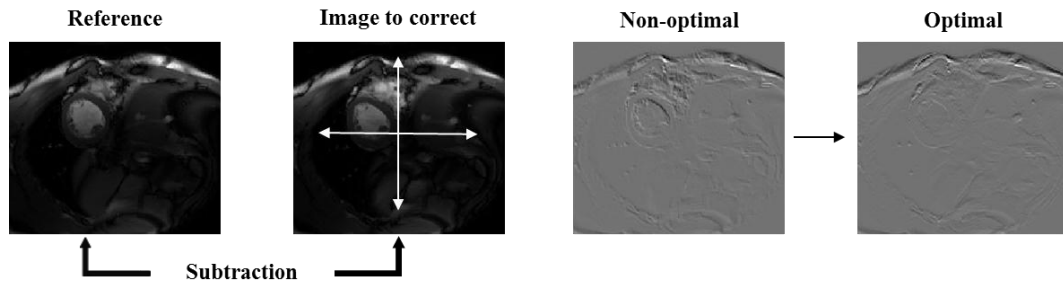
Figure 3.16 – Global Moco procedure. The image to correct and the reference image are sequentially subtracted while the latter is shifted in x/y directions (white arrows). The algorithm choose the position in which the subtracted signal in the previously defined ROI is minimum.

Similar to the originally proposed selection, the local Moco uses a Canny-Deriche edge-enhancement filter.

The algorithm calculates the cross-correlation coefficient (CC) of contour image pairs in a specific segment (ROI drawn by the user as presented in Figure 3.17). The contour to correct is sequentially shifted in x/y directions to calculate the highest possible correlation with the reference contour. This establishes a xy-shift space of correlation values, the minimum of which corresponds to the optimal position (black on the map representation of this space shown below).
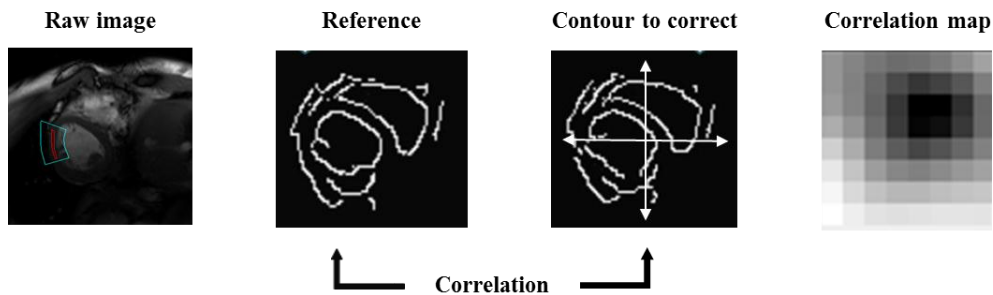

Figure 3.17 – Local Moco procedure. Correction is applied only to a specific segment of the myocardium (blue ROI). The algorithm calculates the highest possible correlation between the two contours, by sequentially shifting one contour map versus the other in x/y directions. This calculates a correlation map whose maximum corresponds to the optimal position. The small red ROI will then be used to quantify myocardial perfusion.

Perfusion quantification

As it has been proposed in the originally developed post-processing procedure, a CC acceptance window is finally defined by the user to choose the percentage of best correlated combinations that have to be kept.

In the original post-processing procedure, the signal was measured on the pixels from the same region of interest as that used for the selection procedure (blue ROI in Figure 3.17), and signal masks were used to eliminate blood signal. Since this rather large region includes the surroundings of the myocardium (blood, fat, or air), such signal analysis could lead to errors in MBF quantification. To improve quantification further, the new algorithm now introduces a second and smaller ROI in which the signal is evaluated (red ROI in Figure 3.17). The second ROI includes

only pixels from the myocardium and therefore substantially reduces the potential bias in perfusion quantification.

The Moco algorithm was tested on 6 healthy subjects who underwent a high spatial resolution (156 x 192) spASL scan.

3.3.c.   Results

Global Moco

Figure 3.18 shows tag and control images of the heart and its changing position induced by breathing motion. For better visualization of motion, a ROI covering the anterior myocardium was placed on the reference image and then copied on all other images of the series. On the raw images, the displacement of the myocardium can easily be seen, while motion is reduced on the corrected images.
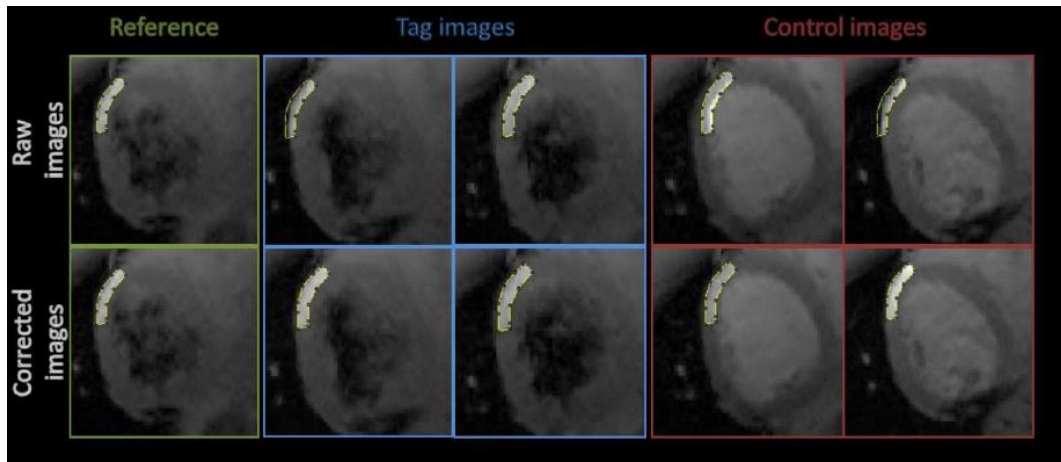
Figure 3.18   –   Displacement of the myocardium compared to a fixed ROI covering the anterior myocardium with and without global Moco for tag and control images, as indicated.

Figure 3.19 shows a comparison between two MBF maps obtained in a volunteer with and without the use of global Moco.

Local Moco

In addition to global correction, the use of the local Moco procedure allows to optimize motion correction over a specific segment of the myocardium. Figure 3.20 shows the discrepancies between two perfusion signal maps ($\Delta M_\infty / M_\infty^c$) without (left) and with (right) motion correction. Compared to the example presented in Figure 3.19, a precise motion correction based on contour correlation was performed on the anterior myocardium in addition to the global correction based on subtraction of images. After correction the myocardial borders are much clearer defined, and the signal appears more homogeneous.
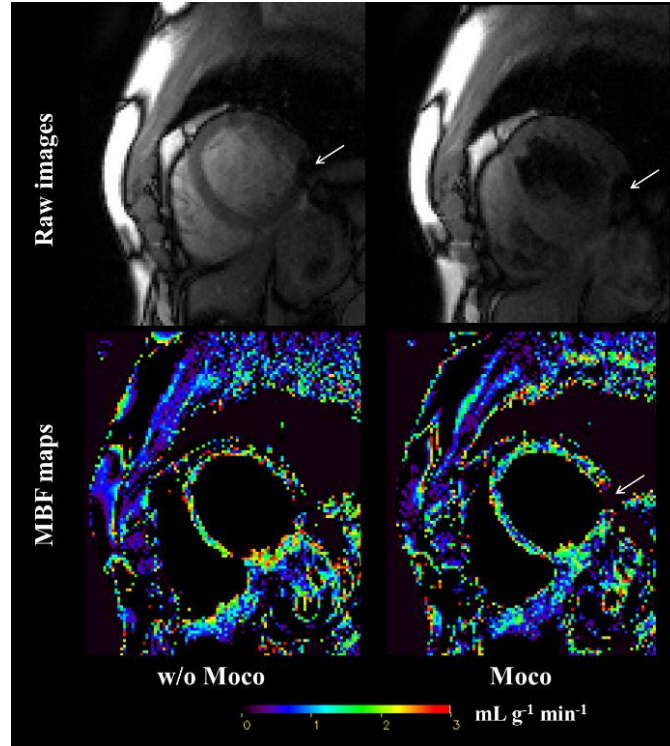
Figure 3.19 – MBF maps from a healthy subject without (left) and with (right) global Moco. Better homogeneity and delineation of the myocardium can be seen. The signal drop (white arrows) was only due to bSSFP artefacts.
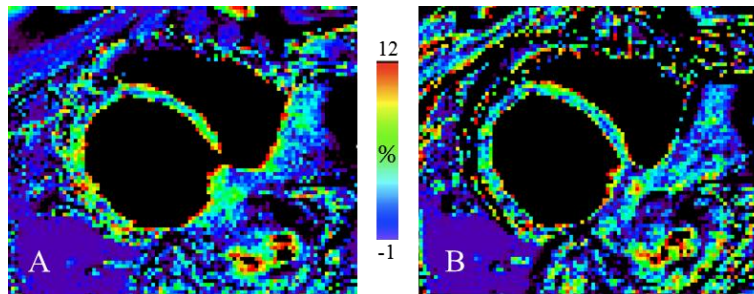
Figure 3.20 – Example of a signal map ($\Delta M_\infty/M_\infty^c$) without (A) and with (B) the use of Moco. A precise motion correction based on contour correlation was performed on the anterior myocardium in addition to the global correction based on subtraction of images with the reference.

Perfusion quantification

The signal difference for 6 subjects was measured in the anterior myocardium for several values of CC acceptance, giving a percentage of data kept ranging from 5 to 100 % of the N_{data} available. To assess signal stability, perfusion signal maps were computed with and without the use of Moco (global and local). To compare between subjects, perfusion signal values were normalized with respect to their signal plateau, as previously defined.

Using the different described steps for motion correction led to significantly improved signal stability. Figure 3.21 shows the mean signal ± SD obtained in the 6 evaluated subjects. Values are represented as a function of the percentage of included images after contour based selection. Without Moco, the lowest SD was found when including between 10 to 30% of all images. With

Moco, the signal reached a plateau around 50% but remained stable between 10 up to 80% of included images.

Figure 3.21 – Evolution of the normalized ASL signal measured in the anterior myocardium without (left) and with (right) the use of global and local Moco. Data were obtained on 6 healthy volunteers and post-processing was repeated for successive cross-correlation acceptance levels.

3.3.d.   Discussion
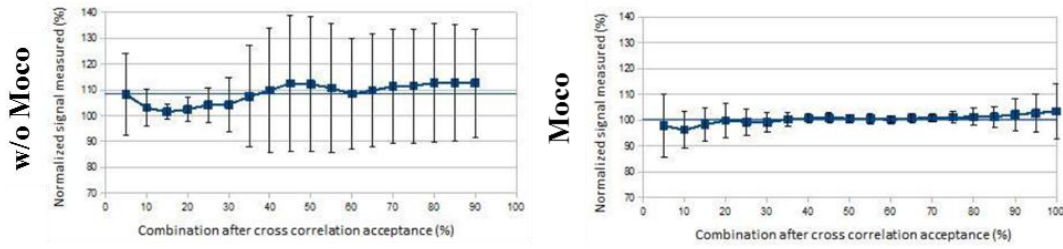
To further improve the spASL technique, we have implemented a dedicated motion correction method, together with an improved signal quantification algorithm which uses smaller ROI to quantify perfusion.

When a global motion correction is applied to the image sets, as shown in Figure 3.18, displacement of the myocardium was roughly corrected. This procedure helped to reduce potential contamination from blood, air, or fat signals. Although deformation of the myocardium were not accounted for, perfusion mapping in some subjects could be attempted as shown in Figure 3.19. Without the use of global Moco, perfusion maps were corrupted by non-myocardial signal which resulted in a blurred map, with sometimes a complete loss of the perfusion signal. This can be seen in the anterior myocardium or the septum in Figure 3.19. Although MBF mapping was possible, no attempt in perfusion quantification was done at that stage of the post-processing. After global correction, indeed, no selection of the 'best overlaid' image pairs was possible such that every combination were used for perfusion mapping.

In the originally proposed selection procedure, the CC acceptance selection was already successful in determining the correct tag/control image pairs used for perfusion quantification. However, (i) no algorithm had been set up to verify the selection quality (obtained here by the correlation map) and (ii) no correction of the misregistration of tag/control pairs between each other was used.

An additional local correction appeared essential for an accurate perfusion quantification. Thus, the local Moco based on contour-correlation was carried out for a specific segment at a time. Such approach can be considered as precise despite the deformation of the heart under free breathing.

With the local correction applied, the position of the segment of interest is corrected before tag/control subtraction and averaging data is less likely to contain false values. Using local Moco helped to reduce significantly blurring in the corrected region, as suggested here by the well delineated anterior myocardium in Figure 3.20. Interestingly, even if the correction was applied only to the anterior myocardium, the septum position was also partially corrected, which was reflected here in a reduced blood contamination in the septal region. We note, however, that

motion correction is reliable and reproducible only in the segment where the local Moco has been done.

The use of semi-automated Moco, combined with the assessment of perfusion signal in a small ROI covering the myocardial tissue only, led to a significant decrease of inter-subject SD when using free-breathing spASL acquisition. The measured signal was found stable within a wider range of included images (Figure 3.21).

The improvement of the spASL technique when using Moco and the associated post-processing algorithm is twofold. On the one hand, it allows inclusion of a much higher number of acquired images in the quantification procedure. On the other hand, it allows evaluating the regional signal by using smaller regions of interest which makes the post-processing chain more robust. As shown in Figure 3.19 and Figure 3.20, these improvements represent a step towards calculation of perfusion maps with high spatial resolution.

3.4.   Conclusion

In conclusion, the first presented study reports the application of a steady-pulsed ASL sequence for the quantitative assessment of myocardial blood flow in humans. Experiments were conducted in a group of healthy volunteers at 3T. The spASL sequence was compared to the previously proposed multi-breath-hold FAIR approach. Higher signal and equivalent performance as compared to FAIR was found. Steady-pulsed ASL appears as a good candidate for non-contrast perfusion assessment, although sequence and more importantly post-processing improvements have to be done.

The application of a dedicated retrospective motion correction tool combined with an increased spatial resolution for spASL acquisitions was then presented. Increasing the spatial resolution by using parallel imaging appears mandatory when a clear delineation of the endo- and epicardial borders is required to reliably study the ASL signal within a ROI. Using global Moco, we were able to compute MBF maps in some subjects with high spatial resolution and a good signal homogeneity in the myocardium. The combined application of global and local Moco allowed us to significantly reduce signal instability due to free-breathing acquisitions. This dedicated Moco, together with signal evaluation in a small region of interest, increase the robustness of the post-processing algorithm to assess the perfusion signal in a specific segment of the myocardium. Alternatively, since the use of motion correction allows including much more data in the quantification, such improvements might also in the future allow for reducing acquisition time.

In this work, we only used rigid Moco in order to guarantee that no uncontrolled modification of the magnetization difference created with the spASL scheme occurred during the post-processing. However, future improvement should investigate the use of non-rigid motion correction to counterbalance the distortion of the heart along the image series. Non-rigid Moco appears now an absolute necessity to calculate reliable perfusion maps in humans.

Retrospective motion correction techniques, however, cannot assess potential bias due to through-plane motion during acquisition. Prospective motion correction (such as 'motion tracking' techniques) would have the additional advantage of addressing these issues. Also, adaptive reconstruction algorithms such as GRICS should enable the use of all images for signal averaging and thereby improve sensitivity *[Odille 2008]*.

Chapter 4 - Cine-ASL: Different Version for Different Needs

Contents

4.1. Introduction

In a first subproject, the goal was to monitor the time course of perfusion in response to a continuous infusion of adenosine as a vasodilator. Cine-ASL had been shown to be a faster alternative method for perfusion quantification than LLFAIRGE, and it therefore offered the possibility of doing frequently repeated measurements during one exam. An optimized cine-ASL version regarding short acquisition time has therefore been derived from its original implementation. An optimized cine-ASL version regarding acquisition time has therefore been derived from its original implementation. Theory of the cine-ASL technique as well as validation against the LLFAIRGE approach are described in the Chapter 2, and we therefore only recall some of its most important aspects.

Briefly, cine-ASL relies on a fast ECG-gated cine-FLASH sequence repeated over several cardiac cycles for each line of k-space. At each cardiac cycle, one single gradient-echo is substituted by a spatially selective inversion pulse, labeling the arterial blood at the level of the aortic root. This labeling has to be performed just before the arterial blood enters through the myocardial tissue via the coronaries, i.e. at end-systole. Using this approach, a continuous cine acquisition can be performed while the blood magnetization feeding the coronaries is driven into a steady-state, leading to a perfusion-dependent stationary regime of tissue magnetization.

By using shorter inversion pulses and TR compared to the originally proposed cine-ASL sequence, higher temporal resolutions became feasible. The aim of the second subproject was to correlate magnetization difference changes and perfusion variations across time. High temporal resolution MBF maps were obtained in rats in order to study dynamic MBF changes over the entire cardiac cycle at rest and during adenosine-induced stress.

In a third study, the fast and optimized cine-ASL version was integrated in a multimodal MRI and MRS protocol to study cardiac function, perfusion and triglyceride contents in small-animal models of type 2 diabetes.

4.2. Dynamics of the Perfusion Reserve

This section constitutes the work of Christian Kenmoe, a Master student under my co-supervision.

While the coronary auto-regulation mechanism is able to maintain resting myocardial blood flow constant in the presence of strong stenosis, it might not be so during exercise or pharmacological stress. In clinical routine, myocardial perfusion MRI is generally performed with a rest/stress protocol to ensure that perfusion regulation is normal in both physiological states *[Gebker 2007]*. To induce differences between normal and ischemic myocardial segments, pharmacological vasodilation is applied in patients using adenosine *[Wilson 1990]* or dipyridamole *[Ranhosky 1990]*. These pharmacological agents proved to be safe and well tolerated. Adenosine, an endogenous nucleotide, is a potent vasodilator of most vascular beds, except for hepatic and renal arterioles. Characterized by a very short half-life of about 10s, it exerts its pharmacological effect through the activation of purine A1 and A2 cell-surface receptors. Dipyridamole is the prodrug of adenosine, and it is activated by metabolism in the liver. Thus, vasodilatory capacity depends on the individual metabolic rate, and a longer half-life potentially translates into prolonged side effects after administration. As such, adenosine is preferable and became the stress agent of choice for myocardial perfusion imaging.

The microcirculation supplied by both normal and stenotic coronary arteries is dilated to its maximum using these drugs. Since autoregulation is already exhausted at rest in stenotic coronaries, these vessels cannot be dilated any further. Thus, pharmacologic vasodilation induces an increase in blood flow in myocardial areas supplied by normal coronary vessels whereas no, or only minimal, change is found in areas supplied by stenotic coronary arteries.

In clinical routine procedures, maximal vasodilation can be achieved safely with intravenous adenosine infusion at a rate of 140 $\mu g\ kg^{-1}\ min^{-1}$. Figure 4.1 presents the two protocols most commonly used for myocardial perfusion imaging. Adenosine is typically injected 3 to 4 minutes prior to imaging. For first pass MRI, adenosine infusion is stopped and immediately replaced by the contrast agent while the patient is asked to hold their breath for imaging the heart *[Nagel 2003]*. For PET studies, two separate lines of injection are used and adenosine is still infused while the contrast agent is injected into the vein of the patient.
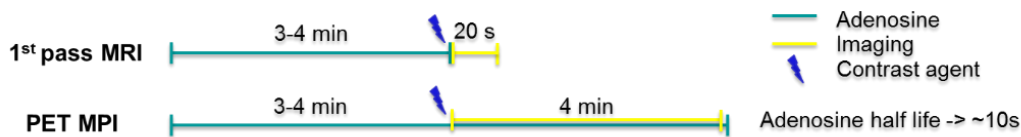

Figure 4.1 – Typical procedures used in clinic for first pass MRI and PET stress perfusion imaging.

To gain insight into perfusion dynamics under stress, we propose to use a shortened version of the cine-ASL sequence to study the longitudinal effect of a continuous injection of adenosine on myocardial blood flow and myocardial perfusion reserve in rats.

4.2.a.   Methods

cine-ASL short version

Compared to the original cine-ASL version proposed initially in Chapter 2, the readout scheme was modified so as to acquire a two-fold segmented cine dataset per cardiac cycle (Figure 4.2). The acquisition time of this sequence is given by:

$$T_{Acq} = 2\left(RR \ N_{cine} \ N_{PE} \right), \quad\quad\quad [4.1]$$

where RR is the interval between two heart beats, N_{cine} the number of cine block repetitions, and N_{PE} the number of phase encoding steps. Acquiring two *k*-space lines per cine block allows reducing the acquisition time by a factor two at the expense of a proportional decreased of the temporal resolution, i.e. the cine frame rate.

As presented in the Chapter 2 – Theory section, the recovery delay between tag and control series affects only the transient regime of tag/control magnetization but not the difference magnetization in the stationary regime, $\Delta M_\infty / M_\infty^c$. Therefore, we removed the recovery delay between tag and control cine blocks to further optimize acquisition time.
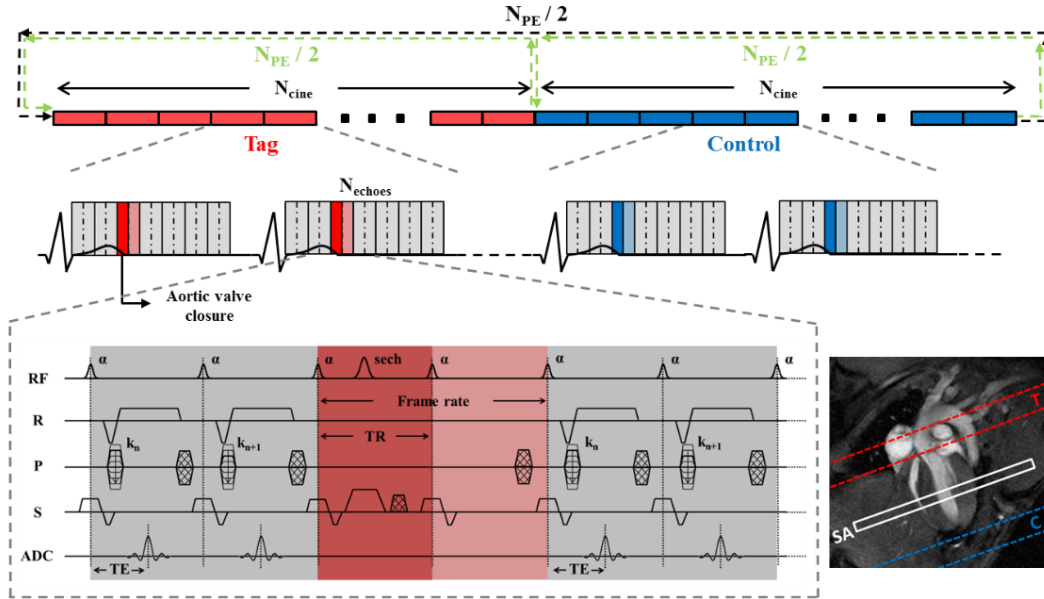
Figure 4.2 – Short version of the cine-ASL sequence. The readout scheme was modified to acquire two k-space lines per cine frame. It allows reducing the acquisition time by a factor two at the expense of a proportional decrease of the temporal resolution. The green arrows highlight the fact that a sequential acquisition can also be performed using this cine-ASL version.

In the first proposed cine-ASL version, tag and control cine blocks were repeated N_{cine} times in an interleaved fashion, that is switched from one steady-state to another for each line of *k*-space. The interleaving was done to reduce potential errors in MBF introduced by long-term motion. However, the data during the transitory phase occurring after each switch could not be used for quantifying MBF and had to be discarded, which appears suboptimal regarding acquisition efficiency. With the new version, the acquisition duration of the blocks became shorter, and it

became possible to acquire the entire tag and control images sequentially, without interleaving (green arrows in Figure 4.2). This sequential approach is similar to the sequential spASL acquisition proposed for human studies. As such, the tag or control steady-state is reached after 10 cine block repetitions for the first encoded *k*-space line, and it is maintained until complete coverage of *k*-space. As presented in Chapter 2, 10 to 15 cine block averages in the steady-state are required to reliably quantify perfusion. Using sequential acquisitions, one can therefore expect to further reduce acquisition time by decreasing the number of acquired cine blocks. Figure 4.3 shows the dynamic of the MR signal behavior during tag and control scans for both interleaved and sequential readout strategies.
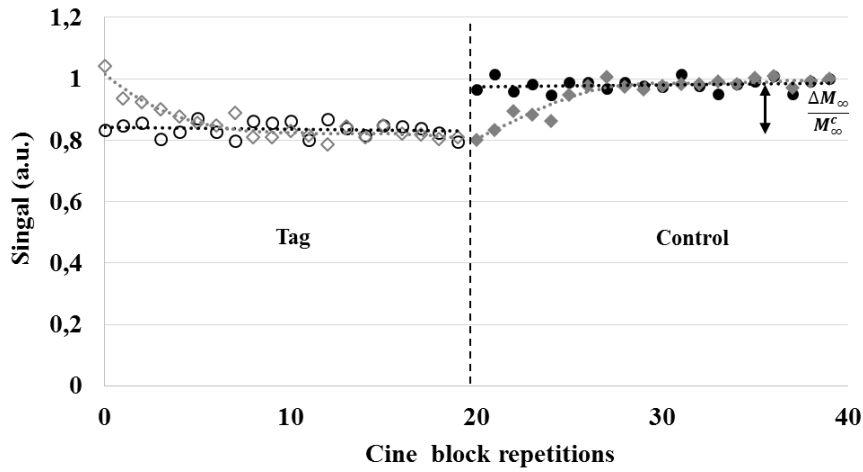
Figure 4.3 – Dynamic MR signal behavior in the anterior myocardium for 20 cine block repetitions during tag (open symbols) and control (filled symbols) acquisitions. For clarity, data were normalized to the last control point and are represented for interleaved (diamonds) and sequential (circles) acquisitions. Using sequential acquisition, a greater portion of the acquired data can be used for perfusion quantification.

However, even with the shorter blocks used here, separating tag and control experiments in a sequential fashion assumes sufficient stability of physiology, which might not be the case in pathological situations or during stress exams. Such acquisition is more sensitive to long-term motion and heart rate variations, while the interleaved approach inherently filters low-frequency drift of physiological parameters along the experiment.

The proposed version was tested in several situations including the rest/stress protocol described here, and its stability was deemed applicable only in healthy animal at rest. We thus decided to keep the interleaved acquisition for this study by acquiring 25 cine blocks per repetition, allowing for 15 averages within the steady-state.

Experimental protocol

Experiments were carried out on 19 healthy rats (body weight 245 ± 80 g) anesthetized with 2% of isoflurane added to 1 L min^{-1} of pure oxygen gas stream. Adenosine was continuously injected via the tail vein at a rate of 140 µg kg^{-1} min^{-1} using a dedicated low-flow pump injector. Perfusion measurements were carried out in the short-axis plane using the fast cine-ASL sequence with the following parameters: imaging slice thickness: 2 mm, field of view: 40 mm, in-plane resolution: 312 x 625 µm², TE/TR: 1.64/6ms, flip angle α: 8° (gaussian pulses, 0.5 ms), labeling slice

thickness: 6 mm (adiabatic hyperbolic secant pulses, 3.7 ms). The number of acquired cardiac phases (N_{echoes}) was fixed to 6, with 25 cine block repetitions. At a mean heart rate of 400 bpm, the acquisition time was 4 minutes.

After localization, all animals first underwent a cine-ASL scan at rest. Myocardial blood flow (MBF) and myocardial perfusion reserve (MPR) were then continuously monitored every 5 minutes for 40 minutes of stress. The group of healthy animals was divided into 3 subgroups (Figure 4.4):

- G1 (N=6), adenosine was continuously infused for 40 minutes.
- G2 (N=6), adenosine was continuously infused for 25 minutes and then stopped for the remaining 15 minutes (recovery period).
- G3 (N=7), the control group, adenosine was replaced by a saline solution to check for eventual long-term isoflurane effect or stress induced by the injection procedure.
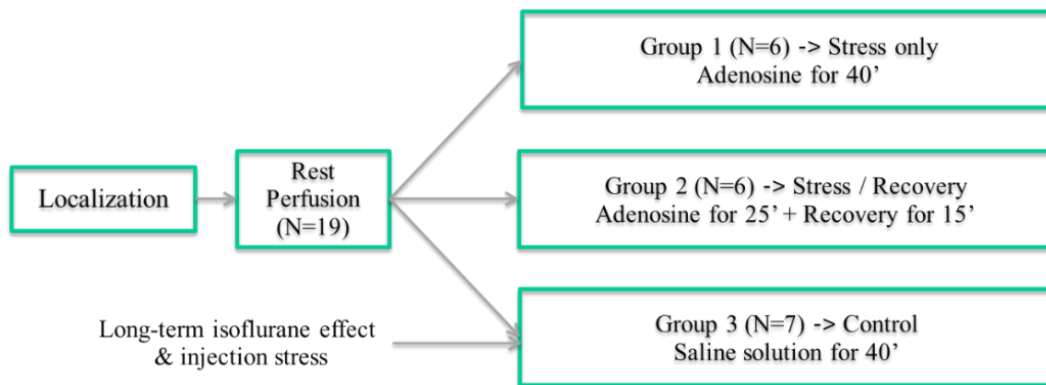
Figure 4.4 – Experimental protocol.

4.2.b. Results

Heart and breath rates were not statistically different between groups along the stress period. Perfusion values obtained in this study cannot be considered as physiological baseline due to the possible influence of isoflurane anesthesia. Perfusion was evaluated in three areas corresponding to the septum, the anterior wall and the lateral wall. Since no differences in MBF were found between these regions (at rest and during stress), MBF values reported afterwards correspond to global MBF which is the average MBF of these three segments.

Figure 4.5 shows MBF maps obtained at rest for the 3 groups (top). Figure 4.5 also shows an example of perfusion map series obtained in two different animals, one from G1 and one from G2, during the 25 minutes stress period (middle) and the remaining 15 minutes (bottom, stress for G1 and recovery for G2). Compared to the perfusion maps obtained with the original cine-ASL sequence (Chapter 2), similar quality was found using the shortened version of cine-ASL. Perfusion maps show a clear MBF increase during the stress period compared to rest. The visual difference in MBF values obtained in the two animals during the stress episode was chosen on purpose to highlight the physiological discrepancies in response to infused adenosine.

For the last 15 minutes of the experiment, MBF was still above resting values in G1 whereas it returned to baseline in G2.
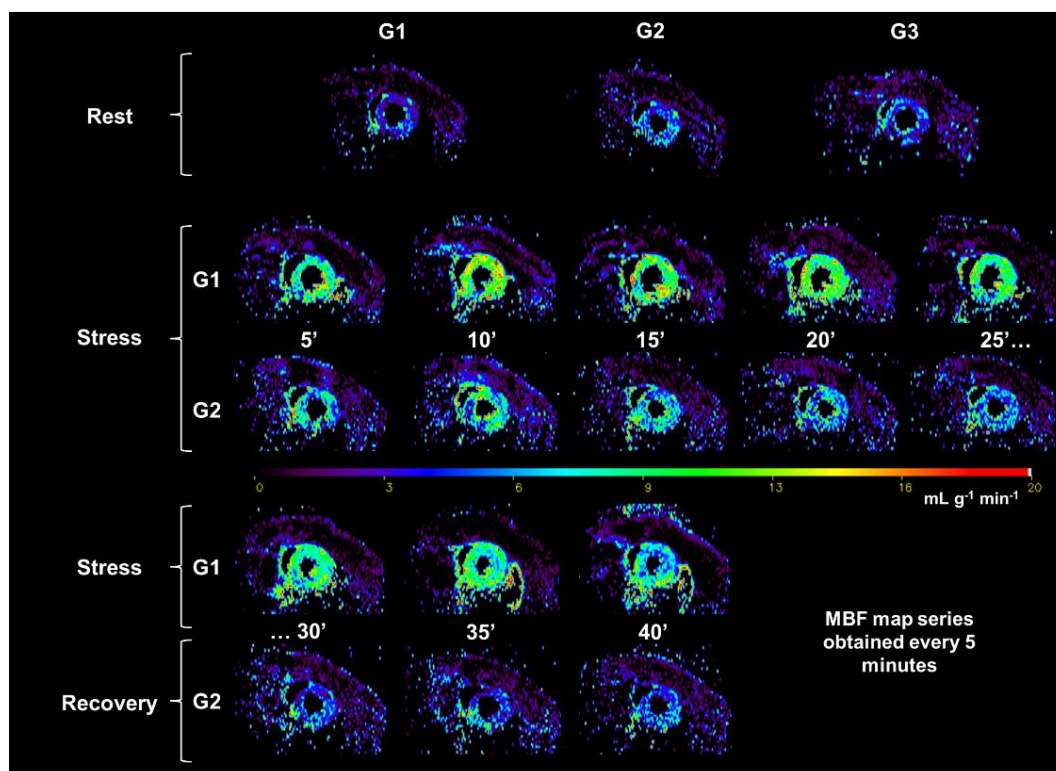
Figure 4.5 – Example of perfusion map series obtained in two animals from the group 1 and 2. During the stress episode of 25 mintues (middle), a clear MBF increase can be seen in both animals compared to rest (top). Vasodilation was maintained for 40 min due to adenosine infusion for the animal in G1 while MBF returned to baseline value for the animal in G2 during the recovery period (bottom).

MBF and MPR variations

Figure 4.6 shows the evolution of the mean myocardial blood flow for the three groups as a function of time after onset of adenosine. Mean group MBF (N=19) at rest was 5.4 ± 0.5 mL g^{-1} min^{-1}. No significant differences were found along the experiment for the control group (MBF = 5.5 ± 0.7). In all studied animals from groups 1 and 2, a significant MBF increase was found during the first 5 minutes of adenosine infusion, but the maximal response to adenosine was always found later, during the time intervals 5-10 or 10-15 minutes. No differences in response was found between these two groups, with a maximum perfusion group value obtained between 5 to 10 min of 10.7 ± 1.5 mL g^{-1} min^{-1} in G1 and 10.9 ± 1.5 mL g^{-1} min^{-1} in G2 ($P = 0.82$). After 15 minutes, a progressive decrease in perfusion response to adenosine was obtained in both groups. After 25 minutes, vasodilation was maintained in G1 and MBF returned to baseline in G2. Table 4.1 summarizes mean MBF values obtained in the three groups over the time course of the study.
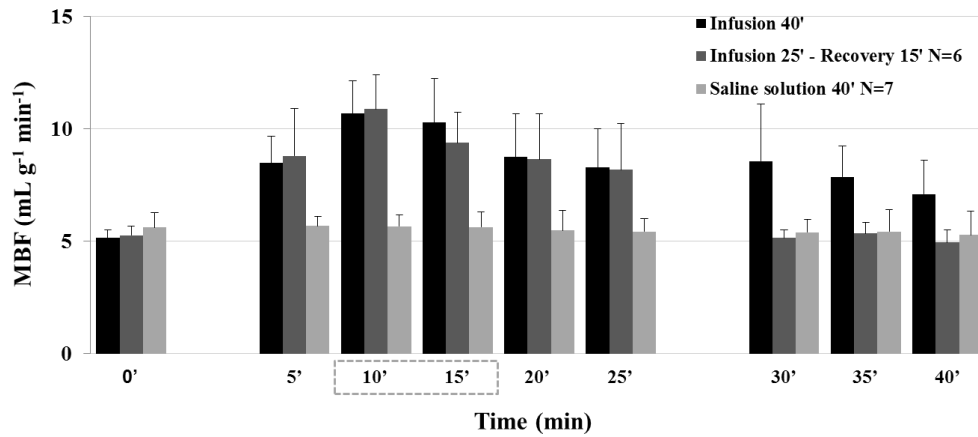
Figure 4.6 – Myocardial blood flow variations as a function of time after onset of adenosine. Mean group MBF values are presented for G1 (black), G2 (dark grey), and G3 (light grey). Error bars represent the standard deviation within each group. Maximal response to adenosine is highlighted with the gray rectangle on the time scale.

Table 4.1 – Summary of the mean group perfusion values obtained in the three groups.

Time intervals (min)	Myocardial Blood Flow (Mean ± SD in mL g^{-1} min^{-1})		
	G1 (Stress only)	G2 (Stress/Recovery)	G3 (Control)
0 (Rest)	5.2 ± 0.4	5.3 ± 0.4	5.6 ± 0.7
0-5	8.5 ± 1.2	8.8 ± 2.1	5.7 ± 0.4
5-10	10.7 ± 1.5	10.9 ± 1.5	5.7 ± 0.5
10-15	10.3 ± 2.0	9.4 ± 1.4	5.6 ± 0.7
15-20	8.8 ± 1.9	8.7 ± 2.0	5.5 ± 0.9
20-25	8.3 ± 1.7	8.2 ± 2.1	5.4 ± 0.6
25-30	8.6 ± 2.6	5.2 ± 0.4	5.4 ± 0.6
30-35	7.9 ± 1.4	5.4 ± 0.5	5.4 ± 1.0
35-40	7.1 ± 1.5	5.0 ± 0.6	5.3 ± 1.0

Since no differences were found between G1 and G2 behaviors in response to adenosine, MBF and MPR values were averaged for the 0-25 minutes time interval, and the mean group values where kept separated for the last 15 minutes. Dynamics of the myocardial perfusion reserve response to adenosine is shown in Figure 4.7. No significant differences were found between the maximal response to adenosine obtained during the 5-10 minutes time interval and that obtained during the 10-15 minutes interval. Compared to the maximal response, however, a significant MPR decrease was found after 20 minutes (2.1 ± 0.3 vs. 1.7 ± 0.4, $P < 0.05$) and 25 minutes (2.1 ± 0.3 vs. 1.6 ± 0.4, $P < 0.01$) of adenosine infusion.

During the last period of the experiment, i.e. the remaining 15 minutes, MPR response to adenosine continued to decrease for group 1 but remained significantly higher than for the resting state. In group 2, perfusion returned directly to baseline after the adenosine infusion was stopped.

Figure 4.7 – Dynamics of the perfusion reserve as a function of time after onset of adenosine. MPR values were averaged between G1 and G2 for the 0-25 minutes time interval. Maximum MPR response to adenosi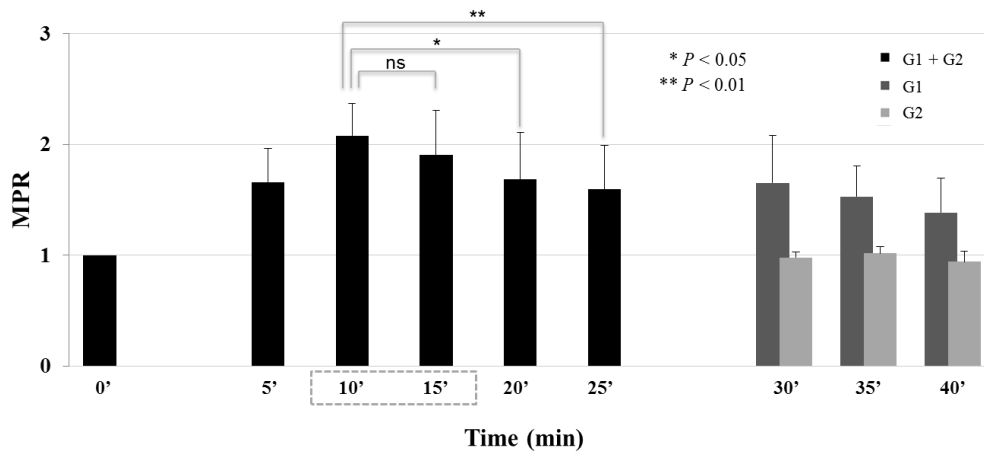ne was found between 5 to 15 minutes of infusion (grey rectangle on the time scale). No significant differences were found between the maximal response obtained during the 5-10 minutes time interval and during the 10-15 minutes interval (ns), whereas a significant MPR decrease was found after 20 minutes (P < 0.05) and 25 minutes (P < 0.01) of adenosine infusion.

4.2.c.   Discussion

In this work we present the use of a shortened version of the cine-ASL sequence. We implemented a 2-fold segmented cine readout scheme acquiring 2 phase encoding steps per cardiac cycle, instead of one. This led to an effective TR between cine frames of 12 ms ($TR_{Eff} = 2*6ms$). We believe that in a cardiac context, TR of a gradient echo readout should be less than 10% of the cardiac cycle duration to avoid blurring artifacts due to cardiac contraction. Also, further reduction of the acquisition time by acquiring additional lines would increase the risk of errors due to through-plane movement of the myocardium. As shown in Figure 4.5, perfusion maps where obtained with a similar quality compared to the previous study in mice.

This study focused on MBF response dynamics to adenosine. The aim of this study was twofold, (i) to validate the shortened cine-ASL sequence, and (ii) to gain detailed insight into rodent coronary reserve and coronary response to an infused vasodilator. MBF increase in response to adenosine was already reported in a previous study by our group using the LLFAIRGE ASL sequence with a similar experimental setup *[Jacquier 2011]*. Our results of maximal vasodilation on MBF and MPR were in accordance with those reported by Jacquier and coworkers. However, considering the long duration of the perfusion sequence used in that study (i.e. ~ 25 minutes with LLFAIRGE) coronary reserve dynamics was inaccessible at that time. Using the fast cine-ASL sequence, we were able to perform such measurements, validating at the same time that the stress with intravenous adenosine injection was indeed maintained during the 25 minutes experiment in rats.

Following adenosine infusion, an initial increase was found within the first 5 minutes, but the maximum coronary response to adenosine was always found later, between 5 and 15 minutes. After 15 minutes, a progressive decrease in response was found over time. MPR significantly decreased in G1 and G2, from 2.1 ± 0.3 after 10 minutes of infusion to 1.6 ± 0.4 after 25 minutes. This behavior persisted in G1 until the 40 minutes of infusion (MPR decreased until 1.4 ± 0.3), while perfusion returned to baseline in G2 as soon as adenosine injection was stopped.

Since adenosine half-life is comparable to the time for blood recirculation in the rat body, i.e. about 10 seconds, it is unlikely that adenosine receptors on arteriolar smooth muscles become saturated when performing a continuous infusion. One possible explanation for this decreasing behavior could be that coronary vessels might strengthen over time after they have reached their maximal dilatation. This would result in progressive narrowing of the vessels, which was reflected here by a progressive decrease in response to adenosine.

Adenosine is characterized by a relatively short time of action. In this study, the injection was performed at a clinical rate which is 140 µg kg^{-1} min^{-1}. Due to the lower body weight of small-animals as compared to humans, the injection flow was proportionally lower. Even though a dedicated low-flow pump injector was used, the infusion process was delicate when applied to small-animals.

Compared to human studies in which perfusion is assessed 3 to 4 minutes after adenosine injection, we found that for rodent studies, it is preferable to wait at least 5 minutes before acquiring perfusion data to ensure that maximal vasodilation is reached. It has to be kept in mind, however, that these results might be partly proper to our experimental setup. Nonetheless, such dynamic measurements give more detailed insight into rodent coronary reserve and coronary responses to infused vasodilators. They may also give complementary information on microvascular functional defects if applied to non-ischemic heart disease models.

In summary, these results were important to validate the short cine-ASL version but, more importantly, to find the time interval during which maximum vasodilation occurs and whether it remains stable. These experiments were therefore useful for a subsequent study presented in the next section, in which a longer version of the cine-ASL sequence was used, and in which the optimal interval of stress observation could be chosen using this result.

4.3. Cyclic Myocardial Perfusion Variation

This section is based on:

In Vivo Characterization of Rodent Cyclic Myocardial Perfusion Variation at Rest and during Adenosine-Induced Stress using cine-ASL Cardiovascular Magnetic Resonance. J. Cardiovasc. Magn. Reson. 2014.

Troalen T, Capron T, Bernard M, and Kober F.

4.3.a. Background

The pulsatility of coronary flow has been studied for several decades *[Sabiston 1957, Hoffman 1990]*: as elsewhere in the arterial circulation, it is the pressure difference between the aorta and the peripheral capillaries that provides the driving force for coronary circulation. In a paradoxical way, the heart, which is dedicated to supply blood to the organs, restricts its own blood supply during peak contraction in systole unlike most other systemic vascular beds which have a fresh oxygenated blood supply in systole. The squeezing effect of myocardial contraction causes arterial blood inflow to peak during diastole and venous blood outflow to peak during systole *[Morgenstern 1973, Spaan 1981]*. Microvessels are abundant in the myocardium so that myocardial blood volume (MBV) and flow (MBF) vary during the cardiac cycle in response to this pulsatile change in coronary circulation and cyclic variation in myocardial tension. Diseases such as diabetes, atherosclerosis, cardiomyopathies, and arterial hypertension result in functional and morphologic microvascular alterations, which may precede clinical signs and symptoms. The mechanical interaction between coronary microcirculation, and myocardial contraction and relaxation is fundamentally important for an understanding of intramural coronary hemodynamics. The morphology and function of capillaries across myocardial wall during a cardiac cycle play a pivotal role on the mechanical control of blood perfusion to regional myocardium together with arteriolar and venular mechanics and responses *[Klassen 1997]*. Determination of the role of systolic extravascular compression on the pattern of blood flow in the microcirculation during the cardiac cycle has been limited to measurements made in those regions of the myocardium where direct observations of these microvessels is possible *[Ashikawa 1986, Kajiya 1989, Yada 1993]*. Quantitative assessment of myocardial perfusion and characterization of cyclic myocardial perfusion variation would help better understand the mechanisms underlying myocardial contractility and may give valuable complementary information on microvascular functional defects in non-ischemic heart diseases.

Cyclic change of regional MBV in the mouse heart has already been reported using cardiovascular MRI based on the correlation with cyclic variation in the steady-state T_2^* shortening effect of an ultrasmall iron oxide nanoparticle intravascular contrast agent *[Ed X Wu 2004]*. Another study focused on noninvasive MBV variation assessment in the canine left ventricle using displacement encoding with stimulated echoes (DENSE) technique *[Rodriguez 2006]*. Nevertheless, no study has assessed MBF variation over the entire cardiac cycle in the rodent heart. In humans, however, Radjenovic *et al.* demonstrated the feasibility of assessing systolic and diastolic MBF changes by dynamic contrast-enhanced MRI *[Radjenovic 2010]*.

By using cine-ASL, the steady-state approach associated with the cine readout allowed us to dynamically map MBF over the entire cardiac cycle with high temporal resolution. In a

preliminary study, cyclic change of regional MBF in healthy mice was measured at rest *[Troalen 2012]*, and a significant MBF increase of 30% from end-systole (ES) to end-diastole (ED) was shown. Based on this finding, we propose a new protocol which compares cyclic MBF changes in healthy Wistar rats between rest and adenosine-induced stress.

4.3.b.   Methods

Animal Preparation

All experiments were conducted according to a protocol approved by the University's animal experimentation committee. Seven healthy female Wistar rats (age 25 weeks, body weight 329 ± 8 g; Janvier Laboratories, Le Genest-Saint-Isle, France) were anesthetized in an induction chamber with 3% isoflurane. During the experiments, a 2% dose of isoflurane mixed with 1L min^{-1} of pure oxygen gas stream was continuously delivered through a face mask. For the present study, isoflurane was chosen as it maintains cardiac function and permits real time regulation of the depth of anesthesia whereas barbiturates such as pentobarbital are known to have depressant effects on hemodynamic parameters *[Takuma 2001]*. Nonetheless, isoflurane has been shown to induce coronary vasodilation and MBF increase at rest compared to other anesthetics *[Iltis 2005b]*. Isoflurane concentration was regulated using a dedicated vaporizer (Ohmeda/General Electric, Milwaukee, WI, USA) so as to obtain regular breathing frequencies in the range of 70 breaths per minute. Respiration was monitored using a pressure sensor connected to an air-filled balloon positioned on the back of the rat. Body temperature was monitored using a rectal probe and maintained at 37°C using a heating blanket with hot water circulation placed around the rat. The electrocardiogram (ECG) signal was monitored by placing two subcutaneous electrodes, one in the right foreleg and one at abdominal level. The electrodes were connected to an ECG trigger unit (Rapid Biomedical, Rimpar, Germany) to record the signal and to trigger the MRI sequence. Oxygen saturation was also monitored to ensure stable physiological conditions along the experiment. A catheter was placed in the tail vein to deliver adenosine. The venous cannula had a dead volume of about 120 µL.

Perfusion MRI

As for all prospectively gated techniques, the original cine-ASL sequence had to be stopped before the next ECG trigger so that the observable time window within the cardiac cycle was only about two third of the cardiac cycle. Also, the waiting delay caused steady-state interruptions that might bias the perfusion signal on the short time scale observed here.

Compared with the original cine-ASL version, the sequence was therefore slightly modified so as to acquire data during almost two cardiac cycles after each trigger pulse (Figure 4.8). We assumed that the heart rate was constant over two cardiac cycles so that ECG-triggering every two heart beats was sufficient. By appropriately adjusting the number of cardiac phases to acquire per cardiac cycle as well as the number of echoes at which the labeling pulses occur (NE_1, NE_2 and NE_3 in Figure 4.8), more than one cardiac cycle coverage without interrupting the steady-pulsed labeling scheme was possible. The repetition time TR between each gradient echo was kept as short as possible to maximize temporal resolution (six milliseconds in these experiments).

In summary, this modification was done for two reasons:

- The cine readout covered almost two cardiac cycles with a negligible interruption of the FLASH steady-state at the end of the second cardiac cycle.
- The labeling was still performed every heart beat which is mandatory to optimize labeling efficiency (see perfusion quantification section below).
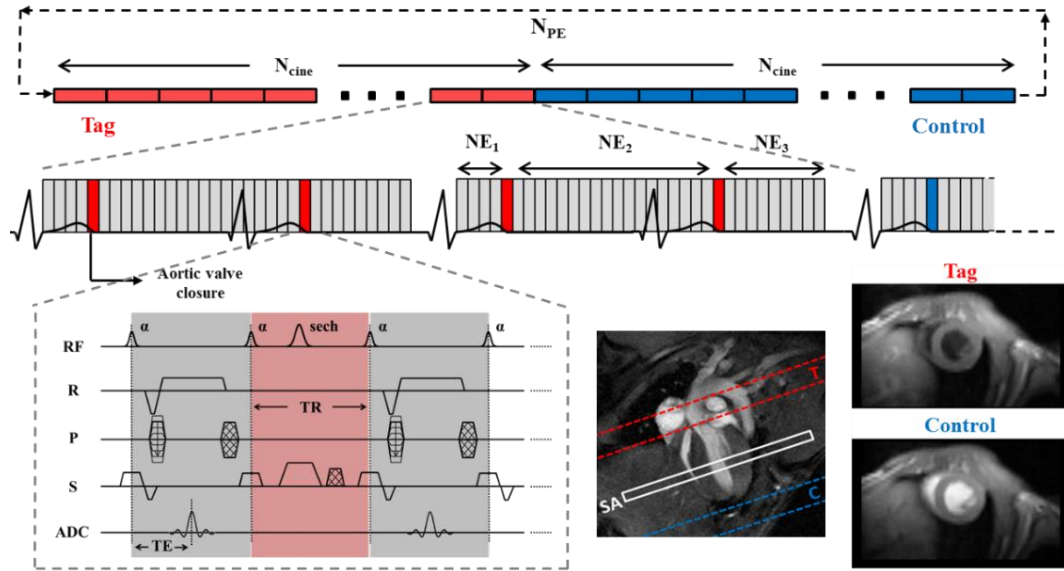

Figure 4.8 – Long version of the cine-ASL sequence used for measurement of cyclic blood flow changes during the cardiac cycle. Compared to the original sequence, the cine readout was extended to cover almost two cardiac cycles. The labeling had to be performed at every cardiac cycle to keep an optimized labeling efficiency despite the extension of the readout over two cardiac cycles. This was done by carefully adjusting the number of echoes before and after each labeling pulse (NE$_1$, NE$_2$ and NE$_3$). Note that no recovery delay was present between tag and control cine block series to optimize acquisition time. The repetition time TR between each gradient echo was kept as short as possible to maximize temporal resolution, six milliseconds in these experiments.

Experimental Protocol

All imaging experiments were performed with the same MR equipment as in the initial experimental study presented in Chapter 2. Prior to the perfusion measurements, scout images were acquired to determine the short-axis plane used for the perfusion imaging sequences. A cine-FLASH sequence in four-chamber long-axis view was used to achieve precise spatial and temporal placement of the labeling pulses at end-systole, just before aortic valve closure.

Perfusion measurements were carried out in the short-axis plane using cine-ASL with the following parameters: imaging slice thickness: 2 mm, field of view: 40 mm, in-plane resolution: 312 x 625 µm², TE/TR: 1.64/6ms, flip angle α: 8° (gaussian pulses, 0.5 ms), labeling slice thickness: 6 mm (adiabatic hyperbolic secant pulses, 3.7 ms). The number of acquired cardiac phases (N$_{echoes}$) was adjusted according to the animal's heart rate, allowing about 30 echoes per cardiac cycle and 50 echoes per cine block (~ 1.7 cardiac cycle). Acquisition time was approximately 12 min at 400 bpm. All animals first underwent MBF quantification at rest. Continuous adenosine infusion was accomplished using a dedicated low-flow pump injector (World Precision Instruments, Sarasota, FL, USA) and a tail vein catheter. The infusion rate was set to 280 µg kg^{-1} min^{-1}, which corresponds to twice the standard clinical rate used in human clinical practice. This rate was shown in preliminary experiments to reliably produce a maximal

response to adenosine. The second cine-ASL sequence was started 5 minutes after an initial heart rate drop observed upon arrival of adenosine and infusion was maintained until completion of the sequence. The criterion for a hyperemic state was a significant increase in MBF compared to rest condition.

Perfusion quantification

Global MBF maps in left ventricular myocardium were computed from the steady-state perfusion-dependent gradient-echo cine images. As a result of the theory presented in Chapter 2, the experimentally measured relevant quantity is the stationary signal difference between control and tag scans $\Delta M_\infty = M_\infty^c - M_\infty^t$, which is related to myocardial blood flow by the following equation:

$$\text{MBF} = \frac{\lambda M_{ss}}{T_1^* M_0} \frac{C_\infty}{2\beta - C_\infty} , \qquad [4.2]$$

where, β corresponds to the average labeling efficiency, $\lambda = 0.95$ the blood-tissue partition coefficient for water *[Waller 2000]* and T_1^* the apparent relaxation time measured under the influence of rapid succession of small flip angle pulses *[Deichmann 1992]*. T_1 was fixed to 1.31 s as reported in a previous study *[Kober 2004]*. M_{SS} is the longitudinal steady-state magnetization observed under FLASH partial saturation and can be directly calculated from M_0, TR, T_1 and the excitation flip angle α:

$$M_{ss} = M_0 \frac{1 - e^{-TR/T_1}}{1 - \cos(\alpha)e^{-TR/T_1}} . \qquad [4.3]$$

It important to recall that the labeling efficiency reached with this particular steady-pulsed scheme was only 0.5, although adiabatic inversion pulses were used. Considering the large extent of the inversion slice of 6mm which covers both atria, pulmonary compartments and the aorta, blood entering into the coronaries has already been inverted several times with different inversion delays before reaching the microvascular compartment. It has been shown that this multiple exposure of blood spins to inversion pulses led to reduced labeling efficiency β of 0.5, also confirmed by absence of signal in the LV blood pool as observed earlier.

Image processing

Transmural MBF was quantified as an average of pixel values for ROIs drawn on every map in the series (about 50 maps per acquisition). Global myocardium was first evaluated from the MBF maps for each rat as a function of time. Since the blood signal coming from the left ventricle and from the coronaries was significantly higher than the measured signal of interest, particular attention was paid at masking this signal on each individual map. Indeed, coronary flow is known to be highly variable within the cardiac cycle *[Davies 2006]*, and taking blood signal into account could lead to a misinterpretation of cyclic myocardial perfusion variation.

Since the cyclic variations observed at rest and during stress were dependent on the animal's heart rate, data were temporally normalized with respect to the individual RR interval. In order to perform a group analysis, MBF data were sorted into bins representing the mean temporal resolution after the normalization process. Finally, myocardial perfusion reserve (MPR) was computed as a ratio of stress and rest MBF for each temporal bin.

To obtain the average change of MBF over the cardiac cycle, the two highest and lowest values found at end-diastole (ED) and end-systole (ES), respectively, were averaged so as to calculate the relative cyclic variation defined as:

$$\Delta MBF_{Cycl} = \frac{\left(MBF_{Max} - MBF_{Min}\right)}{MBF_{Max}} \ .$$

[4.4]

Measurements of systolic and diastolic MBF were done in the first cardiac cycle for each individual rat at rest and during stress before averaging within the group. To assess inter-observer variability, all measurements were performed twice by two different readers.

Statistical method

Data were presented either as group mean value ± SD across the entire cardiac cycle or as group mean value ± SD for each temporal bin within the cardiac cycle. All statistical processing was performed using Prism 5 software (Graph Pad, San Diego, CA, USA). Statistical differences between systolic and diastolic values of MBF and MPR, i.e. minimum and maximum, were evaluated using a paired t-test. A probability value of $P < 0.05$ was taken as statistically significant. Correlation between heart rate and relative cyclic variation ΔMBF_{Cycl} was quantified by the Pearson rank correlation coefficient rho. A paired t-test was also used to compare cyclic variation measurements between the two observers.

4.3.c.   Results

The cine-ASL approach allowed for dynamic quantification of MBF across the cardiac cycle with time-frames given by the cine repetition time of 6 milliseconds. Figure 4.9 shows an example of a perfusion map series over the entire cardiac cycle obtained with cine-ASL from the same rat at rest and during adenosine stress.
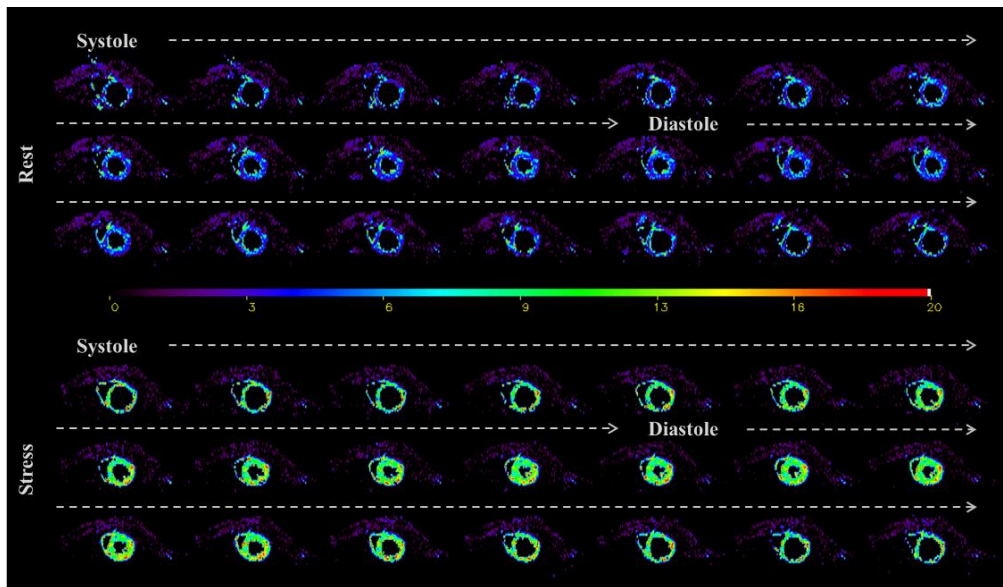

Figure 4.9 – Dynamic MBF mapping. Twenty one consecutive color-coded short-axis perfusion (MBF) maps resulting from a measurement series over the cardiac cycle. The color scale is in mL g^{-1} min^{-1}. Data are shown from the same rat heart at rest (top) and during stress (bottom) while 280 µg kg^{-1} min^{-1} of adenosine were administered intravenously inside the magnet.

By inducing strong hyperemia with adenosine, perfusion significantly increased by a factor of 2.1. In this example, mean perfusion over the entire cardiac cycle in the global myocardium increased from 6.3 ± 0.6 mL g^{-1} min^{-1} at rest to 13.7 ± 1.3 mL g^{-1} min^{-1} during stress. This result demonstrates that cine-ASL has the potential to dynamically map MBF over the cardiac cycle and to study and quantify changes in myocardial perfusion within the cardiac cycle for different physiological states. In terms of breath and heart rates, no statistical differences were found between experiments at rest and during stress (*Table 4.2*).

Table 4.2 – Physiological parameters recorded during the experiment. No statistical differences (ns) were found between rest and stress experiments.

Rat	Body Weight (g)	Heart Rate (bpm)		Breath Rate (bpm)	
		Rest	Stress	Rest	Stress
1	320	370 (±30)	387 (±40)	65	70
2	330	359 (±10)	341 (±20)	70	80
3	325	261 (±40)	256 (±50)	60	65
4	338	359 (±15)	308 (±20)	65	60
5	337	286 (±10)	300 (±20)	60	65
6	320	310 (±5)	330 (±30)	75	70
7	335	308 (±10)	323 (±20)	65	60
Mean	329	322	321 ^{ns}	68	67 ^{ns}
± SD	± 8	± 42	± 40	± 7	± 8

Capillary flow dynamics

In Figure 4.10A all individual MBF data sets observed in the seven normal rats studied are shown as a function of time, at rest and during adenosine stress. Figure 4.10B shows normalized data over the cardiac cycle. Figure 4.11A shows the evolution of MBF across the cardiac cycle at rest and during adenosine-induced stress. These results are plotted as a function of the normalized cardiac cycle averaged over the seven animals studied ± standard deviation within the group. Along the series starting at early-systole, perfusion gradually and significantly decreased, reaching a minimum at ES and then recovered during the diastole. This general behavior was well reproducible in all subjects. The maximal perfusion values were always found to be at ED just before the next QRS complex. One can also notice a slight shift of the maximum MBF during stress compared to rest which was found to be reached sooner within the cardiac cycle. In Figure 4.11B, averaged MPR within the group is reported as a function of the normalized cardiac cycle. MPR behavior was found reversed compared to MBF variation, with an initial increase during systole until a maximum at ES. This maximum value was sustained during most of the diastole. Towards the end of the cardiac cycle, MPR dropped in a sudden way reaching a minimum at ED.
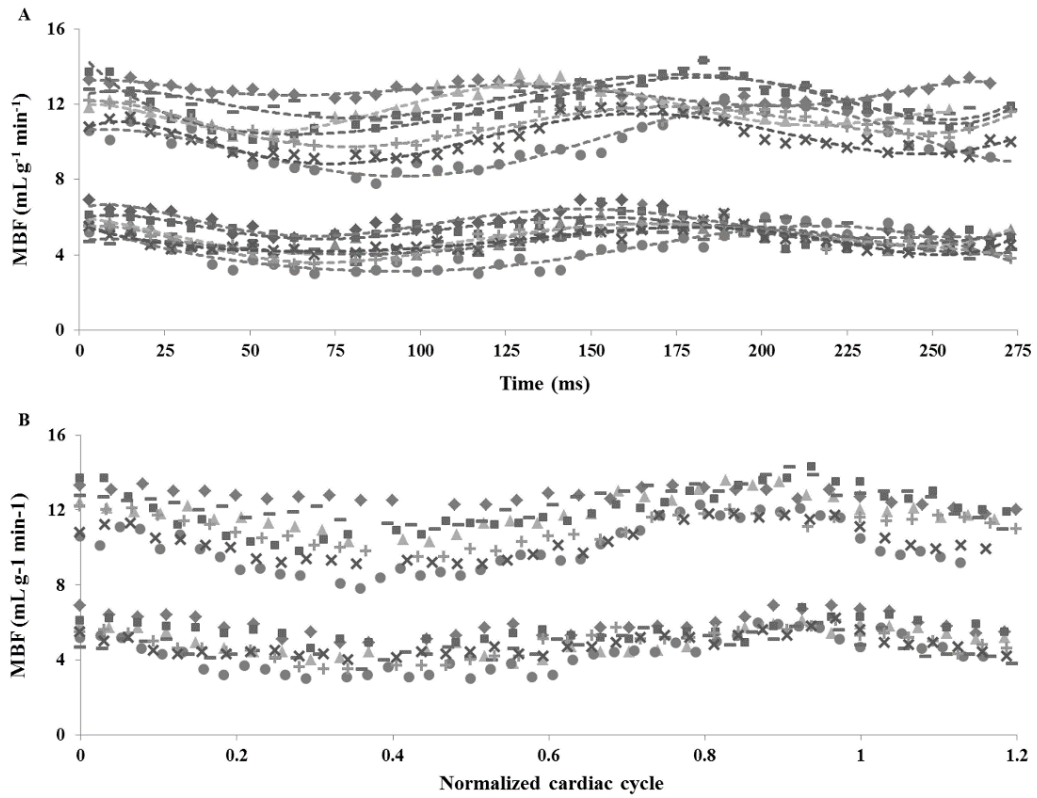
Figure 4.10 – Temporal normalization process. All individual cyclic perfusion dynamics (A) were rebinned relatively to heart rate resulting in curves that represent the MBF evolution as a function of the normalized cardiac cycle (B). Once the data are normalized, a general behavior emerges along the cardiac cycle with variation within the group depending on individual response to adenosine.
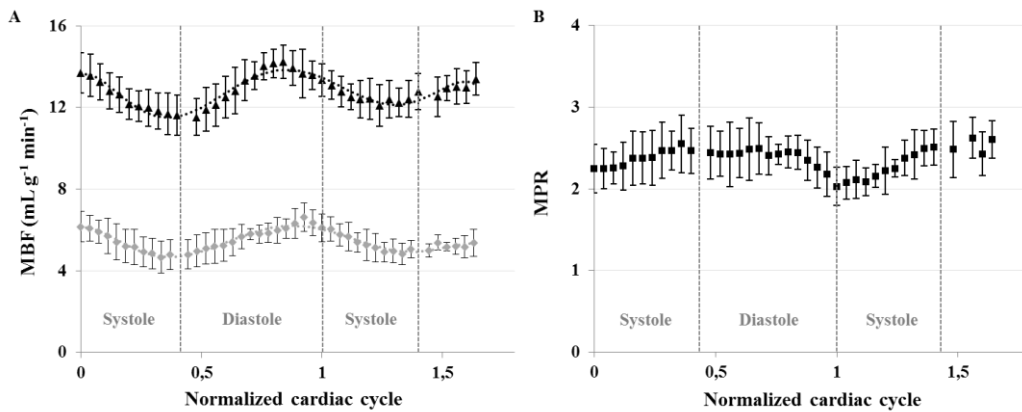
Figure 4.11 – Cyclic myocardial perfusion variation over the cardiac cycle. (A) Mean MBF within the group ± SD of seven healthy rats are reported as a function of the normalized cardiac cycle. These are shown at rest (grey diamonds) and during adenosine-induced stress (black triangles). For clarity, a six orders polynomial regression was used to fit the data. Minimum MBF was found to be at ES for both physiological states. Maximum MBF was found to be at ED at rest and sooner than ED during stress. (B) MPR values are given as free ratios of stress and rest MBF. MPR behavior (black squares) was found reversed compared to MBF variation, with first an initial increase during systole until a maximum at ES. This maximum value was conserved during most of diastole with a minimum at ED.

119

For each temporal bin along the cardiac cycle, mean perfusion values were found in agreement between the two observers. No significant differences were found between the two observers, with a Pearson correlation coefficient of r = 0.88 at rest and r = 0.89 during stress. We found a mean MBF over the cardiac cycle of 5.5 ± 0.6 mL g^{-1} min^{-1} at rest (observer 1, 5.7 ± 0.6 mL g^{-1} min^{-1} and observer 2, 5.4 ± 0.6 mL g^{-1} min^{-1}, $P = 0.12$) which was significantly different from 12.8 ± 0.7 mL g^{-1} min^{-1} obtained during stress (observer 1, 13.1 ± 1.2 mL g^{-1}min^{-1} and observer 2, 12.6 ± 0.7 mL g^{-1} min^{-1}, $P = 0.38$) . Results are presented in Figure 4.12A. A significant difference in myocardial perfusion was found between rest and stress conditions ($P < 0.0001$), leading to a mean perfusion reserve of 2.4 ± 0.2 within the group.

The two lowest values and the two highest values obtained within the cardiac cycle were identified and averaged for each studied animal. The minimum and maximum MBF values found at ES and ED were defined as MBF$_{Min}^{Rest,Stress}$ and MBF$_{Max}^{Rest,Stress}$ respectively. Individual results are reported in Figure 4.12B. Resting transmural MBF extrema were significantly different with MBF$_{Min}^{Rest}$ = 4.7 ± 0.8 mL g^{-1} min^{-1} and MBF$_{Max}^{Rest}$ = 6.5 ± 0.6 mL g^{-1} min^{-1} ($P = 0.0007$). During stress, they were also significantly different with MBF$_{Min}^{Stress}$ = 11.7 ± 1.0 mL g^{-1} min^{-1} and MBF$_{Max}^{Stress}$ = 14.2 ± 0.7 mL g^{-1} min^{-1} ($P = 0.0007$). The mean relative variation ΔMBF$_{Cycl}$ within the group Figure 4.12C), was found significantly different between both conditions. We found 27.2 ± 9.3 % decrease from ED to ES at rest and 17.8 ± 7.1 % during adenosine stress, with paired samples t-test $P = 0.014$. On the other hand, MPR was minimum at ED, 1.9 ± 0.1 and maximum at ES, 2.8 ± 0.3 ($P < 0.0001$). Individual quantifications as well as a statistic summary are reported in Table 4.3 for MBF and Table 4.4 for MPR.
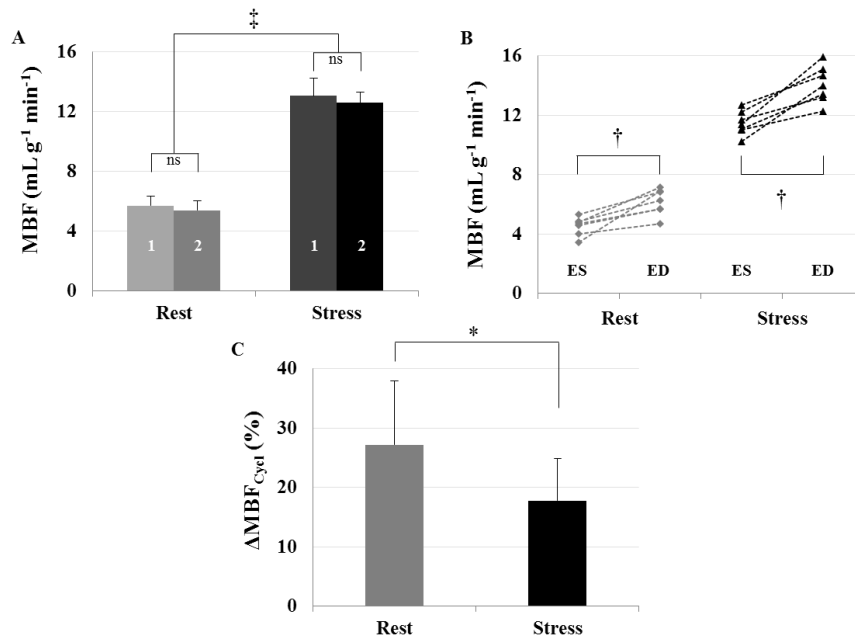
Figure 4.12 – (A) Mean MBF obtained within the group at rest (5.5 ± 0.6 mL g^{-1} min^{-1}) and during adenosine stress (12.8 ± 0.7 mL g^{-1} min^{-1}, P < 0.0001,‡). No statistical differences were found between the two observers (labels #1 and #2). (B) Individual minimum and maximum MBF values found at ES and ED, respectively. Two-tailed paired t-test was performed to compare minimum and maximum MBF, respectively, at rest, 4.7 ± 0.8 vs. 6.5 ± 0.6 mL g^{-1} min^{-1} (P = 0.0007,†) and under stress, 11.7 ± 1.0 vs. 14.2 ± 0.7 mL g^{-1} min^{-1} (P = 0.0007,†). (C) The mean relative variation ΔMBF$_{Cycl}$ was found significantly different (27.2 ± 10.7 % at rest and 17.8 ± 7.1 % at stress (P = 0.014,)).*

Table 4.3 – Individual myocardial blood flow obtained in 7 healthy rats at rest and during adenosine stress. Individual mean and standard deviation has been calculated over the entire cardiac cycle. Two-tailed paired t-test P values: $^*P = 0.014$ (ΔMBF_{Cycl}), $^\dagger P = 0.0007$ (maximum vs. minimum) and $^\ddagger P < 0.0001$ (stress vs. rest for Mean MBF).

Rat	MBF Rest (mL g^{-1} min^{-1})				MBF Stress (mL g^{-1} min^{-1})				ΔMBF_{Cycl} (%)	
	Min	Max	Mean	SD	Min	Max	Mean	SD	Rest	Stress
1	5.5	7.3	6.3	0.6	12.7	13.7	13.2	0.7	25.2	7.3
2	5.4	6.6	5.9	0.5	11.9	13.7	12.7	0.7	19.1	12.8
3	3.5	6.8	4.8	1.0	10.5	14.8	12.3	1.4	48.5	29.2
4	5.3	7.3	6.2	0.6	12.3	15.0	13.5	1.0	28.2	17.8
5	4.5	6.1	5.3	0.5	12.8	15.0	13.7	0.8	26.4	14.7
6	4.0	5.7	5.1	0.6	10.6	13.8	12.5	1.0	29.5	22.8
7	4.7	6.3	5.1	0.5	10.8	13.5	11.8	0.9	25.3	19.8
Mean	4.7	6.6 †	5.5	0.6	11.7	14.2 †	12.8 ‡	0.9	27.2	17.8 *
± SD	0.7	0.6	0.6		1.0	0.7	0.7		9.3	7.1

Table 4.4 – Individual myocardial perfusion reserve obtained in 7 healthy rats. Paired t-test $^*P < 0.0001$ (maximum vs. minimum).

Rat	MPR				
	Min	Max	Mean	SD	ΔMPR (%)
1	1.7	2.8	2.2	0.2	38
2	1.8	2.7	2.2	0.2	35
3	1.8	3.2	2.6	0.4	42
4	1.9	2.8	2.3	0.2	29
5	2.2	3.1	2.7	0.2	29
6	2.1	2.9	2.4	0.2	28
7	2.0	2.7	2.3	0.2	26
Mean	1.9	2.9 *	2.4	0.2	32
± SD	0.2	0.2	0.2		6

Heart rate and cyclic MBF variation amplitude

In Figure 4.13A, the impact of the heart rate on the amplitude of MBF variation is highlighted. This graph shows the two extreme cases found within the group in terms of heart rate, i.e. the animal with the highest heart rate (Rat 1, 370 bpm) and the one with the lowest heart rate (Rat 3, 260 bpm). For clarity, a six orders polynomial regression was used to fit the data. ΔMBF_{Cycl} (Figure 4.13B) was lower for Rat 1 (24% at rest and 9% during stress) compared to the Rat 3

(42% at rest and 31% during stress). We verified whether a linear group correlation existed between individual heart rate and the corresponding relative variation ΔMBF_{Cycl} for both rest and stress conditions (Figure 4.14). There was a significant correlation between ΔMBF_{Cycl} and heart rate during stress (rho = -0.83, P = 0.02) but not at rest (rho = -0.67, P = 0.10).
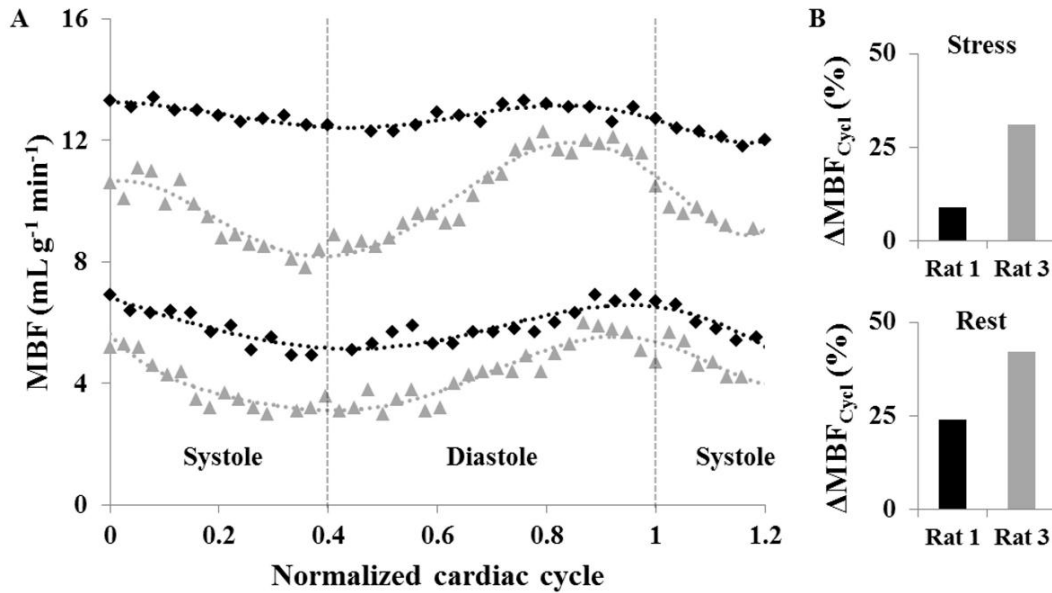
Figure 4.13 – Individual comparison of cyclic myocardial perfusion variation. (A) MBF is shown for two specific animals as a function of the cardiac cycle: Rat 1 with a heart rate of 370 bpm (black diamonds) and Rat 3 with a heart rate of 260 bpm (grey triangles). (B) The variation ΔMBF_{Cycl} was higher for Rat 3 (42% at rest and 31% during stress) compared to Rat 1 (24% at rest and 9% during stress).
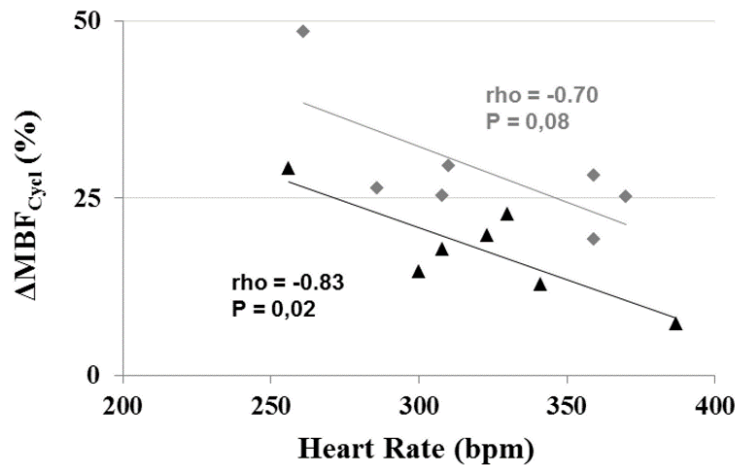
Figure 4.14 – Relationship between heart rate and amplitude of the relative MBF variation. A linear group correlation exists between individual heart rate and the corresponding relative variation ΔMBF_{Cycl} during adenosine stress (black triangles, rho = -0.83, P = 0.02). Even though no correlation was found at rest (gray diamonds, rho = -0.70, P = 0.08), a dependence of ΔMBF_{Cycl} on heart rate can be seen.

122

4.3.d.   Discussion

In this study we report time-resolved absolute quantification of MBF by MRI with a new approach based on a cine-FLASH labeling and readout module. The spatial resolution (313 x 625 μm²) and the sensitivity were sufficient to measure global myocardial perfusion and hemodynamic changes within the cardiac cycle in approximately 12 min. MBF maps were obtained with a high temporal resolution of 6 ms covering almost two cardiac cycles. The tagging scheme used here consists in rapidly repeated local inversions with precise timing within the cardiac cycle. It allows maintaining the labeled blood state throughout the experiment while a cine readout can be achieved during the remaining time with a steady-state acquisition. Tissue magnetization is thus driven into a perfusion-dependent equilibrium state so that signal changes that occur during the cardiac cycle can only reflect changes in momentary tissue blood flow. Arterial spin labeling measures the integrated effect of tagged blood flowing through the vasculature and remaining in the capillary system during the mean transit time (MTT). MTT is of the order of a second in the rodent heart and therefore much longer than a cardiac cycle. The averaged blood flow across the cardiac cycle reported here corresponds to the mean blood flow commonly defined by MBF = MBV/MTT which is understood on a much longer time scale than a cardiac cycle. By using high-temporal resolution cine readouts of 6ms, signal that is acquired within a narrow window allows capturing the time-variant changes in the microvascular status of the myocardium, which is related to the number of patent myocardial microvessels. Thus, the variations observed at different time-points within the cardiac cycle have to be distinguished from the mean blood flow and are due to cyclic variations of momentary flow.

Capillary flow dynamics

Figure 4.11 shows that cyclic temporal variations were measurable using the cine-ASL technique. Left-coronary arterial blood flow is characterized by a diastolic-dominant inflow *[Chilian 1988]* whereas small distal venous flow exhibits a systolic-dominant pattern *[Kajiya 2007]*. Our results are consistent with the expected physiological pattern of preferential coronary diastolic filling.

A clear and complete description of coronary flow patterns across the cardiac cycle in humans has been proposed by Davies *et al.*, who used intracoronary wires for measuring pressure and Doppler velocity waveforms *[Davies 2006]*. Microvascular MBF is closely related to macrovascular coronary flow such that these results can be confronted to ours. During systole, the authors observed a dominant forward-travelling pushing wave in proximal coronary arteries that is reflected when reaching the microvascular bed in distal coronary arterioles, causing blood to move in the opposite direction. Coronary arteries are also known to have a significant capacitance to accommodate for blood supply *[Kajiya 2008]*. Also, during ventricular contraction, the compressive forces on the small vessels lying in the myocardium increase while venous outflow is in its dominant phase. One can therefore expect decreasing capillary flow during systole, which is consistent with our observations. During diastole, however, Davies and coworkers highlighted a dominant backward-travelling 'suction' wave initiated at the beginning of ventricular relaxation along with decreased compressive forces on capillaries and resistance of microvessels. Closure of the aortic valve in early diastole generates a late forward-travelling pushing wave which accelerates blood still further towards the myocardium. Most of the arterial inflow occurs during diastole with a velocity peak at early to mid-diastole. We observed the same pattern with a delay that corresponds to the time for the blood to reach the microvascular compartment.

We showed that momentary blood flow is non-uniform through the cardiac cycle and occurs mainly in diastole when myocardial tension is low. Therefore, the timing of data acquisition in myocardial perfusion experiments may affect the measured MBF and might be considered in the evaluation of perfusion exams in both research and clinical practice. We note here that for studying temporal variations of perfusion using arterial spin labeling MRI, the underlying spin-exchange model has to be kept in mind. One-compartment models are valid for perfusion quantification in the heart *[Wong 1997]*, in which free diffusivity and complete exchange of the blood magnetization with the tissue during the presence of a spin in the arterial capillary compartment is assumed. However, the time scale relevant here is the delay between successive cardiac frames, which is much shorter than the time for spins to travel across the arterial capillary compartment, i.e. the time relevant for perfusion model validity. Taking into account spin exchange between perfusate and tissue, rapid MBF variations are observable if the exchange is fast on the scale of our frame rate. The significant cyclic perfusion change found in this study supports the assumption of sufficiently fast capillary/tissue spin exchange in myocardium. In the literature, there are few studies regarding changes in spin exchange rates in the context of cardiovascular pathologies. Since arterial spin labeling only uses water molecules, we can hypothesize that the fast exchange assumption should be preserved even across pathologies.

Rest versus Stress

Changes in MBF across the cardiac cycle were significant in this study with, in general, a similar behavior between rest and stress experiments. Nevertheless, two major differences arose from these results. First, maximum MBF appeared sooner within the cardiac cycle at stress than at rest. This was the case not only within the averaged group results, but also for each studied animal. This observation is also reflected in the MPR variations, in which a drop was found at the end of the cardiac cycle, corresponding to the delay between both physiological states. Second, we found a mean group decrease of MBF from ED to ES (ΔMBF_{Cycl}) of 27.2 ± 9.3 % at rest, which was significantly higher from ΔMBF_{Cycl} obtained during stress (17.8 ± 7.1 %, $P = 0.014$).

In a study published by Kajiya *et al.*, the authors focused on the phase opposition of velocity waveforms between coronary arteries and veins *[Kajiya 2008]*. They introduced the unstressed volume (UV), which refers to a capacitance accommodating for blood supply during diastole without significant increase in UV pressure to propel venous outflow. But UV can become saturated when diastolic arterial inflow is higher than normal, such as in pharmacologic stress situations causing vasodilation. In this case, the pressure of ordinary capacitance exceeds the venous pressure causing diastolic venous outflow. Such theory might explain why the maximum MBF was found to appear sooner within the cardiac cycle during stress.

When administered intravenously, adenosine effect is mixed, endothelial dependent and non-dependent *[Sato 2005]* and thus causes relaxation of smooth muscles as found inside the arterial walls. This action leads to vasodilation and increases arterial inflow along with a decreased resistance and an increased capacitance of microvessels. Here, the term vascular resistance refers to the impediment offered by the vascular bed to a unidirectional and constant blood flow. The concept of vascular impedance, however, involves the pressure-flow relations at each instantaneous timing change and refers to the impediment offered to flow at the input of a vascular bed where pulsatile flow is involved. Thus, vascular impedance takes into account not only the resistance but also dynamic effects and seems more appropriate in this context. It is defined as

the ratio of arterial pressure and flow. By reaching the maximum coronary response using adenosine, microvessels are already subjected to very high blood flow but also to reduced arterial pressure *[Waller 2000]*, which in our experiments resulted in lower vascular impedance represented in our experiments by a lower ΔMBF_{Cycl} during stress.

Relationship between heart rate and ΔMBF_{Cycl}

There was a linear correlation when comparing heart rate and ΔMBF_{Cycl} amplitude during stress (Figure 4.13 and Figure 4.14). However, no significant correlation was found at rest which might be explained by the lower sensitivity of ASL at rest compared to stress. This might also be due to an insufficient number of animals to reach significance. There is a dependence of ΔMBF_{Cycl} on heart rate under stress, which could be present at rest as well. A likely explanation for this behavior is that the vascular system of the heart has a capacitive property when submitted to pressure variations at its entry. Analogies between electrical circuits and the vascular system, such as the Windkessel model, have been often used for modeling approaches *[Kissling 2000]*. In a similar way as electric current in a capacitor submitted to voltage variations, the pressure oscillations lead to flow oscillations whose amplitude depend on the frequency of the pressure variations, here given by the heart rate.

Absolute MBF and MPR quantification

It should be noted that all MBF values reported in this study, especially at rest, cannot be considered as physiological baseline values due to the influence of isoflurane anesthesia on coronary vasodilation *[Crystal 1996, Iltis 2005b]*. Resting MBF within the group was 5.5 ± 0.6 mL g^{-1} min^{-1} and therefore similar to previously reported values in rats, which are in the range of 3.83-7.89 mL g^{-1} min^{-1}, using MRI *[Kober 2004, Iltis 2005c, Jacquier 2011]* or fluorescent microspheres *[Wicker 1982, Debaene 1990, Jacquier 2011]*. MBF obtained during stress was 12.8 ± 0.7 mL g^{-1} min^{-1}, and mean MPR was 2.4 ± 0.2. To our knowledge, MPR has not been reported to be more than 2.5 in rodents and our results were in accordance with earlier obtained values using MRI in comparison with fluorescent microspheres *[Jacquier 2011]* or contrast-enhanced ultrasound *[Oshita 2002, Raher 2007]*. However, MPR in this experiment was found higher than that reported by Croteau *et al.* (1.4 ± 0.5) in a study using positron emission tomography and ^{13}N-NH_3 as radiotracer *[Croteau 2004]*. In their article, the authors discussed the fact that vasodilation induced by the pharmacologic stress was not maximal in their experimental design with the commonly used clinical injection rate of 140 µg kg^{-1} min^{-1}. In our first experimental trial, we also encountered difficulties to obtain a reproducible stress within a group of healthy rats using this typical infusion rate. Increasing twice the infusion rate and using a small injection line with inner diameter of 0.58 mm resulted in obtaining a maximal MPR more reliably.

Study limitations

In humans, Radjenovic *et al.* found no differences between systolic and diastolic MBF at rest and a significant MBF increase in diastole during adenosine-induced stress *[Radjenovic 2010]*. The authors discussed that cyclic MBF changes may be present also at rest in humans but that the precision of the first-pass gadolinium-based MRI method used in their work might not be sufficient to assess them.

MBF quantification errors may be present by various sources such as respiratory motion. No respiratory gating was done with this sequence. Likely owing to the high number of signal

averages performed with cine-ASL along with randomization of breathing events with myocardial contraction, impact of respiratory motion on MBF quantification and cyclic behavior is expected to be negligible.

Although the heart lengthens longitudinally from systole to diastole, through-plane motion affects both control and tag scans in the same way so that their effects should cancel when calculating the difference maps. Effect of through-plane motion on the magnetization steady-state should also be relatively small considering the rather thick (2mm) slices. With cine-ASL, temporal placement of the labeling pulse cannot be corrected once the acquisition started. Particular attention was paid to heart rate stability so as to ensure regular labeling efficiency throughout the entire 12 minutes scan. As shown in Table 4.2, the heart rate variation in this group of healthy rats did not exceed 15% at rest and 20% during stress, and one can therefore expect limited impact of label pulse timing imperfections on MBF quantifications. Heart rate variations can, however, be larger in models of cardiac pathology and would necessitate individual labeling efficiency determination.

Another potential source of error, especially when assessing dynamic perfusion changes over the cardiac cycle, are the short waiting periods before each ECG trigger that lead to interruptions of the longitudinal magnetization steady-state. Again, these interruptions affect tag and control scans in the same way, but in addition, the acquisition was extended over two cardiac cycles instead of one, such that the second cycle was not affected by the steady-state interruption. Figure 4.10 and Figure 4.11 indeed prove good concordance between the dynamics of the initial phases of the first and the second observed cycle. Finally, it cannot be excluded that tissue and/or blood T_1 as well as T_2^* are submitted to changes throughout the cardiac cycle. T_1 might in addition be altered in a pathological context when tissue structural changes play a role. As a limitation common to many ASL techniques, cine-ASL would indeed require the acquisition of a T_1 map to be fully quantitative. In terms of cyclic changes, the influence of T_1 variations across the cardiac cycle can, however, be expected to remain small and would only linearly affect the resulting MBF values. Given the short echo time used in the cine-ASL sequence, the influence of T_2^* on the signal is also expected to remain small.

In conclusion, this study presents the first attempt to quantify and monitor cyclic MBF variation in vivo in rats using a fully non-invasive arterial spin labeling MRI protocol. These experiments were carried out in a group of healthy rats with a focus on cyclic changes at rest and during adenosine-induced stress. Our observations clearly show that, in rodents, blood flow is phase-dependent and differs significantly between systole and diastole, for both rest and stress conditions. We discussed rat myocardial perfusion changes in response to adenosine as an infused vasodilator in detail and provided complementary information on how cyclic perfusion changes are affected by the vasodilator. Also, maximum absolute blood flow occurs earlier under stress conditions than under resting conditions. This might become relevant when calculating perfusion reserve based on two measurements with equal trigger delays. Considering the nature of coronary hemodynamics, cyclic MBF changes may reveal new physiologic information because they are a function of coronary flow, myocardial contraction and microvascular condition. This technique may be useful in a pathologic context to study microvascular defects in non-ischemic heart disease models.

4.4. A Multi-Modal MRI/MRS Protocol to Study Type-II Diabetes

This section is based on:

A multimodal 30-minutes MRI and MRS protocol for longitudinal monitoring of myocardial function, perfusion and triglyceride content in diabetic mice. Abstract submitted to the 22nd ISMRM congress, Milan, 2014.

Troalen T, Abdesselam I, Pepino P, Bernard M, and Kober F.

The methodological developments made during this thesis led to setup a new sequence to quantify perfusion in small-animal studies. The cine-ASL sequence appeared to be faster than the previously employed techniques based on FAIR labeling, although the only drawback is a potential reduced accuracy in absolute quantification (uncertainty on β, and no T_1 quantification). Beyond the presented studies, this sequence was integrated into several multimodal protocols to study rodent cardiovascular disease models in greater detail.

The cine-ASL sequence has been used for the longitudinal exploration of two particular rodent models of diabetes, the high-fat high-sucrose mouse model and the Goto-Kakizaki rat. Given the longitudinal character of these studies and a rather large number of animals, a multi-modal protocol was setup with the goal of keeping examination times short while providing good estimations of important functional, microvascular and metabolic measurements relevant in diabetes and obesity. These multi-parametric studies are designed to establish the chronological order of the appearance of anomalies associated with diet-induced obesity and insulin resistance.

4.4.a. Methods

Systolic and diastolic function was assessed using a high resolution cine-FLASH sequence (TR: 5 ms, slice thickness: 1.5 mm, in-plane resolution 200 x 200 μm²). Standard full volume coverage of the left-ventricle using multi-slice acquisition is not only time consuming but might also not be compatible with specific cardiovascular disease models in which prolonged anesthesia is undesirable. A two-slice approach using the hemisphere cylinder model (one short-axis and one long-axis view, Figure 4.15) was therefore used for volume approximation. This model has recently been evaluated as one of the better approximations to assess cardiac function in a reduced scan- and post-processing time *[van de Weijer 2012]*.
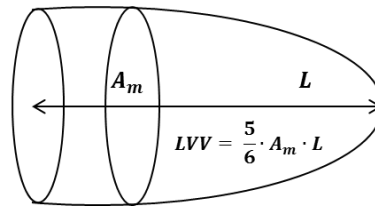
Figure 4.15 – Hemisphere cylinder model. The length (L) is measured on a long-axis view while the surface (A_m) is measured on a short-axis view placed just below the mitral valve. Left ventricular volume (LVV) can thus be approximated using the proposed equation.

Myocardial blood flow was quantified using the shortened version of the cine-ASL sequence as detailed in the first section of this chapter. Again, acquisition time has been reduced to its minimum while keeping compatibility with time constraints in cardiac MR (T_{Acq} = 3.5 min at 500 bpm).

Ectopic fat deposition in the myocardium and the liver was quantified using double-gated Point-RESolved Spectroscopy (PRESS) *[Burtscher 2001]*. To assess myocardial triglyceride content, a first PRESS scan was acquired at end-systole (TR/NA/Tacq = 5s/512/8min, volume 2μL), followed by a reference scan to obtain an unsaturated water peak (TR/NA/Tacq=5s/64/5min). Hepatic triglyceride content was assessed using a larger spectroscopic volume of 8μL allowing for reduced scan time (TR/NA/Tacq=1s/128/3min and TR/NA/Tacq=5s/32/4min for the reference). The entire protocol is summarized in Figure 4.16.

Localization 2' –>   **Function** 4' –>   **Perfusion** 4' –>   **Ectopic Fat** 20'
4-chamber + SA   Rest cine-ASL   4 * Press MRS

Figure 4.16 – Protocol summary

Male C57Bl/6R mice (8 weeks) were subjected to a high fat high sucrose diet (HFHSD, N=10) or a regular diet (RD, N=10) during 4 months. To establish chronological order of anomalies appearance associated to di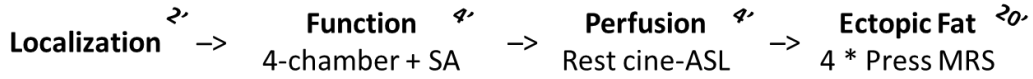et-induced obesity and insulin resistance, mice underwent complete exploration at 4.7T using this multi-modal MR protocol every month (M0 to M4). Mice were anesthetized with isoflurane added to 0.6 L min^{-1} of pure O_2. Compared to the previous studies, isoflurane concentration in these experiments varied from 1.5 to 2%, depending on the physiological stability of the animal during the experiment. One of the multiple parameters measured here was defined as abnormal when difference between both groups was statistically relevant ($P < 0.05$ using unpaired student t-test).

Due to the low scan time, a stress experiment using vasodilators might be added to the proposed protocol in obese mice. The entire protocol, including stress, was already performed in Goto-Kakizaki (GK) rats, a nonobese model of type-2 diabetes. The GK rat model is known to mimic the early stages of diabetes in humans *[Picarel-Blanchot 1996]* and is characterized by hyperglycemia, insulin resistance, endothelial dysfunction, and evidence of peripheral vascular complications *[Cheng 2001, Witte 2002, Desrois 2004, 2010]*. Experiments have been performed at 4.7T on 20 rats (10 GK rats and 10 Wistar control rats) and repeated at 8, 10, 13 and 15 months. However, data post-processing is still ongoing and results are not presented in this manuscript.

4.4.b. Preliminary results

The following presents preliminary results obtained in mice fed with high-fat high-sucrose diet.

The protocol performed well in all studied animals. Mice fed with HFHSD became obese compared to mice fed with RD (47.3 ± 0.7 g vs. 32.9 ± 0.1g at 4 months). Weight difference between both groups was already significant in the first month.

This weight gain was associated with abnormal triglyceride deposition in the liver (+1.9%) but not within the myocardium, in which increased triglycerides could only be seen one month later (+1.0%).

After 2 months of diet, myocardial fat deposition was associated with cardiac dysfunction premises, a significant decrease in end-diastolic volume (EDV, -16.8%) and cardiac output/weight ratio (CO/WR, -5.5%). Stroke volume (SV) was, however, significantly different between both groups only after four months of diet (-19.9%).

During the third month of diet, differences between groups were larger but no additional disorder was observed.

After 4 months of diet, hypertrophy (represented by an increased LV mass) along with reduced stroke volume was observed, which was correlated to a decreased myocardial blood flow (-14.4%). Chronological outcomes are summarized in Table 4.5.

Table 4.5 – Summary of the chronological outcomes obtained during the 4-month study. Abnormalities (increase or decrease) are expressed as relative (%) to the mean data obtained in the regular diet group.

Month	1	2	3	4
↗ Body Weight	+11.8%	+27.4%	+38.2%	+45.2%
↗ Hepatic fat	+1.9%	+11.5%	+25.9%	+26.3%
↗ Myocardial fat	∅	+1.0%	+1.0%	+1.6%
↘ EDV	∅	-16.8%	-17.2%	-23.7%
↘ CO/WR	∅	-5.5%	-9.0%	-11.5%
↘ Stroke volume	∅	∅	∅	-19.9%
↘ MBF	∅	∅	∅	-14.4%

This multimodal protocol allowed establishing chronological order of the appearance of anomalies associated with diet-induced obesity and insulin resistance in mice during a 4-month longitudinal assessment. A larger cohort of animals is currently being prepared following this particular high-fat high-sucrose diet. Measurement are planned to be repeated after four months of diet, and after a specific treatment using different cardio-protective molecules that might improve cardiac function and microcirculation.

4.5. Conclusion

In the first subproject we reported the validation of a strongly shortened cine-ASL sequence. Measurement quality was found to be comparable to the initial results presented in Chapter 2. This fast sequence was used to study the dynamic of the coronary response to a continuous infusion of adenosine as a vasodilator. Compared to human studies in which perfusion is generally assessed 3 to 4 minutes after adenosine injection, we found that for rodent studies, it is preferable to wait at least 5 minutes before acquiring perfusion data to ensure that maximal vasodilation is reached. Such measurements were until now inaccessible with the formerly employed myocardial ASL techniques.

These experiments were also useful for the second study presented in this chapter, which focused on cyclic MBF variation across the cardiac cycle. Our observations clearly showed that, in rodents, myocardial blood flow is phase-dependent and differs significantly between systole and diastole, for both rest and stress conditions. We discussed rat myocardial perfusion changes in response to adenosine as an infused vasodilator in detail and provided complementary information on how cyclic perfusion changes are affected by the vasodilator. Also, we found that maximum blood flow occurs earlier under stress conditions than under resting conditions, which might become relevant when calculating perfusion reserve based on two measurements with equal trigger delays.

The third study reports the use of a low scan time multimodal protocol to study functional, microvascular and metabolic alterations in a mouse model of type-2 diabetes induced by obesity. This fast and robust protocol will be used in a near future to work on a larger group of obese mice to strengthen these preliminary results and to study metabolic and functional improvements following drug therapy.

Conclusion

This thesis is part of a wider project conducted by the members of the '*MR Methods*' team at '*Centre de Résonance Magnétique Biologique et Médicale*' in Marseille. One of the main topics of this team is the development of non-invasive perfusion MRI methods with a transversal approach from animals to humans, dedicated to multiple organs including brain, spinal cord, kidney, and heart. These developments find their place in both basic and clinical research to study different pathologies, in which the microcirculation is altered.

Within the scope of improving cardiac perfusion MRI techniques, I joined the MR methods team in November 2010, supported by a funding from the healthcare division of Siemens France since February 2011.

The aim of this thesis was to develop new, optimized MRI sequences for a non-invasive quantification of myocardial perfusion using arterial spin labeling (ASL) in a translational way, working in parallel on both small-animal and human methods. The following figure summarizes my thesis work.
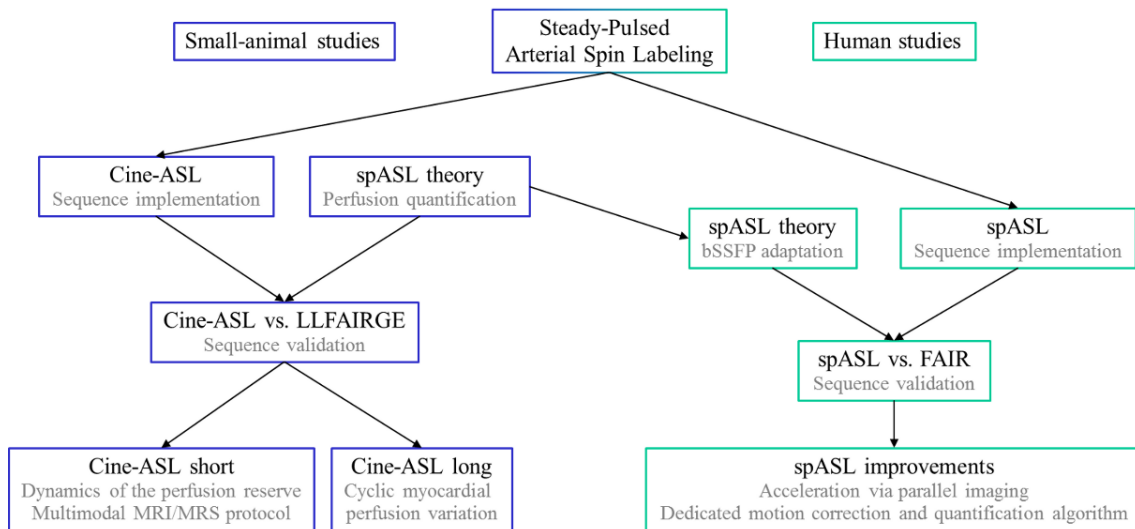
Figure 5.1 – Organization chart of the work realized during this thesis. Blue and green boxes correspond to small-animal and human studies, respectively.

The starting point was to focus on existing myocardial ASL techniques established in the past. Our institute initially developed the Look-Locker FAIR gradient echo (LLFAIRGE) technique for myocardial small-animal studies. This sequence had been successfully applied by several research groups afterwards, but it is characterized by long acquisition times. A first goal therefore was to elaborate a new strategy in the context of rodent studies.

Considering the high pulsatility of coronary flow irrigating the myocardium, all methods that have been developed in the past were based on pulsed ASL using the FAIR labeling scheme. Although FAIR is known to have a quasi-perfect inversion efficiency, it has the drawback of a poor acquisition efficiency in the context of cardiac ASL. Keeping in mind continuous ASL techniques, which are known to provide better sensitivity than pulsed ASL methods, a so called steady-pulsed

technique was developed. The objective of the steady-pulsed labeling scheme is to maintain the labeled blood state along the entire experiment, despite motion and pulsatility constraints imposed by cardiac physiology. A regularly repeated pulsed labeling strategy was therefore used to build up a perfusion-dependent stationary magnetization regime in the myocardial imaging slice. The cine-ASL sequence implemented this strategy by inserting a slice-selective inversion pulse inside the echo train of a cine-FLASH sequence. This sequence was developed and implemented on the 4.7T Bruker MRI system at CRMBM. In parallel Thibaut Capron (a postdoctoral fellow in our group from 2010/2012) elaborated an associated theoretical model, which was essential for the quantification of myocardial blood flow (MBF) with steady-pulsed labeling sequences. A different implementation of the spASL strategy was then developed, implemented, and evaluated for human cardiac ASL applications on CRMBM's Siemens Verio 3T scanner.

Small-animal myocardial ASL

Chapter 2 presents the initial setup of the so called steady-pulsed ASL (spASL) strategy initially developed for small-animal studies under the name cine-ASL. The spASL scheme combined with a cine-FLASH readout module were used to integrate over several cardiac cycles the steady perfusion-dependent magnetization difference. According to our findings, results on myocardial blood flow measured with cine-ASL in mice were not different from those obtained with the previously employed LLFAIRGE approach. Furthermore, cine-ASL has been shown to shorten acquisition time by improving acquisition efficiency and ASL sensitivity.

As a limitation in common with many other ASL techniques, cine-ASL requires a separate T_1 measurement to be fully quantitative, while LLFAIRGE has the advantage of providing T_1 maps inherently. In many applications one can, however, expect T_1 to remain constant throughout the study, so that a simultaneous (and repeated) T_1 measurement is not always necessary.

Specific optimizations of the cine-ASL technique were made for various applications subsequently to these validation steps and are presented in Chapter 4. In particular, high temporal resolution MBF maps were obtained in rats in order to study dynamic MBF changes over the entire cardiac cycle at rest and during adenosine-induced stress. Our observations in rodents clearly show that myocardial blood flow is phase-dependent and differs significantly between systole and diastole.

With the goal of investigating the dynamics of the hyperemic response to an infused vasodilator in rats, an accelerated cine-ASL sequence was developed to further reduce the acquisition time with minimal impact on the quality of the measurement. The accelerated cine-ASL version was also integrated in a still ongoing multimodal MRI/MRS protocol to study functional, microvascular and metabolic alterations in rodent models of type-2 diabetes.

Beyond the proposed technical improvements, we believe that an external comparison of the cine-ASL technique against microspheres or micro-PET will ultimately be necessary as validation. Also, future investigations will focus on adapting the cine-ASL sequence on a horizontal 11.75T Bruker system. This scanner have stronger and faster gradients which might help further reduce acquisition time.

Even if cardiac ASL is recognized as a well-established technique to study myocardial perfusion in rodents, first pass MRI techniques have recently shown very promising advances. By using

132

contrast agents, first pass MRI is superior to ASL in terms of signal and acquisition time, and it has the advantage of providing tissue blood volume within the same measurement, whereas ASL appears as simpler in terms of absolute quantification. It would now be interesting to experimentally compare ASL techniques with first pass techniques in several aspects including acquisition time, reproducibility and mapping quality.

Human myocardial ASL

The major challenge associated with ASL when applied to humans is in improving its inherently low sensitivity. Because myocardial blood flow is relatively low compared to rodents, it produces much smaller ASL signal changes. In addition, the acquisition efficiency is reduced because of the necessity of handling cardiac and respiratory motion. When applied at rest, the noise in flow measurements done with existing ASL methods is therefore relatively large even when compared with the flow values themselves. This also causes significant variability in measurements of perfusion reserve, which impedes its widespread application in clinical studies.

Despite this, earlier trials using a FAIR-bSSFP technique had already provided evidence that myocardial ASL was able to characterize perfusion defects in some patients, but the dominance of physiological noise was pointed out at the same time.

Considering the improvements in ASL sensitivity obtained with the spASL approach in small-animals, we considered it as a good candidate for improving ASL sensitivity in the human myocardium as well. A free-breathing acquisition strategy combined with the spASL labeling scheme was implemented on CRMBM's Siemens Verio 3T clinical MRI system and compared with a previously proposed multi-breath-hold FAIR technique. Higher signal and equivalent performance as compared to FAIR was found. Although steady-pulsed ASL showed promising results for non-contrast perfusion assessment, sequence improvements have to be developed and, more importantly, an optimized dedicated post-processing strategy has to be found. The use of non-rigid motion correction algorithms, as well as the feasibility of adaptive reconstruction algorithms such as GRICS, should be investigated. Both of them should enable the use of all images for signal averaging and thereby improve sensitivity. Alternatively, prospective motion correction, such as 'motion tracking' techniques, would have the additional advantage of reducing a potential bias due to through-plane motion during acquisition.

From an acquisition point of view, the labeling pulse is currently an important point leaving room for improvements. Due to a rather large spatial coverage of the labeling, myocardial ASL currently suffers from a large apparent ASL signal in the LV blood pool due to inadvertent tagging of blood in both atrium and the thoracic region. But more importantly, the multiple exposure of blood spins to an inversion pulse leads to a reduced labeling efficiency as compared to other PASL techniques. Future investigations should therefore include the study of 2D spatially selective adiabatic inversion pulses that can produce an inversion only focusing on the proximal aorta while leaving both atrium and left ventricular blood undisturbed.

Clinical validations on patient populations including a pharmacological stress would be an important point to investigate the robustness of the spASL technique for detecting perfusion defects in humans. These validation steps may be accomplished in the near future through the numerous clinical collaborations of our institute. Finally, as for rodent studies, an external validation against other perfusion imaging modalities (first pass MRI or PET) would be desirable in order to highlight the true value of our proposed approach.

French Synopsis

Ce manuscrit retrace mes travaux de thèse réalisés au sein du Centre de Résonance Magnétique Biologique et Médicale (CRMBM) de Marseille, sous la direction du Docteur Frank Kober et la codirection du Docteur Monique Bernard. Ce projet de thèse s'intitule : « IRM quantitative de la perfusion myocardique par marquage de spins artériels » (*Quantitative myocardial perfusion MRI using arterial spin labeling*) et a été financé par une bourse CIFRE issue de la collaboration entre le CNRS et la société Siemens Healthcare France.

Le travail réalisé au cours de ces trois dernières années s'inscrit dans un projet plus global mené par l'équipe de développements méthodologiques du CRMBM. Ce projet vise à concevoir, améliorer et exploiter des approches innovantes pour la mesure non-invasive de la perfusion par IRM, que ce soit chez l'homme en recherche clinique ou chez le petit animal en recherche préclinique, et ce pour différents organes, du cerveau aux reins, en passant par la moelle épinière et bien-sûr le cœur.

J'ai donc rejoint cette équipe dans le but bien précis de développer de nouvelles techniques pour la mesure de la perfusion myocardique par IRM. Ces développements ont été conduits avec une approche transversale, l'objectif étant de les appliquer à la fois en recherche fondamentale et clinique. La première étape de ce projet a consisté à concevoir et mettre en place une nouvelle méthode de cartographie de la perfusion myocardique chez le petit animal. Cette technique a ensuite été validée chez des animaux sains par comparaison avec une approche précédemment développée au sein de notre laboratoire (Chapitre 2). La seconde étape a consisté à adapter cette technique pour une utilisation chez l'homme (Chapitre 3). Les travaux de développements de séquence réalisés chez l'homme ont été possibles grâce à l'aide apportée par l'ingénieur Benjamin Robert de la société Siemens. Enfin, en considérant les avantages que cette nouvelle approche nous a apportés chez l'animal, nous nous sommes intéressés à diverses optimisations de la séquence IRM afin de répondre à des besoins particuliers (Chapitre 4).

1. Contexte de l'étude

Cette partie résume le premier chapitre de ce manuscrit et reprend les points clés utiles à la compréhension du travail effectué au cours de cette thèse.

Le cœur

Le cœur est un organe musculaire qui pompe le sang à travers les différents vaisseaux sanguins de l'organisme grâce à des contractions rythmiques et répétées. En fournissant ce travail, le muscle cardiaque, le myocarde, dépend lui-même d'un approvisionnement constant en sang oxygéné et en nutriments. L'architecture et la vascularisation de cet organe sont présentées dans la figure 1.

La perfusion cardiaque se réfère au phénomène de transport du sang et se situe à l'échelle de la microcirculation tissulaire. Les vaisseaux sanguins irriguant le cœur s'adaptent en permanence pour moduler la perfusion afin de répondre aux besoins de l'organe. De nombreuses pathologies cardiaques affectent de façon directe ou indirecte cette fonction de régulation. La mesure de la

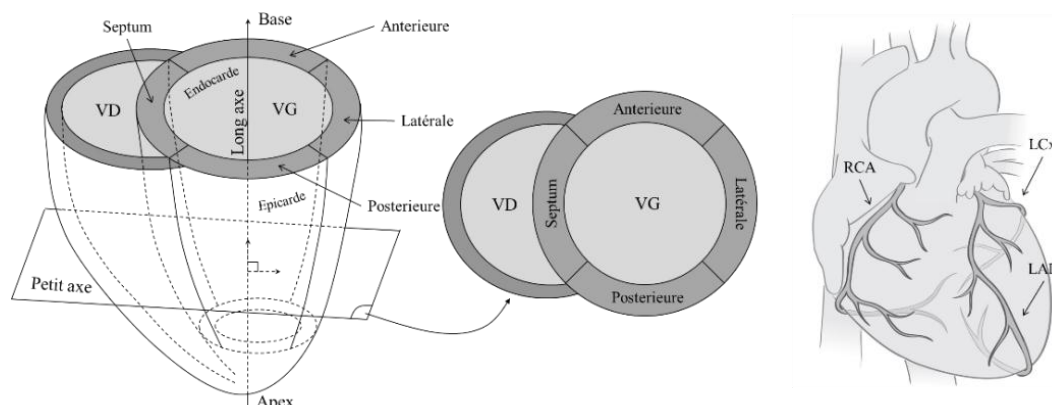perfusion tissulaire permet donc de déterminer l'état de la microvascularisation régionale d'un organe.

Figure 1 – Architecture et vascularisation cardiaque. Le cœur est un organe creux composé de deux cavités, le ventricule gauche (VG) et le ventricule droit (VD). Le muscle du VG, le myocarde gauche, peut être divisé en quatre segments (le septum (séparant les deux ventricules), la paroi antérieure, latérale et postérieure). La vascularisation du myocarde se fait par l'intermédiaire des artères coronaires gauche et droite (RCA, LCx et LAD) qui ont pour origine la racine aortique et qui donnent ensuite naissance à une multitude de micro-vaisseaux, les capillaires, qui permettent d'approvisionner le myocarde en sang à un niveau tissulaire.

Le cœur, contrairement aux autres organes, a la particularité d'être en mouvement perpétuel et impose donc des contraintes temporelles spécifiques lorsqu'il s'agit de l'imager. L'acquisition des images doit être synchronisée à l'activité cardiaque afin de s'affranchir d'artéfacts liés aux mouvements cardiaques. De plus, le cœur étant placé dans la région thoracique, les mouvements respiratoires font que l'organe bouge au cours du temps ce qui impose donc des contraintes supplémentaires.

Imagerie de la perfusion myocardique par IRM

Actuellement, l'imagerie par résonance magnétique (IRM) de perfusion est appliquée en routine sur des patients porteurs de lésions macrovasculaires (sténose coronarienne, infarctus du myocarde). Le but est principalement de caractériser les zones hypoperfusées dans le cadre de la maladie coronarienne afin de déterminer les zones ischémiques et/ou de nécrose. Par comparaison avec une région dite saine de l'organe, l'étendue de la lésion peut ainsi être évaluée.

La technique la plus largement utilisée, dite IRM de premier passage, est basée sur l'injection d'un agent de contraste qui modifie les temps de relaxation en fonction de la concentration de cet agent dans le système vasculaire. Une série d'images est acquise à la suite de l'injection d'un bolus afin de capturer les changements dynamiques d'intensité induits par le passage du produit de contraste. Au-delà d'une mesure relative de la perfusion, cette technique permet aussi de quantifier de manière absolue le flux sanguin au niveau d'une région tissulaire (exprimée alors en mL g^{-1} min^{-1}). Cependant, cette quantification absolue n'est toujours qu'à un stade de développement et est basée sur des modèles mathématiques complexes qui ne lui permettent pas d'être utilisée en routine clinique sans qu'il n'y ait d'interactions avec des physiciens spécialistes de l'IRM de premier passage.

136

Une autre approche a vu le jour il y a une vingtaine d'années et se nomme marquage de spins artériels (ASL pour *Arterial Spin Labeling*, cf. figure 2). Celle-ci a émergé en tant que technique totalement non-invasive car c'est le sang qui est utilisé comme traceur et non un produit de contraste exogène. C'est un outil puissant pour la mesure quantitative du flux sanguin tissulaire qui a été appliqué au cerveau, aux reins mais aussi au cœur. Ne nécessitant pas d'injection, le principal avantage de cette technique est qu'elle peut être répétée sans limitation. Un autre avantage, comparé aux techniques de premier passage, est que la quantification est relativement simple et ne repose pas sur la dynamique de l'injection d'un bolus. C'est cette technique qui a fait l'objet du travail méthodologique mis en place durant cette thèse. La finalité de ce travail n'est pas de reproduire la cartographie de la perfusion obtenue par premier passage en utilisant l'ASL, mais de mesurer quantitativement le débit sanguin régional dans le myocarde afin de caractériser des maladies non-ischémiques du cœur et d'étudier des pathologies et des phénomènes qui jusqu'alors étaient inaccessibles par IRM.
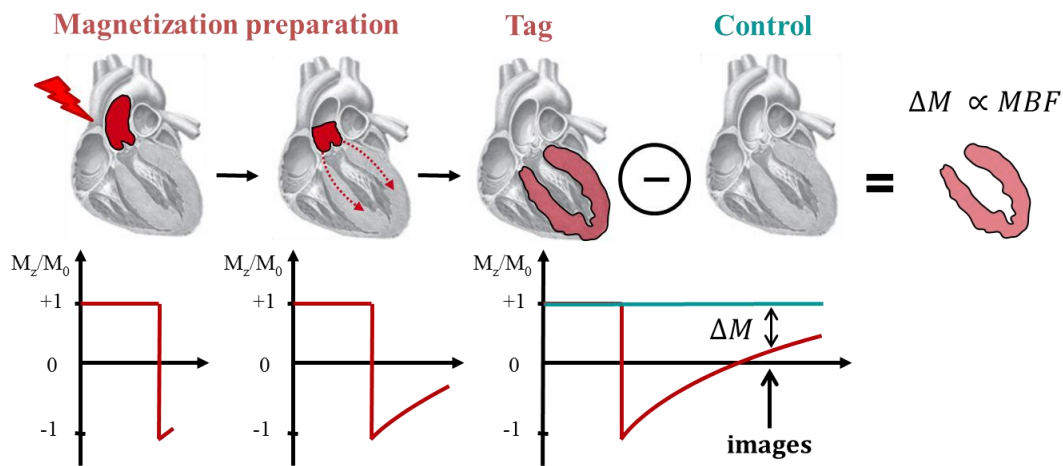

Figure 2 – Principe de base du marquage de spins artériels (ASL). L'eau contenue dans le sang artériel est marquée magnétiquement à l'aide d'une impulsion radiofréquence en amont de la région d'intérêt. Le sang ainsi marqué perfuse ensuite le tissu tandis que la relaxation longitudinale T1 a déjà été initiée (courbe rouge). Une fois que le sang marqué a atteint le compartiment microvasculaire, une image dite marquée ('tag') est acquise. La même image est acquise sans qu'il n'y ait de marquage initial (image contrôle). Enfin, la différence de ces deux images permet d'obtenir le signal ASL (ΔM) qui est directement proportionnel au flux sanguin tissulaire.

La majorité des techniques utilisées jusqu'alors pour la mesure de la perfusion myocardique par ASL se basent sur un marquage de type pulsé (*Pulsed ASL*) en utilisant le marquage FAIR (*Flow-sensitive Alternating Inversion Recovery*). Cette méthode consiste à réaliser deux inversions successives. L'une se fait sur l'ensemble du cœur (inversion non-sélective ou globale) et donne l'image marquée (ou '*tag*'). L'autre se fait seulement au niveau de la région à imager (inversion sélective) et donne l'image contrôle.

L'ASL myocardique chez le rongeur

Cette technique de marquage a été utilisée dans un premier temps chez l'animal *[Belle 1998]*, combinée avec un module de lecture basé sur la séquence d'imagerie snapshot-FLASH (*snapshot-Fast Low-Angle SHot, [Haase 1990]*). Le but était alors de réaliser une image à chaque cycle cardiaque afin de caractériser la repousse de l'aimantation longitudinale à la suite de ces deux

inversions (T_1^{sl} pour l'inversion sélective et T_1^{gl} pour l'inversion globale). On parle alors d'inversion récupération (IR) à multiples temps d'inversions (approche *multiple TI*), comme présenté ici dans la figure 3.
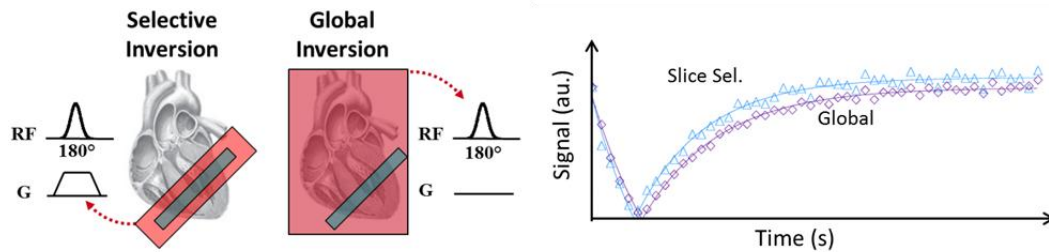

Figure 3 – Principe de la technique FAIR avec plusieurs temps d'inversion. Deux séquences d'inversion récupération sont acquises à la suite des préparations globale et sélective. L'échantillonage des courbes de relaxation T1 permet de quantifier la perfusion.

Le temps pour réaliser une image snapshot-FLASH n'est pas négligeable et est de l'ordre de quelques centaines de millisecondes. Du fait des contractions très rapides du cœur du rongeur (~ 400-500 pulsation par minute (*bpm*) contre 50-100 chez l'homme), l'acquisition d'une image par cycle cardiaque n'était alors pas très adaptée. Plus récemment, cette technique a été améliorée au sein de notre laboratoire afin de s'affranchir des contraintes liées aux contractions rapides de l'animal (LLFAIRGE, *[Kober 2004]*). Le module de marquage FAIR a été conservé mais le module de lecture a été modifié. Celui-ci a en fait été segmenté afin de réduire la fenêtre de temps de lecture. A l'échelle du cycle cardiaque rapide de l'animal, le temps d'acquisition par écho devient relativement faible ce qui améliore la précision. En outre, cela permet d'obtenir des résolutions spatiales élevées en répétant la mesure jusqu'à ce que l'intégralité des images soit obtenue. La contrepartie d'une telle avancée technique est que le temps d'acquisition total devient assez long, environ 25 minutes chez le rat et la souris.

Dans le but d'améliorer l'efficacité et la sensibilité des techniques d'ASL myocardique chez le rongeur, sans pour autant réduire la résolution spatiale et temporelle des techniques précédemment développées, nous avons mis en place une approche alternative basée sur un module de marquage pulsé et répété (*steady-pulsed ASL, spASL*). Cette technique a été développée pour une utilisation chez la souris et nous avons montré qu'elle permet d'obtenir une meilleure efficacité d'acquisition et, par conséquent, un temps d'acquisition significativement réduit. Les résultats sont présentés dans le Chapitre 2 de ce manuscrit.

L'ASL myocardique chez l'homme

Bien que l'ASL myocardique ait rencontré un certain succès chez le rongeur (en raison notamment d'un flux sanguin tissulaire cinq fois plus important que chez l'homme), cette technique, une fois appliquée au cœur humain, n'en est qu'à un stade initial de développement. De nombreuses équipes se sont intéressées à son utilisation mais sans obtenir de résultats fiables et pertinents, permettant une utilisation en routine clinique.

Chez l'homme, la durée du cycle cardiaque est de l'ordre de la seconde ce qui permet de capturer une image complète par cycle sans pour autant que celle-ci ne soit affectée par les mouvements de contraction (image *snapshot* généralement obtenue en diastole quand le cœur est stable). De

plus, l'acquisition d'images en IRM cardiaque chez l'homme se fait généralement au cours d'une apnée afin de minimiser l'impact de la respiration.

Dans le passé, plusieurs essais ont été entrepris pour quantifier la perfusion myocardique chez l'homme en utilisant un principe similaire de mesure du temps T_1 à la suite de deux préparations d'aimantation (inversion ou saturation) *[Poncelet 1999, Wacker 2003, Fidler 2004]*. Alors que les pulsations cardiaques rapides du rongeur permettent un échantillonnage précis de la courbe de récupération T_1, cela n'est pas le cas pour le cœur humain. Obtenir une image par cycle cardiaque n'était pas suffisant pour bien échantillonner ces courbes d'inversion récupération, entrainant alors des erreurs systématiques dans la quantification absolue de la perfusion.

Plus récemment, l'ASL myocardique a été amélioré de manière significative grâce à l'implémentation à 3 Tesla du marquage de type FAIR avec une lecture *snapshot*-bSSFP (*balanced Steady-State Free-Precession*) *[Zun 2009]*. Cette séquence, comparée à la séquence FLASH, a été montrée supérieure en termes de rapport signal sur bruit et de sensibilité aux artéfacts de flux sanguin.

Cette même séquence a ensuite été évaluée dans une situation clinique sur plusieurs patients. Ces mesures ont été obtenues lors d'un protocole de type repos/stress (injection d'un vasodilatateur) afin de détecter les régions du myocarde qui étaient affectées par la maladie coronarienne *[Zun 2011]*. Bien que cette technique ait permis de révéler des signes cliniques de défaut de la perfusion, les résultats ont cependant montré que la mesure de la perfusion par ASL chez l'homme était limitée par un rapport signal sur bruit trop faible (principalement en raison d'un fort bruit physiologique), ne permettant pas d'obtenir une mesure fiable et reproductible de la perfusion myocardique chez l'homme.

Afin d'améliorer cette situation, une nouvelle approche a vu le jour au cours de cette thèse. A la suite de la validation de la technique spASL chez le rongeur, nous nous sommes intéressés à un transfert de cette technique vers l'imagerie clinique. Les résultats sont présentés au Chapitre 3 de ce manuscrit.

2. Steady-pulsed ASL, une méthode pour quantifier la perfusion myocardique chez le rongeur

Cette section résume le second chapitre de ce manuscrit qui présente la séquence cine-ASL développée au début de cette thèse.

Ce travail a fait l'objet de deux publications scientifiques dans le journal *Magnetic Resonance in Medicine* (2013) :

Cine-ASL: A Steady-Pulsed Arterial Spin Labeling Method for Myocardial Perfusion Mapping in Mice. Part I: Experimental Study.

Troalen T, Capron T, Cozzone PJ, Bernard M, et Kober F.

Cine-ASL: A Steady-Pulsed Arterial Spin Labeling Method for Myocardial Perfusion Mapping in Mice. Part II: Theoretical Model and Sensitivity Optimization.

Capron T, **Troalen T**, Cozzone PJ, Bernard M, et Kober F.

L'approche de type FAIR présentée précédemment consiste en un marquage pulsé qui doit être répété pour chaque ligne de l'espace des k. L'inconvénient majeur est que le marquage s'évanouit au cours du temps (avec la relaxation T_1) après chaque inversion. Nous avons cherché à mettre en place une alternative qui permet de maintenir l'aimantation du sang dans un état marqué au cours de la mesure. Ces développements devaient néanmoins rester compatibles avec les contraintes associées à l'imagerie cardiaque et la forte pulsatilité du flux sanguin artériel dans l'aorte ascendante. En effet, les coronaires irrigants le myocarde ont pour origine la racine aortique et la majorité du sang qui perfuse ces coronaires est expulsé à la fin de la systole.

Nous avons modifié la séquence dynamique *cine-FLASH* en y intégrant une impulsion de marquage à l'intérieur du train d'échos (technique cine-ASL présentée dans la figure 4). Le marquage est positionné au niveau de la racine aortique et a lieu à la fin de la systole. Avec cette approche, une imagerie continue du cœur peut être réalisée tandis que le sang est marqué en amont de la région à imager *[Troalen 2013]*. Cette alternance image/marquage est ensuite répétée à chaque cycle cardiaque afin de créer un état stationnaire de l'aimantation (*steady-state*) sous l'influence de la perfusion. Une série d'expériences contrôles est aussi nécessaire pour corriger les effets de transfert d'aimantation. Le marquage contrôle est placé symétriquement par rapport à la coupe d'imagerie et ne marque aucun sang artériel. Enfin, ce schéma de marquage et de lecture est alors répété pour chaque ligne de l'espace des k afin de compléter les séries images marquées et contrôles.

Le signal du tissu myocardique évolue vers un état d'équilibre qui diffère entre les deux expériences. Parallèlement à la mise en place expérimentale de cette séquence, nous avons travaillé sur l'aspect théorique afin de quantifier la perfusion à partir de la différence entre les images marquées et contrôles dans le régime stationnaire *[Capron 2013]*.
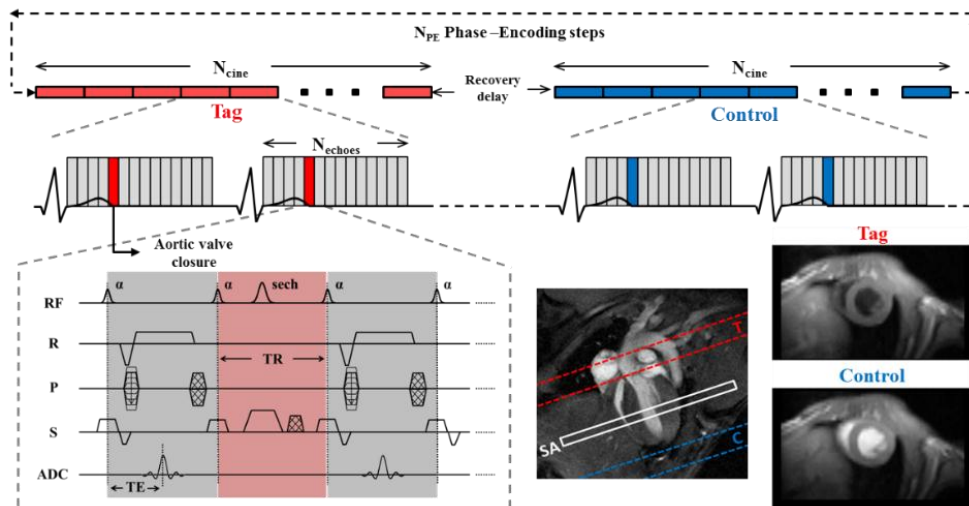
Figure 4 – Description de la séquence cine-ASL. Une séquence cine-FLASH synchronisée à l'ECG a été modifiée et intègre un module de marquage pulsé à l'intérieur du train d'écho. La position du plan de marquage (T), du plan contrôle (C) et de la coupe d'imagerie (SA) sont représentés sur une vue 4-chambre du cœur de souris. La présence de sang noir au niveau des ventricules droit et gauches sur l'image Tag provient du marquage qui couvre l'aorte mais aussi une partie des oreillettes.

Afin de valider cette nouvelle séquence, nous avons effectué des mesures de la perfusion myocardique sur 14 souris C57Bl6 saines en comparant nos résultats obtenus avec cine-ASL avec la technique initialement développée au laboratoire (*Look-Locker FAIR gradient-echo*, LLFAIRGE, *[Kober 2005]*). Nous avons pu montrer que la séquence cine-ASL permettait de mesurer efficacement la perfusion au niveau du myocarde avec des résultats similaires entre les deux techniques.

L'avantage de cette nouvelle séquence est un gain non négligeable en sensibilité, ce qui permet de réduire le temps d'acquisition d'un facteur trois (8 min contre 25 min). En revanche, l'inconvénient de cette technique par rapport à LLFAIRGE est une possible diminution dans la précision de la quantification absolue de la perfusion. En effet, l'approche LLFAIRGE permet de façon inhérente d'obtenir une mesure fiable du T_1 tissulaire. Cette constante de temps entre en compte dans les modèles de quantification et peut être perturbée dans certains cas de pathologies. Aussi, il existe avec cine-ASL quelques incertitudes sur l'efficacité du marquage qui elle aussi entre en compte dans la quantification.

Néanmoins, et nous le verrons dans la quatrième partie de ce résumé, cette nouvelle technique a permis d'améliorer significativement la sensibilité de l'ASL dans le contexte de l'imagerie de la perfusion cardiaque chez le rongeur et a permis de réaliser un certain nombre d'études à la suite de cette étape de validation.
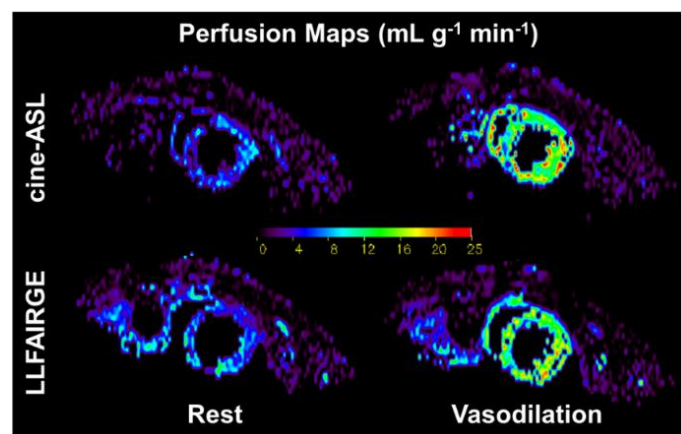
Figure 5 – Cartes de perfusion obtenues chez une souris saine au repos et lors d'un épisode de vasodilatation induit par augmentation de l'isoflurane. Comparaison directe des séquences cine-ASL et LLFAIRGE.

3. Transition de l'approche spASL vers une application chez l'homme.

Cette section résume le troisième chapitre de cette thèse qui concerne l'adaptation de cette technique chez l'homme.

Ce travail est en cours de révision pour publication dans le journal *Magnetic Resonance in Medicine* :

Myocardial Perfusion Assessment in Humans using Steady-Pulsed Arterial Spin Labeling.

Capron T, **Troalen T**, Robert B, Jacquier A, Bernard M, et Kober F.

Au vu des résultats encourageants obtenus avec la séquence cine-ASL chez le rongeur, il semblait intéressant d'entreprendre un transfert de cette approche *steady-pulsed* sur les imageurs cliniques. La figure 5 présente le schéma de cette séquence spASL appliquée à l'homme. La stratégie de marquage est similaire avec un marquage pulsé localisé au niveau de la racine aortique qui a lieu à la fin de la systole. Une image est ensuite acquise à chaque cycle cardiaque au cours de la diastole. Plutôt que d'être restreints par la durée d'une apnée, nous avons décidé de réaliser ces acquisitions en respiration libre afin d'accumuler les données sur des temps plus longs. L'inconvénient d'une acquisition en respiration libre est le déplacement et la déformation du cœur qui rendent le post-traitement plus complexe.

Cette combinaison marquage/lecture est répétée 128 fois afin de construire l'état d'équilibre sous l'influence de la perfusion. Le marquage contrôle corrigeant les effets de transfert d'aimantation a aussi été conservé.
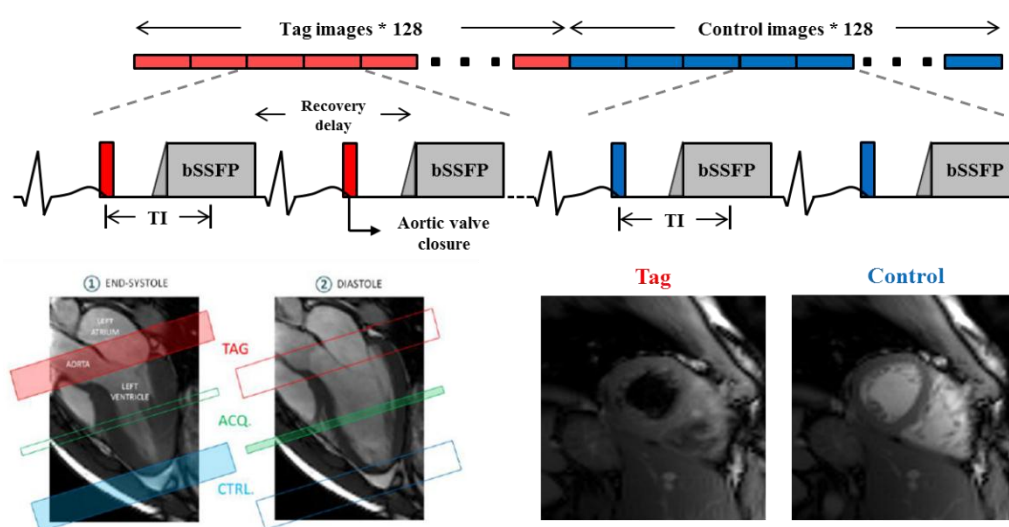
*Figure 6 – Description de la séquence spASL développée pour une application chez l'homme. Le marquage est réalisé à la fin de la systole à chaque battement cardiaque et l'image est acquise à la fin de la diastole avec une séquence snapshot-bSSFP. Les 2*128 images marquées et contrôles sont acquises séquentiellement en respiration libre.*

Nous avons évalué la faisabilité de la séquence spASL chez 13 sujets sains en respiration libre. Afin de s'affranchir des contraintes imposées par les mouvements respiratoires, un algorithme de sélection rétrospective basé sur la détection régionale des contours du myocarde a été développé. Nous avons comparé les résultats avec la séquence FAIR-SSFP à multiples apnées proposée précédemment *[Zun 2009a]*. Les deux techniques ont donné des valeurs de perfusion similaires mais le signal de perfusion mesuré était supérieur avec la séquence spASL.

A la suite de cette étude, nous avons entrepris d'améliorer des points précis de la méthode. Tout d'abord nous avons modifié le module de lecture en y intégrant l'imagerie parallèle afin d'accélérer le temps de lecture et d'augmenter la résolution spatiale de nos images. Ensuite, nous nous sommes penchés sur l'amélioration du post-traitement en y intégrant un algorithme de correction de mouvement. Ce travail a fait l'objet d'un stage de Master 2 sous ma cotutelle.

Du fait des mouvements respiratoires, la simple sélection d'images basée sur la correspondance des contours initialement proposée ne permettait d'inclure qu'environ 30% des données acquises. Le nouvel algorithme comprend deux étapes supplémentaires et distinctes de correction rigide du mouvement (correction globale puis locale), ainsi que l'utilisation de régions d'intérêt plus petites afin d'éviter toute contamination du signal par le sang ou la graisse avoisinante.
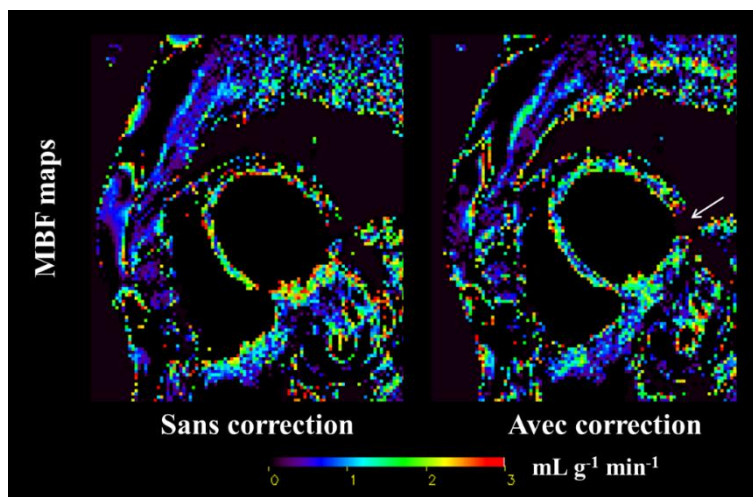

Figure 6 – Cartes de perfusion avec et sans correction globale de mouvement. Une fois cette correction appliquée les contours du myocarde sont mieux définis et le signal est plus homogène.

Jusqu'à maintenant, l'algorithme a été testé sur 6 sujets et a permis de réduire significativement les variabilités du signal entre les sujets. Ce nouveau post-traitement permet aussi d'inclure un nombre plus important de données, ce qui rend la quantification plus fiable.

4. Application de la séquence cine-ASL

Parallèlement à l'adaptation de la séquence pour une utilisation chez l'homme, nous avons cherché à exploiter et optimiser la séquence cine-ASL. Trois études distinctes ont alors vu le jour.

Etant donné la sensibilité que nous avons obtenue avec cette séquence, nous avons cherché à réduire d'avantage le temps d'acquisition en accélérant la lecture (deux lignes de l'espace des *k* à chaque répétition). Cela a permis de réduire le temps d'acquisition pour une carte de perfusion chez le rongeur à seulement environ 4 minutes.

Cette version de cine-ASL a été utilisée dans un protocole qui visait à caractériser la dynamique de la réponse à un agent vasodilatateur, l'adénosine. Une mesure de perfusion a été réalisée toutes les 5 minutes lors de l'injection continue de cet agent. Nous avons pu déterminer l'intervalle de temps pour lequel la vasodilatation était maximale chez le rat.

Une autre étude a consisté en la mise en place d'un protocole multimodal pour caractériser des altérations cardiaques (la fonction avec l'imagerie dynamique et la microcirculation avec cine-ASL) ainsi que la proportion de graisse dans le cœur et dans le foie (par spectrométrie). Ce protocole est utilisé actuellement dans deux modèles animaux de diabète de type 2 afin d'établir l'ordre chronologique d'apparition des anomalies cardiaques associées à l'obésité et l'insulino-résistance. .

La dernière étude que nous avons menée visait à exploiter l'aspect dynamique de nos acquisitions 'ciné'. La résolution temporelle du module de lecture a été optimisée de façon à bien caractériser l'évolution de la perfusion au cours du cycle cardiaque. Cette étude nous a permis de mettre en évidence que, chez le rat, le flux sanguin au niveau des capillaires du myocarde était variable au cours du cycle et que le maximum de perfusion n'était pas obtenu exactement au même moment entre le stress et le repos.

Le travail suivant a fait l'objet d'une publication scientifique dans le *Journal of Cardiovascular Magnetic Resonance* (2014) :

In Vivo Characterization of Rodent Cyclic Myocardial Perfusion Variation at Rest and during Adenosine-Induced Stress using cine-ASL CMR.

Troalen T, Capron T, Bernard M, et Kober F.
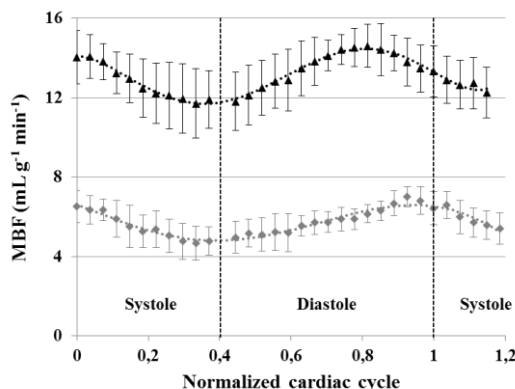
Variation cyclique de la perfusion au cours du cycle cardiaque au repos et lors d'un stress pharmacologique

5. Conclusion

En conclusion, ce travail de thèse a permis de mettre en place des approches alternatives de mesure non-invasive de la perfusion myocardique par IRM. La technique spASL qui permet de maintenir le signal dans un état marqué a permis d'augmenter significativement la sensibilité de détection du signal ASL, que ce soit chez l'animal ou chez l'homme.

Pour les études sur le petit animal, il a été mis en évidence que la séquence cine-ASL permettait de réduire considérablement le temps d'acquisition tout en conservant une qualité de mesure similaire aux techniques existantes. Alternativement, ce gain en sensibilité permet aussi d'augmenter la résolution spatiale tout en conservant un temps d'acquisition raisonnable.

Il subsiste quelques incertitudes par rapport à la quantification absolue de la perfusion (inhabilité à mesurer T_1 et l'efficacité d'inversion simultanément, les deux étant nécessaires pour la quantification absolue du flux). Ceci est également le cas pour d'autres techniques d'ASL continu.

Afin d'améliorer l'efficacité du marquage et donc de gagner encore en signal, il serait possible d'utiliser des impulsions RF à deux dimensions spatiales pour ne couvrir que l'aorte ascendante et non les régions avoisinantes. Ces impulsions 2D ont, cependant, la particularité d'être plus longues que les impulsions adiabatiques à une dimension et ne seraient donc pas forcément compatibles avec notre approche telle qu'elle a été développée jusqu'alors.

L'adaptation de cette séquence spASL pour une mesure de la perfusion myocardique chez l'homme a donné des résultats très encourageants. En effet, nous avons observé que le signal créé avec notre approche était supérieur à celui créé avec FAIR, bien que l'efficacité d'inversion soit moindre. De la même manière que chez le rongeur, il serait intéressant de mettre en place une

impulsion de marquage 2D de façon à essayer d'améliorer l'efficacité d'inversion. Cette amélioration semble plus envisageable chez l'homme dans le sens où la fréquence cardiaque est bien plus faible.

L'approche spASL en respiration libre permet d'accumuler un plus grand nombre de données que si nous avions effectué ces mesures lors d'une apnée. Il parait maintenant important d'orienter nos efforts vers des méthodes plus performantes de correction de mouvement respiratoire non-rigides afin de corriger non seulement la position mais aussi les déformations du cœur. Cela permettrait de calculer avec une meilleure reproductibilité des cartes de perfusion à haute résolution chez l'homme. Au-delà des améliorations purement techniques et afin de démontrer une véritable valeur de notre approche, des mesures comparatives en utilisant d'autres modalités d'imagerie de perfusion (IRM de premier passage ou PET) seront souhaitables. Une analyse dans des conditions de stress pharmacologique serait aussi un point important de validation. Ceci pourra être accompli à travers les collaborations du CRMBM.

References

Aguor ENE, Arslan F, van de Kolk CWA, Nederhoff MGJ, Doevendans PA, van Echteld CJA, Pasterkamp G, Strijkers GJ . Quantitative T 2* assessment of acute and chronic myocardial ischemia/reperfusion injury in mice. *Magma*. 2012;25:369–379.

Al-Saadi N, Gross M, Paetsch I, Schnackenburg B, Bornstedt A, Fleck E, Nagel E . Dobutamine Induced Myocardial Perfusion Reserve Index with Cardiovascular MR in Patients with Coronary Artery Disease. *J. Cardiovasc. Magn. Reson.* 2003;4:471–480.

Aletras AH, Ding S, Balaban RS, Wen H . DENSE: displacement encoding with stimulated echoes in cardiac functional MRI. *J. Magn. Reson.* 1999;137:247–252.

Alsop DC, Detre JA . Multisection cerebral blood flow MR imaging with continuous arterial spin labeling. *Radiology*. 1998;208:410–416.

An J, Voorhees A, Chen Q . SSFP Arterial Spin Labeling Myocardial Perfusion Imaging at 3 Tesla. *Proc. 13th Annu. Meet. ISMRM Miami Beach*. 2005;253.

Anderson LJ, Holden S, Davis B, Prescott E, Charrier CC, Bunce NH, Firmin DN, Wonke B, Porter J, Walker JM, Pennell DJ . Cardiovascular T2-star (T2*) magnetic resonance for the early diagnosis of myocardial iron overload. *Eur. Heart J.* 2001;22:2171–2179.

Ashikawa K, Kanatsuka H, Suzuki T, Takishima T . Phasic blood flow velocity pattern in epimyocardial microvessels in the beating canine left ventricle. *Circ. Res.* 1986;59:704–711.

Axel L, Dougherty L . MR imaging of motion with spatial modulation of magnetization. *Radiology*. 1989;171:841–845.

Barbier EL, Lamalle L, Décorps M . Methodology of brain perfusion imaging. *J. Magn. Reson. Imaging*. 2001a;13:496–520.

Barbier EL, Silva AC, Kim HJ, Williams DS, Koretsky AP . Perfusion analysis using dynamic arterial spin labeling (DASL). *Magn. Reson. Med.* 1999;41:299–308.

Barbier EL, Silva AC, Kim SG, Koretsky AP . Perfusion imaging using dynamic arterial spin labeling (DASL). *Magn. Reson. Med.* 2001b;45:1021–1029.

Bauer WR, Hiller KH, Roder F, Rommel E, Ertl G, Haase A . Magnetization exchange in capillaries by microcirculation affects diffusion-controlled spin-relaxation: a model which describes the effect of perfusion on relaxation enhancement by intravascular contrast agents. *Magn. Reson. Med.* 1996;35:43–55.

Bauer WR, Roder F, Hiller KH, Han H, Fröhlich S, Rommel E, Haase A, Ertl G . The effect of perfusion on T1 after slice-selective spin inversion in the isolated cardioplegic rat heart: measurement of a lower bound of intracapillary-extravascular water proton exchange rate. *Magn. Reson. Med.* 1997;38:917–923.

Beek AM, Kühl HP, Bondarenko O, Twisk JWR, Hofman MBM, van Dockum WG, Visser CA, van Rossum AC . Delayed contrast-enhanced magnetic resonance imaging for the prediction of regional functional improvement after acute myocardial infarction. *J. Am. Coll. Cardiol.* 2003;42:895–901.

Belle V, Kahler E, Waller C, Rommel E, Voll S, Hiller KH, Bauer WR, Haase A . In vivo quantitative mapping of cardiac perfusion in rats using a noninvasive MR spin-labeling method. *J. Magn. Reson. Imaging*. 1998;8:1240–1245.

Ben-Haim S, Murthy VL, Breault C, Allie R, Sitek A, Roth N, Fantony J, Moore SC, Park M-A, Kijewski M, Haroon A, Slomka P, Erlandsson K, Baavour R, Zilberstien Y, Bomanji J, Di Carli MF . Quantification of Myocardial Perfusion Reserve Using Dynamic SPECT Imaging in Humans: A Feasibility Study. *J. Nucl. Med.* 2013;54:873–879.

Bergmann SR, Fox KA, Rand AL, McElvany KD, Welch MJ, Markham J, Sobel BE . Quantification of regional myocardial blood flow in vivo with H215O. *Circulation*. 1984;70:724–733.

Beyers RJ, Smith RS, Xu Y, Piras BA, Salerno M, Berr SS, Meyer CH, Kramer CM, French BA, Epstein FH . T_2 -weighted MRI of post-infarct myocardial edema in mice. *Magn. Reson. Med.* 2012;67:201–209.

Botnar RM, Kim WY, Bornert P, Stuber M, Spuentrup E, Manning WJ . 3D coronary vessel wall imaging utilizing a local inversion technique with spiral image acquisition. *Magn Reson Med*. 2001;46:848–54.

Bratis K, Mahmoud I, Chiribiri A, Nagel E . Quantitative myocardial perfusion imaging by cardiovascular magnetic resonance and positron emission tomography. *J. Nucl. Cardiol.* 2013;20:860–870; quiz 857–859, 871–873.

Burtscher IM, Holtås S . Proton MR spectroscopy in clinical routine. *J. Magn. Reson. Imaging JMRI*. 2001;13:560–567.

Buxton RB, Frank LR, Wong EC, Siewert B, Warach S, Edelman RR . A general kinetic model for quantitative perfusion imaging with arterial spin labeling. *Magn. Reson. Med.* 1998;40:383–396.

Calamante F, Williams SR, van Bruggen N, Kwong KK, Turner R . A model for quantification of perfusion in pulsed labelling techniques. *NMR Biomed.* 1996;9:79–83.

Campbell-Washburn AE, Price AN, Wells JA, Thomas DL, Ordidge RJ, Lythgoe MF . Cardiac arterial spin labeling using segmented ECG-gated Look-Locker FAIR: variability and repeatability in preclinical studies. *Magn. Reson. Med.* 2013;69:238–247.

Campbell-Washburn AE, Zhang H, Siow BM, Price AN, Lythgoe MF, Ordidge RJ, Thomas DL . Multislice cardiac arterial spin labeling using improved myocardial perfusion quantification with simultaneously measured blood pool input function. *Magn. Reson. Med.* 2012;

Capron T, Troalen T, Cozzone PJ, Bernard M, Kober F . Cine-ASL: A steady-pulsed arterial spin labeling method for myocardial perfusion mapping in mice. Part II. Theoretical model and sensitivity optimization. *Magn. Reson. Med.* 2013;70:1399–1408.

Caudron J, Mulder P, Nicol L, Richard V, Thuillez C, Dacher J-N . MR relaxometry and perfusion of the myocardium in spontaneously hypertensive rat: correlation with histopathology and effect of anti-hypertensive therapy. *Eur. Radiol.* 2013;23:1871–1881.

Cerqueira MD, Weissman NJ, Dilsizian V, Jacobs AK, Kaul S, Laskey WK, Pennell DJ, Rumberger JA, Ryan T, Verani MS, American Heart Association Writing Group on Myocardial Segmentation and Registration for Cardiac Imaging . Standardized myocardial segmentation and nomenclature for tomographic imaging of the heart. A statement for healthcare professionals from the Cardiac Imaging Committee of the Council on Clinical Cardiology of the American Heart Association. *Circulation*. 2002;105:539–542.

Chareonthaitawee P, Kaufmann PA, Rimoldi O, Camici PG . Heterogeneity of resting and hyperemic myocardial blood flow in healthy humans. *Cardiovasc. Res.* 2001;50:151–161.

Cheng ZJ, Vaskonen T, Tikkanen I, Nurminen K, Ruskoaho H, Vapaatalo H, Muller D, Park JK, Luft FC, Mervaala EM . Endothelial dysfunction and salt-sensitive hypertension in spontaneously diabetic Goto-Kakizaki rats. *Hypertension*. 2001;37:433–439.

Chilian WM, Eastham CL, Layne SM, Marcus ML . Small vessel phenomena in the coronary microcirculation: phasic intramyocardial perfusion and coronary microvascular dynamics. *Prog. Cardiovasc. Dis.* 1988;31:17–38.

Chow K, Flewitt JA, Green JD, Pagano JJ, Friedrich MG, Thompson RB . Saturation recovery single-shot acquisition (SASHA) for myocardial T1 mapping. *Magn. Reson. Med.* 2013;

Coolen BF, Geelen T, Paulis LEM, Nauerth A, Nicolay K, Strijkers GJ . Three-dimensional T1 mapping of the mouse heart using variable flip angle steady-state MR imaging. *NMR Biomed.* 2011;24:154–162.

Coolen BF, Moonen RPM, Paulis LEM, Geelen T, Nicolay K, Strijkers GJ . Mouse myocardial first-pass perfusion MR imaging. *Magn. Reson. Med.* 2010;64:1658–1663.

Coolen BF, Simonis FFJ, Geelen T, Moonen RPM, Arslan F, Paulis LEM, Nicolay K, Strijkers GJ . Quantitative T2 mapping of the mouse heart by segmented MLEV phase-cycled T2 preparation. *Magn. Reson. Med. Off. J. Soc. Magn. Reson. Med. Soc. Magn. Reson. Med.* 2013;

Croteau E, Bénard F, Bentourkia M, Rousseau J, Paquette M, Lecomte R . Quantitative myocardial perfusion and coronary reserve in rats with 13N-ammonia and small animal PET: impact of anesthesia and pharmacologic stress agents. *J. Nucl. Med.* 2004;45:1924–1930.

Crystal GJ . Vasomotor effects of isoflurane in the coronary circulation. *Anesthesiology*. 1996;84:1516–1518.

Dai W, Garcia D, de Bazelaire C, Alsop DC . Continuous flow-driven inversion for arterial spin labeling using pulsed radio frequency and gradient fields. *Magn. Reson. Med.* 2008;60:1488–1497.

Davies JE, Whinnett ZI, Francis DP, Manisty CH, Aguado-Sierra J, Willson K, Foale RA, Malik IS, Hughes AD, Parker KH, Mayet J . Evidence of a dominant backward-propagating "suction" wave responsible for diastolic coronary filling in humans, attenuated in left ventricular hypertrophy. *Circulation*. 2006;113:1768–1778.

Debaene B, Goldfarb G, Braillon A, Jolis P, Lebrec D . Effects of ketamine, halothane, enflurane, and isoflurane on systemic and splanchnic hemodynamics in normovolemic and hypovolemic cirrhotic rats. *Anesthesiology*. 1990;73:118–124.

Deichmann R, Haase A . Quantification of T1 values by SNAPSHOT-FLASH NMR imaging. *J. Magn. Reson.* 1992;96:608–612.

Desrois M, Clarke K, Lan C, Dalmasso C, Cole M, Portha B, Cozzone PJ, Bernard M . Upregulation of eNOS and unchanged energy metabolism in increased susceptibility of the aging type 2 diabetic GK rat heart to ischemic injury. *Am. J. Physiol. Heart Circ. Physiol.* 2010;299:H1679–1686.

Desrois M, Sidell RJ, Gauguier D, King LM, Radda GK, Clarke K . Initial steps of insulin signaling and glucose transport are defective in the type 2 diabetic rat heart. *Cardiovasc. Res.* 2004;61:288–296.

Detre JA, Leigh JS, Williams DS, Koretsky AP . Perfusion imaging. *Magn. Reson. Med.* 1992;23:37–45.

Detre JA, Wang J, Wang Z, Rao H . Arterial spin-labeled perfusion MRI in basic and clinical neuroscience. *Curr. Opin. Neurol.* 2009;22:348–355.

Detre JA, Zhang W, Roberts DA, Silva AC, Williams DS, Grandis DJ, Koretsky AP, Leigh JS . Tissue specific perfusion imaging using arterial spin labeling. *NMR Biomed.* 1994;7:75–82.

Dijkmans PA, Knaapen P, Sieswerda GTJ, Aiazian E, Visser CA, Lammertsma AA, Visser FC, Kamp O . Quantification of Myocardial Perfusion Using Intravenous Myocardial Contrast Echocardiography in Healthy Volunteers: Comparison with Positron Emission Tomography. *J. Am. Soc. Echocardiogr.* 2006;19:285–293.

Do HP, Jao TR, Nayak KS . Myocardial arterial spin labeling perfusion imaging with improved sensitivity. *J. Cardiovasc. Magn. Reson.* 2014;16:15.

Duhamel G, Prevost V, Girard OM, Callot V, Cozzone PJ . High-resolution mouse kidney perfusion imaging by pseudo-continuous arterial spin labeling at 11.75T. *Magn. Reson. Med.* 2013;n/a–n/a.

Ed X Wu, Haiying Tang, Wong KK, Wang J . Mapping cyclic change of regional myocardial blood volume using steady-state susceptibility effect of iron oxide nanoparticles. *J. Magn. Reson. Imaging.* 2004;19:50–58.

Edelman RR, Siewert B, Darby DG, Thangaraj V, Nobre AC, Mesulam MM, Warach S . Qualitative mapping of cerebral blood flow and functional localization with echo-planar MR imaging and signal targeting with alternating radio frequency. *Radiology.* 1994;192:513–520.

Epstein FH, Meyer CH . Myocardial perfusion using arterial spin labeling CMR: promise and challenges. *JACC Cardiovasc. Imaging.* 2011;4:1262–1264.

Fidler F, Wacker CM, Dueren C, Weigel M, Jakob PM, Bauer WR, Haase A . Myocardial perfusion measurements by spin-labeling under different vasodynamic states. *J. Cardiovasc. Magn. Reson.* 2004a;6:509–516.

Fidler F, Wacker CM, Dueren C, Weigel M, Jakob PM, Bauer WR, Haase A . Myocardial perfusion measurements by spin-labeling under different vasodynamic states. *J. Cardiovasc. Magn. Reson. Off. J. Soc. Cardiovasc. Magn. Reson.* 2004b;6:509–516.

Fuster V, Hurst JW . Hurst's the Heart, 12th Edition: Vol. 1. 2008;. McGraw Hill Professional.

Gaborit B, Jacquier A, Kober F, Abdesselam I, Cuisset T, Boullu-Ciocca S, Emungania O, Alessi M-C, Clément K, Bernard M, Dutour A . Effects of bariatric surgery on cardiac ectopic fat: lesser decrease in epicardial fat compared to visceral fat loss and no change in myocardial triglyceride content. *J. Am. Coll. Cardiol.* 2012;60:1381–1389.

Garot J, Bluemke DA, Osman NF, Rochitte CE, McVeigh ER, Zerhouni EA, Prince JL, Lima JA . Fast determination of regional myocardial strain fields from tagged cardiac images using harmonic phase MRI. *Circulation.* 2000;101:981–988.

Gebker R, Paetsch I, Neuss M, Schnackenburg B, Bornstedt A, Jahnke C, Gomaa O, Fleck E, Nagel E . Determinants of myocardial response in CMR perfusion imaging using Gd-BOPTA (Multihance). *J. Cardiovasc. Magn. Reson.* 2005;7:565–572.

Gebker R, Schwitter J, Fleck E, Nagel E . How we perform myocardial perfusion with cardiovascular magnetic resonance. *J. Cardiovasc. Magn. Reson.* 2007;9:539–547.

Gervais M, Démolis P, Domergue V, Lesage M, Richer C, Giudicelli JF . Systemic and regional hemodynamics assessment in rats with fluorescent microspheres. *J. Cardiovasc. Pharmacol.* 1999;33:425–432.

Gibbons RJ . Myocardial perfusion imaging. *Heart Br. Card. Soc.* 2000;83:355–360.

Gilson WD, Yang Z, French BA, Epstein FH . Complementary displacement-encoded MRI for contrast-enhanced infarct detection and quantification of myocardial function in mice. *Magn. Reson. Med.* 2004;51:744–752.

Gould KL, Kirkeeide RL, Buchi M . Coronary flow reserve as a physiologic measure of stenosis severity. *J. Am. Coll. Cardiol.* 1990;15:459–474.

Gould KL, Lipscomb K . Effects of coronary stenoses on coronary flow reserve and resistance. *Am. J. Cardiol.* 1974;34:48–55.

Griswold MA, Jakob PM, Heidemann RM, Nittka M, Jellus V, Wang J, Kiefer B, Haase A . Generalized autocalibrating partially parallel acquisitions (GRAPPA). *Magn. Reson. Med.* 2002;47:1202–1210.

Grözinger G, Pohmann R, Schick F, Grosse U, Syha R, Brechtel K, Rittig K, Martirosian P . Perfusion measurements of the calf in patients with peripheral arterial occlusive disease before and after percutaneous transluminal angioplasty using Mr arterial spin labeling. *J. Magn. Reson. Imaging.* 2013;n/a–n/a.

Günther M, Bock M, Schad LR . Arterial spin labeling in combination with a look-locker sampling strategy: inflow turbo-sampling EPI-FAIR (ITS-FAIR). *Magn. Reson. Med.* 2001;46:974–984.

Haase A . Snapshot FLASH MRI. Applications to T1, T2, and chemical-shift imaging. *Magn. Reson. Med.* 1990;13:77–89.

Harms HJ, Nesterov SV, Han C, Danad I, Leonora R, Raijmakers PG, Lammertsma AA, Knuuti J, Knaapen P . Comparison of clinical non-commercial tools for automated quantification of myocardial blood flow using oxygen-15-labelled water PET/CT. *Eur. Heart J. Cardiovasc. Imaging.* 2013;

Hoffman JI, Spaan JA . Pressure-flow relations in coronary circulation. *Physiol. Rev.* 1990;70:331–390.

Hunold P, Maderwald S, Eggebrecht H, Vogt FM, Barkhausen J . Steady-state free precession sequences in myocardial first-pass perfusion MR imaging: comparison with TurboFLASH imaging. *Eur. Radiol.* 2004;14:409–416.

Iltis I, Kober F, Dalmasso C, Cozzone PJ, Bernard M . Noninvasive characterization of myocardial blood flow in diabetic, hypertensive, and diabetic-hypertensive rats using spin-labeling MRI. *Microcirc. N. Y. N 1994*. 2005a;12:607–614.

Iltis I, Kober F, Dalmasso C, Lan C, Cozzone PJ, Bernard M . In vivo assessment of myocardial blood flow in rat heart using magnetic resonance imaging: effect of anesthesia. *J. Magn. Reson. Imaging.* 2005b;22:242–247.

Iltis I, Kober F, Desrois M, Dalmasso C, Lan C, Portha B, Cozzone PJ, Bernard M . Defective myocardial blood flow and altered function of the left ventricle in type 2 diabetic rats: a noninvasive in vivo study using perfusion and cine magnetic resonance imaging. *Invest. Radiol.* 2005c;40:19–26.

Ishida N, Sakuma H, Motoyasu M, Okinaka T, Isaka N, Nakano T, Takeda K . Noninfarcted myocardium: correlation between dynamic first-pass contrast-enhanced myocardial MR imaging and quantitative coronary angiography. *Radiology.* 2003;229:209–216.

Jacquier A, Kober F, Bun S, Giorgi R, Cozzone PJ, Bernard M . Quantification of myocardial blood flow and flow reserve in rats using arterial spin labeling MRI: comparison with a fluorescent microsphere technique. *NMR Biomed.* 2011;24:1047–1053.

Jerosch-Herold M . Quantification of myocardial perfusion by cardiovascular magnetic resonance. *J. Cardiovasc. Magn. Reson.* 2010;12:57.

Jerosch-Herold M, Swingen C, Seethamraju RT . Myocardial blood flow quantification with MRI by model-independent deconvolution. *Med. Phys.* 2002;29:886–897.

Jerosch-Herold M, Wilke N, Stillman AE . Magnetic resonance quantification of the myocardial perfusion reserve with a Fermi function model for constrained deconvolution. *Med. Phys.* 1998;25:73–84.

Jogiya R, Makowski M, Phinikaridou A, Patel AS, Jansen C, Zarinabad N, Chiribiri A, Botnar R, Nagel E, Kozerke S, Plein S . Hyperemic stress myocardial perfusion cardiovascular magnetic resonance in mice at 3 Tesla: initial experience and validation against microspheres. *J. Cardiovasc. Magn. Reson.* 2013;15:62.

Kajiya F, Tsujioka K, Ogasawara Y, Hiramatsu O, Wada Y, Goto M, Yanaka M . Analysis of the characteristics of the flow velocity waveforms in left atrial small arteries and veins in the dog. *Circ. Res.* 1989;65:1172–1181.

Kajiya F, Yada T, Hiramatsu O, Ogasawara Y, Inai Y, Kajiya M . Coronary microcirculation in the beating heart. *Med. Biol. Eng. Comput.* 2008;46:411–419.

Kajiya M, Hirota M, Inai Y, Kiyooka T, Morimoto T, Iwasaki T, Endo K, Mohri S, Shimizu J, Yada T, Ogasawara Y, Naruse K, Ohe T, Kajiya F . Impaired NO-mediated vasodilation with increased superoxide but robust EDHF function in right ventricular arterial microvessels of pulmonary hypertensive rats. *Am. J. Physiol. Heart Circ. Physiol.* 2007;292:H2737–2744.

Kaufmann PA, Gnecchi-Ruscone T, Yap JT, Rimoldi O, Camici PG . Assessment of the reproducibility of baseline and hyperemic myocardial blood flow measurements with 15O-labeled water and PET. *J. Nucl. Med.* 1999;40:1848–1856.

Kellman P, Hansen MS . T1-mapping in the heart: accuracy and precision. *J. Cardiovasc. Magn. Reson.* 2014;16:2.

Kim H-S, Cho S-G, Kim JH, Bom H-S . Indirect Radionuclide Coronary Angiography to Evaluate Gradients of Myocardial Blood Flow and Flow Reserve Through Coronary Stenosis Using N-13 Ammonia PET/CT. *Chonnam Med. J.* 2013;49:69–74.

Kim RJ, Fieno DS, Parrish TB, Harris K, Chen EL, Simonetti O, Bundy J, Finn JP, Klocke FJ, Judd RM . Relationship of MRI delayed contrast enhancement to irreversible injury, infarct age, and contractile function. *Circulation*. 1999;100:1992–2002.

Kim SG . Quantification of relative cerebral blood flow change by flow-sensitive alternating inversion recovery (FAIR) technique: application to functional mapping. *Magn Reson Med*. 1995;34:293–301.

Kissling G, Blickle B, Pascht U . Modified heart-lung preparation for the evaluation of systolic and diastolic coronary flow in rats. *Am. J. Physiol. Heart Circ. Physiol.* 2000;278:H277–284.

Klassen GA, Barclay KD, Wong R, Paton B, Wong AY . Red cell flux during the cardiac cycle in the rabbit myocardial microcirculation. *Cardiovasc. Res.* 1997;34:504–514.

Knobelsdorff-Brenkenhoff F von, Dieringer MA, Prothmann M, Greiser A, Niendorf T, Schulz-Menger J . Segment-based myocardial T1 and T2 mapping at 3T: feasibility and normal values. *J. Cardiovasc. Magn. Reson.* 2013;15:P37.

Kober F, Duhamel G, Cozzone PJ . Experimental comparison of four FAIR arterial spin labeling techniques for quantification of mouse cerebral blood flow at 4.7 T. *NMR Biomed.* 2008;21:781–792.

Kober F, Iltis I, Cozzone PJ, Bernard M . Myocardial blood flow mapping in mice using high-resolution spin labeling magnetic resonance imaging: influence of ketamine/xylazine and isoflurane anesthesia. *Magn. Reson. Med.* 2005;53:601–606.

Kober F, Iltis I, Izquierdo M, Desrois M, Ibarrola D, Cozzone PJ, Bernard M . High-resolution myocardial perfusion mapping in small animals in vivo by spin-labeling gradient-echo imaging. *Magn. Reson. Med.* 2004;51:62–67.

Kwong KK, Chesler DA, Weisskoff RM, Donahue KM, Davis TL, Ostergaard L, Campbell TA, Rosen BR . Mr perfusion studies with t1-weighted echo planar imaging. *Magn. Reson. Med.* 1995;34:878–887.

Larghat AM, Maredia N, Biglands J, Greenwood JP, Ball SG, Jerosch-Herold M, Radjenovic A, Plein S . Reproducibility of first-pass cardiovascular magnetic resonance myocardial perfusion. *J. Magn. Reson. Imaging*. 2013;37:865–874.

Lee DC, Simonetti OP, Harris KR, Holly TA, Judd RM, Wu E, Klocke FJ . Magnetic resonance versus radionuclide pharmacological stress perfusion imaging for flow-limiting stenoses of varying severity. *Circulation*. 2004;110:58–65.

Look DC, Locker DR . Time Saving in Measurement of NMR and EPR Relaxation Times. *Rev. Sci. Instrum.* 1970;41:250–251.

Lusitano A . Curationum Medicinalium Centuriæ Septem. 1st. edition. 1551;

Makowski M, Jansen C, Webb I, Chiribiri A, Nagel E, Botnar R, Kozerke S, Plein S . First-pass contrast-enhanced myocardial perfusion MRI in mice on a 3-T clinical MR scanner. *Magn. Reson. Med.* 2010;64:1592–1598.

Marinelli M, Positano V, Nekolla SG, Marcheschi P, Todiere G, Esposito N, Puzzuoli S, L'Abbate GA, Marraccini P, Neglia D . Hybrid image visualization tool for 3D integration of CT coronary anatomy and quantitative myocardial perfusion PET. *Int. J. Comput. Assist. Radiol. Surg.* 2013;8:221–232.

Meng Y, Wang P, Kim S-G . Simultaneous measurement of cerebral blood flow and transit time with turbo dynamic arterial spin labeling (Turbo-DASL): application to functional studies. *Magn. Reson. Med.* 2012;68:762–771.

Merabet N, Bellien J, Glevarec E, Nicol L, Lucas D, Remy-Jouet I, Bounoure F, Dreano Y, Wecker D, Thuillez C, Mulder P . Soluble epoxide hydrolase inhibition improves myocardial perfusion and function in experimental heart failure. *J. Mol. Cell. Cardiol.* 2012;52:660–666.

Messroghli DR, Radjenovic A, Kozerke S, Higgins DM, Sivananthan MU, Ridgway JP . Modified Look-Locker inversion recovery (MOLLI) for high-resolution T1 mapping of the heart. *Magn. Reson. Med.* 2004;52:141–146.

Miller CA, Naish JH, Ainslie MP, Tonge C, Tout D, Arumugam P, Banerji A, Egdell RM, Clark D, Weale P, Steadman CD, McCann GP, Ray SG, Parker GJ, Schmitt M . Voxel-wise quantification of myocardial blood flow with cardiovascular magnetic resonance: effect of variations in methodology and validation with positron emission tomography. *J. Cardiovasc. Magn. Reson.* 2014;16:11.

Moon JC, Messroghli DR, Kellman P, Piechnik SK, Robson MD, Ugander M, Gatehouse PD, Arai AE, Friedrich MG, Neubauer S, Schulz-Menger J, Schelbert EB . Myocardial T1 mapping and extracellular volume quantification: a Society for Cardiovascular Magnetic Resonance (SCMR) and CMR Working Group of the European Society of Cardiology consensus statement. *J. Cardiovasc. Magn. Reson.* 2013;15:92.

Morgenstern C, Höljes U, Arnold G, Lochner W . The influence of coronary pressure and coronary flow on intracoronary blood volume and geometry of the left ventricle. *Pflüg. Arch.* 1973;340:101–111.

Moro P-J, Flavian A, Jacquier A, Kober F, Quilici J, Gaborit B, Bonnet J-L, Moulin G, Cozzone PJ, Bernard M . Gender differences in response to cold pressor test assessed with velocity-encoded cardiovascular magnetic resonance of the coronary sinus. *J. Cardiovasc. Magn. Reson.* 2011;13:54.

Nagel E, Klein C, Paetsch I, Hettwer S, Schnackenburg B, Wegscheider K, Fleck E . Magnetic Resonance Perfusion Measurements for the Noninvasive Detection of Coronary Artery Disease. *Circulation.* 2003;108:432–437.

Nahrendorf M, Streif JU, Hiller K-H, Hu K, Nordbeck P, Ritter O, Sosnovik D, Bauer L, Neubauer S, Jakob PM, Ertl G, Spindler M, Bauer WR . Multimodal functional cardiac MRI in creatine kinase-deficient mice reveals subtle abnormalities in myocardial perfusion and mechanics. *Am. J. Physiol. Heart Circ. Physiol.* 2006;290:H2516–2521.

Northrup BE, McCommis KS, Zhang H, Ray S, Woodard PK, Gropler RJ, Zheng J . Resting myocardial perfusion quantification with CMR arterial spin labeling at 1.5 T and 3.0 T. *J Cardiovasc Magn Reson.* 2008;10:53.

Odille F, Vuissoz P-A, Marie P-Y, Felblinger J . Generalized Reconstruction by Inversion of Coupled Systems (GRICS) applied to free-breathing MRI. *Magn. Reson. Med.* 2008;60:146–157.

Oshita A, Ohmori K, Yu Y, Kondo I, Takeuchi H, Takagi Y, Wada Y, Yukiiri K, Mizushige K, Kohno M . Myocardial blood flow measurements in rats with simple pulsing contrast echocardiography. *Ultrasound Med. Biol.* 2002;28:459–466.

Park S-H, Wang DJJ, Duong TQ . Balanced steady state free precession for arterial spin labeling MRI: Initial experience for blood flow mapping in human brain, retina, and kidney. *Magn. Reson. Imaging.* 2013;31:1044–1050.

Pell GS, Thomas DL, Lythgoe MF, Calamante F, Howseman AM, Gadian DG, Ordidge RJ . Implementation of quantitative FAIR perfusion imaging with a short repetition time in time-course studies. *Magn. Reson. Med.* 1999;41:829–840.

Petersen ET, Lim T, Golay X . Model-free arterial spin labeling quantification approach for perfusion MRI. *Magn. Reson. Med.* 2006;55:219–232.

Picarel-Blanchot F, Berthelier C, Bailbé D, Portha B . Impaired insulin secretion and excessive hepatic glucose production are both early events in the diabetic GK rat. *Am. J. Physiol.* 1996;271:E755–762.

Piechnik SK, Ferreira VM, Dall'Armellina E, Cochlin LE, Greiser A, Neubauer S, Robson MD . Shortened Modified Look-Locker Inversion recovery (ShMOLLI) for clinical myocardial T1-mapping at 1.5 and 3 T within a 9 heartbeat breathhold. *J. Cardiovasc. Magn. Reson.* 2010;12:69.

Pohmann R, von Kienlin M, Haase A . Theoretical Evaluation and Comparison of Fast Chemical Shift Imaging Methods. *J. Magn. Reson.* 1997;129:145–160.

Pollock JM, Tan H, Kraft RA, Whitlow CT, Burdette JH, Maldjian JA . Arterial Spin Labeled MRI Perfusion Imaging: Clinical Applications. *Magn. Reson. Imaging Clin. N. Am.* 2009;17:315–338.

Poncelet BP, Koelling TM, Schmidt CJ, Kwong KK, Reese TG, Ledden P, Kantor HL, Brady TJ, Weisskoff RM . Measurement of human myocardial perfusion by double-gated flow alternating inversion recovery EPI. *Magn Reson Med.* 1999;41:510–9.

Pruessmann KP, Golay X, Stuber M, Scheidegger MB, Boesiger P . RF pulse concatenation for spatially selective inversion. *J Magn Reson*. 2000;146:58–65.

Radjenovic A, Biglands JD, Larghat A, Ridgway JP, Ball SG, Greenwood JP, Jerosch-Herold M, Plein S . Estimates of systolic and diastolic myocardial blood flow by dynamic contrast-enhanced MRI. *Magn. Reson. Med.* 2010;64:1696–1703.

Raher MJ, Thibault H, Poh KK, Liu R, Halpern EF, Derumeaux G, Ichinose F, Zapol WM, Bloch KD, Picard MH, Scherrer-Crosbie M . In vivo characterization of murine myocardial perfusion with myocardial contrast echocardiography: validation and application in nitric oxide synthase 3 deficient mice. *Circulation*. 2007;116:1250–1257.

Ranhosky A, Kempthorne-Rawson J . The safety of intravenous dipyridamole thallium myocardial perfusion imaging. Intravenous Dipyridamole Thallium Imaging Study Group. *Circulation*. 1990;81:1205–1209.

Reeder SB, Atalay MK, McVeigh ER, Zerhouni EA, Forder JR . Quantitative cardiac perfusion: a noninvasive spin-labeling method that exploits coronary vessel geometry. *Radiology*. 1996;200:177–184.

Rodriguez I, Ennis DB, Wen H . Noninvasive measurement of myocardial tissue volume change during systolic contraction and diastolic relaxation in the canine left ventricle. *Magn. Reson. Med.* 2006;55:484–490.

Rudolph AM, Heymann MA . The circulation of the fetus in utero. Methods for studying distribution of blood flow, cardiac output and organ blood flow. *Circ. Res.* 1967;21:163–184.

Sabiston DC, Gregg DE . Effect of Cardiac Contraction on Coronary Blood Flow. *Circulation*. 1957;15:14–20.

Saeed M, Wendland MF, Szolar D, Sakuma H, Geschwind J-F, Globits S, Derugin N, Higgins CB . Quantification of the extent of area at risk with fast contrast-enhanced magnetic resonance imaging in experimental coronary artery stenosis. *Am. Heart J.* 1996;132:921–932.

Sakuma H, Fujita N, Foo TK, Caputo GR, Nelson SJ, Hartiala J, Shimakawa A, Higgins CB . Evaluation of left ventricular volume and mass with breath-hold cine MR imaging. *Radiology*. 1993;188:377–380.

Sato A, Terata K, Miura H, Toyama K, Loberiza FR Jr, Hatoum OA, Saito T, Sakuma I, Gutterman DD . Mechanism of vasodilation to adenosine in coronary arterioles from patients with heart disease. *Am. J. Physiol. Heart Circ. Physiol.* 2005;288:H1633–1640.

Sawada S, Muzik O, Beanlands RS, Wolfe E, Hutchins GD, Schwaiger M . Interobserver and interstudy variability of myocardial blood flow and flow-reserve measurements with nitrogen 13 ammonia-labeled positron emission tomography. *J. Nucl. Cardiol.* 1995;2:413–422.

Scheffler K . On the transient phase of balanced SSFP sequences. *Magn. Reson. Med.* 2003;49:781–3.

Scheffler K, Lehnhardt S . Principles and applications of balanced SSFP techniques. *Eur. Radiol.* 2003;13:2409–2418.

Schindler T, Zhang X-L, Prior J, Cadenas J, Dahlbom M, Sayre J, Schelbert H . Assessment of intra- and interobserver reproducibility of rest and cold pressor test-stimulated myocardial blood flow with 13N-ammonia and PET. *Eur. J. Nucl. Med. Mol. Imaging*. 2007;34:1178–1188.

Schmitt P, Griswold MA, Jakob PM, Kotas M, Gulani V, Flentje M, Haase A . Inversion recovery TrueFISP: quantification of T(1), T(2), and spin density. *Magn. Reson. Med.* 2004;51:661–7.

Schreiber WG, Schmitt M, Kalden P, Mohrs OK, Kreitner K-F, Thelen M . Dynamic contrast-enhanced myocardial perfusion imaging using saturation-prepared TrueFISP. *J. Magn. Reson. Imaging.* 2002;16:641–652.

Schwitter J, DeMarco T, Kneifel S, von Schulthess GK, Jörg MC, Arheden H, Rühm S, Stumpe K, Buck A, Parmley WW, Lüscher TF, Higgins CB . Magnetic resonance-based assessment of global coronary flow and flow reserve and its relation to left ventricular functional parameters: a comparison with positron emission tomography. *Circulation.* 2000;101:2696–2702.

Schwitter J, Wacker CM, Rossum AC van, Lombardi M, Al-Saadi N, Ahlstrom H, Dill T, Larsson HBW, Flamm SD, Marquardt M, Johansson L . MR-IMPACT: comparison of perfusion-cardiac magnetic resonance with single-photon emission computed tomography for the detection of coronary artery disease in a multicentre, multivendor, randomized trial. *Eur. Heart J.* 2008;

Schwitter J, Wacker CM, Wilke N, Al-Saadi N, Sauer E, Huettle K, Schonberg SO, Debl K, Strohm O, Ahlstrom H, Dill T, Hoebel N, Simor T . Superior diagnostic performance of perfusion-cardiovascular magnetic resonance versus SPECT to detect coronary artery disease: The secondary endpoints of the multicenter multivendor MR-IMPACT II (Magnetic Resonance Imaging for Myocardial Perfusion Assessment in Coronary Artery Disease Trial). *J. Cardiovasc. Magn. Reson.* 2012;14:61.

Schwitter J, Wacker CM, Wilke N, Al-Saadi N, Sauer E, Huettle K, Schönberg SO, Luchner A, Strohm O, Ahlstrom H, Dill T, Hoebel N, Simor T . MR-IMPACT II: Magnetic Resonance Imaging for Myocardial Perfusion Assessment in Coronary artery disease Trial: perfusion-cardiac magnetic resonance vs. single-photon emission computed tomography for the detection of coronary artery disease: a comparative multicentre, multivendor trial. *Eur. Heart J.* 2013;34:775–781.

Spaan JA, Breuls NP, Laird JD . Diastolic-systolic coronary flow differences are caused by intramyocardial pump action in the anesthetized dog. *Circ. Res.* 1981;49:584–593.

Streif JU, Nahrendorf M, Hiller KH, Waller C, Wiesmann F, Rommel E, Haase A, Bauer WR . In vivo assessment of absolute perfusion and intracapillary blood volume in the murine myocardium by spin labeling magnetic resonance imaging. *Magn. Reson. Med.* 2005;53:584–92.

Takuma S, Suehiro K, Cardinale C, Hozumi T, Yano H, Shimizu J, Mullis-Jansson S, Sciacca R, Wang J, Burkhoff D, Di Tullio MR, Homma S . Anesthetic inhibition in ischemic and nonischemic murine heart: comparison with conscious echocardiographic approach. *Am. J. Physiol. Heart Circ. Physiol.* 2001;280:H2364–2370.

Talagala SL, Barbier EL, Williams DS, Silva AC, Koretsky AP . Multi-slice perfusion MRI using continuous arterial water labeling: controlling for MT effects with simultaneous proximal and distal RF irradiation. *Proc. 6th Annu. Meet. ISMRM Syd.* 1998;381.

Tran-Gia J, Stäb D, Wech T, Hahn D, Köstler H . Model-based Acceleration of Parameter mapping (MAP) for saturation prepared radially acquired data. *Magn. Reson. Med.* 2013a;70:1524–1534.

Tran-Gia J, Troalen T, Köstler H, Kober F . A Model-based Reconstruction Technique for Look-Locker FAIR Gradient Echo ASL Perfusion Data. *Proc. 21st Annu. Meet. ISMRM Salt Lake City.* 2013b;

Troalen T, Capron T, Cozzone P, Bernard M, Kober F . Cyclic Variation of Myocardial Blood Flow Assessed with cine-ASL. *Abstr. ESMRMB - MAGMA.* 2012;25 Suppl 1:94.

Troalen T, Capron T, Cozzone PJ, Bernard M, Kober F . Cine-ASL: A steady-pulsed arterial spin labeling method for myocardial perfusion mapping in mice. Part I. Experimental study. *Magn. Reson. Med.* 2013;70:1389–1398.

156

Van de Weijer T, van Ewijk PA, Zandbergen HR, Slenter JM, Kessels AG, Wildberger JE, Hesselink MKC, Schrauwen P, Schrauwen-Hinderling VB, Kooi ME . Geometrical models for cardiac MRI in rodents: comparison of quantification of left ventricular volumes and function by various geometrical models with a full-volume MRI data set in rodents. *Am. J. Physiol. Heart Circ. Physiol.* 2012;302:H709–715.

Van Nierop BJ, Coolen BF, Dijk WJR, Hendriks AD, de Graaf L, Nicolay K, Strijkers GJ . Quantitative first-pass perfusion MRI of the mouse myocardium. *Magn. Reson. Med.* 2013;69:1735–1744.

Vandsburger MH, French BA, Helm PA, Roy RJ, Kramer CM, Young AA, Epstein FH . Multi-parameter in vivo cardiac magnetic resonance imaging demonstrates normal perfusion reserve despite severely attenuated beta-adrenergic functional response in neuronal nitric oxide synthase knockout mice. *Eur. Heart J.* 2007;28:2792–2798.

Vandsburger MH, Janiczek RL, Xu Y, French BA, Meyer CH, Kramer CM, Epstein FH . Improved arterial spin labeling after myocardial infarction in mice using cardiac and respiratory gated look-locker imaging with fuzzy C-means clustering. *Magn Reson Med*. 2010;63:648–57.

Wacker CM, Bock M, Hartlep AW, Beck G, van Kaick G, Ertl G, Bauer WR, Schad LR . Changes in myocardial oxygenation and perfusion under pharmacological stress with dipyridamole: assessment using T*2 and T1 measurements. *Magn. Reson. Med.* 1999;41:686–695.

Wacker CM, Fidler F, Dueren C, Hirn S, Jakob PM, Ertl G, Haase A, Bauer WR . Quantitative assessment of myocardial perfusion with a spin-labeling technique: preliminary results in patients with coronary artery disease. *J Magn Reson Imaging*. 2003;18:555–60.

Wagner A, Mahrholdt H, Holly TA, Elliott MD, Regenfus M, Parker M, Klocke FJ, Bonow RO, Kim RJ, Judd RM . Contrast-enhanced MRI and routine single photon emission computed tomography (SPECT) perfusion imaging for detection of subendocardial myocardial infarcts: an imaging study. *Lancet*. 2003;361:374–379.

Waller C, Hiller KH, Voll S, Haase A, Ertl G, Bauer WR . Myocardial perfusion imaging using a non-contrast agent MR imaging technique. *Int. J. Cardiovasc. Imaging*. 2001;17:123–132.

Waller C, Kahler E, Hiller KH, Hu K, Nahrendorf M, Voll S, Haase A, Ertl G, Bauer WR . Myocardial perfusion and intracapillary blood volume in rats at rest and with coronary dilatation: MR imaging in vivo with use of a spin-labeling technique. *Radiology*. 2000;215:189–197.

Wang DJ, Bi X, Avants BB, Meng T, Zuehlsdorff S, Detre JA . Estimation of perfusion and arterial transit time in myocardium using free-breathing myocardial arterial spin labeling with navigator-echo. *Magn Reson Med*. 2010;64:1289–95.

Wang J, Alsop DC, Li L, Listerud J, Gonzalez-At JB, Schnall MD, Detre JA . Comparison of quantitative perfusion imaging using arterial spin labeling at 1.5 and 4.0 Tesla. *Magn. Reson. Med.* 2002;48:242–254.

Wang Y, Moin K, Akinboboye O, Reichek N . Myocardial first pass perfusion: steady-state free precession versus spoiled gradient echo and segmented echo planar imaging. *Magn. Reson. Med.* 2005;54:1123–1129.

Wapcaplet . Diagram of the human heart. http://commons.wikimedia.org/wiki/File:Diagram_of_the_human_heart_(cropped).svg. 2006;

Wei K, Jayaweera AR, Firoozan S, Linka A, Skyba DM, Kaul S . Quantification of Myocardial Blood Flow With Ultrasound-Induced Destruction of Microbubbles Administered as a Constant Venous Infusion. *Circulation*. 1998;97:473–483.

Weiss RG, Bottomley PA, Hardy CJ, Gerstenblith G . Regional Myocardial Metabolism of High-Energy Phosphates during Isometric Exercise in Patients with Coronary Artery Disease. *N. Engl. J. Med.* 1990;323:1593–1600.

Wicker P, Tarazi RC . Coronary blood flow measurements with left atrial injection of microspheres in conscious rats. *Cardiovasc. Res.* 1982;16:580–586.

Wilke N, Kroll K, Merkle H, Wang Y, Ishibashi Y, Xu Y, Zhang J, Jerosch-Herold M, Mühler A, Stillman AE . Regional myocardial blood volume and flow: first-pass MR imaging with polylysine-Gd-DTPA. *J. Magn. Reson. Imaging*. 1995;5:227–237.

Williams DS, Detre JA, Leigh JS, Koretsky AP . Magnetic resonance imaging of perfusion using spin inversion of arterial water. *Proc. Natl. Acad. Sci.* 1992;89:212–216.

Williams DS, Grandis DJ, Zhang W, Koretsky AP . Magnetic resonance imaging of perfusion in the isolated rat heart using spin inversion of arterial water. *Magn. Reson. Med.* 1993;30:361–365.

Wilson RF, Wyche K, Christensen BV, Zimmer S, Laxson DD . Effects of adenosine on human coronary arterial circulation. *Circulation*. 1990;82:1595–1606.

Witte K, Jacke K, Stahrenberg R, Arlt G, Reitenbach I, Schilling L, Lemmer B . Dysfunction of soluble guanylyl cyclase in aorta and kidney of Goto-Kakizaki rats: influence of age and diabetic state. *Nitric Oxide Biol. Chem. Off. J. Nitric Oxide Soc.* 2002;6:85–95.

Wong EC . Quantifying CBF with pulsed ASL: technical and pulse sequence factors. *J. Magn. Reson. Imaging*. 2005;22:727–731.

Wong EC, Buxton RB, Frank LR . Implementation of quantitative perfusion imaging techniques for functional brain mapping using pulsed arterial spin labeling. *NMR Biomed.* 1997;10:237–249.

Wong EC, Buxton RB, Frank LR . A theoretical and experimental comparison of continuous and pulsed arterial spin labeling techniques for quantitative perfusion imaging. *Magn Reson Med*. 1998;40:348–355.

Wu W-C, Fernández-Seara M, Detre JA, Wehrli FW, Wang J . A theoretical and experimental investigation of the tagging efficiency of pseudocontinuous arterial spin labeling. *Magn. Reson. Med.* 2007;58:1020–1027.

Yada T, Hiramatsu O, Kimura A, Goto M, Ogasawara Y, Tsujioka K, Yamamori S, Ohno K, Hosaka H, Kajiya F . In vivo observation of subendocardial microvessels of the beating porcine heart using a needle-probe videomicroscope with a CCD camera. *Circ. Res.* 1993;72:939–946.

Yang Z, Berr SS, Gilson WD, Toufektsian M-C, French BA . Simultaneous evaluation of infarct size and cardiac function in intact mice by contrast-enhanced cardiac magnetic resonance imaging reveals contractile dysfunction in noninfarcted regions early after myocardial infarction. *Circulation*. 2004;109:1161–1167.

Zeng L, Hu Q, Wang X, Mansoor A, Lee J, Feygin J, Zhang G, Suntharalingam P, Boozer S, Mhashilkar A, Panetta CJ, Swingen C, Deans R, From AHL, Bache RJ, Verfaillie CM, Zhang J . Bioenergetic and functional consequences of bone marrow-derived multipotent progenitor cell transplantation in hearts with postinfarction left ventricular remodeling. *Circulation*. 2007;115:1866–1875.

Zerhouni EA, Parish DM, Rogers WJ, Yang A, Shapiro EP . Human heart: tagging with MR imaging--a method for noninvasive assessment of myocardial motion. *Radiology*. 1988;169:59–63.

Zhang H, Qiao H, Frank RS, Huang B, Propert KJ, Margulies S, Ferrari VA, Epstein JA, Zhou R . Spin-labeling magnetic resonance imaging detects increased myocardial blood flow after endothelial cell transplantation in the infarcted heart. *Circ. Cardiovasc. Imaging*. 2012;5:210–217.

Zhang W, Williams DS, Koretsky AP . Measurement of rat brain perfusion by NMR using spin labeling of arterial water: in vivo determination of the degree of spin labeling. *Magn. Reson. Med.* 1993;29:416–421.

Zhang Y, Yeung HN, O'Donnell M, Carson PL . Determination of sample time for T1 measurement. *J. Magn. Reson. Imaging JMRI*. 1998;8:675–681.

Zun Z, Varadarajan P, Pai RG, Wong EC, Nayak KS . Arterial Spin Labeled CMR Detects Clinically Relevant Increase in Myocardial Blood Flow With Vasodilation. *JACC Cardiovasc. Imaging*. 2011;4:1253–1261.

Zun Z, Wong EC, Nayak KS . Assessment of myocardial blood flow (MBF) in humans using arterial spin labeling (ASL): feasibility and noise analysis. *Magn. Reson. Med.* 2009a;62:975–983.

Zun Z, Wong EC, Nayak KS . Myocardial ASL Perfusion Imaging Using Pulsed 2D Tagging of the Proximal Aorta. *Proc. 17th Annu. Meet. ISMRM Honol.* 2009b;1737.

Appendix

Supplementary Theory for spASL signal quantification

Here we present details of the resolution of the master equations presented in Chapter 2 - Theory section, in particular the calculations for the initial conditions.

We recall that phase A correspond to the period during which the signal is acquired with the cine-FLASH sequence (tag or control) and phase B the recovery period at the end of each cine train.

The magnetization in phase A is governed by the master equation:

$$\frac{dM_z}{dt} = \frac{M_{ss} - M_z}{T_1^*} + fM_a^{tag,ctrl} - f\frac{M_z}{\lambda},$$ [5.1]

And the magnetization in phase B is governed by the master equation:

$$\frac{dM_z}{dt} = \frac{M_0 - M_z}{T_1} + f\frac{M_0}{\lambda} - f\frac{M_z}{\lambda}.$$ [5.2]

Provided these master equations, the general solutions yield the magnetization time evolutions:

$- M_c^A(t) = M_\infty^{Ac} + \left(M_A^c - M_\infty^{Ac}\right)e^{-t/T_1^{app*}}$ for control scan during phase A.

$- M_t^A(t) = M_\infty^{At} + \left(M_A^t - M_\infty^{At}\right)e^{-t/T_1^{app*}}$ for tag scan during phase A.

$- M_c^B(t) = M_0 + \left(M_B^c - M_0\right)e^{-t/T_1^{app}}$ for control scan during phase B.

$- M_t^B(t) = M_0 + \left(M_B^t - M_0\right)e^{-t/T_1^{app}}$ for tag scan during phase B.

In these expressions, the unknown initial conditions have been written as $M_{t,c}^{A,B}(t=0) = M_{A,B}^{t,c}$.

The initial conditions are linked together by continuity of the magnetization along the four successive periods considered:

Phase A, tag → Phase B, tag → Phase A, control → Phase B, control.

We consider M_{An}^t as the initial condition for the magnetization in phase A, tag scan, line n. In this period, time evolves in an interval $t \in \left[n\left(t_p + RD\right); \left((n+1)t_p + nRD\right)\right]$, and the general solution is written:

$$M_t^{An}(t) = M_\infty^{At} + (M_{An}^t - M_\infty^{At})e^{-(t-n(t+RD))/T_1^{app*}}.$$ [5.3]

For the following period, the time interval is $t \in \left[(n+1)t_p + nRD; (n+1)(t_p + RD) \right]$, the initial condition M_{Bn}^t, and the general solution is written:

$$M_t^{Bn}(t) = M_0 + (M_{Bn}^t - M_0)e^{-(t-((n+1)t_p+nRD))/T_1^{app}}.$$ [5.4]

The continuity between these two periods implies:

$$M_t^{An}(t = (n+1)t_p + nRD) = M_t^{Bn}(t = (n+1)t_p + nRD),$$ [5.5]

which leads

$$M_\infty^{At} + (M_{An}^t - M_\infty^{At})e^{-t_p/T_1^{app*}} = M_{Bn}^t.$$ [5.6]

Similarly, the following period is described by:

$$M_c^{An+1}(t) = M_\infty^{Ac} + (M_{An+1}^c - M_\infty^{Ac})e^{-(t-(n+1)(t_p+RD))/T_1^{app*}}$$ [5.7]

By continuity,

$$M_c^{An+1}(t = (n+1)(t_p + RD)) = M_t^{Bn}(t = (n+1)(t_p + RD)),$$ [5.8]

And thus

$$M_{An+1}^c = M_0 + (M_{Bn}^t - M_0)e^{-RD/T_1^{app}}.$$ [5.9]

Combining equations [5.6] and [5.9], we obtain:

$$M_{An+1}^c = M_{An}^t e^{-RD/T_1^{app}} e^{-t_p/T_1^{app*}} + M_0 \left(1 - e^{-RD/T_1^{app}}\right) + M_\infty^{At}\left(1 - e^{-t_p/T_1^{app*}}\right)e^{-RD/T_1^{app}}.$$ [5.10]

By repeating this calculation, we obtain the equations linking successive initial conditions of the same phase:

$$M_{Bn+1}^t = y_B^t + xM_{Bn}^c; \ M_{Bn+1}^c = y_B^c + xM_{Bn}^t; \ M_{An+1}^t = y_A^t + xM_{An}^c; \ M_{An+1}^c = y_A^c + xM_{An}^t,$$

where the $y_{A,B}^{t;c}$ factors are given by:

$$y_B^t = M_0 \left(1 - e^{-RD/T_1^{app}}\right)e^{-t_p/T_1^{app*}} + M_\infty^{At}\left(1 - e^{-t_p/T_1^{app*}}\right),$$ [5.11]

$$y_B^c = M_0 \left(1 - e^{-RD/T_1^{app}}\right)e^{-t_p/T_1^{app*}} + M_\infty^{Ac}\left(1 - e^{-t_p/T_1^{app*}}\right),$$ [5.12]

$$y_A^t = M_0 \left(1 - e^{-RD/T_1^{app}}\right) + M_\infty^{Ac}\left(1 - e^{-t_p/T_1^{app*}}\right)e^{-RD/T_1^{app}},$$ [5.13]

163

$$y_A^c = M_0 \left(1 - e^{-RD/T_1^{app}}\right) + M_\infty^{At} \left(1 - e^{-t_p/T_1^{app*}}\right) e^{-RD/T_1^{app}} , \qquad [5.14]$$

and
$$x = e^{-RD/T_1^{app}} e^{-t_p/T_1^{app*}} . \qquad [5.15]$$

More precisely, the recurrence relation for each period can be written in the form:

$$M_{A,B,N+1}^{t,c} = Y_{A,B}^{t,c} + X M_{A,B,N}^{t,c} , \qquad [5.16]$$

with $X = x^2$, $Y_{A,B}^{t,c} = y_{A,B}^{t,c} + x y_{A,B}^{c,t}$, and $N = 2n$.

The initial conditions are thus linked by a relation of the type $u_{n+1} = a + b u_n$, which can be expressed for an arbitrary n by:

$$u_n = \sum_{i=0}^{n-1} a b^i + b^n u_0 . \qquad [5.17]$$

This yields the relation:

$$M_{A,B,N}^{t,c} = Y_{A,B}^{t,c} \frac{1 - X^N}{1 - X} + X^N M_{A,B,1}^{t,c} . \qquad [5.18]$$

As $x \ll 1$ (and therefore $X \ll 1$), the dependence on N is rapidly converging, so that:

$$M_{A,B}^{t,c} = \frac{Y_{A,B}^{t,c}}{1 - X} . \qquad [5.19]$$

Note that $x \ll 1$ allows the additional simplification $M_{A,B}^{t,c} \approx y_{A,B}^{t,c}$, which is used to derive the formula in the Theory section.

Model-based reconstruction of LLFAIRGE data

Independently from the development of alternative strategies for both rodent and human myocardial ASL, a study was carried out during the period of this thesis to improve LLFAIRGE quantification. This work was done in partnership with Johannes Tran-Gia, a PhD student, and Dr. Herbert Köstler, a Professor from the Institute of Radiology at the University of Würzburg, Germany and has been presented at the 21st ISMRM in Salt Lake City last year *[Tran-Gia 2013b]*. This cooperation was supported by the 'France – Bavaria center for university cooperation (Bayerisch-Französisches Hochschulzentrum, BFHZ).

Purpose

Arterial Spin Labeling (ASL) provides quantitative measurements of tissue blood flow and has been used for quantification of myocardial perfusion in small animals. The most common methodological approach is a FAIR preparation combined with an ECG-gated Look-Locker gradient echo (LLFAIRGE) acquisition scheme *[Kober 2004]*. Details of the sequence can be found in Chapter 1 – Myocardial ASL section.

The fast heart rates of rodents enable a high sampling rate of the T_1 relaxation curve but limit the acquisition to only one phase-encoding (PE) per inversion (IR) pulse if blurring by cardiac motion is to be avoided. The IR pulse needs to be repeated for each PE step leading to long scan times of about 20-25 min. In the initial implementation, inversion times (TI) are obtained as an average over the measured TI of all PE steps. A long scan time associated with variable heart rates can cause inconsistencies in the TI used for the T_1 fitting process which has been addressed in *[Vandsburger 2010]*.

In this work, an adjustment of the model-based MAP reconstruction technique presented in *[Tran-Gia 2013a]* to a LLFAIRGE acquisition (IR-MAP) was developed featuring two major improvements: (i) the ability to take into account any variations of TI in the reconstruction and (ii) the ability to apply *k*-space undersampling for eventually reducing the total acquisition time. This technique paves the way for quantitative myocardial blood flow mapping on small animals from prospectively undersampled datasets, promising shorter scan times in future studies.

Method

In the course of an LLFAIRGE experiment, varying heart rates as well as missed ECG triggers usually lead to a variation in the TI of every PE step growing with the temporal distance to the inversion pulse (see histogram of TIs in Figure A.1). Thus, the use of averaged TI (dotted lines in Figure A.1) is a source of error in the T_1 fit and therefore in the measured perfusion values.
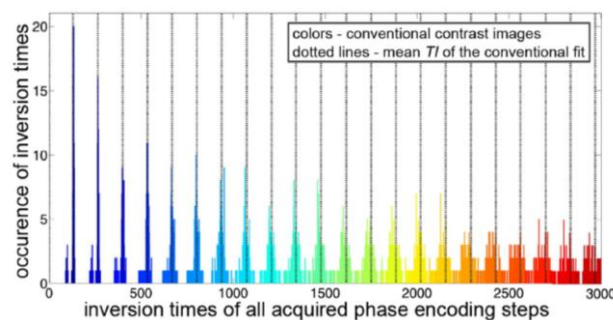

Figure A.1 – Partial histogram of all inversion times.

To improve the precision of the fit, the exact time points of every acquired PE step after the IR pulse were recorded during the experiment. Based on this time log, all PE steps were assigned to bins of a temporal resolution of 20ms. The result was a set of highly undersampled *k*-spaces. For reconstruction, the IR-MAP algorithm (based on the MAP algorithm presented in *[Tran-Gia 2013a]*) was applied to these undersampled *k*-spaces in order to reconstruct one fully sampled *k*-space for each of the temporal bins.

The mono-exponential function:

$$M\left(TI\right) = M_0^* - \left(M_0 + M_0^*\right)e^{-TI/T_1^*},$$
[5.20]

was used to model the signal after the IR pulse, with M_0 the equilibrium magnetization, M_0^* the steady-state magnetization and T_1^* the apparent relaxation time in the presence of continuous RF excitation [6].

The reconstruction scheme of the IR-MAP algorithm is shown in Figure A.2. For initialization, all undersampled *k*-spaces were Fourier transformed into image space. Subsequently, a pixel-wise least-squares fit of the model function was applied, resulting in a set of parameters $M_0(x,y)$, $M_0^*(x,y)$ and $T_1^*(x,y)$ for every pixel (x,y).

Using these parameters, model images were calculated for all TI (*model*). In order to ensure data consistency, the initial *k*-spaces were finally substituted into the corresponding model *k*-spaces (*consistent model*). The consistent model was then passed on to the subsequent iteration. A fixed number of 100 iterations was used as termination criterion throughout this work.
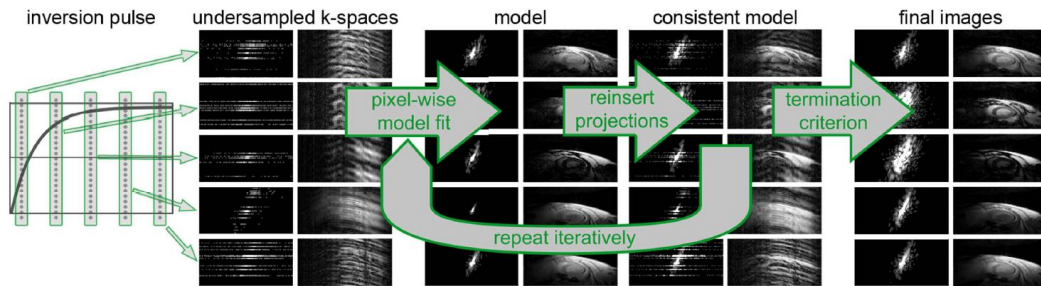

Figure A.2 – Basic reconstruction scheme.

For proof of concept, an experiment was performed with a healthy C57Bl6J mouse on a Bruker 4.7T animal scanner. As described in *[Kober 2004]*, every repetition started with an ECG- and respiratory-gated IR pulse, followed by the acquisition of 55 ECG-gated gradient echoes. This was repeated for all 64 PE steps with an additional repetition delay of 3 seconds.

Post-processing was performed in three different ways:

(A) The complete dataset including all 55 acquired images of the relaxation process was used for slice-selective (SS) and global (GL) measurement.

(B) All images visibly affected by respiratory movement were excluded.

(C) The binning process resulted in sets of 357 highly undersampled *k*-spaces for both SS and GL measurement (5 examples for the GL case are given in Figure A.2).

Applying the IR-MAP algorithm then resulted in 357 complete model images and a set of parameters M_0, M_0^* and T_1^* for every pixel. There parameters were used with the mean values of TI (dotted lines in

Figure A.1) to calculate a new model dataset which was used for post-processing. Perfusion maps were calculated as described in the introduction and in *[Kober 2004]*.

Results

Figure A.3 shows three perfusions maps of the *in-vivo* measurement obtained by the different post-processing techniques (A-C) as described above.

Table A.1 lists the corresponding perfusion values obtained from different myocardial regions (anterior and lateral) as well as the entire myocardium and the chest muscle. Good concordance was found between myocardial perfusion assessed after excluding images affected by respiratory movements (B) and the model-based reconstruction (C).
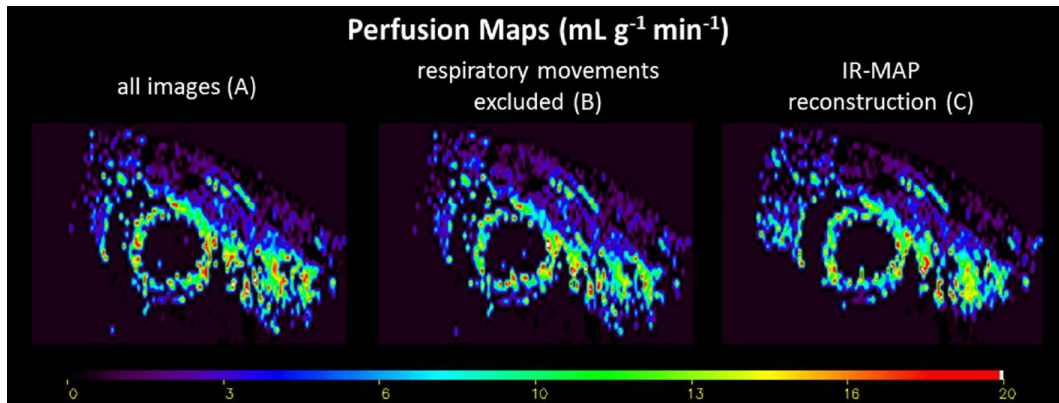

Figure A.3 – Perfusion maps obtained with (A) the conventional reconstruction using every data, (B) with respiratory movements manually excluded and (C) with the IR-MAP reconstruction algorithm.

Table A1 – Perfusion values

Region	Conventional Reconstruction		IR-MAP Reconstruction
	All images (A)	Respiratory movement excluded (B)	
Anterior	10.4 ± 5.2	8.6 ± 5.5	8.0 ± 5.9
Lateral	12.0 ± 4.3	7.4 ± 5.5	7.5 ± 6.2
Global Myocardium	10.3 ± 5.0	8.1 ± 5.8	8.1 ± 5.8
Chest Muscle	0.3 ± 1.5	0.3 ± 1.5	0.4 ± 1.7

Discussion

An extension of the MAP algorithm for the model-based reconstruction of LLFAIRGE datasets is presented. The IR-MAP algorithm can perform parameter mapping from highly undersampled k-spaces acquired after magnetization preparation. In conjunction with a time log of all acquired PE steps, it allows taking into account any variations in *TI*, which can be caused by variable heart rates or imperfect

R-wave detection. Sorting the acquired data more accurately leads to an excellent temporal resolution < 20 ms in TI for the model-based T_1 fit. Although the three perfusion maps seem visually similar, perfusion is overestimated if images affected by respiratory movements are not excluded from the T_1 fit (A vs. B). By using the constraint of a mono-exponential relaxation, the IR-MAP algorithm automatically suppresses respiratory artefacts. Additionally, a time log of the respiratory movement of the animals could be included in the post-processing to further decrease respiratory artefacts. Finally, the new technique holds the potential for a quantification of myocardial perfusion from further undersampled k-spaces, promising shorter scan times in the future.

List of Publications

Peer review articles

Capron T, **Troalen T**, Robert B, Jacquier A, Bernard M, Kober F. *Myocardial Perfusion Assessment in Humans using Steady-Pulsed Arterial Spin Labeling*. Magn Reson Med. (under revision).

Troalen T, Capron T, Bernard M, Kober F. *In Vivo Characterization of Rodent Cyclic Myocardial Perfusion Variation at Rest and during Adenosine-Induced Stress using cine-ASL Cardiovascular Magnetic Resonance*. J. Cardiovasc. Magn. Reson. 2014. In press.

Troalen T, Capron T, Cozzone PJ, Bernard M, Kober F. *Cine-ASL: A Steady-Pulsed Arterial Spin Labeling Method for Myocardial Perfusion Mapping in Mice. Part I: Experimental Study*. Magn Reson Med. 2013;70:1389–98.

Capron T, **Troalen T**, Cozzone PJ, Bernard M, Kober F. *Cine-ASL: A Steady-Pulsed Arterial Spin Labeling Method for Myocardial Perfusion Mapping in Mice. Part II: Theoretical Model and Sensitivity Optimization*. Magn Reson Med. 2013;70:1399–408.

Scientific reviews

Kober F, Bernard M, **Troalen T**, Capron T. *Cardiovascular Magnetic Resonance of Myocardial Structure, Function, and Perfusion in Mouse and Rat Models*. Current Cardiovascular Imaging Report. 2012;5:109-115.

Kober F, **Troalen T**, Bernard M. *Recent developments in small animal cardiovascular MRI*. Current Cardiovascular Imaging Report. 2014;7:9249.

Oral communications

Troalen T, Christian Kenmoe, Pugnaire J, Cozzone PJ, Bernard M, Kober F. *Dynamic of the perfusion reserve during adenosine-induced stress in rats*. ESMRMB 2013, Toulouse, France.

Troalen T, Capron T, Cozzone PJ, Bernard M, Kober F. *Feasibility of cyclic myocardial perfusion variation assessment during adenosine-induced stress in rats*. ISMRM 2013, Salt Lake City, USA.

Capron T, **Troalen T**, Robert B, Jacquier A, Cozzone PJ, Bernard M, Kober F. *Myocardial perfusion assessment in humans using steady-pulsed arterial spin labeling*. ISMRM 2013, Salt Lake City, USA.

Capron T, **Troalen T**, Cozzone PJ, Bernard M, Kober F. *Myocardial perfusion assessment in humans using steady-pulsed arterial spin labeling*. Printemps de la cardiologie (GRRC) 2013, Marseille, France.

Troalen T, Capron T, Bernard M, Cozzone PJ, Kober F. *Cyclic Variation of Myocardial Blood Flow Assessed with cine-ASL*. GDR Imagiv 2012, Lyon, France.

Troalen T, Capron T, Bernard M, Cozzone PJ, Kober F. *Cyclic variation of myocardial blood flow assessed with cine-ASL*. ESMRMB 2012, Lisbon, Portugal.

Troalen T, Capron T, Bernard M, Cozzone PJ, Kober F. *Cine-ASL : Une nouvelle méthode de marquage de spins artériels pour la cartographie de la perfusion myocardique chez la souris.* SFRMBM 2012, Marseille, France.

Troalen T, Capron T, Bernard M, Cozzone PJ, Kober F. *Cine-ASL: A new arterial spin labeling method for myocardial perfusion mapping in mice using a cine-FLASH labeling and readout module.* SCMR 2012, Orlando, USA.

Poster communications

Troalen T, Pugnaire J, Capron T, Robert B, Bernard M, Kober F. *Improved Spatial Resolution and Post-Processing for Myocardial Blood Flow Quantification in Humans using Steady-Pulsed Arterial Spin Labeling.* ISMRM 2014, Milan, Italia.

Tran-Gia J, **Troalen T**, Köstler H, Kober F. A Model-based Reconstruction Technique for Look-Locker FAIR Gradient Echo ASL Perfusion Data. ISMRM 2013, Salt Lake City, USA.

Troalen T, Capron T, Cozzone PJ, Bernard M, Kober F. *Cine-ASL: A non-invasive MRI method for myocardial perfusion mapping in rodents using arterial spin labeling.* Printemps de la cardiologie (GRRC) 2013, Marseille, France. Poster Price from the French Society of Cardiology (SFC).

Troalen T, Capron T, Bernard M, Cozzone P, Kober F. *Cine-ASL: new arterial spin labeling method for myocardial perfusion mapping in mice using a cine- FLASH labeling and readout module.* ISMRM 2012, Melbourne, Australia.

Capron T, **Troalen T**, Cozzone PJ, Bernard M, Kober F. *A theoretical model describing the cine-ASL perfusion mapping technique: steadily-pulsed labeling provides better acquisition efficiency than FAIR.* ISMRM 2012, Melbourne, Australia.

Capron T, **Troalen T**, Bernard M, Cozzone PJ, Kober F. *A New Arterial Spin Labeling MRI Scheme for the Assessment of Myocardial Perfusion.* SFRMBM, 2012, Marseille, France.

RESUME

La perfusion est un facteur important dans la viabilité et la fonction du myocarde. Des atteintes microvasculaires diffuses, précédant l'infarctus ou l'insuffisance cardiaque sont impliqués dans bon nombre de pathologies cardiaques. Ce travail vise à améliorer les techniques existantes de mesure quantitatives et non-invasive de la perfusion myocardique par marquage de spins artériels (ASL). La première partie de mon travail de thèse a consisté en la mise place chez la souris d'une technique alternative pour mesurer la perfusion myocardique. Celle-ci est basée sur un marquage pulsé et régulièrement répété afin de construire un état d'équilibre de l'aimantation sous l'influence de la perfusion (approche steady-pulsed ASL). Le modèle théorique associé à cette technique spASL a été développé en parallèle afin de quantifier le flux sanguin tissulaire. Il a été montré que spASL permettait d'obtenir un résultat similaire aux techniques existantes avec en plus, les avantages d'améliorer la sensibilité au signal de perfusion ainsi que de réduire le temps d'acquisition. Dans un second temps, un transfert vers l'imagerie clinique pour une application chez l'homme a été entrepris. Le marquage de type spASL a été conservé et le module de lecture a été adapté aux spécificités de l'imagerie cardiaque chez l'homme pour une acquisition en respiration libre. Un post-traitement dédié qui comprend une correction de mouvement rétrospective a ensuite vu le jour afin d'améliorer la robustesse de nos mesures. Parallèlement aux développements conduits chez l'homme, nous avons exploité l'approche spASL chez l'animal en proposant diverses améliorations en fonction des études menées.

MOTS CLES

ABSTRACT

Myocardial blood flow is an important factor of tissue viability and function. Diffuse changes in microcirculation preceding heart failure are involved in various cardiac pathologies. This work aim at improving existing techniques allowing quantitative and non-invasive myocardial perfusion assessment using arterial spin labeling. The first step of my work was to design an alternative approach to quantify myocardial blood flow in mice. The so called steady-pulsed ASL (spASL) is based on a regularly repeated pulsed labeling in order to build up a stationary regime of the magnetization under the influence of perfusion. The associated theoretical model has been developed in parallel to quantify tissue blood flow. We have shown that spASL allows to obtain similar results than the previously employed techniques, with the additional advantages of an increased sensitivity to the perfusion signal and a reduced acquisition time. A transfer towards clinical imaging for human applications was then undertaken. The spASL labeling scheme has been preserved while adapting the readout module to the specificities of cardiac MRI when applied to free-breathing human acquisitions. A dedicated post-processing, which includes a retrospective motion correction, has emerged subsequently to improve the robustness of our measurements. In parallel to the developments made for human studies, some optimization of the spASL technique when applied to rodent have been carried out depending on the conducted studies.

KEY WORDS